

Hip & Spine Mechanics - Understanding the linkage from several perspectives of injury
mechanisms to rehabilitation using biomechanical modelling

by

Edward Douglas John Cambridge

A thesis
presented to the University of Waterloo
in fulfilment of the
thesis requirement for the degree of
Doctor of Philosophy
in
Kinesiology

Waterloo, Ontario, Canada, 2019
© Edward Douglas John Cambridge 2019

Author's Declaration

I hereby declare that I am the sole author of this thesis. This is a true copy of the thesis, including any required final revisions, as accepted by my examiners. I understand that my thesis may be made electronically available to the public.

Examination Committee Membership

The following served on the Examining Committee for this thesis. The decision of the Examining Committee is by majority vote.

External Examiner	Cara Lewis, PT, PhD Associate Professor
Supervisor	Stuart McGill, PhD Professor Emeritus
Internal Member	Clark Dickerson, PhD Professor
Internal Member	Steven Fischer, PhD Associate Professor
Internal-external Member	John McPhee, PhD Professor

Abstract

One recent megatrend in medicine is that of “precision medicine” whereby a precise diagnosis leads to a precise intervention for superior results. This thesis was undertaken to enhance the understanding of spine and hip interactions and facilitate precision in both detection and the intervention of mechanical and neurological based disorders. The hip and spine are highly integrated structures. In order to adequately examine and improve the understanding of the complex mechanical linkage between the two, development of a highly biofidelic Hip-Spine Model (HSM) was pursued. Given that no model existed that incorporated the necessary detail, several challenges regarding model development needed to be addressed. It was clear that biofidelity of the model depended on a better understanding and representation of the passive hip stiffness in both males and females. Thus, the experimental data of passive stiffness was evaluated in conjunction with the HSM passive stiffness model predictions. Next, known Anterior Cruciate Ligament (ACL) injury risk factors, such as dynamic knee valgus (DKV) were examined in a female population where both the kinetic and kinematic variables of the hip and spine were evaluated to assist in differentiating those deemed at-risk and not-at-risk during the drop vertical jump (DVJ) procedure. Finally, an atlas of rehabilitation exercises was constructed to guide program design and progression/regressions of rehabilitation protocols for those with back and hip concerns. Each of these themes were unified around the overall goal of this thesis, that being the understanding of the hip-spine mechanical linkage pertaining to injury mechanisms and a guide for rehabilitation of hip-spine disorders.

The first task was the development of the HSM. This model is anatomically detailed and driven by biological signals obtained from the individual to provide new insights into the

understanding of the linkage in a way that was sensitive to the unique movement strategies of the individual. The HSM is an expansion of the previously established 'Spine Model' (SM), developed by Stuart McGill and his team over the past 37 years. The model anatomy was expanded from the current SM using the most complete single subject lower limb data set available known as the Twente Lower Extremity Model (TLEM). Hip ligaments were also added to enhance the passive behaviour of the model. An electromyographic (EMG) driven approach with subject specific kinematics was used to compute the model outputs that consisted of tissue and joint loads. Thus, the first objective of this thesis was to examine the interactions of hip and spine mechanics using a newly developed Hip-Spine Model (HSM) and then to investigate a spectrum of injury mechanisms and rehabilitation exercises.

The next objective was to evaluate passive hip stiffness to enhance the biofidelity of the model and the understanding of hip mechanics in both males and females. A novel testing apparatus was designed and fabricated for measuring hip stiffness which could easily be adapted to clinical settings. This study also serves to establish normative baselines for passive hip stiffness *in vivo*.

The third objective of this thesis was to examine issues of normal function and potential injury mechanisms. For example, ACL injury risk has been linked with some knee kinematic and kinetic patterns however, hip and spine interactions have not been appropriately explored nor have neuromuscular control strategies. This thesis linked the mechanical variables which differentiate at-risk landings of the DVJ task versus non-at-risk landing in females to enhance the understanding of risk behaviours. Clear differences in hip and spine control were documented to

differentiate high and low valgus landings. Adding this knowledge to the current understanding of ACL injury risk will lead to the development of superior and more specific coaching cues to decrease tissue stress/strain concentrations. This approach will underpin intervention strategies leading to lower risk behaviour and correspondingly lower injury risk among female athletes.

The final objective of this thesis was to evaluate the appropriateness of rehabilitation exercises to address hip spine disorders. Currently, there exists a myriad of exercises but little evidence to guide clinical reasoning or decisions for exercise choice, progression, volume and technique. Currently missing from the literature is knowledge of tissue and joint loads in combination with muscle activation patterns. This knowledge will facilitate better matching of specific exercises for specific disorders.

The main objectives of this thesis were: (1) The development of the anatomically detailed, biologically driven HSM which successfully computes joint and tissue loads unique to the individual and their neuromuscular control strategy. (2) The establishment of passive hip stiffness for males and females. (3) To enhance understanding of both neurological and tissue loading characteristics associated with ACL injury risk which when added to the current knowledge provides the opportunity for more precise interventions. (4) The beginning of the development of an atlas for rehabilitation exercises to guide prescriptions that can be matched to specific hip-spine disorders. These findings have the potential to enhance precision medicine in the area of musculoskeletal health – where precision medicine is currently lacking.

Acknowledgements

There are a several people I need to acknowledge, who have given me the tutelage, guidance and support required to make this journey possible.

First, I would like to thank Dr. Stuart McGill, my supervisor. His knowledge, expertise and mentorship have been overwhelming. I am truly humbled to be one of his students and learn from his years of experience, as a world leader in the field who has transcended the area of spine biomechanics. His research and years of investigation have created a paradigm shift in the scientific and clinical community second to none. I consider myself blessed and privileged to have learnt from, shared ideas with, and researched alongside Dr. McGill. Thank you, Stu!

I'd like to acknowledge all of my previous research supervisors who provided me with much needed skills that have served me well at the University of Waterloo. This includes Dr. David Gabriel, PhD, Dr. John J Triano DC, PhD, FCCCS(Hon) and Dr. Kim Ross BSc, MSc, DC, PhD. Drs. Triano and Ross forever changed the course of my life with their mentorship and guidance, I am forever indebted to these fine men.

Next, I'd like to thank all the teachers and trainers who shared their knowledge and expertise with me throughout my many years of schooling. I wish to mention a few here but this is by no means a complete list. Drs. Richard Wells and McGill (KIN 611), Dr. Andrew Laing (KIN 612), Dr. Clark Dickerson (KIN 613), Dr. Wells (KIN 713), Dr. McGill (KIN 727). Thank you to the many others through the years. Dr. Dominique Yedon, DC, FRCCSS and Dr. Brad Muir, DC, FRCCSS for my clinical training as a fourth-year intern, and Dr. Jason Pajaczkowski, DC, FRCCRS, FRCCSS for always willing to share his wealth of knowledge with me. Lastly, Dr. Mark Erwin, DC, PhD for my clinical externship and being the first to show me the role of non-surgical spine specialist firsthand. I have learnt much clinical wisdom from these great clinicians and this knowledge continues to serve me well to this day.

Thanks to all of my friends and colleges through the various institutions and educational arenas that I have learnt from and grown with - there are too many to name. However, I wish to name a few of these individuals, in the McGill Lab here including, Natalie Sidorkewics and Christian Balkovec, who started in the lab with me in 2010. As well as Jordan Cannon, who has worked on a number of projects together. We have all become not only good colleges but great friends. I value your friendship and feel lucky that we shared the journey through graduate school with you all. Diane Ikeda thank you for teaching me the "ways of the lab" from her experience as one of the senior lab members when I started. Thank you to the many others through the years.

Next, I'd like to thank the Undergraduate students who have helped me collect and process data - your collective efforts saved me many hours and work help was very much appreciated: Elliot Perkins, Alex Paluka, Brooke Skerritt, Sam Hogenho and Jake Misener. David Kingston and Jeff Barrett thank you for helping with a few programming tips in MATLAB! I would also like to thank the wonderful staff who made me feel it feel like a Waterloo family: Denise Hay - you are the best!, Jeff Rice - always there to help, Jenny Crowley - you always had what we needed in the lab!, and Craig McDonald - for everything I needed with a computer! Thank you all!

I'd like to acknowledge the guidance and support of my proposal committee Drs. Richard Wells, Clark Dickerson and Jim Frank as well as all of the members of the defense examination committee Drs. Clark Dickerson, Steven Fischer, John McPhee and Cara Lewis (Boston University, School of Medicine). Your collective knowledge and expertise have enhanced the academic contribution of this work and will therefore also improve upon its clinical impact in the years to come. I cannot thank you all enough for your time, effort and contribution to my training.

Lastly, and most importantly, I'd like to thank my loving family who have been my biggest supporters and given me the courage to continue this journey of life. My loving wife Dr. Melanie Abbott-Cambridge - I believe she alone makes me the luckiest man in the world. My parents Helen and Ted, for their life lessons and upbringing, my first teachers! I could not have had better parents. My brother, Andrew and sister-in-law Erin, along with my niece Abigail and nephew Hunter, wonderful supporters. To my late Grandma Barbara Cambridge, thanks for the inspiration of lifelong learning and dedication to education. Also, my extended family Mrs. Wilda and Dr. David Abbott who have supported me like one of their own as well the entire Abbott family. I am so lucky to have an amazing family to encourage and support me emotionally, financially, and in so many other ways. I am blessed to have such a wonderful family - Thank you all!

Dedication

This thesis and the work to produce it is dedicated to my family. To my wife Melanie, thank you for your ongoing and unwavering support. To my wonderful children, Douglas and Julianna – you both mean the world to me. I love you all more than you'll ever know.

Table of Contents

Author’s Declaration	ii
Examination Committee Membership	iii
Abstract	iv
Acknowledgements	vii
Dedication	viii
List of Figures:.....	xii
List of Tables:.....	xix
1.0 Introduction:.....	1
1.1 The Problem	3
1.2 Background & Justification of the Problem	4
1.2.1 Low Back Disorders	5
1.2.2 Lower Limb Disorders	5
1.3 Potential Thesis Impact & Theory Development.....	7
1.4 Objectives.....	9
1.5 Thesis outline and guide to this document	10
2.0 Literature Review:	14
2.1 Modelling Review:.....	15
2.1.1 Relevant Anatomy for Modelling	16
2.1.1.1 Anatomical Relationships to joint coordinate systems (JCS).....	17
2.1.2 Muscle Modeling	18
2.1.2.1 Force-Length Relationship.....	18
2.1.2.2 Force-Velocity Relationship.....	19
2.1.2.3 Force-Length-Velocity Relationship	19
2.1.2.4 EMG to Force.....	20
2.1.3 Neurologically Driving Muscle Mechanics with EMG.....	22
2.1.4 Passive Tissue Properties & Modeling.....	23
2.1.5 Spine Models	24
2.1.6 Hip Models.....	26
2.1.7 Passive Hip Mechanics.....	30
2.1.8 Solving the Indeterminacy Problem	33
2.2 Clinical issues of the knee, the hip, & the spine:.....	35
2.2.1 Hip-Spine Syndrome	35
2.2.2 Hip & Spine ROM	37
2.2.3 Hip & Spine Movement	39
2.2.4 Hip & Spine Loads.....	43
2.2.5 Hip & Spine - Neuromuscular Patterns & Fatigue	44
2.2.6 Hip & Spine - Muscle Strength, Imbalances & Endurance	47
2.2.7 Hip and Spine Rehabilitation and Manual Therapy.....	50
2.2.8 Knee injuries and the hip and spine	51
2.3 Summary of Literature Review	53
3.0 Study 1: Developing the Hip-Spine Model.....	55
3.1 Input Variables.....	57
3.1.1 Kinetics	58
3.1.2 Anthropometrics	58
3.1.3 Kinematics	58
3.1.4 Electromyography	60

3.2 Model Parameters.....	62
3.2.1 Modified Skeletal Geometry	62
3.2.2 Modified Muscle Parameters	65
3.2.2.1 Muscle Wrapping and Geodesics	70
3.2.2.2 Modified Muscle Rest Lengths & Sensitivity Testing.....	81
3.2.3 Ligament Parameters	85
3.2.3 Kinematics	86
3.2.4 Muscle Activation	87
3.2.5 Calculation of Muscle and Ligament Lengths and Velocities	88
3.2.6 Calculation of Muscle Force	88
3.2.7 Calculation of Ligament Force	92
3.3 Model Tuning – EMG driven model and Inverse Dynamics	101
3.4 Results	103
3.5 The Integrated Hip-Spine Model Validation.....	106
3.6 Discussion	107
4.0 Study 2: Passive Moment-Angle Curves and Joint Rotational Stiffness of the Hip in the sagittal and frontal planes: Implications for modelling and model evaluation, sex comparisons, and injury mechanisms.	111
4.1 Introduction.....	111
4.2 Methods	115
4.2.1 Participants.....	115
4.2.2 Data Collection Procedures & Equipment.....	116
4.2.3 Data Analysis	121
4.2.4 Statistical Analysis	122
4.2 Results.....	122
4.3.1 Hip passive ROM profile.	122
4.3.2 Compare male and female passive ROM profile.....	135
4.3.3 Evaluate the model performance estimating angle-moment curves.	144
4.4 Discussion	145
4.4.1 Hip passive ROM profile	145
4.4.2 Compare male and female passive ROM profile.....	147
4.4.3 Evaluate the model performance estimating angle-moment curves.	149
4.4.4 General Discussion	150
4.5 Conclusion	152
5.0 Study 3: Analysis of hip and spine mechanics: Implications for the risk for Anterior Cruciate Ligament injury	153
5.1 Introduction.....	153
5.2 Methods	156
5.2.1 Study Design	156
5.2.2 Participants.....	156
5.2.3 Tasks	156
5.2.4 Procedures.....	157
5.2.5 Outcome Measures & Statistical Design	161
5.3 Results	163
5.3.1 Primary Analysis	163
5.3.1.2 Joint Loads (Inverse Dynamics)	169
5.3.3 Joint Loads Estimates from the HSM.....	175
5.3.2 Secondary Analysis of Continuous Variable Data.....	183

5.4 Discussion	191
5.5 Conclusions.....	194
6.0 Study 5: Quantifying the demands and exposures in commonly used rehabilitation exercises	
- Towards the development of an atlas of exercises for clinical use	195
6.1 Introduction.....	195
6.2 Methods	197
6.2.1 Participants.....	198
6.2.2 Tasks and Apparatus.....	198
6.2.3 Procedure	199
6.2.1. Statistical Analysis	203
6.3 Results	204
6.3.1 Movement Patterns.....	204
6.3.2 Motor Patterns	207
6.3.3 Joint Loads	209
6.4 Discussion	217
7.0 Global Discussion of the Thesis: Hip-Spine Mechanics	221
References.....	226
Appendix A: Hip Anatomy Parameters.....	244
Appendix B: Joint Coordinate Systems.....	247
Appendix C: Passive Tissue Torque-Angle Curves – Tuning the model.....	248
Appendix D: Data Collection, Processing and Analysis.....	254
Data Collection	254
Data Processing	255
Appendix E: Model Congruency	257
Appendix F: Data from Hip Passive Resistance & Stiffness	260
Appendix G: Data from ACL study – Tuning the Model.....	288
Appendix H: Data from ACL study – Statistical Analysis.....	290

List of Figures:

Figure 1.1: A conceptual model of healthy and pathological tissue loading, and interaction links between the hip and spine function. The individual's MSK system forms the basis of the tissue model, which is modulated by unique movement patterns and postures, which in turn influence joint loading (McGill, 2007). Tissue demands are matched by their capacity to bear load; two possible outcomes result, the demands are within the system's capacity or they exceed it. Demands have been discussed elsewhere by Kumar (2001) in relation to repetitive loading and acute over exertion along with imbalances in the muscular system or differential fatigue. If tissue capacity exceeds the demands place on the tissue, then the "healthy tissue loading" cascade will ensue (blue). If the demands exceed tissue capacity, then the "pathological tissue loading" cascade ensues (red). Several theoretical interaction points exist to promote healthy tissue loading and healing as well as encourage tissue overload and failure. In other words, hip and spine mechanics may serve to promote load sharing or encourage tissue overload and injury depending on the individual movement and motor patterns, as well as postures, and loading conditions experienced. Similarly, during the tissue healing process a similar interaction between the hip and spine joint mechanics may promote or retard the healing process based on the same principle of tissue demands and capacity.	8
Figure 1.2: The flow of data through two major data collections and four thesis studies.....	13
Figure 3.1: A schematic diagram of the HSM. Biological signals drive the anatomical detail (model parameters) found within the model which are used to estimate the joint reaction forces and moments.....	57
Figure 3.2: Schematic diagram of axis definitions for the spine and hip in two view, frontal and sagittal plans, in a right-hand coordinate system. Flexion occurs about the z axis, lateral bend of the spine and adduction of the hip occur about the x axis, while axial rotation (twist) occurs about the y axis.	59
Figure 3.3: Reflective Marker Set-Up Anatomical (Single) and marker cluster (4-5) markers.	60
Figure 3.4: Twenty-Four EMG channels were collected including 6 bilateral core muscles (Rectus Abdominis (RA), External Oblique (EO), Internal Oblique (IO), Lower Erector Spinae (LES), Upper Erector Spinae (UES), and Latissimus Dorsi (LD)) and 6 bilateral hip/leg muscles (Rectus Femoris (RF), Tensor Fascia Latae (TFL), Gluteus Medius (GMed), Gluteus Maximus (GMax), Biceps Femoris (BF), and Adductor Longus (ADD).	61
Figure 3.5: Custom MATLAB EMG processor normalized the EMG signals to a MVC for later force estimation calculations in the model. (Top) Raw EMG is filtered 30-500H and bias removed, then (Middle) full wave rectified (FWR) and low pass filtered (Bottom).....	61
Figure 3.6: Correction factor for hip posture off-set in the TLEM as shown in the 2D axial plane view. The off-set accounts for the fixation posture of the cadaveric specimen during the fixation process. The magnitudes are 12.465 degrees of extension, 6.24 degrees of adduction, and 26.28 degrees of medial rotation. The mid-point of the femoral epicondyles is also graphed here however, it perfectly over lays the hip-joint-center and is therefore not visualized. Note: The left side is also shown here	

for comparison in the uncorrected position with the right side demonstrating the corrected posture. L5 = Fifth lumbar vertebra center.	65
Figure 3.7: Correction factor for hip posture off-set in the TLEM as shown in the 2D sagittal plane view. The off-set accounts for the fixation posture of the cadaveric specimen during the fixation process. The magnitudes are 12.465 degrees of extension, 6.24 degrees of adduction, and 26.28 degrees of medial rotation. Note: The femoral and tibial epicondyles and the hip joint center are now aligned vertically. Rectus abdominis is shown as an example of a muscle and provides a relative reference point attaching on the inferior aspect of the rib cage and the pubic bone of the pelvis.	66
Figure 3.8: Sagittal view (left) and frontal view (right) of psoas major with an anatomical representation (top) and the model 3D point representation (bottom) with spherical warping object and wrapping points in anatomical position (right side only displayed).	74
Figure 3.9: Sagittal view (left) and frontal view (right) of psoas major with spherical warping points in anatomical position (right side muscle displayed).	75
Figure 3.10: Iliacus with its 6 proximal segments on the ilium passing through the common psoas and iliacus via point prior to wrapping around the hip/pelvis sphere and attaching to the lesser trochanter of the femur (right side only displayed).	75
Figure 3.11: Gluteus maximus as it passes posterior to the hamstring group and ischial tuberosity.	77
Figure 3.12: Gluteus maximus inferior reduces its moment arm to non-physiological amounts above ~70 degrees. (Extension is negative – flexion is positive, moments are calculated in flexion-extension plane.)	77
Figure 3.13: Gluteus maximus inferior was wrapped to provide realistic anatomical muscle mapping. (Extension is negative – flexion is positive, moments are calculated in flexion-extension plane.)	78
Figure 3.14: Semimembranosus (left), Semitendinosus (middle) and Biceps Femoris Long Head (right) each muscle was wrapped around the inferior margin of a sphere which represented the ischial tuberosity, the bony pelvis and the extensive ligamentous structures present in vivo.	79
Figure 3.15: The effect of wrapping on changes in length for semimembranosus. Wrapping begins at 45 degrees of hip flexion and continues until terminal flexion.	79
Figure 3.16: The effect of wrapping on changes in length for semitendinosus. Wrapping begins at 45 degrees of hip flexion and continues until terminal flexion.	80
Figure 3.17: The effect of wrapping on changes in length for biceps femoris. Wrapping begins at 59 degrees of hip flexion and continues until terminal flexion.	80
Figure 3.18: Adjusted physiological optimal muscle length to achieve more appropriate operating ranges for the force-length and PEC equations for Adductor Magnus Middle section 5. Here a compromise is struck between the flexion/extension plane and the abduction/adduction plane, selecting 22.9 cm as the optimal rest length.	84
Figure 3.19: Adjusted physiological optimal muscle length to achieve more appropriate operating ranges for the force-length and PEC equations for Adductor Magnus Middle section 6. Here a compromise is struck between the flexion/extension plane and the abduction/adduction plane, selecting 23 cm as the optimal rest length.	84

Figure 3.20: Passive resistive moment created by sections iliacus. (Extension is negative – flexion is positive, moments are calculated in flexion-extension plane.).....	85
Figure 3.21: Active (Blue) and passive (orange) muscle force-length modulation. Active dynamics are a piece wise equation and PEC operates above rest lengths of 1.....	91
Figure 3.22: Hip ligaments and capsule.	95
Figure 3.23: Anatomical illustration of the iliofemoral ligament.....	96
Figure 3.24: Experimental data from Hewitt 2002. Orange lines indicate key target points in the curve to identify the inferior iliofemoral ligament characteristics.....	97
Figure 3.25: Model estimated force-displacement curve for inferior iliofemoral ligament. Coefficients in the Barrett equations are as follows: K=55, s=1.5 and m=-3.3.....	97 98
Figure 3.26: Experimental data from Hewitt 2002. Orange lines indicate key target points in the curve to identify the superior iliofemoral ligament characteristics.	98
Figure 3.27: Model estimated force-displacement curve for superior iliofemoral ligament. Coefficients in the Barrett equations are as follows: K=41, s=0.8 and m=-2.05.....	98
Figure 3.28: Anatomical illustration of the ischiofemoral ligament.....	99 99
Figure 3.29: Experimental data from Hewitt 2002. Orange lines indicate key target points in the curve to identify the ischiofemoral ligament characteristics.....	99
Figure 3.30: Model estimated force-displacement curve for ischiofemoral ligament. Coefficients in the Barrett equations are as follows: K=8, s=1.5 and m=-2.0.....	100
Figure 3.31: Anatomical illustration of the pubofemoral ligament.	101
Figure 3.32: Reference voluntary contraction (RVC) positions for evaluating and tuning the model. Position one (left) standing erect with the weight held in front and position 2 (right) standing in a semi-squat position.	102
Figure 3.33: Right hip moment data comparing the HSM and ID (subject 13 in the ACL study, right hip gain of 1.12). This data is used in the model to calculate the tuning factor by which the HSM is adjusted to the ID prediction during the RVC trial. In this trial the data collection captured the posture demonstrated in position 1 in Figure 3.32.	104
Figure 3.34: Left hip moment data comparing the HSM and ID (subject 13 from the ACL study, left hip gain of 0.94). This data is used in the model to calculate the tuning factor by which the HSM is adjusted to the ID prediction during the RVC trial. In this RVC trial the participant moves into and out of the posture in position 2 in Figure 3.32.	104
Figure 3.35: Lumbar spine moment data comparing the HSM and ID (subject 13 of the ACL study with a lumbar spine gain of 0.72). This data is used in the model to calculate the tuning factor by which the HSM is adjusted to the ID prediction during the RVC trial. In this RVC trial the participant moves into and out of the posture in position 2 in Figure 3.32.....	105
Figure 4.1: Schematic diagram of the passive ROM profile characteristics on a generic extension-flexion moment-angle curve. (A) Peak Moment; (B) Peak Angle; (C) Neutral Zone Barrier (NZB) ; (D) Neutral Zone Width (NZW). Note: Not included on the curve is the exponential curve fit $M=ae^{b\theta}$	114
Figure 4.2: Experimental set-up, (A) Kinematic clusters, (B) Suspension Straps in-line with adjusTable connectors and suspension ropes, (C) Pelvic restraint(s).....	117
Figure 4.3: Experimental set-up for measuring sagittal motion (flexion and extension) moment-angle curves.	118

Figure 4.4: Experimental set-up for measuring frontal plane motion (abduction and adduction) moment-angle curves.....	118
Figure 4.5: Schematic diagram of flexion and extension procedures for measuring angle-moment curves. Left – Extension, Middle – Flexion (Knee Bent), Right – Flexion (Straight Leg).....	120
Figure 4.6: Schematic diagram of adduction (left) and abduction (right) procedures for measuring angle-moment curves.	121
Figure 4.7: Subjects’ mean torque-angle plots for (a) FSL, (b) FKB, (c) Ext, (d) Abd, (e) Add.	124
Figure 4.8: Passive hip resistance trials flexion straight leg (left) and flexion knee bent (right), individual means, and group means with a fitted exponential for the group mean.	125
Figure 4.9: Passive hip resistance trials, abduction (left) and adduction (right), individual means, and group means with a fitted exponential for the group mean.	125
Figure 4.10: Passive hip resistance extension trials, individual means, and group means with a fitted exponential for the group mean.	126
Figure 4.11: Mean male angle-moment curve for Flexion-Straight Leg and one standard deviation (Std) for both angle and moment data.....	126
Figure 4.12: Mean male angle-moment curve for Flexion-Knee Bent and one standard deviation (Std) for both angle and moment data.....	127
Figure 4.13: Mean male angle-moment curve for Extension and one standard deviation (Std) for both angle and moment data.....	127
Figure 4.14: Mean male angle-moment curve for Extension and one standard deviation (Std) for both angle and moment data.....	128
Figure 4.15: Mean male angle-moment curve for Extension and standard deviation (Std) for both angle and moment data.	128
Figure 4.16: Subjects’ mean torque-ROM plots for (a) FSL, (b) FKB, (c) Ext, (d) Abd, (e) Add.....	130
Figure 4.17: Mean male ROM-moment curve (black) with one standard deviation (Std) for moment data (grey ticks) for (a) FSL, (b) FKB, (c) Ext, (d) Abd, (e) Add.....	131
Figure 4.18: Torque-ROM curves with exponential curves fitted (black) to the individual trials (light grey) for (a) FSL, (b) FKB, (c) Ext, (d) Abd, (e) Add.....	132
Figure 4.19: Angle-moment plots for males with fitted curves to the exponential function $M=ae^{b\theta}$. Subplots are defined as (a) Flexion – straight leg; (b) Flexion – bent knee; (c) Abduction; (d) Adduction; (e) Extension curves with mean experimental data (grey) and fitted curve (black).....	134
Figure 4.20: Passive hip joint rotational stiffness ($k=abe^{b\theta}$), subplots are defined as (a) Flexion – straight leg; (b) Flexion – bent knee; (c) Abduction; (d) Adduction; (e) Extension (males).	135
Figure 4.21: Mean male (blue) and female (magenta) angle-moment curves for hip flexion straight leg (FSL) with one standard deviation for angle (horizontal) and moment (vertical).	139
Figure 4.22: Mean male (blue) and female (magenta) angle-moment curves for hip flexion – knee bent (FKB) with one standard deviation for angle (horizontal) and moment (vertical).	139
Figure 4.23: Mean male (blue) and female (magenta) angle-moment curves for hip extension (Ext) with one standard deviation for angle (horizontal) and moment (vertical).	140
Figure 4.24: Mean male (blue) and female (magenta) angle-moment curves for hip abduction (ABD) with one standard deviation for angle (horizontal) and moment (vertical).....	140

Figure 4.25: Mean male (blue) and female (magenta) angle-moment curves for hip adduction (ADD) with one standard deviation for angle (horizontal) and moment (vertical).	141
Figure 4.26: Female (magenta) and male (blue) moment-angle curves for (a) Flexion – straight leg; (b) Flexion – bent knee; (c) Abduction; (d) Adduction; (e) Extension curves with mean experimental data (light) and fitted curve (dark).	142
Figure 4.27: Comparison of female (magenta) and male (blue) passive hip joint rotational stiffness $k=abe^{b\theta}$. Subplots are defined as (a) Flexion – straight leg; (b) Flexion – bent knee; (c) Abduction; (d) Adduction; (e) Extension.	143
Figure 4.28: Experimental data (blue) and model predicted (red) passive hip angle-moment curves for extension to flexion straight leg (solid line) and knee bent (dash line).....	144
Figure 4.29: Experimental (blue) and model predicted (red) passive hip angle-moment curves for abduction and adduction.	145
Figure 4.30: Flexion - extension passive torque-angle curves with both FSL (solid line) and FKB (dash-line) respective contribution from Biceps Femoris, Semitendinosus, and Semimembranosus. The change in knee angle effects the muscle length enough to greatly reduce the predicted hamstring contribution to total hip moment.	149
Figure 5.1: The drop vertical jump (DVJ) task is portrayed from start (A) to completion (E). The participant makes a small jump off the box (A-B), lands with one foot on each of the force plates (C), and performs a maximum vertical jump (D), and lands a second time with one foot on each force plate (E).	157
Figure 5.2: Twenty-Four EMG channels will be collected including 6 bilateral core muscles (Rectus Abdominis (RA), External Oblique (EO), Internal Oblique (IO), Lower Erector Spinae (LES), Upper Erector Spinae (UES), and Latissimus Dorsi (LD)) and 6 bilateral hip/leg muscles (Rectus Femoris (RF), Tensor Fascia Latae (TFL), Gluteus Medius (GMed), Gluteus Maximus (GMax), Biceps Femoris (BF), and Adductor Longus (ADD)).	159
Figure 5.3: A subjected landing in DVJ (top). An accompanying schematic representation of the body fixed hip-ankle plane and the perpendicular medial knee displacement which quantifies the knee valgus measure (bottom).	162
Figure 5.4: Knee displacement during the first landing of the DVJ task. Median (solid) and dashed ($\pm 20\%$) reveal the barrier between high and low valgus, which creates the comparison groups.	164
Figure 5.5: Mean and std of spine flexion-extension angles during first land for “valgus group” (Unilateral and Bilateral Valgus) vs the No Valgus group. *SSD in peak angles between valgus group and no valgus group.	164
Figure 5.6: Time histories of the mean (black line) and standard deviation (shaded area) of hip (top), and knee (bottom) flexion-extension angles during first land for the high valgus group (HVG) and low valgus group (LVG), on left and right respectively. *SSD in peak angles between HVG and LVG.....	165
Figure 5.7: Time histories of the mean (black line) and standard deviation (shaded area) of hip (top), and knee (bottom) abduction-adduction angles during first land for the high valgus group (HVG) and low valgus group (LVG), on left and right respectively.	166
Figure 5.8: Time histories of the mean (black line) and standard deviation (shaded area) of hip (top), and knee (bottom) medial-lateral rotation angles during first land for the high valgus group (HVG) and low valgus group (LVG), on left and right respectively.	167

Figure 5.9: Time histories of the mean (black line) and standard deviation (shaded area) of spine (top), hip (middle) and knee (bottom) flexion-extension angles during first land for the bilateral valgus group (BVG, left), Unilateral Valgus Group (UVG, center), and No valgus group (NVG, right), on left and right respectively. *SSD in peak angles between NVG and the other two groups.....	168
Figure 5.10: Comparisons of spine forces (inverse dynamics) between the high and low valgus groups. *SSD between LVG and HVG, $p < 0.05$	169
Figure 5.11: Comparisons of hip forces (inverse dynamics) between the HVG and the LVG. *SSD between LVG and HVG, $p < 0.05$	170
Figure 5.12: Comparisons of knee forces (inverse dynamics) between the HVG and the LVG. *SSD between LVG and HVG, $p < 0.05$	170
Figure 5.13: Histogram of the peak (maximum) inverse dynamics forces for the spine, hip and knee. *SSD between LVG and HVG, $p < 0.05$	171
Figure 5.14: Histogram of the peak (minimum) inverse dynamics forces for the spine, hip and knee.....	171
Figure 5.15: Lumbar spine moments for the DVJ first landing, initial contact to take-off, for the HVG (left) and LVG (right), with flexion across the top, lateral bend in the center, and axial twist along the bottom.....	173
Figure 5.16: Hip moments for the DVJ first landing, initial contact to take-off, for the HVG (left) and LVG (right), with flexion across the top, abduction-adduction in the center, and medial-lateral torque along the bottom.	173
Figure 5.17: Knee moments for the DVJ first landing, initial contact to take-off, for the HVG (left) and LVG (right), with flexion across the top, abduction-adduction in the center, and medial-lateral torque along the bottom.	174
Figure 5.18: Peaks (max) moments for high and low valgus group means with standard error bars. * Indicates statically significantly different comparisons ($P \leq 0.01$). (L_Flex = Lumbar Spine Flexion/Extension Moment; H=Hip; K=Knee)	174
Figure 5.19: Figure xx: Peaks (min) moments for high and low valgus group means with standard error bars. * Indicates statically significantly different comparisons ($P \leq 0.01$). (L_Flex = Lumbar Spine Flexion/Extension Moment; H=Hip; K=Knee).....	175
Figure 5.20: Mean lumbar spine compression force and StE (shaded area) for the DVJ trails comparing the high valgus bilateral, unilateral and no valgus groups. ** Indicates significantly different from both comparisons for peak minimum compression.....	176
Figure 5.21: Mean lumbar spine flexion-extension moments and StE (shaded area) for bilateral valgus (left), unilateral valgus (middle) and no valgus (right) for the DVJ trails comparing the high valgus bilateral and unilateral with low (“No”) valgus groups. *Indicates significantly different from “No Valgus” comparison.	176
Figure 5.22: Mean hip spine forces (Compression (top), AP Shear (middle) and ML shear (bottom)) and StE (shaded area) for the DVJ trails comparing the high valgus bilateral and unilateral with low (“No”) valgus groups. Note: Left hip forces were normalised to the right side (ML shear Left *-1). * Significantly different ($p < 0.05$), ** significantly different ($p < 0.01$); *above the curve indicates peak max score difference, * below the line indicates peak min score difference.....	178
Figure 5.23: Mean hip moments (Flexion-Extension (top), Abduction-Adduction (middle) and Internal-External (bottom)) and StE (shaded area) for the DVJ trails comparing the high valgus bilateral and unilateral with low (“No”) valgus groups. Note: Left hip forces were normalised to the right side (ML shear Left *-1). * Significantly	

different ($p < 0.05$), ** significantly different ($p < 0.01$); *above the curve indicates peak max score difference, * below the line indicates peak min score difference..... 179

Figure 6.1: Bosu™ ball with a semi-domed rubber and firm plastic platform..... 199

Figure 6.2: Pilates adductor ring with padded handles and ring structure. 201

Figure 6.3: Green Mini-Band from Perform Better™ 202

Figure 6.4: Twenty-Four EMG channels will be collected including 6 bilateral core muscles (Rectus Abdominis (RA), External Oblique (EO), Internal Oblique (IO), Lower Erector Spinae (LES), Upper Erector Spinae (UES), and Latissimus Dorsi (LD)) and 6 bilateral hip/leg muscles (Rectus Femoris (RF), Tensor Fascia Latae (TFL), Gluteus Medius (GMed), Gluteus Maximus (GMax), Biceps Femoris (BF), and Adductor Longus (ADD). 204

Figure 6.5: Mean and standard deviation (SD) bars for the median peak EMG values for each squat sub-type by neural driver..... 208

List of Tables:

Table 3.1: Bony Landmarks (cm)	62
Table 3.2: Spine Muscle Attachments.....	67
Table 3.3a: Hip Muscles Attachments.....	68
Table 3.3b: Hip Muscles Origination on the Pelvis (Con't).....	69
Table 3.3c: Hip Muscles Origination on the Pelvis (Con't)	70
Table 3.4: Muscle crossing the hip and spine.	70
Table 3.5: Muscle Via Points	73
Table 3.6: Modified muscle parameters from the TLEM data set based on physiological muscle length operating range over a physiological range of motion.....	83
Table 3.7: HSM ligament attachments.....	86
Table 3.8: Input parameters for ligament force calculations.....	94
Table 3.9: Point of application (degree of flexion) when ligaments start to strain	94
Table 3.10: Muscle gains for study 3: ACL injury risk.....	105
Table 3.11: Muscle gains for study 4: HRA.....	106
Table 4.1: Equations of curve fit and goodness of fit measures for mean angle-moment data (males).....	129
Table 4.2: Coefficients and goodness of fit measures for mean moment-ROM data (males).....	133
Table 4.3: Coefficients and goodness of fit measures for moment-ROM curves of each trial (females).....	133
Table 4.4: Comparison of neutral zone angle widths for passive resistance of the hip between sexes.....	137
Table 4.5: Comparison of peak hip angle for passive resistance between sexes.	137
Table 4.6: Comparison of hip angle neutral zone barrier for passive resistance between sexes.....	138
Table 4.7: Comparison of peak hip moment for passive resistance between sexes.	138
Table 4.8: Equations of curve fit and goodness of fit measures for mean angle-moment data (females).	141
Table 5.1: Specific Research Questions and Hypothesis for the primary outcome measures.....	155
Table 5.2: Mean (SD) of peak spine loads during DVJ first landing for bilateral, unilateral and no valgus.	180
Table 5.3: Mean (SD) of peak hip loads during DVJ first landing for bilateral, unilateral and no valgus.	181
Table 5.4: Peak EMG collapsed across right and left sides.	182
Table 5.5: iEMG (%Movement * %EMG) collapsed across right and left sides.....	183
Table 5.6: Multiple Regression Models for Right Knee Valgus using a stepwise approach.	184
Table 5.7: ANOVA results of the Right Knee Valgus stepwise multiple regression models.	185
Table 5.8: Multiple Regression model analysis of the Right DKV.....	186
Table 5.9: Multiple Regression Models for Left Knee Valgus using a stepwise approach.....	186
Table 5.10: ANOVA results of the Left Knee Valgus stepwise multiple regression models.	187
Table 5.11: Multiple Regression model analysis of the left DKV.	188
Table 5.12: Right Knee Stepwise Regression Analysis Model Summary.....	189

Table 5.13: iEMG (%Movement * %EMG) on the right side for Hi vs Low Valgus on the right knee.	190
Table 5.14: iEMG (%Movement * %EMG) on the left side for Hi vs Low Valgus on the left knee.	190
Table 6.1: Squat variations with illustrations and descriptions.	200
Table 6.2: Descriptive data for mean spine angle (degree) across five squat sub-types.....	205
Table 6.3: Peak spine flexion angle during five squat types and statistical analysis.....	205
Table 6.4: Spine compression peaks (minimum) estimated from HSM for five squat types.....	209
Table 6.5: Spine AP shear peaks estimated from HSM for five squat types.	210
Table 6.6: Spine Flexion Moment peaks estimated from HSM for five squat types.....	211
Table 6.7: Spine Lateral Bend Moment peaks estimated from HSM for five squat types.....	211
Table 6.8: Right Hip compression peaks estimated from HSM for five squat types.....	213
Table 6.9: Right Hip AP Shear peaks estimated from HSM for five squat types.	213
Table 6.10: Right Hip ML shear peaks estimated from HSM for five squat types.	214
Table 6.11: Right hip peak extension moment estimated from HSM for five squat types.....	214
Table 6.12: Right hip Abduction rotation moment peaks estimated from HSM for five squat types.	215
Table 6.13: Right hip adduction moment peaks estimated from HSM for five squat types.	215
Table 6.14: Right hip medial rotation moment peaks estimated from HSM for five squat types.....	216
Table 6.15: Right hip lateral rotation moment peaks estimated from HSM for five squat types.....	216

1.0 Introduction:

A mega trend in medicine is “precision medicine” or what is sometimes referred to as “personalised medicine”. This is a move away from the “one size fits all” approach to care towards matching an intervention to a specific mechanism. This thesis seeks to contribute to this developing trend through a more complete assessment of the biomechanical variables and mechanisms leading to hip-spine disorders. Every system in biology has a tipping point where loading below the tipping point adds resiliency and loading exceeding the point causes damage, or pain, or dysfunction, or all three. Analysis of hip/spine disorders have centered around kinematic variables or muscle activation usually in isolation. To further the advances of the aforementioned mega trend of precision medicine this thesis was directed towards developing tools to assess complex kinetics, neuromuscular control and kinematics in a more holistic examination of hip/spine disorders and then assess the influence of these variables on stress and strategies to enhance resilience and performance.

The spine and hip joints form very complex neural, muscular and skeletal systems. While they thrive under optimal loading conditions, they become painful and disabled when mechanical loading is either too much or too little. The hip and spinal joints form linkages in the kinetic chain that exhibits regional interactions and interdependence of function. Their interaction across the continuum of injury mechanics, rehabilitation, and performance, are of interest. If spine load can

their synergistic relationships that optimize function along the kinetic chain will prove beneficial. This information can be used to modify risk for athletes and inform clinicians in the management of musculoskeletal disorders (MSD). For example, finding ways to reduce spine load in a patient with load back pain (LBP) may enable function while mitigating pain triggers (Ikeda & McGill 2012). Similarly, altering movement or motor strategy along the kinetic chain in an at risk athlete may enhance performance while reducing injury risk, in this case injury to the knee (Hewett & Myer 2011). These are just two examples of potential benefits gained from understanding the complex interdependence of the hip and spine along the kinetic chain.

A review of the clinical research examining the interplay between hip and spine function is presented in detail in the literature review section of this thesis. While the interactions of the hip and spinal regions have been of interest clinically for some time (Offierski & MacNab 1983), there is a paucity of research examining the mechanical and functional relationships between them. Furthermore, the review in this thesis shows the spine has generally been modeled and analysed in isolation and likewise analysis of the lower limb has rarely if ever incorporated structures above the pelvis. It makes sense to study the hip and spine function together. But the impediments lie in the complexity of properly accounting for all of the structures, in sufficient detail, with respect to anatomy and mechanics.

Biomechanical modelling is performed to gain understanding of joint and tissue loading and mechanisms of musculoskeletal (MSK) function and dysfunction in both healthy and pathological populations (Buchanan et al. 2004). Direct measurement of joint and tissue load is often not possible in vivo. Specifically, this thesis will consider the interactions between hip and spine

function with the development of an anatomically detailed, biologically driven, hip-spine model (HSM). To improve model biofidelity an examination of passive hip stiffness will be conducted and together with differences in males and female passive hip stiffness, range of motion (ROM) and neutral zone (NZ) size, to name a few. The ability of the HSM to predict the behaviours of the male passive hip stiffness was assessed with comparison to experimental data. Next, examining the mechanisms underlying ACL injury risk in females will be investigated including both hip and spine kinetics using this novel approach. Finally, the quantification of hip-centric rehabilitation exercises will assist in informing clinicians regarding exercise choice, dosage, progression and regression for specific disorders. The grand intention of this thesis is to better understand the interplay between the mechanics of these two regionally interdependent joint complexes, and ultimately provide leadership with clinical aspects of assessment, treatment and management, and performance enhancement.

1.1 The Problem

There are two main inadequacies in the current body of knowledge that this thesis attempts to address, one concerning the limited investigation of the regional interdependency of hip and spine function outlined in the clinical literature; and, the second being the MSD which propagate along the kinetic/kinematic chain, in this case involving the knee, hip and spine. The first problem is due to the lack of an experimental approach with sufficient detail. This thesis addressed this first problem with the development of a novel HSM which provides new insights in the function of each joint as well as the interplay between these joints. The second major problem is the inadequate understanding of the kinetics and kinematics concurrently linked with non-contact ACL injuries. Thus, the injury mechanisms remain associations rather than specific cause-and-

effect. Addressing the neuromuscular control and modelling tissue and joint stresses is a powerful approach that will deepen the understanding of cause-and-effect.

1.2 Background & Justification of the Problem

While it may seem odd to include a discussion of LBP and ACL injury mechanisms into the same thesis justification, I will argue that it is more than appropriate. The unifying theme of this thesis is that it is the mechanics which underpin injury mechanisms, management of pain and disorders, and enhancement of performance. One biomechanical principle applied to the articulating linkage is: *'proximal stiffness is required for distal mobility and athleticism'* – the most proximal segment linkage is the torso – sometime referred to as the core. Enhancing core stiffness allows for both the initiation and the resistance of motion in the lower limb (McGill and Karpowicz 2009), it has been shown to enhance athletic performance, for example, improved striking performance (Lee and McGill 2016; McGill et al. 2010), enhanced the management of spine disorders (Cholewicki and McGill 1996) and the elimination of pain triggers in back pain individuals (McGill 2004; Ikeda & McGill 2012). To this effect muscles of the torso are activated to stop motion and enhance control of the thigh across the hip (Brown & McGill 2005; McGill & Cholewicki 2001) which in turn influences load and mechanics at the knee. Further control of the hip (Hewett et al. 2010; Hewett & Myer 2011; Hewett et al. 2005) as well as neuromuscular patterning (Myer, Brent, et al. 2011; Myer et al. 2007a) is linked to dynamic valgus which in turn are associated with ACL injuries. Clearly, more understanding of the regional interdependence justifies this thesis.

1.2.1 Low Back Disorders

Clinically, there has been an interest in hip-spine interplay as hip dysfunction has been linked with disorders of the spine (Offierski & MacNab 1983). Back pain presents a vast economic burden on society in both direct and indirect costs (Dagenais et al. 2008). The numbers are staggering. In the United States alone, cost estimates range from \$84.1 to 624.8 billion, annually. In nationwide surveys, Deyo et al. (2006) reported LBP as the most common source of pain, with 26.4 percent of the respondents reporting pain within the last three months, followed by headaches and neck pain, rounding out the top three categories. In addition to the financial burden, the health care system is also encumbered by LBP. This is evident in primary care physician offices where LBP is among the most common reasons for visits to primary care physicians (Deyo et al. 2006). When examining the severity of spine pain cases the majority (low back and neck) are acute/sub-acute and graded either one or two, on a four point severity scale (Manchikanti et al. 2009; Cote, Cassidy, and Carroll 1998). This lower severity level of pain is associated with disorders that are likely to be amendable to approaches utilising conservative management strategies. This provides a great opportunity for conservative interventions to impact the LBP burden on society. Obviously, working to obtain a better understanding of the conditions and mechanisms which lead to mild and moderate levels of pain is a logical next step.

1.2.2 Lower Limb Disorders

Lower limb injuries are a significant problem in sport accounting for over 50% of injuries in collegiate athletics and ACL injuries are on the rise (Hootman et al. 2007). The majority of ACL injuries are non-contact injury mechanisms (Gianotti et al. 2009). Even more staggering is that an ACL injury history leads to a sevenfold increase in the odds of having a total knee replacement as

a result of osteoarthritis later in life (Khan et al. 2018). These injuries are important not only for their immediate effects but also the long-term effects. As many as 51% of female athletes who sustain an ACL injury will show radiographic evidence of knee arthritis, and 75% report symptoms affecting their quality of life just 12 years post-injury (Lohmander et al. 2004). The implications of sport related lower limb injuries have serious implications on future health, making prevention and rehabilitation strategies, a worth while pursuit for further investigation.

Identifying injury risk is important. Targeting an at-risk group could lead to large reductions in injury and subsequent functional limitations, pain, disability and decreased quality of life after the injury. Dynamic knee valgus (DKV) has been and is evolving as predictor for several knee disorders (Powers 2010). Hewett and Myers (Hewett et al. 2005; Ford et al. 2000; Timothy E Hewett et al. 2004; Hewett, Ford, et al. 2006; Hewett, Myer, et al. 2006a) have linked DKV to ACL injury risk, while Powers and colleagues have linked DKV to a myriad of knee injuries (Sigward et al. 2011) but most commonly patellofemoral pain syndrome (PFPS) (Powers 2003; Powers 2010). While identifying the phenomena of DKV and its link to injury is a terrific accomplishment little has been done to understand the mechanism which drive this movement pattern until recently (Cannon, Cambridge, McGill; in press). This further suggests investigation on the kinetic and kinematic chain will lead to improvement in prevention and rehabilitation strategies downstream.

A final justification for inquiry into kinetic/kinematic chain dysfunction are several sub-groups of patients with low back, hip and knee disorders who have common links. For example, hip dysfunction and asymmetry have been suggested to lead to earlier back pain (relevant references

provided in detail in the literature review). All of this evidence suggests the efforts to develop a novel biomechanical model to evaluate hip-spine function and utilize this HSM to evaluate mechanics and mechanisms of joint function in a more comprehensive way will bear fruit.

1.3 Potential Thesis Impact & Theory Development

As shown in the MSK literature (Lu & Chang 2012); inappropriate loads, postures, and movements can cause joint injury and tissue damage leading to pain. The contrary is also true: appropriate loads, postures and movements can be both therapeutic and prophylactic. A conceptual model for this framework is proposed in Figure 1.1. To formalize these thoughts, the dynamic relationships between joint and tissue loading through applied loads, postures and movements govern both injury causation and injury prevention. The notion that tissue load may fall within the tissue's capacity or exceed tissue capacity is the key to understanding both mechanism of injury and designing effective intervention strategies. The potential intervention sites of hip-spine function with potential to influence the injury cascade are demonstrated in the conceptual model entitled "Hip-Spine Integration Model (HSIM)". This conceptual model lays out the foundation and theory development of the current thesis as well as a general guiding principle as to how understanding mechanics and mechanism lead to the development of improved clinical scenarios.

The HSIM is a culmination of years of research and work from many scientists, distilled here to provide a conceptual framework to guide scientific inquiry. Kumar (2001) and McGill (1997, 2007) are two in particular who have made a significant contribution to MSK injury theory literature. This HSIM is a conceptualization that provides a framework to wage future

Conceptual Model of Tissue Loading – Hip & Spine Integration

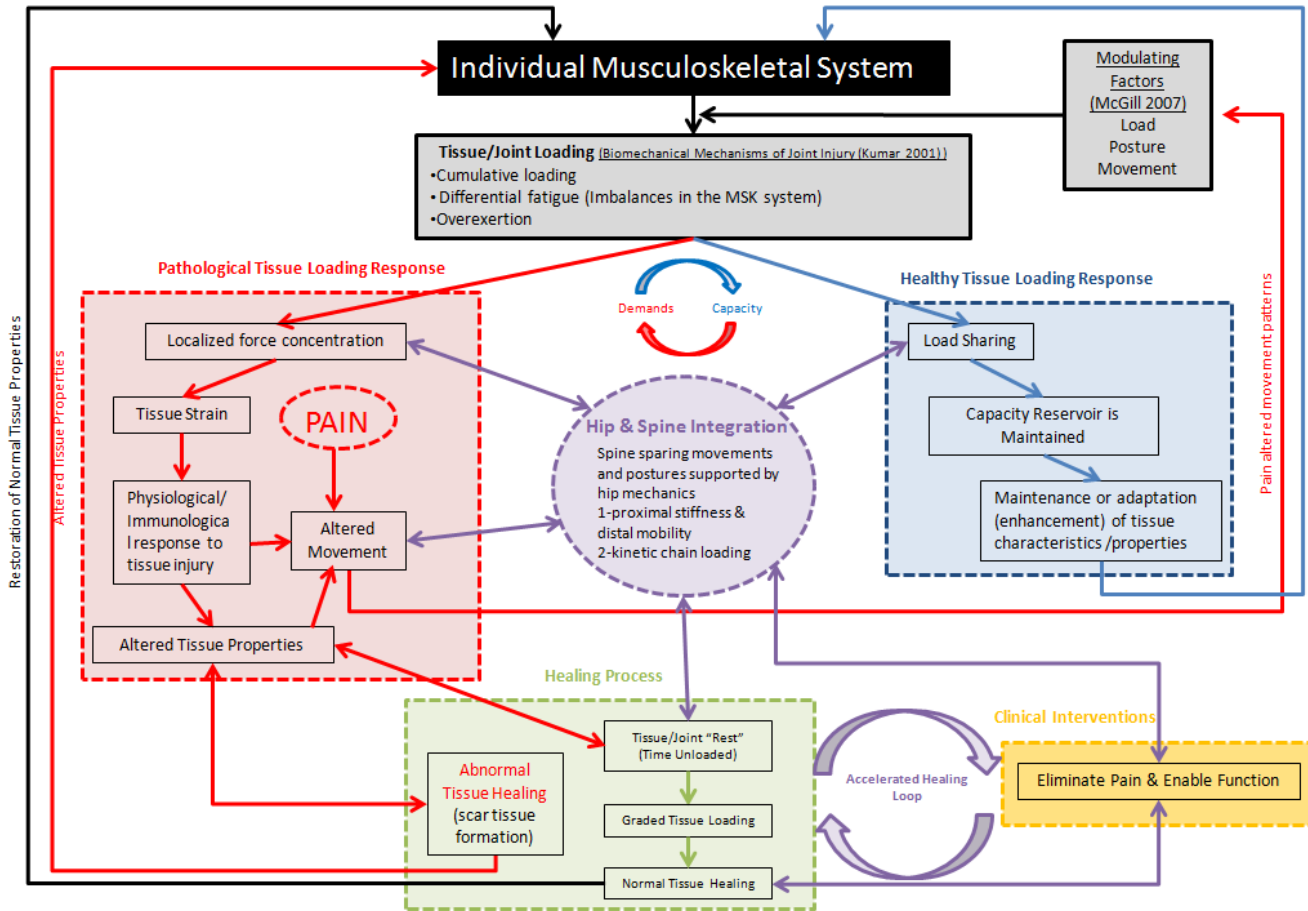


Figure 1.1: A conceptual model of healthy and pathological tissue loading, and interaction links between the hip and spine function. The individual's MSK system forms the basis of the tissue model, which is modulated by unique movement patterns and postures, which in turn influence joint loading (McGill, 2007). Tissue demands are matched by their capacity to bear load; two possible outcomes result, the demands are within the system's capacity or they exceed it. Demands have been discussed elsewhere by Kumar (2001) in relation to repetitive loading and acute over exertion along with imbalances in the muscular system or differential fatigue. If tissue capacity exceeds the demands place on the tissue, then the "healthy tissue loading" cascade will ensue (blue). If the demands exceed tissue capacity, then the "pathological tissue loading" cascade ensues (red). Several theoretical interaction points exist to promote healthy tissue loading and healing as well as encourage tissue overload and failure. In other words, hip and spine mechanics may serve to promote load sharing or encourage tissue overload and injury depending on the individual movement and motor patterns, as well as postures, and loading conditions experienced. Similarly, during the tissue healing process a similar interaction between the hip and spine joint mechanics may promote or retard the healing process based on the same principle of tissue demands and capacity.

investigations of the various interactions and model nodes. In summary, filling in understanding of the various intersections in the framework will improve patient care through better prevention; earlier assessment/diagnosis of MSK disorders and more effective and efficient treatment protocols, all of which are the ultimate objective of this work.

1.4 Objectives

The objectives of this thesis are: 1, to improve upon the fundamental understanding of the biomechanical relationship between hip and spine function developing and using a biologically driven model to address research questions; and 2, to improve the mechanical and mechanistic understanding of the interplay between the spine, hip and knee. This process will require several stages to achieve these two main objectives.

The first major objective was the development of a "Hip-Spine Model" (HSM). To achieve this objective, the existing anatomically detailed, biologically driven spine model was expanded to include a more detailed pelvis and hip. This new HSM allowed for the investigation of the mechanical relationship between hip and spine function. New questions and hypotheses in the relationships involving the hips and spine were investigated with the use of the HSM. In addition, because of the utilization of the muscle activation and kinematics was obtained from each individual, the HSM provided unique insights into the mechanical load sharing capacity arising from the individual neurological control strategies. The capability of this type of unique and robust analysis of loads, postures and movement does not currently exist in a single data base or model that considers the hip and spine together. This in turn has the potential to enhance the

design and application of preventative, therapeutic, and rehabilitative interventions for superior management of spine and hip disorders and even enhance performance.

Following the development of the HSM model and the analysis of passive hip stiffness, two additional biomechanical themes were proposed to investigate hip and spine interplay. The first theme examined the influence of the hip and spine interplay on ACL injury risk. Through the monitoring of motor patterns, movements, postures, and loads, the associations between the hip and spine interplay was investigated for their role in contributing to ACL injury risk behaviour, namely DKV. Deeper insights into the already established body of knowledge related to ACL injury risk and knee disorders related to DKV was obtained. The second theme was to create an atlas of hip centric spine sparing rehabilitation exercises designed to promote appropriate motor patterns, motions, postures and loads in the hip and spine to guide clinical decision making. In this manner, the prospective and retrospective analyses using the detailed biological HSM, allowed for unparalleled understanding of fundamental mechanics, activity demands, and therapeutic exercise dosages.

1.5 Thesis outline and guide to this document

The thesis is subdivided around thematic topics for the presentation of the data. Two major data collections served to provide the experimental data for this thesis along with the extraction of data from the literature to develop the HSM and refine it from the current data sets available.

Chapter two outlined the relevant literature that served to inform this thesis and direct the investigations to provide greater insights into the issue of hip and spine function and the associated disorders of the spine, hip and knee. The literature review first examined issues in

musculoskeletal modelling pertinent to the proposed modelling approach. The literature review then examined the clinical theoretical framework for the studies investigating the various hip-spine disorders. The review concluded with a statement of what is known and what is yet to be discovered. This shall serve as the rationale, in part, for the work of this thesis.

Chapter three addressed the development of an anatomically detailed, biologically driven, HSM for the estimation of joint and tissue loading. A description of the model as well as relevant equations and utilizations of model parameters are found here. Data related to the model tuning and estimation of gain factors is also documented here, as well as the modifications and updates to maintain the biofidelity of the anatomical function of various muscles. Ligaments and passive tissue properties were also enhanced at the hip with the use of previous literature and experimental data capture in the next chapter.

Chapter four documented the passive hip stiffness properties of males and females in vivo. Experimental data was evaluated to enhance the understanding of hip mechanics from a foundational knowledge perspective as well as a direct input to the HSM. It was hypothesised that males and females would have different passive hip properties and the model would predict male passive hip properties sufficiently well.

Chapter five documented the investigation of ACL non-contact injury mechanisms in females and the underlying mechanisms which differentiate high and low valgus groups, a known injury risk predictor. It was hypothesized that the neuromuscular patterns as well as kinetic analysis will lead to a better understanding of underlying mechanism for dynamic valgus.

Chapter six documented the development of an atlas of hip rehabilitation exercise progressions that spare the spine, while challenging the hip for conservative management of many hip and spine disorders as well as potentially impactful knee injury mechanisms. It was hypothesised that differences in kinematics, neuromuscular patterns and kinetics will be revealed and knowledge of these differences can be utilised by clinicians to prescribe exercise selection, volume and programming more specifically to the individual.

Finally, chapter seven, provided a global discussion of the thesis and the impact of the results on the objectives set out in the thesis. This provides the capstone impressions and considerations of this data as well as directions for future work.

This thesis developed organically, while the first objective the thesis was model development, experimental data was required to inform and utilize the model. Two major data collections were used to create this data set. The first, was a group of females primarily collected for the “ACL study” in Chapter 5 (study 3). The second, was a group of males primarily collected for the “Hip Rehab study” in Chapter 6 (study 4). Each of these data sets also contributed to the “passive hip stiffness study” in Chapter 4 (study 2). This brings us full circle back to model development in chapter 3 (study 1) where the model gain factors, and tuning was documented. The general flow of the data sets and studies is provided in Figure 1.2.

Hip-Spine Thesis

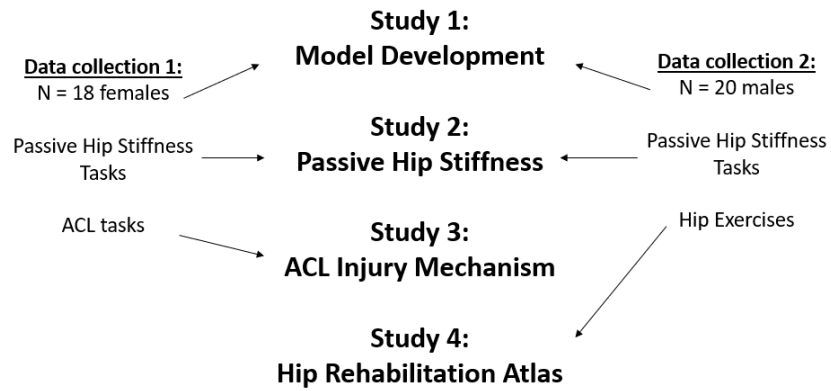


Figure 1.2: The flow of data through two major data collections and four thesis studies.

2.0 Literature Review:

The purpose of this literature review is to establish what is known and identify what remains unknown, forming the rationale for this thesis. Given the need to create an anatomically detailed, biologically driven, hip model which was married to the existing spine model (McGill & Norman 1986), the first section of the literature review, entitled '*Modelling Review*', addresses pertinent information related to model development. This information was used in development of the hip model including anatomical and tissue properties along with a review of fundamental concepts in modeling. In addition, the review includes a selection of current hip and spine models available in the literature and discusses the current status of these models. The second major section of the literature review entitled '*Clinical issues of the knee, the hip, & the spine*' is focused on the clinical and practical applications of the model as well as the current status of the clinical evidence surrounding knee, hip and spine disorders as they relate to the dynamic interplay of the interactions between these joints. This section of the review includes various forms of a condition referred to as 'Hip-Spine Syndrome' as well as the relationships between hip and spine mechanics and low back pain. In addition, Anterior Cruciate Ligament (ACL) injuries are discussed along with dynamic knee valgus (DKV) and the current evidence relating these issues. How these clinical theories are related to loads, postures and movements was reviewed together with the available evidence to support the underlying mechanism of injury propagation along the kinetic/kinematic chain. In this way, this review has served as the foundation knowledge to provide an understanding of hip and spine mechanics and they relate to injury prediction, prevention, rehabilitation, pain and dysfunction. From this understanding a path for future discovery and development of new ideas is presented.

2.1 Modelling Review:

The focus of musculoskeletal modelling included in this review will be inverse dynamics and EMG driven modelling approaches, as they relate to the spine and hip joints. This will also include anatomical considerations, muscle modelling, passive tissue properties and model tuning or the indeterminacy problem. A fundamental issue in biomechanics is the understanding of tissue loading characteristics. Direct measurement of tissue loading, including joint load, is very difficult and usually highly invasive (Erdemir et al. 2007). For this reason, modelling is an essential and critical process in biomechanics. Modelling has been used to estimate joint loads from surrogate biological signals. This is possible through the understanding of the relationship to intermediate variables. For example, surface electromyography (EMG) is readily measured in the laboratory and relationships to muscle force are well established from previous research (Hof 1984). Combining EMG, anatomical data (muscle attachment sites), and kinematics provides the modelling inputs and model guts required to estimate joint loads. For instance, in a biologically driven model such as the one proposed here, the EMG is used to estimate muscle force, couple with attachment sites located in the model are tracked via the individual's kinematics measured in the laboratory. These variables are then used to estimate muscle parameters (line of action, moment arm lengths, muscle lengths, muscle velocities and force) and this process is repeated for each muscle of interest and summed to estimate joint force. The advancement of modelling techniques and new applications of models is essential to the advancement of biomechanics and the understanding of tissue and joint loading. This knowledge then serves as a foundation for applied and clinical applications as well as future research.

2.1.1 Relevant Anatomy for Modelling

One issue with modelling is the generalizability of anatomical data and matching the research pool to the data set from which the model parameters were derived. Two approaches have been used to attempt to resolve this issue. Brand and colleagues (1982) examined attachment sites for the hip, knee, and ankle used as model parameters in a gait analysis. They attempted to provide scaling factors to individualize these model parameters for the participant pool for which the model was applied. While these authors were proponents of using scaling factors, moment arm estimates were associated with errors in the accuracy identifying locations of origins and insertions. Based on sensitivity analysis the error represented inaccurately identifying specific muscle attachment locations would likely be less than a 10 percent. In contrast, a recently detailed data set of lower limb anatomy was published “The Twente Lower Extremity Model” (TLEM) (Horsman et al. 2007) using a single cadaveric specimen. These authors suggested that the relative relationship of the anatomy was more important than removing the biological variance. Therefore, they suggested that this data set with a robust set of biological parameters (muscle rest length, muscle PCSA, muscle and ligament attachment points, muscle 'via' points, segment inertial parameters) for modelling inputs would be superior to piecing together norms and averages from multiple data sets and specimens. How well the participant pool matches the model parameters continues to present challenges for gender matching. There are statistically significant differences in pelvic morphology (Bonneau et al. 2012). However, it remains unknown whether or not these differences are practically significant when it comes to modelling and the application of the model to participant pools. The Twente Lower Extremity Model (TLEM) (Horsman et al. 2007) was chosen to be used to here to construct the HSM in chapter three. The

model parameters are listed in Appendix A (Table A-1). These model parameters will be integrated with the existing spine model and are discussed in detail in chapter three. Finally, realizing that these anatomical studies are done on cadaveric specimens or static CT or MR imaging it is noteworthy that dynamic movements of the limb do not greatly change the inertial properties of the limbs. Clark & Hawkins (2010) found a less than 0.01% effect when correcting for tissue movement within the limb during dynamic tasks. There are always limitations and assumptions when it comes to model inputs and anatomical data is no exception.

2.1.1 .1 Anatomical Relationships to joint coordinate systems (JCS)

Identifying anatomical landmarks and their relationship to joint centers of rotation has been a challenge. Bell et al.(1990) compared methods of estimating hip joint center from palpable anatomical landmarks. Errors in hip joint center estimation ranged from 3.79 cm using 'the rotational method' (based on radiographs) to 3.61 cm using 'Andriacchi's method' (again based on radiographic data). None of the methods at this time reached a predetermined standard of accuracy of 2.0 cm and were deemed inaccurate. Moreover, the implications for joint axes of rotation and calculations of joint Euler angles, thereafter, rely on the accuracy of marker placement to be able to define joint rotation accurately.

An updated approach to identifying joint centers and joint axes of rotation is using '[functional] joint centers (FJC)' (Schwartz & Rozumalski 2005). Begon et al. (2007) examined the effects of movement in calibration trials to inform users of FJC how best to calibrate and calculate hip joint center location. For example, using at least 10 cycles of movement was critical for accuracy, and circumduction was better than flexion/extension or abduction/adduction motion

in isolation. Interestingly smaller amplitude motions were also more accurate than large movements. In fact, when considering clinical populations with reduced hip ROM this newer FJC approach remains the preferred method (Piazza et al. 2001). Overall, this approach is more objective and precise when compared to the standard clinical approach. It was also considered more accurate in calculating knee joint motion for example by limiting signal bleeding between axes of rotation and thereby producing more accurate valgus measures in the knee (Schwartz & Rozumalski 2005).

2.1.2 Muscle Modeling

Muscle modeling is a major area of investigation in biomechanics research, it is worthy of a textbook to review the entirety of the issues related to the understanding and complications. This review will highlight a few of the areas pertinent to this thesis and assist in the justification and rationale of the modeling approached proposed for the use in these investigations.

2.1.2.1 Force-Length Relationship

The force-length (F-L) relationship was formalized by Gordon et al. (1966) through a series of experiments examining tension and sarcomere length. It was discovered that muscles, or more accurately sarcomeres, have an optimal length and shortened or lengthened beyond this optimal length there is a reduced capability for force production. The cause of this relationship relates to the cross-bridging capabilities with respect to the sliding filament theory. At optimal lengths the congruency of the cross-bridging of actin and myosin fibers as well as force production are maximized. When the fiber is shortened or lengthened the cross-bridge integration is reduced and force production capability is diminished. More recently, this has been

documented in the abdominal musculature to better understand the physiological range of the sliding filament theory as it relates to these torso muscles (Brown & Gerling 2012). Muscle length is a critical intermediate in the prediction of muscle force and ultimately joint load.

2.1.2.2 Force-Velocity Relationship

Demonstrated as early as the 1930s, by A.V. Hill, there is an inverse non-linear relationship between shortening velocity of the sarcomere and force production capacity (Hill 1938). While simplifying complexity is often done to improve comprehension of a relationship, a single linear relationship is not appropriate for the force-velocity (F-V) relationship for isometric contractions (Chapman & Harrower 1977). Contraction velocity ought to be accounted for in any EMG driven modelling approach.

2.1.2.3 Force-Length-Velocity Relationship

It would appear that the interaction effect of the length and velocity parameters should also be considered as these are inseparable in vivo. Bahler (1968) was one of the first to examine the combined effects of length and velocity on muscle force capabilities. Several equations were developed to explain the mechanics of parallel and serial elastic properties combined with the contractile properties of muscle. The stimulation parameters were also considered not only in terms of stimulation frequencies and intervals but also force development, since muscle is not a first order mechanical system. In short, rest length and lower velocity conditions provide maximal muscle force capabilities while deviations from rest length and higher velocities decrease the available force capacity of the muscle. To summarise the individual constraints of length and velocity were maintained in this examination.

2.1.2.4 EMG to Force

Direct measurements of muscle force are difficult and invasive in human subjects. Therefore, understanding the relationship between muscle force and neural drive is important for biomechanical modeling. Since neural drive is readily measured in the laboratory, it makes this an ideal surrogate for muscle force. The development of this relationship has been ongoing for many decades and continues to be refined even today. In a four part series Hof and Van den Berg (1981a, 1981b, 1981c, 1981d) examined the Hill-Type Model, which remains today as "The Standard" for modelling the relationship between neural drive and muscle force, both conceptually and mathematically. In part one of the examination, the Hill-Type Model's linearity was investigated (Hof & Van den Berg 1981a). Muscle torque was directly measured and force and lengths were extrapolated and corrections for length and velocity are discussed. The importance of these scaling factors remain as key elements of the EMG to force relationship. Part two examined the passive elastic component of the system and torque-angle relationships (Hof & Van den Berg 1981b). NoTable hysteresis was observed requiring different equations for increasing and decreasing force. Unfortunately, individual differences observed in hysteresis were larger than the effects themselves. Therefore, correction factors were never adopted into the Hill-Type Model. Yet, the EMG processor presented here remains quite accurate. Similarly, each muscle had its own torque-angle relationship. In other words, at a given joint angle each muscle that crosses that joint will be at a unique location on the force-length curve. Results suggest factors from muscle architecture to single or multiple crossing articulations account for these unique relationships. It is important to remember, given this information, joint torque is the sum of all muscles components and each component requires consideration for its unique

scaling factors. However, there were commonalities found in calf muscles given the conditions of the task, similarities in activation profiles were observed. Therefore, it is reasonable to extrapolate certain variables like torque-velocity to both calf muscles as being equivalent. This is important when there is limited access to some muscles, as is found in the spine and hip. In these situations, with deep musculature and no accessible surface electrode recording sites, neurological surrogates must be identified. The third paper continues to examine the torque-angle relationship in even more detail (Hof & Van den Berg 1981c). Here the model is tested and is found to be able to closely represent measured torque from predicted torque. Also, mean rectified EMG is linearly proportional to the muscle torque in quasi-static conditions (Hof & van den Berg 1977). However, there seems to be more of a quadratic relationship during dynamic contractions. On the contrary, when corrected with SEC (tendon compliance) the relationship restores its linearity as seen in part three of the examination (Hof & Van den Berg 1981c). Lastly, part four of the examination of muscle modeling investigates contraction dynamics in both concentric and eccentric scenarios (Hof & Van den Berg 1981d). This EMG processor was able to handle both concentric and eccentric processing with good congruency. However, in this work the authors commented on the importance of a non-linear conversion for fast dynamic movements. This non-linear approach was able to characterize the fast rise and slower decline of the active muscle state in a more accurate way. While others (Guimaraes et al. 1994) have noted that the linearity of the EMG to force relationship, between 5 and 88% of the activation spectrum is a reasonable estimation for most applications. This debate remains at some level even today. In summary, this series of papers (parts one to four) demonstrated the ability to

digitally program the Hill-Type Muscle Model with good success for predicting force profiles under different conditions.

2.1.3 Neurologically Driving Muscle Mechanics with EMG

Consideration of neuromuscular compartments, including physical anatomical separations and unique neurological activation patterns, are important for EMG driven modelling approaches. Mechanical separations have been described to influence muscle lines of action and moment arm lengths (Pereira et al. 2004; Johnson et al. 1996; Van der Helm & Veenbaas 1991) and the representative PCSA of these muscles sections are also of important consideration. The neurological aspect to these compartments is far more theoretical and has been referred to as "the partitioning hypothesis" (English et al. 1993). There is some empirical support for this concept with much of this work investigating shoulder muscles and function including the pectoralis, deltoid and latissimus dorsi (Brown, Wickham, McAndrew, & Huang, 2007; Wickham & Brown, 1998; Wickham & Brown, 2011) and others have examined gluteus maximus (McAndrew et al. 2006). Identifying neurological patterning within and between muscles is important for identifying the number of unique muscle drivers. In other words, do groups of muscle share common activation patterns? If yes, then these muscles can be well represented by a single neural driver (i.e. one EMG channel). If not, then some muscle may have multiple activation patterns requiring more than one neural driver. The examination of neuromuscular compartments is of course not without controversy, a critical appraisal of the methodology to identify these compartments is the nature of the tasks used to demonstrate these unique compartments is often highly controlled in posture, direction of force, and task objective (Brown et al. 2007). This is especially true when comparing these highly controlled tasks to a dynamic

task like a drop vertical jump off a box to a maximal vertical height. The presence of neuromuscular compartments requires further examination for the hip and thigh muscles as well as for less controlled and more common or even dynamic tasks. This knowledge will then guide the development of EMG driven modelling approaches to improve anatomical and neurological fidelity.

2.1.4 Passive Tissue Properties & Modeling

Any joint load modelling approach must consider the role of passive tissue not only within the muscular system but also the joint complex. In this manner, the joint load is a culmination of both the active muscle, and the passive forces and moments. Here the passive moment is the contribution of all tissues crossing the joint that restrict movement while the musculature remains inactive (Yoon & Mansour 1982). However, it should be noted that in vivo both of these forces and moments produce may act simultaneously and even synergistically and therefore are not mutually exclusive. Yoon and Mansour (1982) brought this issue to the forefront as it relates to hip modelling. Previous hip models have omitted ligaments altogether suggesting they are not relevant in gait analysis (Crowninshield et al. 1978). This is in stark contrast to the work of Bresler & Frankel (1950), who found the passive elements contributed 30-50% of the hip moment during gait at toe-off. Contributions at heel strike were between 20-40 Nm as well (percent contributions were not stated as the total hip moment changes so rapidly during this phase of gait). It seems clear that the passive elements ought to be included in any detailed model of hip which seeks to predict joint loading.

Skeletal muscle, as mentioned above, also comprises a series of passive elements. The passive component contributions are greatly impacted when considering the bi-articular muscles. These are of particular interest since the adjacent joints may greatly influence these passive element characteristics by altering the length-tension relationship at the adjacent joint. This was more closely considered at the hip when it was discovered that knee angle greatly affects the passive load on the hip due to the hamstring group (Yoon & Mansour 1982). It is reasonable to suggest that rectus femoris, and psoas might have similar effects on the passive contribution to hip joint loading during extension activities when considering spine and knee kinematics, respectively. As a result, the importance of quantifying the passive contribution of joint loading is obvious. The viscoelastic nature of the passive structures to contribute in the counter movement has been made in many different circumstances from running (Cavagna et al. 1964) to general exercise (Thys et al. 1972). Clearly, the forces and moments at any joint ought to consider the contribution from passive tissue as well as the effects adjacent joints may influence this phenomenon. Our model first assigns passive forces based on joint position then allocates the remaining force to muscle, where the distribution is EMG based - recognizing the individual motor control strategies. Passive force from muscles and articular structures should not be overlooked and with this new model both the hip and the knee will now be incorporated and the passive tissues which are influenced by joint posture will be considered along this kinetic chain.

2.1.5 Spine Models

Over five decades ago began the formalization of the biomechanical investigation of spinal loading (Morris, Lucas, & Bresler, 1961; Chaffin, 1969). Many assumptions were made in these pioneering spine models which provided just as many limitations. As these models were a

static analysis, acceleration and momentum were neglected, in part due to the lack of technology. Major muscle groups were assumed to have negligible contribution to the task at hand and were omitted from the analysis. Anatomical details were simplistic in nature. Though these models had significant limitations it began the awareness of biomechanical spine modelling and prompted more detailed analysis in hopes of better understanding of mechanical issues related to LBP and spine function in general.

Since then there have been advancements to the biomechanical investigation of spine loading (Andersson, Ortengren, & Schultz 1980; Schultz et al. 1982; Marras & Sommerich 1991; Marras & Sommerich 1991; Larivi & Gagnon 1999; Gagnon, Larivière, & Loisel 2001). However, it is still the McGill and Norman model (1986) which has been regarded as the most anatomically detailed, and complex model (Delleman & Drost 1992). Kingma noted in his keynote (CSB Kingston) that it best balances predicted and measured moments when compared to other available models (de Looze et al. 1992). This model was greatly enhanced with the addition of a spine stability index (Jacek Cholewicki & McGill 1996), a concept first formalized by Bergmark (1989) as it relates to the lumbar spine. Stability analysis of the lumbar spine provides new insights into spine function. Aside from the addition of spine stability this model has had numerous updates and enhancements to improve its predictions of spine loading (Grenier & McGill, 2007). This model remains to be the best choice to enhance further with the addition of anatomy sufficient to investigate hip-spine interactions.

These models have enhanced the understanding of spine function, loading, and injury mechanics. In addition to the biomechanical advancements in understanding function, these

models have also been used to design therapeutic exercises based on various criterion such as tolerable loading and the targeting of specific tissues (Grenier & McGill, 2007; Grenier & McGill, 2007; Kavcic, Grenier, & McGill, 2004a, 2004b; McGill & Karpowicz, 2009; McGill, 1997; 1998) as well as diagnostic tests (McGill 2007; Ikeda & McGill, 2012). The role of spine modelling in biomechanics has major impacts on the understanding of normal function, injury mechanics and therapeutic interventions right on through to maximising human performance (McGill et al. 2010; McGill 2001; Lee & McGill 2015; Lee & McGill 2016; Green et al. 2002).

2.1.6 Hip Models

Multiple hip models are currently available in the literature and the majority of them utilize various optimization techniques to solve the indeterminate problem. Understanding hip and spine loading, and more importantly the distribution of load, requires knowledge of muscle activation time histories. Muscle activation is the single highest contributor to joint force in human movement for the hip (Lewis et al. 2010) and the spine (McGill & Norman, 1986) alike. In addition, of the available hip models in the literature, none have been developed to include the mechanics of the spine. Below I will review and highlight some of the advancements and limitations to the currently available models, which will highlight the need for the development of the proposed model.

Crowninshield and colleges (1978) developed one of the earliest and most sophisticated hip models of their time. However, some important limitations are observed, namely the omission of ligaments and the absence of EMG data to assist the indeterminate problem. Ligaments were omitted as the authors suggested the tasks being observed (walking and stair climbing and

descents) were within the range of motion (ROM) where ligaments would not contribute to the joint loading profile. Essentially these authors were suggesting all the motion required occurs in the neutral zone of the joint and the passive contribution is negligible. This was refuted earlier in the literature (Bresler & Frankel 1950), as the passive components do indeed contribute to joint loading during gait. In addition, the absence of EMG data requires the authors to rely solely on optimization techniques, which are known to be non-physiological by relying on a given philosophical phenomenon – like minimization of muscle stress cubed, for example. Given these limitations the model developed was well within its capability to handle gait and stair ascents and descents.

Another of the earlier anatomically detailed models of the hip was developed by Dostal & Andrews (1981). This model was considered by the investigators as a "muscle model" (pg. 803). The model incorporated straight line actuators to represent the hip musculature. Physical model simulations identified some important limitation with the effects of joint angle and muscle paths. Namely, gluteus maximus required a manual override for the moment arm calculation at hip flexion angles greater than five degrees of flexion. These manual overrides are also used in other models to maintain the anatomical integrity of muscle moment arms (Cholewicki et al., 1995; Cholewicki & McGill, 1994; McGill & Norman, 1986). Limitations considered, this model was validated with normal walking and pathological gait data.

One important issue for any joint loading predictive model is the biological fidelity and anatomical detail as it relates to the application of the model. Brand and colleges (1982) published one of the earlier data bases of lower limb muscle anatomy, and since used by Delp in

his lower limb models (Arnold et al. 2010). This data used straight lines for muscles and used previous research (Jensen & Davy 1975) to justify their approach. These authors (Brand et al. 1982) demonstrated the need to scale the anatomy to the individual. Their approach featured the use of variation in the anatomical landmarks taken from cadaveric specimens with a scaling factor for in vivo use. Another example, is the importance of hip joint center location when considering force and moment production at the hip (Delp & Maloney, 1993). Small changes in modeling technique or even anatomical land marking can have noticeable changes in joint loading as was demonstrated by Frost and colleagues (CSB, Burnaby, BC). The challenge remains how best to define and locate critical anatomical structures when developing modelling approaches. Moreover, Lenaerts et al. (2008) showed that individualized hip joint geometry is important and relevant to the accuracy of modelled results. However, these authors were additionally limited by the optimization approach and inherent assumptions in their modelling technique. None the less they found femoral neck length could be used to predict changes in hip loading while the femoral neck angle was not as critical to individualize. This study was followed up by Scheys and colleagues(2011), who found hip muscle moment arm lengths were affected by subject specific anatomical data versus generic data sets based on percentiles. However, it remains unclear how the modelling approach would affect these results and, whether or not, this research simply identifies a weakness in the modelling approach. Recently, palpation of anatomical land marks, have been used to scale model anatomy to the individual (Luo et al. 2009). Regression equations require two or more independent variables to achieve sufficient predictive ability for anatomical scaling. No matter the approach, tuning the model to the individual of interest is an important

aspect to biomechanical modelling, yet no unanimous method exists, and the issue is not without controversy.

In a paper by Arnold and colleagues (2010) a group of 21 cadavers were used to create a data set for model inputs, however these 21 specimens were elderly and considered to be at risk for illness leading to disuse atrophy in the lower limb. There were limitations in this model as 61 N/cm² maximum isometric force per PCSA was used to tune the results to attain equilibrium. This relatively higher force/PCSA may be a result of the sample as age can change the prediction of force based on PCSA (Jones et al. 2008). In addition, the 21 specimens seemed to be from a homogeneous population, defeating the purpose of estimating anatomical variability in the broadest sense. There continued to be some outputs which were none physiological in this model and systematic manual adjustments were made. The authors were critical of a common gain and elected instead to take the approach of relying on the variance of the 21 specimens.

In more recent years, with the development of both refined modeling approaches and software applications, open source software has been developed for biomechanical use. One of the earliest open source models was developed by Professor Delp and colleagues (1990). This model was equipped with interactive platform which allows for user manipulation of input parameters to better understand consequences of surgical interventions. Building on this foundation, one of the more popularized lower limb models is the that of Delp and colleagues (2007), named the "OpenSim" model. This model was designed for estimating the effects of pathology on joint and muscle mechanics. Obviously, the pathology being investigated must have well understood impairments and limitations in order to make meaningful insights. For example,

shortened musculotendinous units like those found in cerebral palsy patients can be examined with simulation trials in this model. Others (Modenese et al. 2011a) have also used generations of the OpenSim models combining them with the most robust anatomical data set available (Horsman, Koopman, van der Helm, Prosé, & Veeger, 2007) to validate their optimization modelling approaches. The approach by Modenese (2011a) and colleagues seems to be limited by identifying the appropriate objective function based on a predetermined physiological criterion, which is a common criticism of optimization - What is the most physiological criterion? On the other hand, this demonstrates the ability of these models to be shared and developed by fellow scientists to advance our ultimate understanding of the biological system.

Validation of a biomechanical model of the hip, or any joint for that matter, offers many challenges. Generally speaking this is not often accomplished directly though it is possible to do so if direct measures are possible (Lu, O'Connor, Taylor, & Walker, 1998). A more practical approach is verification and validation in parts. Meaning the individual parts within the model have been validated separately and therefore when combined they are assumed to also be valid. The approach described above to validate in parts and verify with established approaches will be used in this thesis. These are only some of the aspects related to model validity, which is a major consideration for any modeling approach (Anderson et al. 2007; Henninger et al. 2010).

2.1.7 Passive Hip Mechanics

2.1.7.1 Stability

Passive structures at the hip contribute to joint mechanics in several ways. One important way is the contribution to hip stability. In fact, even the periarticular tissues (muscles, skin, and

fat) can contribute to hip kinematic stability in multiple planes by controlling motion of the femoral head and limiting translations in the acetabulum (Safran et al. 2013). However, the contribution of the ligaments should not be overlooked. In particular when considering repair strategies surgically theoretical anatomical evidence suggests both the iliofemoral ligament and the acetabular labrum play unique and significant roles in limiting external rotation and anterior translation of the femur (Myers et al. 2011). This was updated and confirmed more recently, with experimental data demonstrating the multiple postures and the interactions with specific ligaments. It was clear that passive resistance is posture dependant and that the joint capsule as well as ligaments have a significant role in hip stability and limiting translations of the femur which is suspected to contribute the progression of hip osteoarthritis (van Arkel et al. 2015).

2.1.7.2 Models

As mentioned above in the hip modelling section these contributions have not been incorporated into many if any modelling approaches. One consideration of passive structures is their effects on joint range of motion, this includes bone, ligament, joint capsule and labrum when considering the hip. One approach is a lumped parameter to sum the effects of all these tissues into one algorithm. However, some experimental data exists to partition the contribution of at least the individual ligaments into a biomechanical model (Hewitt et al. 2002), and this data is used and described in more detail in Hip-Spine Model (HSM) section of this document.

2.1.7.3 In vivo clinical studies

Evaluating passive joint stiffness is often a clinical target – hip stiffness and even hamstring ‘tightness’ is no exception. Some have investigated passive force and stiffness changes with hamstring stretching (Miyamoto et al. 2015; Reid & McNair 2004) but few have asked the more

fundamental question, should we stretch? Or even more fundamental should reducing 'joint stiffness' or 'tissue stiffness' be a clinical target? There was a small sample of a sub-group of LBP patients (with spondylolysis) and tight hamstrings compared to healthy controls (Barash et al. 1970) and in addition to a multimodal rehabilitation program (Khalil et al. 1992). Similarly, Individuals with LBP have been shown to have stiffer hamstrings (Tafazzoli & Lamontagne 1996). While passive stretching has been shown to change mechanical properties at the joint, like increases ROM and decreased rotational stiffness (Reid & McNair 2004; Marshall, Cashman, et al. 2011) it remains unclear who will benefit from these changes in both the patient population and in an injury resilience points of view. Moreover, the refinement of stretching technique can also make a difference on the clinical effect (Miyamoto et al. 2015). In addition to all these clinical questions, one more is while the patients learn to use the greater access to joint motion? Studies (Moreside & McGill 2011) have shown that skillfully improving one's ROM does not translate into the utilization of improvements in ROM during function tasks. Utilizing new movement strategies requires equally skillful movement coaching.

It is also important to consider how these clinical studies measure hip joint motion or stiffness – since clinical studies may lose accuracy in order to gain access to a clinical population. With respect to the hip many studies (Marshall, Cashman, et al. 2011; Lee & Munn 2000; Reid & McNair 2004) actually evaluate angle between the leg (femur) and the global space horizontal, or clinically, the straight leg raise (SLR). This is problematic mainly because this angle is not a direct measure of the hip, and the definition of zero degrees may not in fact be anatomically zero degrees and even more importantly the spine and pelvis have the potential to rotate and therefore contribute

to the total femur-horizontal angle. This is a major limitation in the clinical evaluation and skillfulness of the assessment techniques.

2.1.8 Solving the Indeterminacy Problem

As mentioned above, direct measurement of muscle force, tissue and joint loading is highly invasive and not available in most clinical or research settings. Currently the most advanced clinical settings have access to inverse dynamics analysis systems like OpenSim software. Inverse dynamics calculations are able to acquire quite reasonable estimates of joint loading in most cases (perhaps with the exception of the spine). However, making the leap to capture individual muscle forces has been of significant challenge due to the complexity of the control system (Erdemir et al. 2007). This is due to the indeterminacy, the number of muscles creating forces and moments about the joint far exceed the number of equations to solve the problem. One of the early spine models by Schultz(1982) employed an optimization approach. This is solved mathematically to balance the moments and forces by using a predetermined objective function. This objective function is often an attempt to minimize or maximize some value thought to relate to a control strategy. For example, minimizing muscle stress might be an objective function. This approach will solve the equation of equilibrium however; the solutions are not always physiologically similar to observed control strategies. Crowninshield and colleagues (Crowninshield et al. 1978) noted the issue of co-contraction and physiological representation when using the optimization approach in their examination of hip mechanics and elected to ignore the contribution of co-activation. Another example in the hip was Brand and colleagues (Brand et al. 1994), who attempted to solve the indeterminate solution with optimization and compared the results to implanted transducer measurements. The mathematically predicted hip

joint force was similar in this analysis, while the authors alluded to over estimation in earlier attempts utilizing the optimization technique. General configuration of the force curves were also adequately represented in the modelling approach. The authors (Brand et al. 1994) noted, however, that performing more physiologically based measurements would likely improve mathematical modelling predictions. It seems the complexity of the task being measured may have had a role to play in the accuracy of the model predictions. In this study, post-operative patients were walking at relatively slow speeds. While variability is in the magnitude of 10 percent for most gait variables, moment calculations are as high as 10-30 percent (Winter 2009). This alludes to the variability in control strategy, especially when walking speed is controlled. The more robust the model, the more versatile its capabilities.

Another early approach to address the indeterminate problem employed EMG driven models. In this case normalized EMG was used to predict individual muscle contribution to the overall joint force profile. In theory, the sum of each muscle equals the reactive moment. While this approach is sensitive to individual motor control strategies it does not always provide a balanced equilibrium equation. McGill & Norman (1986) were the first to develop an EMG driven spine model and use an EMG assisted optimization (Cholewicki & McGill, 1994; Cholewicki et al., 1995) to solve the indeterminacy problem in a spine model. They investigated this by comparing traditional optimization and EMG assisted optimization (EMGAO) approaches while solving for muscle force. In addition, Gagnon and colleagues (Gagnon et al. 2001) reviewed traditional optimization, EMG driven, and EMG assisted optimization (EMGAO) approaches during a dynamic lifting task using an L5-S1 partitioned spine model. Not surprisingly they found similar results, the optimization techniques were best able to handle the mechanical equilibrium, while

the physiological fidelity was upheld through the EMG approaches (Cholewicki et al. 1995; Gagnon et al. 2001).

2.2 Clinical issues of the knee, the hip, & the spine:

Given the close anatomical, biomechanical and neurological relationship between the knee, hip and spine, due in part to their proximity, many symbiotic relationships exist between these joints. Many muscles have shared functions between these joints and the neurological relationships are obvious from the lumbar plexus on down. These regional interdependent relationships exist in pairs, for example the knee and hip (Taylor et al. 2018; Reiman, Bolgia, et al. 2009; Powers 2010) as well as the hip and spine (Offierski & MacNab 1983; Reiman, Weisbach, et al. 2009; Wong & Lee 2002) and also the knee and spine (Li & Zhang 2009). As a result, the knee, hip and spine function have been of interest to clinicians within the context of LBP for some time. The nature of the relationships, between hip and spine function as related to the clinical presentation, present themselves in many forms including movement patterns, (Wong & Lee 2004; Haugstad et al. 2006; Shum et al. 2005a), neuromuscular control strategies (Freeman et al. 2013; Nelson-wong et al. 2008; Nadler et al. 2002; Leinonen et al. 2000; Hungerford et al. 2003; Murphy et al. 2006), and fatigue characteristics (Kankaanpää et al. 1998; Marshall, Patel, et al. 2011; Nourbakhsh & Arab 2002). Each of these relationships will be reviewed here beginning with the earliest documented hip and spine disorder called "hip-spine syndrome" (Offierski & MacNab 1983). This section of the literature review will reveal the clinical importance of this thesis and detail the implications for clinical research moving forward.

2.2.1 Hip-Spine Syndrome

The formalization of hip-spine syndrome was made by Offierski in 1983 (Offierski & MacNab 1983). In this report a series of clinical cases suggested an increase in the prevalence of spine disorders with those who also had hip osteoarthritis (OA). This association was more recently confirmed by Saunders and colleagues (1979) who demonstrated that patients with hip OA had increased incidence of spine OA (lumbar and thoracic), especially at younger ages. Moreover, these associations were not made in the hands or wrists and therefore, are not thought to be part of a generalized arthritis but rather a more localized relationship between the hip and spine. Simple hip-spine syndrome was classified as concurrent pathology (degeneration). Secondary hip-spine syndrome included the cases of LBP that were aggravated by hip deformity. Finally, complex hip-spine syndrome included those patient experiencing symptoms in both joints making the casual etiology more difficult to identify (Offierski & MacNab 1983). Clearly this first attempt to classify these conditions was limited, however, important none the less as the first real identification of the clinical phenomenon. Offierski and MacNab (1983) also discussed the challenges with complex cases and the need for ancillary diagnostic and investigative approaches to be better enable accurate diagnosis and appropriately treat these patients. Since this initial reporting there have been additional investigations examining the relationship of LBP associated with hip dominate pathologies. Matsuyama et al. (2004) examined the effects of secondary hip-spine syndrome on spine posture in a group of patients with LBP. Specifically, they examined patients with bilateral congenital hip dysplasia and reported increases in anterior angulations of the pelvis leading to hyperlordosis. This population demonstrated higher reporting of LBP compared to hip pain despite the obvious hip pathology and comparatively less obvious spine deformity. Later, Yoshimoto and colleagues (2005) investigated the a group of patients with hip

OA and compared them to a spine group, which included patients with 'degenerative joint disease' (DJD) and other spinal pathologies. A number of measurements were used to quantify the biomechanical relationships within these patient populations including increases in lumbar lordosis, sacral base angle, pelvic incidence angle (the angle formed by the coccyx to the midpoint of the acetabulum, passing through the midpoint of the sacral base - measured in the sagittal plane) and sharp angle (the angle between a line passing through the bilateral tear drops and a line from one tear drop to the ipsilateral superior lateral edge of the acetabulum - measured in the frontal plane) found in the hip OA population. In addition, the hip OA population had greater pelvic obliquity and leg length inequalities. Lastly, the hip OA group had decreased pelvic tilt when compared with the spine group. In support of this theory, patients with LBP and OA of the hip requiring total hip replacement (THR) are likely to benefit from addressing the primary lesion, in this case, hip pathology. After THR patients reported clinically significant reductions in LBP (Ben-Galim et al. 2007). Based on these observations further analysis is warranted to elucidate the relationship between the hip and spine function, and how they are related pain and pathology.

2.2.2 Hip & Spine ROM

Movement aberrations are associated with pained individuals and LBP is no exception (Luomajoki, Kool, Bruin, et al. 2008). Yet, the issue is controversial when considering causality of movement aberrations and pain, in regards to the precipitating factor (Williams et al. 2010). However, ROM has been investigated as a potential contributor to the development of LBP. Sjolie et al. (2004) investigated LBP in adolescents and found an association with hip mobility and body mass index (BMI) with LBP. Hip extension demonstrated a trending relationship between

decreased ROM and LPB, and active ROM was found to be decreased in hip flexion and hamstring flexibility (two independent tests) in the LBP group. Moreover, when attempting to identifying those who will develop LBP in physically active and inactive adolescents, decreased spine motion and restricted hip motion have been shown to have predictive values among males (Kujalal et al. 1994), and weight, height, lumbar extension ROM and previous LBP were predictive among females (Kujalal et al. 1994). Importantly, higher levels of physical activity were not shown to be detrimental to pain development in these adolescents. Two other reports (Ellison, Rose, & Sahrman, 1990; Van Dillen, Bloom, Gombatto, & Susco, 2008) have used ROM testing in clinical settings to investigate the relationship between hip ROM and LBP. During passive ROM testing a group of patients with chronic low back pain (cLBP) displayed less hip ROM than healthy participants. Specifically, these deficits were noted with less medial and lateral rotation, than the non-LBP group. In addition, the cLBP individuals had ROM imbalances with the right side having less total ROM than the left; this relationship was not evident in the non-LBP group (Van Dillen et al. 2008). In relation to absolute ROM is the notion of balance and symmetry from side to side. This has long been thought of as clinically important for normal function. Ellison et al.(1990) have demonstrated hip ROM imbalances are associated with LBP. During hip ROM testing, patients with LBP were more likely to have less medial rotation of the hip than lateral. In fact, 48% of this patient population demonstrated a restricted hip pattern during internal rotation. On the other hand, this pattern was only present in 27% of the healthy population. Identifying when hip ROM or imbalances side to side might contribute to LBP development and chronicity are important next steps.

As another example, in a group of professional golfers associations were investigated between LBP and non-LBP groups to identify relationships associated with the development of LBP in this at risk group (Vad 2004). It is important to note; this elite group of golfers would likely form a sub-group of LBP if a common presentation could be identified and may not reflect the general population. None the less, associations were seen for decreased lumbar extension, Patrick's test ROM (AKA FABER's test: flexion, abduction and external rotation), and decreased hip internal rotation of the lead side in the LBP group. Prospective studies would be the next logical step to investigate whether there is clinical efficacy in attempting to change these variables in hopes of preventing or managing LBP.

2.2.3 Hip & Spine Movement

Movement coordination involves both joint mechanics and neural control. The result of coordinated movement can be thought of as movement quality. Rather than simply quantifying the amount of movement as evaluated by ROM testing, assessing movement quality reflects aspects of coordination of movement patterns, typically in goal-oriented movement. In this sense, goal directed movement relates to both the mechanical capabilities of the joint as well as the neurological control strategy to control and coordinate movement thus forming movement patterns over time. These movement patterns have been a clinical focus for some time by many researchers (Van Dillen, Maluf, & Sahrman, 2007; J B Ellison, Rose, & Sahrman, 1990; Gombatto, Collins, Sahrman, Engsborg, & Van Dillen, 2007; Lewis & Sahrman, 2009; Luomajoki, Kool, de Bruin, & Airaksinen, 2008; Sahrman, 2001; Van Dillen, Maluf, & Sahrman, 2009). Unfortunately, there is a paucity of empirical data characterizing Hip-Spine syndrome, due to the lack of investigation into this area and comparative data to healthy controls. Researchers

(Haugstad et al. 2006) studying posterior pelvic pain have developed reliable analysis tools, though these analysis systems lack clinical validation. Yet, characteristic stance, including a narrowed stance, anterior translation of the pelvis, posterior translation of the upper back and shoulder girdle; and sitting posture, including a cross legged and lumbar kyphotic posture were evident in the patient population. Moreover, balance and coordination was compromised as well as a lack of hip mobility during gait (Haugstad et al. 2006). Further examination of the differences in movement quality and movement patterns are warranted for a better understanding of the mechanisms in this population of patients as well as in other low back, pelvis and hip pain syndromes.

One of the most clinically important analyses are of movements that are performed daily. These are the movements that have the potential to contribute in a meaningful way to cumulative loading injuries. Research (for example, Lamothe et al., 2002) has shown LBP populations and healthy controls use different strategies during walking for example. Movement patterns between the thorax and pelvis are in-phase at walking velocities below 3km/h. During faster speeds the thorax and pelvis move out of phase to conserve and transfer angular momentum between the lower limb and the pelvis, however, patients with LBP may remain in-phase walking at higher walking speeds potentially leading to increased joint loading in the lumbar spine. Strategies for the pained patient during walking have been identified by Callaghan and colleagues (1999) which included appropriate arm swing to counter the angular momentum created by the lower limb. Recently, researchers (Shum et al. 2005b; Shum et al. 2005a; Wong & Lee 2004) have demonstrated reduced lumbar flexion in two sub-groups of LBP patients with and without limited side-lying leg raise (SLR) during activities of daily living (ADLs). Loss of lumbar

flexion movement was accompanied by increased axial rotation in some patients (Shum et al. 2005b), those with nerve root symptoms used even less lumbar flexion while performing ADLs than the LBP and the control groups (Shum et al. 2005b) and while performing ROM testing (Wong & Lee 2004). Interestingly, only the nerve root sub-group demonstrated less hip flexion than the health controls in activities such as putting on a sock (Shum et al. 2005b). In relation to the quality of movement, lumbar flexion velocity and right hip flexion velocity were significantly reduced in both LBP groups (Shum et al. 2005b), while movement time was as much as doubled in this group (Wong & Lee 2004). Perhaps more importantly, spine to hip flexion ratio was increased indicating a dominance of spine motion, especially in the SLR sub-group (Shum et al. 2005b; Shum et al. 2005a; Wong & Lee 2004). Further, the coordination of motion (cross-correlation analysis) demonstrated a significant reduction in the similarity of hip and spine sagittal plane motion, while there was an increase in frontal plane coordination in both symptomatic groups. These changes in movement strategy are interesting, however, it is difficult to fully understand the origin of these movement patterns. Are those with back troubles moving because of pain or attempting to avoid pain resulting in altered movement patterns or does their movement pattern pre-exist their pain? This is a difficult question and more research is needed to understand the relationships between injury mechanics, movement patterns and pain behaviour.

Excessive motion of the spine can be detrimental to some patients while too little motion may be pain provoking in others. For example, those who experience pain associated with prolonged postures (Marshall, Patel, et al. 2011). Clinical wisdom would suggest this group might benefit from alternating postures in an attempt to create tissue load sharing capacity. An in vivo

investigation of segmental movement in a severely degenerative group of patients showed a significant reduction in segmental rotation and a lack of coupled motion (Lund et al. 2002). Though it was only possible to make this assessment in a surgical population due to the invasiveness of the procedure it is unclear if these patterns are related to pain. However, the general theory in this group may create increased force concentrations to a specific region of the tissue due to the lack of mobility leading to inappropriate load sharing and diminishing capacity. On the other hand, the ability to create proximal stiffness as discussed earlier can be fundamentally important for some patients with back troubles who demonstrate hip rather than spine dominated movement patterns. Scholtes et al.(2009) demonstrated that a subgroup of patients with LBP who participate in rotation related sports (i.e. racket sports) demonstrate earlier and greater amplitudes of spine motion during extremity movements. This is theorized to contribute to cumulative trauma injuries due to the repetition of motion associated with their sporting activities (McGill, 1997). This example likely demonstrates why a signal treatment technique has failed to help all LBP conditions, yet, a single theory of how to manage LBP conditions may still be possible if it is robust enough to account for individual differences and multiple aetiologies.

It is unclear whether poor movement causes pain, potentially through tissue overload, or poor movement patterns develop as a result of pain and pain avoidance or possibly both. However, anatomical asymmetries, limitations or biases may be an important factor in the understanding of the relationship between movement and pain. Al-Eise et al.(2006) demonstrated pelvic asymmetries were more prevalent in those with LBP. Moreover, the LBP group was more likely to have asymmetries in spine motion. Therefore, understanding the

adaptability of hip and spine motion based on a structural limitation, functional adaptation or selective motor pattern is important. Recently, Hoffman et al.(2011) demonstrated the ability to decrease spine motion and increase the amount of hip motion prior to engaging in movement requiring spine motion during a controlled clinical movement screen. The authors suggested that this would over time provide a more favourable pattern of hip dominate movement leading to spine sparing movement patterns. A critical next step in the understanding of this phenomenon and the association between movement and pain is identifying the precipitating factors. Hence, the ability to develop the desired ROM and train new movement patterns assumed to be more beneficial from a LBP perspective will only be possible when the cascade of events leading to pain is understood.

2.2.4 Hip & Spine Loads

Movements and postures will define the joint load and which tissues will bear the load within the joint. Pain is associated with changes in movement regardless of whether or not the issue of causation can be resolved. Movement related changes in sagittal plane motion, during forward bending, translate to increases in moments in the early and mid-ranges of motion, while reduced at the end range in subjects with LBP (Shum et al. 2010). This was accompanied by increases in adduction moment at the hips during forward bending. The authors suggested tissue stiffness and muscle splinting as potential mechanisms for this change in behaviour however, their use of models (inverse dynamics) does not have the capacity to reveal these changes. These changes were more likely a result of the observed changes in ROM and movement patterns. A more sophisticated model is required to understand loading behaviour between tissues in the hip and spine.

In some earlier work, Vleeming and colleagues (1995) were among the first to provide a theoretical anatomical rationale for the inherent relationship between the hip and spine with their work on the posterior fascia, and biceps femoris with its relationship to sacrotuberous ligament provides some evidence of a direct anatomical link (van Wingerden et al. 1993). This was followed by their work with the dorsal sacral ligament and here the authors are far less subtle with the potential contribution to the development of LBP and the relationships between the spine, pelvis and hip (Vleeming et al. 1996). Essentially this body of work sought to understand the theoretical mechanisms by which the transmission of force, through mainly the muscles and fascia, might influence spine and hip behaviour and the potential influence of low back pain. Though this work was purely theoretical in nature its influence on the understanding of the management of LBP has been highly influential in clinical thought processing. These theories require further investigation and more sophisticated approaches to reveal the nature of the relationships between the anatomical regions of the spine, pelvis and hip as well as the potential to transmit load. Moreover, the potential effects of low back pain and how movement and motor patterns in different populations might affect this theory is also important for the understanding of joint loading and LBP.

2.2.5 Hip & Spine - Neuromuscular Patterns & Fatigue

Spine pain has been shown to effect neurologic reflex loops and alter motor firing patterns (Graven-Nielsen et al. 1997; Graven-Nielsen 2006). The question remains to what extent does this affect have on whole muscle activation and joint mechanics? Hungerford et al.(2003) demonstrated this effect with sacroiliac joint pain (SIJP) during a simple hip flexion task. In comparison to a control group the patient population displayed a delayed firing onset of internal

oblique, multifidus and GMax on the side of the SIJP. This phenomenon was not true of all hip extensors, biceps femoris was increased, theoretically to support the extension moment otherwise produced by GMax. In addition, Leinonen and colleagues(2000), also demonstrated these types of effects in another population of LBP patients. During flexion and extension movements the gluteal muscles in LBP patients were significantly less active in comparison to their healthy counter parts. Variability was also seen in onset latency, though this was much less predictable. This is some of the newer evidence in support of an older theory of crossed pelvic syndrome first described by Vladimir Janda (in Page et al. 2010) and discussed by Professor McGill as "gluteal amnesia" (McGill, 2007). Additional support for the "gluteal amnesia" phenomenon is provided by the investigation of muscular fatigue (Kankaanpää et al. 1998). During repetitive trunk extension endurance testing patients with (chronic low back pain) cLBP, who were initially similar in motor patterns to a healthy control group, demonstrated a divergent pattern with fatigue. It was again the gluteal muscle group that was early to fatigue which separated the groups in the investigation. Interestingly, the erector spinae (ES) EMG characteristics remained similar between groups. In contrast, during twisting and torque producing movements Pirouzi and colleagues (2006) found increased co-activation of the erector spinae muscles and gluteal muscles in back pain patients as compared to healthy controls. This muscle splinting was suggested to provide stiffness and limit motion to prevent further spine injury during these more demanding twisting and torque producing tasks. On the other hand, great compressive force is applied to the spine during these twisting tasks, which may have been pain producing depending on the nature of the back disorder (McGill, 2007). This example highlights the challenges ahead when attempting to identify the specific etiology of spine pain versus the compensatory responses to

protect the injured area. In other words, it appears the effects of LBP may be as diverse as the causes of LBP – making the argument for heterogeneity very relevant in the study and management of back disorders.

Several diagnostic tests have been used to identify and quantify neuromuscular patterns, strength and fatigue behaviour in patients with LBP. One such test was first described by Janda (Page et al. 2010), as the prone hip extension test, has been the focus of much research in an attempt to quantifying the validity of Janda's original findings (Vogt & Banzer 1997; Arab et al. 2011; Lewis & Sahrman 2009; Bruno & Bagust 2006; Sakamoto et al. 2009). Generally, the pattern is assumed to be normal when a predicted pattern is followed based on 'clinical wisdoms' of motor patterns seen in upright gait patterns (Page et al. 2010). However, this predicted pattern has not shown to be valid in healthy subjects when more sophisticated instrumentation like EMG has been used versus visual inspection (Arab et al. 2011; Lewis & Sahrman 2009; Bruno & Bagust 2006; Sakamoto et al. 2009; Vogt & Banzer 1997). Although the original hypothesis for the mechanism of this test has not been supported (aberrant neuromuscular timing), Murphy and colleagues (2006) have proposed its utility and reliability when identifying the ability of a patient with LBP to create "punctum fixum" during the prone leg raise movement. This is theorized to provide insights into the ability of the patient to create core control to stabilise the spine while performing leg movements (proximal stiffness and distal mobility). This is an excellent example of a 'functional test' which interacts with the kinetic chain and may provide insights into the motion/motor pattern used but some cohorts of low back pain patients. Much work is needed to validate these clinical observations and better understand, neuromuscular patterns, gluteal amnesia, and fatigue with respect to the LBP patient.

In the management of musculoskeletal disorders, one more recently popularized approach is neuromuscular compartment training. This concept has been of considerable interest in the clinical management of musculoskeletal disorders, especially at the shoulder, when considering the ability to selectively activate muscular compartments (Holtermann et al. 2010; Holtermann et al. 2009) as well as shoulder rehabilitation to reduce shoulder impingement syndromes through neural control strategies (Cools et al. 2007; Cools et al. 2002; Cools et al. 2003). The clinical goal is to either redirect the load through changes in movement patterns and/or change the motor pattern in an attempt to shelter injured tissues with the training of new motor patterns. In this way it is a similar approach to the proposed theoretical model of this thesis – namely, load sharing will optimise loading capacity and tissue tolerance.

Motor patterns and the selection of neuromuscular patterns likely play a role in the development of musculoskeletal disorders. The next step is to identify the mechanism of injury and the development of faulty motor patterns as well as the effects of pain on motor patterning. Then the best approach for managing these disorders through motor pattern training and rehabilitation techniques can follow.

2.2.6 Hip & Spine - Muscle Strength, Imbalances & Endurance

Muscle imbalances are hypothesized to contribute to unfavourable joint loading causing localized force concentrations leading to tissue overload. For example, tight hamstrings are thought to create excessive pelvic torque and are associated with LBP (Nourbakhsh & Arab 2002; Sjolie 2004). Clinical theory would suggest as noted above the hamstrings overload the posterior kinetic chain, namely via the sacrotuberous ligament, and lead to tissue overload. Arab and

Nourbakhsh (2010), investigate interplay between tensor fascia latae and the iliotibial band (ITB) as it is thought to relate to LBP. Janda theorized (Page et al. 2010) that this relationship is a result of weakness in the gluteals and the TFL compensation results in unfavourable loading on the ITB leading to ITB syndromes. Again, in light of observational data (Arab & Nourbakhsh 2010) it seems that ITB tightness may or may not be associated with LBP. However, in both groups of LBP patients (with and without ITB tightness) hip abduction strength was significantly less than those without LBP. In contrast, during a prolonged standing task, used as an experimental pain model, hip strength was not related to the development of LBP but GMed muscle endurance was able to adequately predict those who would develop LBP (Marshall, Patel, et al. 2011). Yet again, others (Nadler et al. 2000; Nadler et al. 2001) have observed that muscle strength alone is not a predictor of LBP but rather an imbalance from side to side in hip abduction strength was able to differentiate athletes with and without LBP. Similarly, when examining co-activation of the torso and hip muscle in prolonged standing experimental data has shown those likely to develop back pain are more likely to co-contract GMed (Nelson-wong et al. 2008). This was theorized to be related to excessive joint loading leading to pain. Nadler et al.(2002) reported a significant benefit to training the muscle imbalances in a group of female athletes with LBP. To further confuse the situation, muscle imbalances in males at the hip were not found to be predictive of LBP; and once trained the association between muscle imbalances and LBP were no longer predictive in trained female patients. Interestingly, core strengthening was shown to facilitate gluteal strength, demonstrating an integration of hip and spine mechanics. There were limitations in this study since the severity of pain was not significant enough to require treatment. However, athletes are known not to report injury and seek treatment due to fears of lost time in sport among others

(Garrick & Requa 1993). As a result, it may be difficult to evaluate the severity of these injuries. On the contrary, Nourbakhsh and Arab(2002) found back extensor endurance to have the strongest association with LBP followed by hip flexion strength, back extensor endurance and hip adductor strength. There seems to be a relationship between hip muscle characteristics and the development of LBP, however, the specific mechanisms and nature of the relationship continue to elude clinicians and researchers alike.

Next, related more specifically to hip disorders, motor patterns and muscle imbalances have been shown to be equally as important as the previous work examining LBP. In an examination of hip pain related to hip instability and labral tears, Lewis and colleagues(2007) found gluteal and "iliopsoas" (note due to their clearly different functions these should not be considered one muscle) to be contributing factors. Finding motor control strategies to alleviate pain by reducing anterior shear forces is often the clinical goal in managing these conditions. The gluteal muscles are a major target of these interventions. Similarly, Freeman and colleges(2013), have also found gluteal activation an important factor in hip capsule pathology. Tightness in the hip capsule, associated with osteoarticular joint disorders, as an example, is detrimental to gluteal function. There is more than enough evidence to promote and suggest the further examination of the contribution and effects of motor pattern selection on joint and tissue loading characteristics. In order to achieve this a model capable of handling individual motor pattern selection will be required.

2.2.7 Hip and Spine Rehabilitation and Manual Therapy

A critical question for rehabilitation design and exercise prescription is knowledge of the target muscle demands. For example, targeted rehabilitation programs may desire maximizing the target muscle demands while minimizing the joint load, thus optimizing the benefit of the strengthening/endurance while minimizing the risk for joint injury, in perhaps a patient with a degenerative hip condition. On the other hand, a younger athlete may not want to limit joint/bone loading with the desire to maximise muscle demands for strength gains as an example. Unfortunately, the rehabilitation literature for hip exercises are lacking the knowledge of relative joint demands while solely focusing on muscle activation levels. This has been the case for extensor (posterior chain) training (Arokoski et al. 1999), hip abduction exercises in healthy people (Bolglia & Uhl 2005) as well as in total hip arthroplasty patients (Jacobs et al. 2009), in single and double leg support in athlete (McCurdy et al. 2010) and non-athlete (Krause et al. 2009; Schmitz et al. 2002) populations, and even when using "Janda sandals"(Bullock-Saxton et al. 1993). The approach of only assessing EMG has also been used when a myriad of exercises were used in various rehabilitation purposes for the hip (Distefano et al. 2009; Krause et al. 2009; Schmitz et al. 2002; Arokoski et al. 1999; Bolglia & Uhl 2005) as well as the spine (Oliver et al. 2010). A more holistic analysis of muscle activation, joint motion and loading for the hip is likely to provide an enhanced analysis and improve the recommendations made for prevention and rehabilitation exercises. Only recently, has the consideration for spine sparing hip rehabilitation been made evident in the literature(Cambridge et al. 2012). Here the concept is introduced as exercises are intended at producing hip motion and gluteal activation while minimizing spine

movement, as thought to be more spine sparing. Further research is warranted and this will be the focus of the final study of this thesis.

In addition to tradition rehabilitation, grade IV hip mobilization has been used to successfully enhance GMax strength, experimentally (Yerys et al. 2002). Surgically, this has been confirmed with therapeutic arthrograms stretching the hip capsule will affecting gluteal activation(Freeman et al. 2013). When comparing manual therapy to exercise therapy in a randomized controlled trial (RCT) conducted on patients with hip osteoarthritis, manual therapy was shown to be more advantageous to exercise(Lubbe et al. 2004). This research likely identified a sub-population of patients, likely with hip mobility deficits, who are more responsive to mobility enhancement verse strength or endurance gains. Pragmatically, in clinical setting those trained in both practices will apply both techniques to maximize the individual benefits, unfortunately, a combination intervention group was not included, as they rarely are in these highly constrained RCT designs. None the less, there are vast opportunities to inform clinical practice with more sophisticated analysis of rehabilitative techniques.

2.2.8 Knee injuries and the hip and spine

Non-contact ACL injuries are yet another area of interest where more recent investigations are leading the importance of neuromuscular control strategies of the spine, hip and knee rather than simply understanding this injury as a knee dominate problem. Early work (Hewett et al. 2005) investigating ACL injury among young female athletes in jumping and cutting sports (basketball and soccer) focused on knee variables (Knee abduction (shank relative to the femur), knee flexion, knee abduction moment (KAM), differences in leg dominance. This began from the

original observations during a drop vertical jump (DVJ) task there major differences were seen between gender and even leg dominance. Females had significantly higher maximum valgus scores than their male counterparts and this was most prominent on their dominant side (Ford et al. 2000). Also in the literature others (Powers 2003) have investigated dynamic knee valgus (DKV) as a predictor of patellofemoral pain syndromes. In an attempt to identify the mechanism behind ACL injury which are linked to dynamic knee valgus (DKV) was the investigation of knee abduction moment (KAM) which was proposed with a threshold value of 25.25 Nm as the most sensitive variable to dichotomize between 'at-risk' and 'not-at-risk' groups for ACL injury (Myer et al. 2014; Myer, Brent, et al. 2011; Myer et al. 2007a; Myer et al. 2010b). However, isolating the KAM as a single measure for ACL injury is less than perfect. This is not surprising since this was really an attempt to find a threshold value which was related to DKV which was considered the injury mechanism leading to ACL strain and injury.

In more recent work, Hewett et al. (2016) used a more robust approach to develop three pools of female athletes, low-, moderate- and high-risk, respectively. In this analysis additional biomechanical variables such as, ground reaction force (GRF), hip moments, pelvis angle (pelvis in global space), were used to enhance the understanding of mechanical differences between risk levels. This has brought the understanding of hip and spine control into the discussion of ACL injury risk. Further clinical studies are required to better understand the most critical characteristics; however, this is an important study which demonstrates ACL injury is far more complicated than a single variable such as a threshold value of KAM. Understanding the regional interdependency of injury propagation along the kinetic chain is a worthy pursuit and justified by this recent work.

2.3 Summary of Literature Review

In summary, missing from the biomechanics literature is an integrated hip and spine model which is anatomically detailed and biologically driven capable of investigating the neuromusculoskeletal implications of hip and spine interplay as it relates to normal and clinical populations at the individual level. Equally missing from the clinical literature is understanding of how this relationship between hip and spine mechanics contributes to and/or is affected by disorders which arise from an interaction of the kinetic chain (i.e. non-contact ACL injuries and low back pain). Many clinical wisdoms and scientific evidence are available to suggest and support the notion of an important interaction of hip and spine function with injury mechanism, yet there is a paucity of studies with the breadth and depth of analysis to fully examine the hip and spine interplay. Even more so, there is a scarcity of highly sophisticated analysis of the rehabilitation techniques being used for the management of hip disorders and little consideration for the effects on knee and spine mechanics. All of this provides an opportunity for a robust analysis of the hip and spine in an integrated approach using biomechanical modelling to examine mechanics of hip and spine function as well as knee injuries. With this understanding of hip and spine function there is an opportunity to enhance the clinical management of knee, hip and spine disorders through the development of superior exercise and therapy regimes. Limitations in the scientific investigations were also evident throughout the review. Modelling approaches are no exception. Nonetheless the details in physiology, mechanics and anatomy coupled with using a method sensitive to the individual variation in motor strategy will add to understanding of the links between the spine and more caudal structures. It is the intention of this thesis to bolster

the mechanical understanding of hip and spine function in order to ultimately improve clinical outcomes for patients.

3.0 Study 1: Developing the Hip-Spine Model

Biomechanical modelling is used to predict variables that are not readily nor directly measurable. In doing so, biomechanical modelling provides a window into a biological system and the ability to gain a deeper understanding of the underlying behaviour of that system. The objective of this study was to build an anatomically detailed, biologically driven, three-dimensional (3D) Hip-Spine Model (HSM). The purpose of this model is to evaluate the distribution of joint and tissue loads within the hip and spine complex, based on a well-established muscle modelling approach (Hill-Type Model), and the best available data sets for the spine (McGill & Norman, 1986; Cholewicki & McGill, 1994; Cholewicki et al., 1995) and the lower limb anatomy (Horsman et al. 2007). For simplicity, these data sets will be referred to as the McGill dataset and the Twente Lower Extremity Model (TLEM) dataset, respectively. The mechanical relationship between these areas have been neglected in a large way in the past. There is sufficient clinical evidence to suggest the investigation into the mechanical behaviour may provide valuable insights into both injury mechanisms, prevention and rehabilitation of spine, hip and even knee disorders. Hence, this new anatomically detailed, biologically driven HSM provides a foundation for the understanding of regional interdependency of the hip and spine and will allow for novel investigations into injury mechanisms, rehabilitation strategies, and athletic performance.

Creating the HSM was an extensive process which involved re-writing the original McGill spine model into MATLAB™ and amalgamating additional anatomical details for the pelvis and lower limb from the TLEM dataset to create an integrated model. It is noted that this was not trivial process and was intensive and extensive process to transform the world's most detailed spine

model with a complete set of hip and pelvis data. This formed the basis of the HSM and allow for an enhancement of each model as well as the combination of both models. For example, the psoas attachment was extended into the femur from the pelvis allowing the movement at the hip and the spine to enhance the biofidelity of the muscle behaviour with respect to both spine and the lower limb models. Further enhancements were integrated into the model based on problem solving which were presented as the model was examined and proofed. Details are provided below, however, to highlight some of these enhancements this is the first model we are aware of to incorporate ligaments into this type of whole joint modelling at the hip. Moreover, refinements were made to maintain the biological fidelity, such as adjusting anatomical muscle lengths to match the physiological properties. With the development of this model there is great potential for novel investigative approaches which may lead to an improved understanding of the mechanical relationship of the interdependence of the hip and spine.

This chapter outlines the major components of the model in detail. Included is a description of the equations which represent the physiological and behavioural characteristics of the ligaments, muscles and joints represented in this model. The model is driven by biological signals; it calculates ligament and muscle lengths, velocities, vectors, and forces and then sums them to estimate joint loading characteristics as shown in the schematic diagram in Figure 3.1. While further refinements and improvements are always possible and will evolve with this model over time, the current fundamentals and sophistication of the model provides valuable insights in the mechanical linkage of the hip and spine.

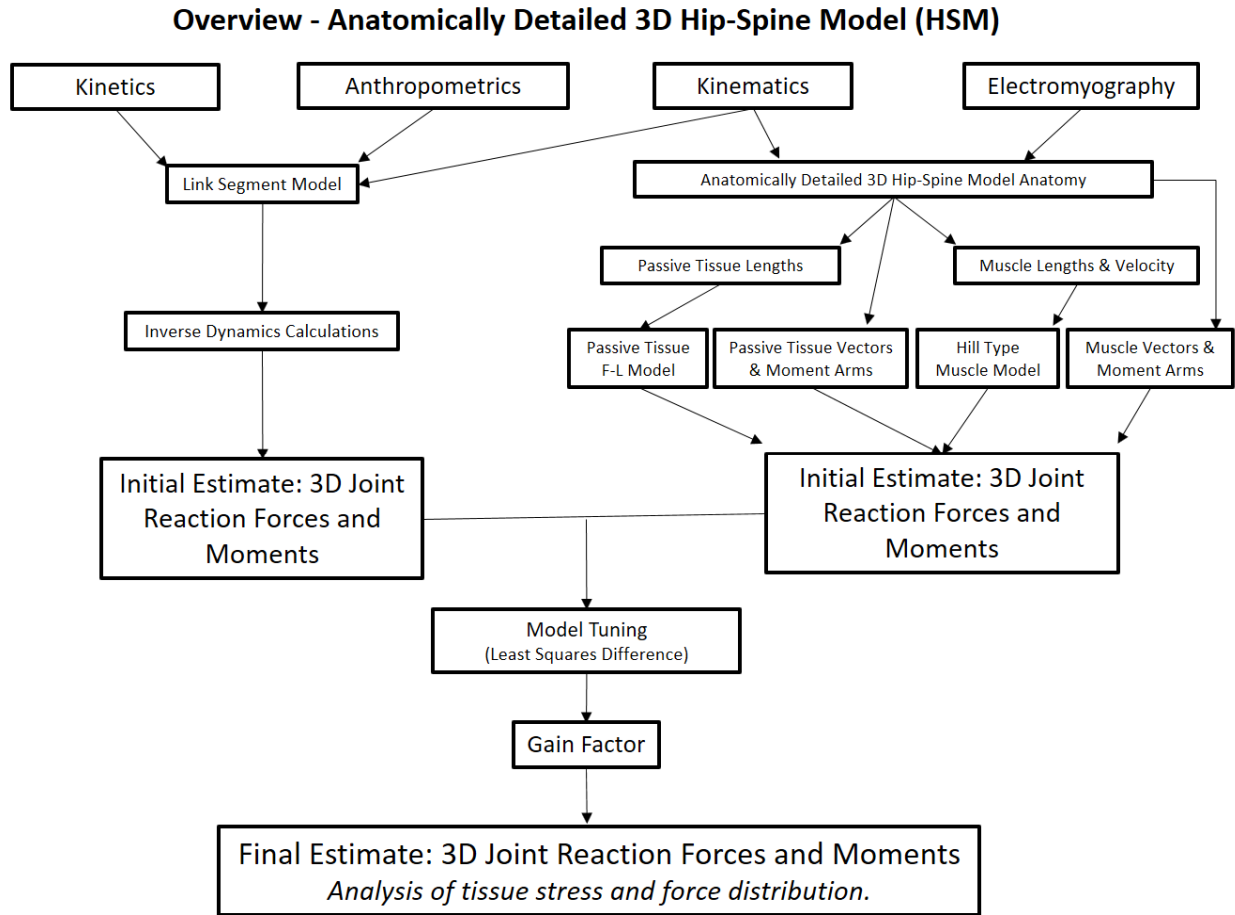


Figure 3.1: A schematic diagram of the HSM. Biological signals drive the anatomical detail (model parameters) found within the model which are used to estimate the joint reaction forces and moments.

3.1 Input Variables

Input variables are considered all of the biological signals which drive the model. These biological signals are recorded during the trial/task/activity for which the model is to be applied. Each of the input parameters are illustrated in Figure 3.1 across the top of the schematic of the model. Namely, the input variables are kinetics, anthropometrics, kinematics and electromyography. Here I will describe the variables directly related to the modelling procedures.

In some cases, there are pre-processing procedures required which are described in detail in appendix D, along with the data collection procedures to acquire these input signals.

3.1.1 Kinetics

Kinetic data, namely, the ground reaction force (GRF), provides inputs in the linked segment inverse dynamics modelling. Inverse dynamics is calculated using Visual 3D software from the data collected by Vicon Nexus software. The linked segment model data calculated reaction moments which are used to tune the EMG driven initial model estimations, providing model verification from this established modelling approach (Figure 3.1).

3.1.2 Anthropometrics

Anthropometrics are collected to support inverse dynamics calculations and serve as scaling factors for segment parameters in Visual 3D. Pelvis depth, chest depth and greater trochanter width, as well as, height and weight are all utilised to scale the segment parameters in the linked segment model.

3.1.3 Kinematics

The definitions of the joint orientation definitions are shown in Figure 3.2. Anatomical markers were placed on anatomical landmarks so that segments can be defined in 3D (Figure 3.3). Marker clusters were placed on each segment with 4 to 5 tracking markers per cluster. Markers were tracked and then labelled using Vicon Nexus software and segments are formed. Data was then imported to Visual 3D where kinematic segments and joints were defined and Euler rotations (Z, X, Y: Flex, Bend/AbAd, Twist/MedLat) were computed to calculate orthopaedic angles.

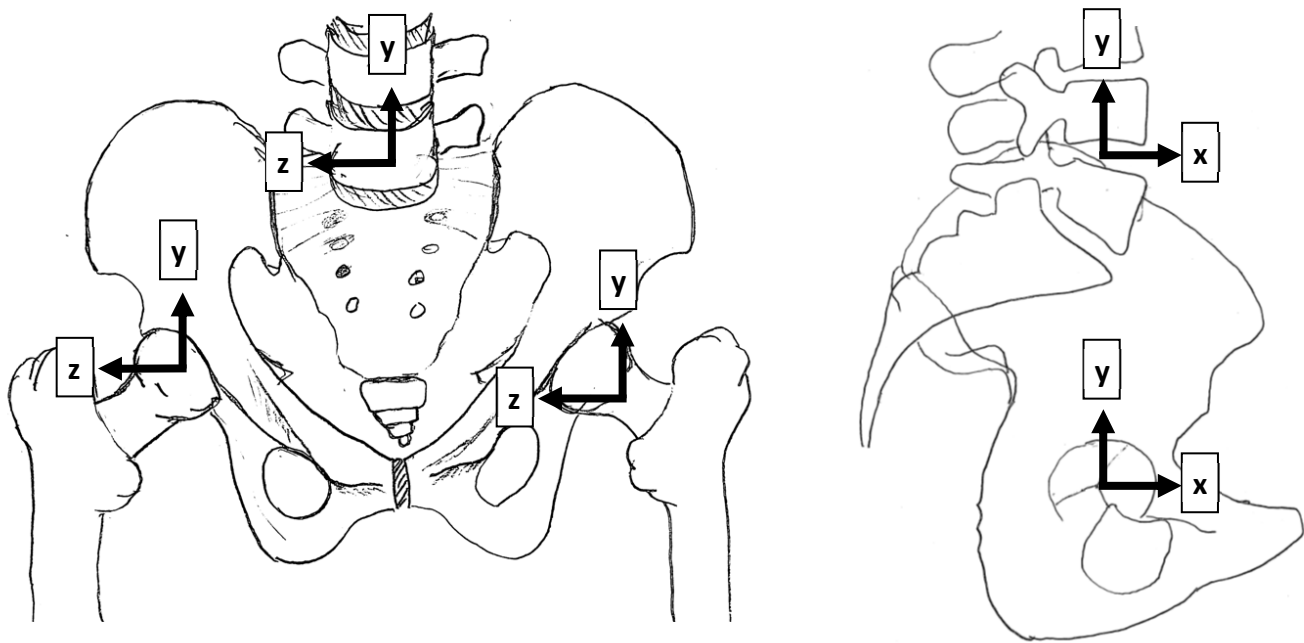


Figure 3.2: Schematic diagram of axis definitions for the spine and hip in two view, frontal and sagittal plans, in a right-hand coordinate system. Flexion occurs about the z axis, lateral bend of the spine and adduction of the hip occur about the x axis, while axial rotation (twist) occurs about the y axis.

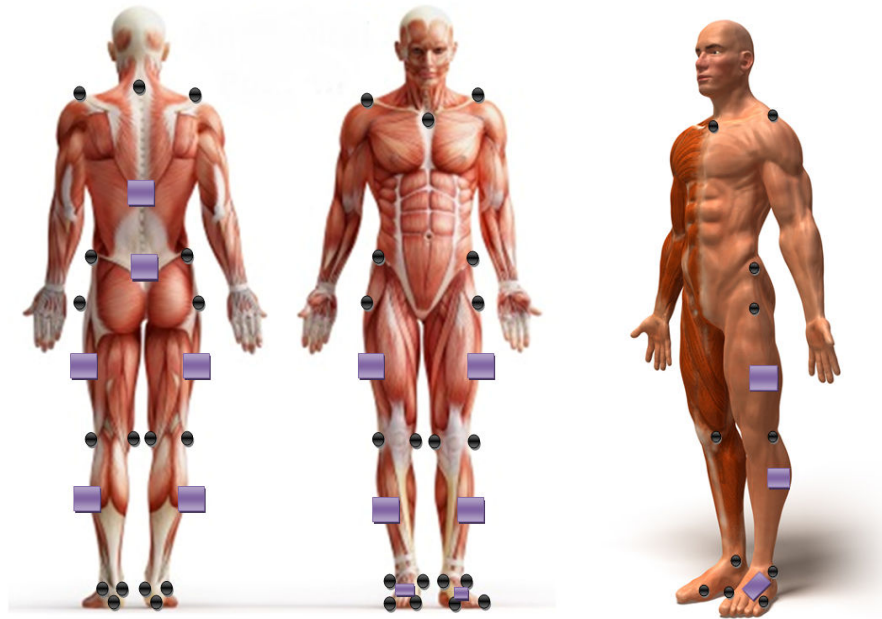


Figure 3.3: Reflective Marker Set-Up Anatomical  (Single) and marker cluster  (4-5) markers.

3.1.4 Electromyography

Myoelectric activity was recorded from 24 muscles of the spine and hip (Figure 3.4). The signals were processed using a custom MATLAB program. The signals were band pass filtered at 30-500 Hz, then DC bias was captured using quiet lying trial and removed from the motion trials, the signals were then full wave rectified (FWR), linear enveloped (2.5 Hz) and normalised to MVC trials (Figure 3.5). These signals then served as input variables into the HSM EMG-Force conversion calculations after McGill's approach in the spine model described in detail below.

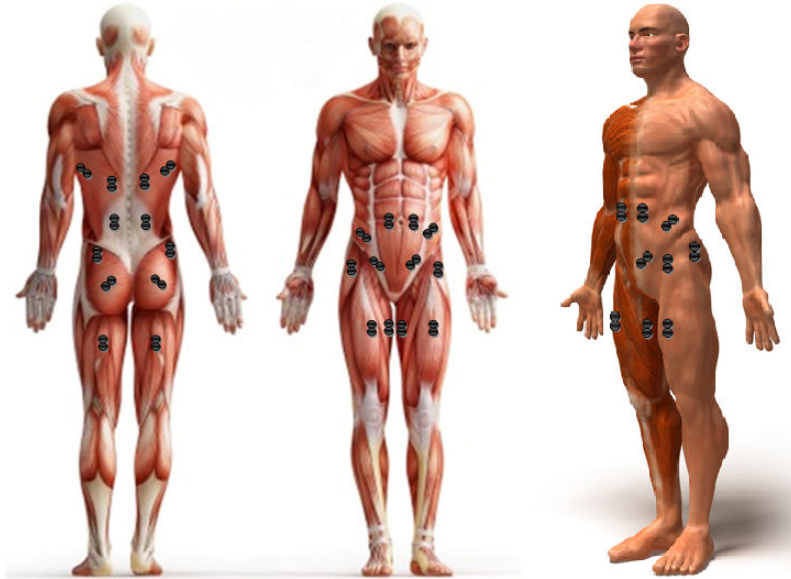


Figure 3.4: Twenty-Four EMG channels were collected including 6 bilateral core muscles (Rectus Abdominis (RA), External Oblique (EO), Internal Oblique (IO), Lower Erector Spinae (LES), Upper Erector Spinae (UES), and Latissimus Dorsi (LD)) and 6 bilateral hip/leg muscles (Rectus Femoris (RF), Tensor Fascia Latae (TFL), Gluteus Medius (GMed), Gluteus Maximus (GMax), Biceps Femoris (BF), and Adductor Longus (ADD)).

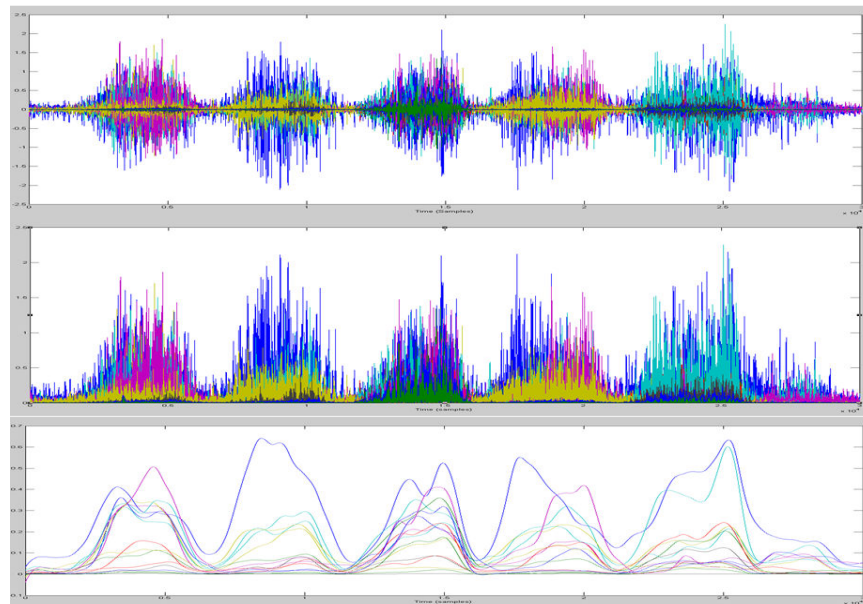


Figure 3.5: Custom MATLAB EMG processor normalized the EMG signals to a MVC for later force estimation calculations in the model. (Top) Raw EMG is filtered 30-500H and bias removed, then (Middle) full wave rectified (FWR) and low pass filtered (Bottom).

3.2 Model Parameters

Model parameters are predetermined equations, variables and data points which were used to define the anatomical characteristics and behaviours of the biological system. Detailed attachment sites for muscles and ligaments were incorporated from the evolved McGill dataset while the pelvis and lower limb data were adopted from the TLEM in Table 3.1 and appendix A.

Table 3.1: Bony Landmarks (cm)

Segment	Bony Landmark	X	Y	Z
Pelvis	<i>Anterior Superior Iliac Spine (R)</i>	14.16	15.58	13.35
	<i>Anterior Superior Iliac Spine (L)</i>	14.16	15.58	-12.88
	<i>Posterior Superior Iliac Spine (R)</i>	-0.93	15.38	4.67
	<i>Posterior Superior Iliac Spine (L)</i>	-0.74	15.77	-4.13
	<i>Public Tubercle (R)</i>	16.5	6.78	1.87
	<i>Pubic Tubercle (L)</i>	16.04	6.75	-2.88
Femur	<i>Greater Trochanter</i>	7.65	3.80	16.31
	<i>Medial Epicondyle</i>	10.40	-33.98	2.70
	<i>Lateral Epicondyle</i>	10.40	-33.44	12.49
Shank (Tibia)	<i>Medial Epicondyle</i>	10.41	-37.29	3.46
	<i>Lateral Epicondyle</i>	10.42	-37.06	12.02
	<i>Tibial Tuberosity *</i>	14.39	39.80	8.29
	<i>Fibular Head*</i>	8.60	-38.81	13.03
	<i>Medial Maleolus</i>	12.95	-72.72	3.42
	<i>Lateral Maleolus</i>	9.00	-74.59	9.87

*coordinate switched in original publication from TLEM was an error

3.2.1 Modified Skeletal Geometry

Several model enhancements and improvements were undertaken in the creation of the HSM. This section will outline in detail both the rationale and the improvement made in the enhanced datasets.

3.2.1.1 Correction of Fixation position back to Anatomical

Accurate anatomical data including skeletal, muscle and ligament geometry is critical to the development of an accurate model. This model was supported with two main sources of anatomical data; (1) the existing spine model, which has had several updates and refinements from the original version (Table 3.2); and, (2) the TLEM, which has laid out an in-depth and systematic description of model inputs for the pelvis and lower limb. The original McGill model (McGill & Norman, 1986) was developed based on a single source data set from archived radiographic records based on the 50th percentile from Dreyfuss (1966). Since this time several updates and improvements have been added in order to enhance the anatomical detail of the spine (Cholewicki et al., 1995; Grenier & McGill, 2007). In a sense, this thesis continued to develop this work through the expansion of the model to the hip joint with the TLEM.

In order to mesh the two data sets an off-set and a correction factor was applied to the TLEM for the pelvis and lower limb anatomical coordinates. First the off-set was created from the position of the hip-joint-center in the McGill data set 10.4, 6.8, and 7.6 for x, y and z, respectively. However, the z coordinated had to be altered based on the symmetry of the pelvis coordinates in the TLEM. The off-set for the z axis was based on the calculated mean of the mid sagittal location of the ASIS, PSIS and pubic tubercles (which was 9.205). The resulted in the adjusted off-set of 10.4 6.8, and 9.2, for x, y, and z, respectively. This improved the congruency of the relative position of the anatomical data when it was reflected (about the z axis) for the left side hip, femur and tibia. Next, a correction factor was created to adjust the anatomical data points in the TLEM dataset to a neutral position. A description of the anatomical correction factor for the fixation procedure has yet to be described or even discussed by others using this anatomical dataset

(Modenese et al. 2011a). The position of the femur relative to the pelvis was described as “externally rotated, the knee extended with the patella in the corresponding position and the foot in plantar flexion and supination” pp.240 (Horsman et al., 2007). However, when examining the data set and precisely analysing the anatomical data the hip was also flexed and abducted, while the knee was hyperextended and laterally rotated, only slightly. Therefore, a hip and knee a joint correction factor was applied to the dataset. The hip was rotated 12.47 degrees in extension, adducted 6.24 degrees and medially rotated 26.26 degrees. As shown in Figure 3.6 and Figure 3.7 this brought the femoral epicondyles into the same plane as the hip-joint-center.

The approach to the correction factor was justified by Dostal (1981), who dealt with a similar issue when using a non-articulated femur and defining anatomical attachment sites when constructing his muscle model. The femur was oriented in anatomical position by setting the mid-point between the medial and lateral femoral epicondyles to intersect with the vertical position of the hip joint center. This was deemed to be a reasonable assumption and the orientation of the femur was positioned in a similar manner here (see Figure 3.7). The tibial epicondyles were also aligned with the same assumptions and this left the medial and lateral malleoli straddling the frontal plane as one would expect in anatomical position. For the correction factor at the knee to achieve an anatomical position the shank needed to be rotated relative to the femur. The knee joint was rotated far less than that of the femur, the rotation was 5 degrees of flexion and 5 degrees of medial rotation. The meshed data set used in this model with the correction factor applied can be found in Tables 3.2, 3.3 a, b, c and 3.4 for the spine, hip, and hips-spine muscles, respectively.

3.2.2 Modified Muscle Parameters

Form and function are critical interrelated constructs in biomechanics. In order for muscles to function in a predictable way their anatomical relationships to the surrounding joint(s) must be maintained. This section outlines modifications made to muscle parameters to enhance the function of the muscles throughout the physiological range of motion thereby maintaining the expected muscle behaviour and relationship to the hip joint.

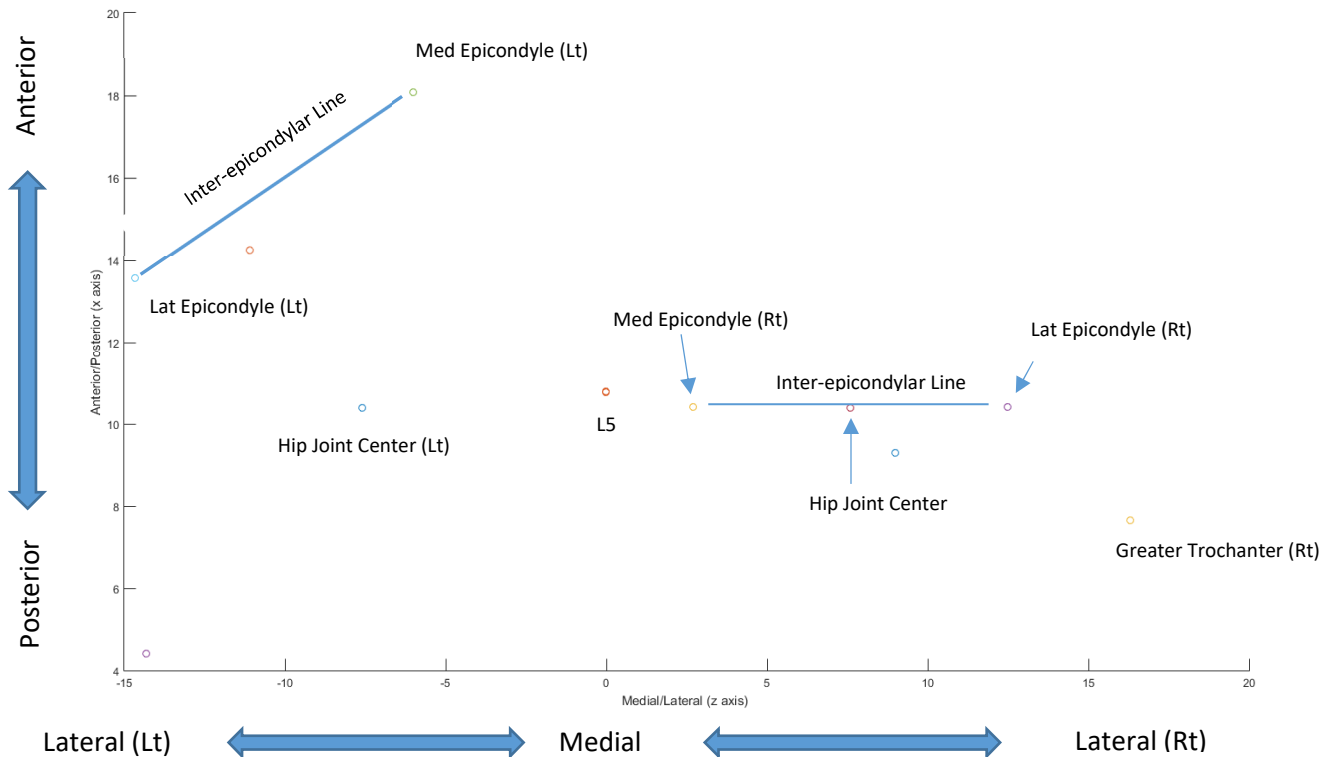


Figure 3.6: Correction factor for hip posture off-set in the TLEM as shown in the 2D axial plane view. The off-set accounts for the fixation posture of the cadaveric specimen during the fixation process. The magnitudes are 12.465 degrees of extension, 6.24 degrees of adduction, and 26.28 degrees of medial rotation. The mid-point of the femoral epicondyles is also graphed here however, it perfectly over lays the hip-joint-center and is therefore not visualized. Note: The left side is also shown here for comparison in the uncorrected position with the right side demonstrating the corrected posture. L5 = Fifth lumbar vertebra center.

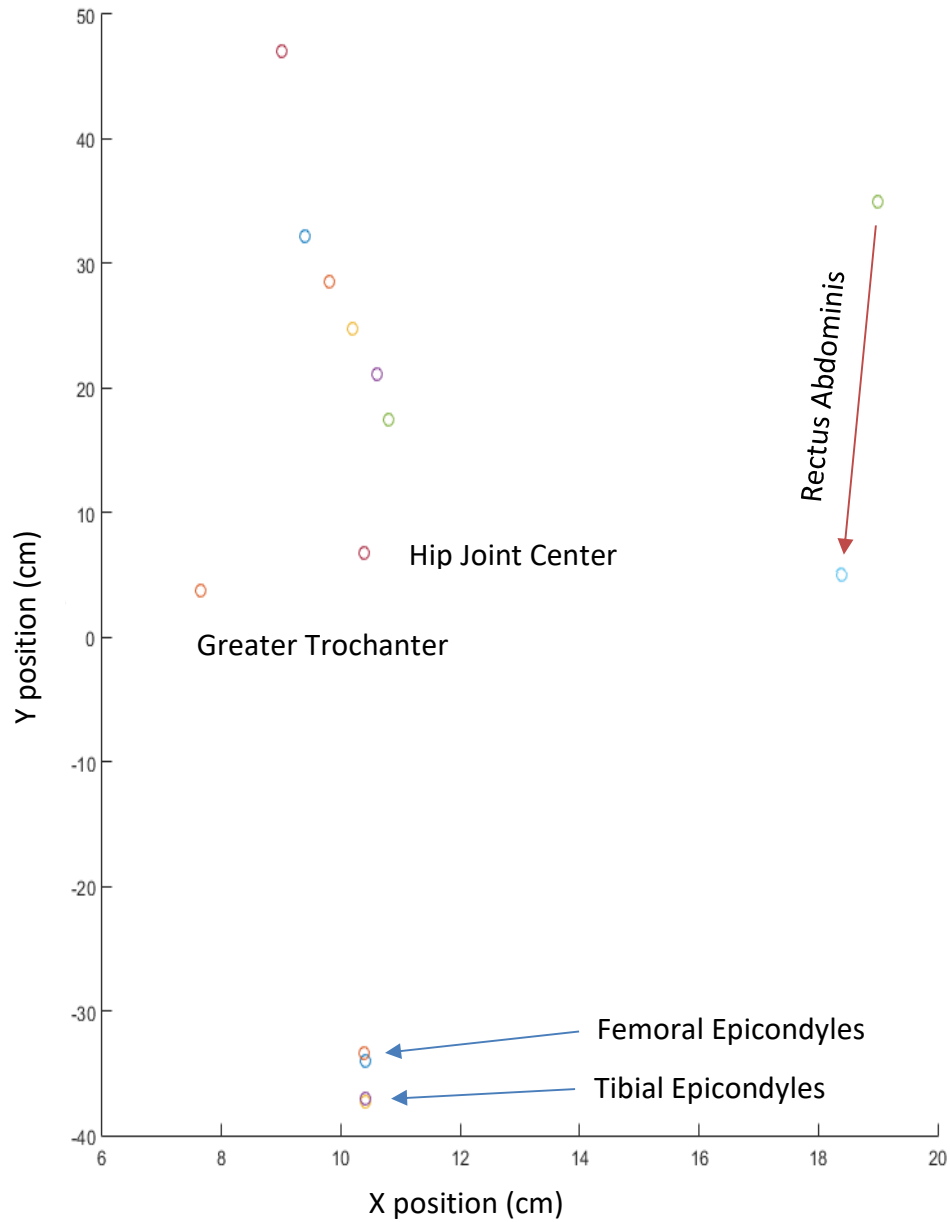


Figure 3.7: Correction factor for hip posture off-set in the TLEM as shown in the 2D sagittal plane view. The off-set accounts for the fixation posture of the cadaveric specimen during the fixation process. The magnitudes are 12.465 degrees of extension, 6.24 degrees of adduction, and 26.28 degrees of medial rotation. Note: The femoral and tibial epicondyles and the hip joint center are now aligned vertically. Rectus abdominis is shown as an example of a muscle and provides a relative reference point attaching on the inferior aspect of the rib cage and the pubic bone of the pelvis.

Table 3.2: Spine Muscle Attachments

Muscle (part)	#	Origin (cm)				Insertion (cm)			
		X	Y	Z	SEG	X	Y	Z	SEG
REC AB	1	18.4	5	3	Pelvis	19	35	4	RC
REC AB (AH) *	1	12.4	5	3	Pelvis	14	35	7	RC
EXT OBL	1	11	19	13	Pelvis	6	30	12.5	RC
	2	18.4	5	3	Pelvis	12.5	29	12.5	RC
IN OBL	1	9	21.5	12.5	Pelvis	15	29	11.5	RC
	2	16	16	12	Pelvis	19	38	0	RC
PARS LUMB	1	2.4	17.8	6	Pelvis	7.4	23.4	2.6	L4
	2	2.4	17.8	6	Pelvis	6.9	26.6	3	L3
	3	2.4	17.8	6	Pelvis	5.9	29.8	2.7	L2
	4	2.4	17.8	6	Pelvis	4.4	32.8	2.4	L1
ILIO LUMB	1	1.4	16.6	6.8	Pelvis	1.6	39	8.4	RC
LONG THOR	1	1.4	16.6	3.3	Pelvis	12	44	5	RC
	2	4	20.4	0.2	L5	2	53.5	2	RC
QUAD LUMB	1	6	21.4	9	Pelvis	3.5	35.5	7.2	RC
	2	6	21.4	9	Pelvis	4	33	3.6	L1
	3	6	21.4	9	Pelvis	5.2	30	3.8	L2
	4	6	21.4	9	Pelvis	6.2	26.8	3.8	L3
	5	6	21.4	9	Pelvis	7.2	23.8	4.4	L4
LAT	1	3.6	19.2	3	Pelvis	9	47	12	RC
	2	4.8	21.5	6	Pelvis	3.6	24.2	6.5	RC
MULT	1	2	13.8	1.5	Pelvis	4.1	21.5	0.5	L4
	2	2.6	18	3.6	Pelvis	4	24	0.5	L3
	3	2.6	18	3.6	Pelvis	3.2	26.9	0.5	L2
	4	2.6	18	3.6	Pelvis	2.2	30.2	0.5	L1
	5	5.8	19.1	1.5	L5	4	24	0.5	L3
	6	5.8	19.1	1.5	L5	3.2	26.9	0.5	L2
	7	5.8	19.1	1.5	L5	2.2	30.2	0.5	L1
TRANS AB (SP)	1	5	25	60	Pelvis	3.6	20.4	0	L5
	2	5	25	60	Pelvis	3.6	22.3	0	L4
	3	5	25	60	Pelvis	2.9	25.4	0	L3
	4	5	25	60	Pelvis	2.4	28	0	L2
TRANS AB (TVP)	5	5	25	60	Pelvis	7.9	19.8	3	L5
	6	5	25	60	Pelvis	6.8	23.2	3.4	L4
	7	5	25	60	Pelvis	6.8	25.4	3.8	L3
	8	5	25	60	Pelvis	6	29.6	3.8	L2

Ten Muscles and 34 (+1) Muscle Parts x 2 (Right and Left).

*Indicates modification based on anatomical variation (AH = abdominal hollowing).

Table 3.3a: Hip Muscles Attachments

Muscle (part)	#/ SEG	Origin (cm)			Insertion (cm)				
		X	Y	Z	SEG	X	Y	Z	SEG
AD BREV (PROX)	1	15.02	5.5	2.28	Pelvis	9.08	-1.27	11.49	Femur
	2	15.47	5.48	2.08	Pelvis	9.41	-2.54	11.34	Femur
AD BREV (MID)	3	14.97	4.98	1.59	Pelvis	9.58	-3.82	11.24	Femur
	4	15.33	4.96	1.42	Pelvis	9.64	-5.11	11.13	Femur
AD BREV (DIST)	5	14.26	4.23	0.86	Pelvis	9.69	-6.40	10.97	Femur
	6	14.49	4.22	0.75	Pelvis	9.82	-7.67	10.69	Femur
AD LONG	1	15.65	5.88	2.56	Pelvis	10.62	-10.82	9.84	Femur
	2	15.84	5.64	2.31	Pelvis	10.64	-12.03	9.56	Femur
	3	15.97	5.43	2.01	Pelvis	10.70	-13.27	9.34	Femur
	4	16.03	5.24	1.69	Pelvis	10.78	-14.53	9.15	Femur
	5	16.01	5.07	1.35	Pelvis	10.83	-15.77	8.92	Femur
	6	15.90	4.92	1.00	Pelvis	10.80	-16.98	8.63	Femur
AD MAG (DIST)*	1	8.30	-0.30	4.35	Pelvis	8.81	-29.33	4.36	Femur
	2	8.89	0.09	3.63	Pelvis	8.81	-29.33	4.36	Femur
	3	10.61	1.02	2.17	Pelvis	8.81	-29.33	4.36	Femur
AD MAG (MID)	1	7.61	-0.10	4.26	Pelvis	10.39	-13.25	9.49	Femur
	2	7.90	0.12	4.67	Pelvis	10.39	-13.25	9.49	Femur
	3	8.28	0.20	3.67	Pelvis	10.46	-16.38	8.72	Femur
	4	8.53	0.38	4.02	Pelvis	10.46	-16.38	8.72	Femur
	5	9.15	0.59	2.96	Pelvis	10.62	-19.56	8.30	Femur
	6	9.34	0.73	3.22	Pelvis	10.62	-19.56	8.30	Femur
AD MAG (PROX)	1	12.26	2.30	1.46	Pelvis	10.23	-3.98	10.39	Femur
	2	10.79	1.47	2.44	Pelvis	10.34	-6.05	10.14	Femur
	3	11.53	1.88	1.95	Pelvis	10.52	-8.13	9.89	Femur
	4	12.26	2.30	1.46	Pelvis	10.66	-10.20	9.64	Femur
BICEPS FEM (LH)	1	6.62	0.71	7.49	Pelvis	8.63	-38.31	12.34	Tibia
GEM (INF)	1	3.90	2.75	6.34	Pelvis	10.28	7.48	14.31	Femur
GEM (SUP)	1	4.84	7.66	4.18	Pelvis	10.90	6.56	13.30	Femur
GLUT MAX (SUP)	1	2.49	14.57	7.63	Pelvis	11.73	12.21	17.52	Femur
	2	1.42	12.31	5.74	Pelvis	11.13	9.00	17.88	Femur
	3	0.76	9.53	4.19	Pelvis	10.47	6.34	18.30	Femur
	4	1.27	15.71	6.52	Pelvis	13.24	11.59	17.01	Femur
	5	0.07	13.57	4.51	Pelvis	12.73	8.61	17.35	Femur
	6	-0.54	10.74	3.01	Pelvis	11.97	5.72	17.79	Femur
GLUT MAX (INF)	1	-0.34	5.97	1.68	Pelvis	6.99	0.44	15.20	Femur
	2	0.53	5.31	1.89	Pelvis	7.13	-0.91	14.67	Femur
	3	1.35	4.24	1.85	Pelvis	7.85	-3.42	13.71	Femur
	4	0.15	6.64	2.34	Pelvis	6.99	0.44	15.20	Femur
	5	1.02	5.98	2.55	Pelvis	7.13	-0.91	14.67	Femur
	6	1.75	4.80	2.40	Pelvis	7.85	-3.42	13.71	Femur

*Error in the TLEM the coordinates were corrected. The Adductor tubercle is the distal attachment of the Adductor Magnus (distal segment) which is on the superior pole of the medial epicondyle of the femur. The coordinates given match the correct anatomical position it was erroneously assigned to the Tibia.

Table 3.3b: Hip Muscles Origination on the Pelvis (Con't)

Muscle (part)	#/ SEG	Origin (cm)			SEG	Insertion (cm)			SEG
		X	Y	Z		X	Y	Z	
GLUT MED (ANT)	1	10.80	16.28	13.66	Pelvis	11.04	6.39	15.66	Femur
	2	11.83	15.83	13.76	Pelvis	11.82	6.01	15.57	Femur
	3	12.89	15.83	13.76	Pelvis	12.53	5.73	15.45	Femur
	4	11.33	16.75	14.42	Pelvis	10.77	5.61	16.08	Femur
	5	12.20	16.16	14.29	Pelvis	11.46	5.03	16.09	Femur
	6	13.21	15.27	13.92	Pelvis	12.16	4.76	15.97	Femur
GLUT MED (POST)	1	6.52	18.67	11.71	Pelvis	9.88	7.82	14.79	Femur
	2	4.38	16.95	8.79	Pelvis	9.51	7.89	14.39	Femur
	3	3.58	14.01	6.89	Pelvis	9.14	7.88	14.18	Femur
	4	5.59	20.26	11.27	Pelvis	9.88	7.82	14.79	Femur
	5	3.06	19.21	8.17	Pelvis	9.31	7.47	15.23	Femur
	6	1.99	16.73	6.14	Pelvis	8.94	7.43	15.06	Femur
GLUT MIN (ANT)	1	10.32	14.69	12.51	Pelvis	12.19	4.07	15.20	Femur
GLUT MIN (MID)	1	8.14	14.35	10.93	Pelvis	12.19	4.07	15.20	Femur
GLUT MIN (POST)	1	6.37	13.31	9.27	Pelvis	12.19	4.07	15.20	Femur
GRACILIS	1	12.05	1.92	1.81	Pelvis	11.32	-41.58	5.38	Tibia
	2	14.07	3.34	1.22	Pelvis	11.32	-41.58	5.38	Tibia
ILIACUS (LAT)	1	7.45	20.03	11.95	Pelvis	8.49	2.12	10.42	Femur
	2	9.27	18.28	12.12	Pelvis	8.49	2.12	10.42	Femur
	3	10.06	16.81	11.98	Pelvis	8.49	2.12	10.42	Femur
ILIACUS (MID)	1	4.82	20.34	9.23	Pelvis	8.49	2.12	10.42	Femur
	2	6.08	17.83	8.99	Pelvis	8.49	2.12	10.42	Femur
	3	7.32	15.41	8.82	Pelvis	8.49	2.12	10.42	Femur
ILIACUS (MED)	1	5.13	19.55	5.30	Pelvis	8.49	2.12	10.42	Femur
	2	5.73	17.57	5.69	Pelvis	8.49	2.12	10.42	Femur
	3	6.72	14.93	5.59	Pelvis	8.49	2.12	10.42	Femur
OBT EXT INF	1	10.36	1.97	2.45	Pelvis	7.62	1.91	13.54	Femur
	2	12.29	2.85	1.22	Pelvis	7.62	1.91	13.54	Femur
OBT EXT SUP	1	14.28	5.03	1.18	Pelvis	9.39	5.86	12.71	Femur
	2	12.51	3.54	1.48	Pelvis	9.39	5.86	12.71	Femur
	3	10.36	2.47	2.33	Pelvis	9.39	5.86	12.71	Femur
OBT INT	1	8.18	8.99	5.01	Pelvis	10.59	7.02	13.81	Femur
	2	8.42	7.15	4.28	Pelvis	10.59	7.02	13.81	Femur
	3	9.47	5.52	3.30	Pelvis	10.59	7.02	13.81	Femur
PECTINEUS	1	13.87	8.18	4.07	Pelvis	9.10	-0.60	11.27	Femur
	2	14.37	7.83	3.72	Pelvis	9.12	-1.48	11.20	Femur
	3	14.87	7.47	3.72	Pelvis	9.13	-2.36	11.14	Femur
	4	15.37	7.12	3.02	Pelvis	9.10	-0.60	11.27	Femur
PIRIFORMIS	1	0.33	9.11	1.78	Pelvis	9.43	7.93	13.05	Femur

Table 3.3c: Hip Muscles Origination on the Pelvis (Con't)

Muscle (part)	#/ SEG	Origin (cm)			Seg.	Insertion (cm)			Seg.
		X	Y	Z		X	Y	Z	
QUAD FEM	1	9.50	1.82	2.90	Pelvis	7.96	4.96	13.64	Femur
	2	8.86	1.56	3.70	Pelvis	7.92	4.18	13.68	Femur
	3	8.23	1.30	4.51	Pelvis	7.88	3.39	13.70	Femur
	4	7.60	1.04	5.31	Pelvis	7.84	2.60	13.73	Femur
REC FEM	1	13.42	11.07	11.23	Pelvis	15.06	-31.47	6.83	Patella
	2	13.42	11.07	11.23	Pelvis	15.06	-31.47	6.83	Patella
SARTORIUS	1	13.60	14.29	12.70	Pelvis	11.61	-41.19	5.36	Tibia
	2	13.60	14.29	12.70	Pelvis	11.61	-41.19	5.36	Tibia
SEMIMEM	1	7.60	0.19	7.17	Pelvis	6.88	-36.51	4.62	Tibia
SEMITEN	1	6.37	0.73	6.42	Pelvis	10.59	-42.58	5.17	Tibia
TFL	1	13.23	14.79	13.96	Pelvis	11.97	-32.24	11.56	Tibia
	2	12.77	15.81	14.33	Pelvis	11.97	-32.24	11.56	Tibia

Table 3.4: Muscle crossing the hip and spine.

Muscle (part)	#	Origin (cm)			SEG	Insertion (cm)			SEG
		X	Y	Z		X	Y	Z	
PSOAS	1	10.2	16.8	5	L5	8.5	2.12	10.42	Femur
	2	10.6	23	2.3	L4	8.5	2.12	10.42	Femur
	3	10.1	26.7	2.1	L3	8.5	2.12	10.42	Femur
	4	9.1	30.5	2	L2	8.5	2.12	10.42	Femur
	5	8.8	33.6	1.9	L1	8.5	2.12	10.42	Femur

3.2.2.1 Muscle Wrapping and Geodesics

In order to maintain anatomical relationships and muscle functions, such as muscles which follow a curved path, additional wrapping points were required. The spine model and the TLEM data set utilized numerous via points to ensure anatomical relationships of the muscle paths. A list of muscle via points for the spine and hip muscles can be found in Table 3.5. These via points (sometimes referred to as nodal points) help maintain the anatomical relationship to ensure

appropriate muscle function. For example, with a high degree of joint movement straight line muscles from origin to insertion may cross or flip to the opposite side of the joint, thereby, changing muscle function. Via points are used to maintain the anatomical relationship and relative anatomical constraints from other muscles, ligaments, bony surfaces and fascia. However, these were not always sufficient for all muscles in the TLEM, especially when testing full ranges of motion. The main areas of concern were the muscle segments most proximal to the hip. Research by Aronld et al. (2000) have examined the erroneous moment arm values when wrapping is not considered. They used a similar technique to that used in the current model and their data showed a high level of congruency with experimental cadaveric data. Therefore, geodesics, specifically spherical wrapping techniques, were added to this model to improve the biofidelity of muscle parameters and maintain expected muscle functional properties. The effect of adding wrapping spheres to some of the hip muscles resulted in altering the muscle length estimations since the muscle now followed a longer path. These length changes also altered the force estimates, as normalised muscle length augments model predicted force, details are outlined in the next section 3.2.2.2 Modified Muscle Rest Lengths & Sensitivity Testing.

3.2.2.1.1 Psoas Major

A sphere was used to wrap psoas major and iliacus muscle around the pelvis and hip bony anatomy. The same sphere for both muscles was positioned at the hip joint center (10.4, 6.8, 9.205) with a radius of 3.5 cm. The pelvis hybrid node was the suprajacent point prior to contacting the sphere. This point was used in order to maintain the contact point on the superior ramus of the pubic bone. Thick connective fascia and the inguinal ligaments hold the psoas major muscle/tendon in place as it wraps around the bony pelvis. At the inferior end the muscle freely

releases from the sphere to the femoral attachment in a straight line to the muscles' distal attachment (insertion) on the lesser trochanter of the femur. The psoas major and the iliacus share a similar function at their distal end, since the point before and after the sphere, the pelvis node and lesser trochanter of the femur, respectively. However, only the psoas crosses into the spine making these two muscles as a whole very different in the functional abilities when considering the integration of the hip and spine. Iliacus is a hip flexor, but psoas has a more complex role to stabilize the spine and pelvis – these functional differences can now be quantified in detail with the development of this model.

The geodesics of the wrapping sphere are used to improve muscle length estimation. The length of the arc segments on the sphere are calculated by dividing the arc into 100 points and calculating the straight-line distances of each segment along the entire wrapping arc. The wrapping sphere engages with the muscle/tendon of psoas from full extension to 63° of flexion. Past 63° of flexion the muscle/tendon travels directly to the femoral attachment (lesser trochanter) from the pelvis node (the arch suprajacent to the superior pubic ramus). Notice this maintains approximation with superior ramus, where there is an extensive fascia as well as the inguinal ligament surrounding the psoas major and iliacus muscle/tendon as it passes through the iliopectineal arch under the inguinal ligament (Moore & Dalley 2006). The psoas and iliacus muscles in the new orientation can be visualised in Figures 3.8-3.9 (psoas) and 3.10 (iliacus).

Table 3.5: Muscle Via Points

Muscle (part)	#	Location (cm)			
		X	Y	Z	SEG
EXT OBL 2	1	18.72	21.2	3.54	L4
INT OBL 2	1	18.78	24.2	3.64	L4
LAT 1 (SAC)	1	3.6	24.2	6.5	RC
PSOAS	1	8	32	4.6	L1
	2	9.4	28.8	4.7	L2
	3	10.3	25	4.8	L3
	4	10.5	21.5	4.9	L4
	5	10.2	16.8	5	L5
*PSOAS	6	14.87	7.47	8.17	Pelvis
*ILIACUS	1	14.87	7.47	8.17	Pelvis
OBT EXT SUP	1	9.64	3.69	10.19	Femur
SAR (PROX)	1	13.71	-4.29	5.65	Femur
	2	14.08	-12.94	6.05	Femur
	3	13.67	-13.85	5.74	Femur
	4	13.23	-15.25	5.29	Femur
	5	12.59	-16.20	4.98	Femur
	6	11.83	-17.32	4.72	Femur
	7	11.26	-18.39	4.36	Femur
	8	10.81	-19.58	4.28	Femur
	9	10.30	-20.87	4.10	Femur
	10	9.99	-22.30	3.92	Femur
	11	9.77	-23.76	3.70	Femur
	12	9.42	-25.18	3.43	Femur
	13	9.37	-25.47	3.43	Femur
SAR (DIST)	1	-7.66	-33.13	0.45	Femur
GRACILIS	1	8.13	-36.96	3.67	Tibia
	2	8.77	-37.76	3.81	Tibia
	3	8.85	-37.78	3.76	Tibia
	4	9.41	-38.07	3.75	Tibia
	5	9.94	-38.77	4.08	Tibia
	6	10.03	-38.78	4.03	Tibia
	7	10.99	-39.46	4.69	Tibia
	8	11.87	-39.92	5.40	Tibia
SEMITEN	1	5.91	-36.03	5.33	Tibia
	2	6.04	-36.74	5.21	Tibia
	3	6.66	-37.54	5.13	Tibia
	4	7.41	-38.46	5.08	Tibia
	5	8.04	-39.07	5.00	Tibia
	6	8.46	-39.53	4.95	Tibia
	7	8.75	-40.18	5.09	Tibia

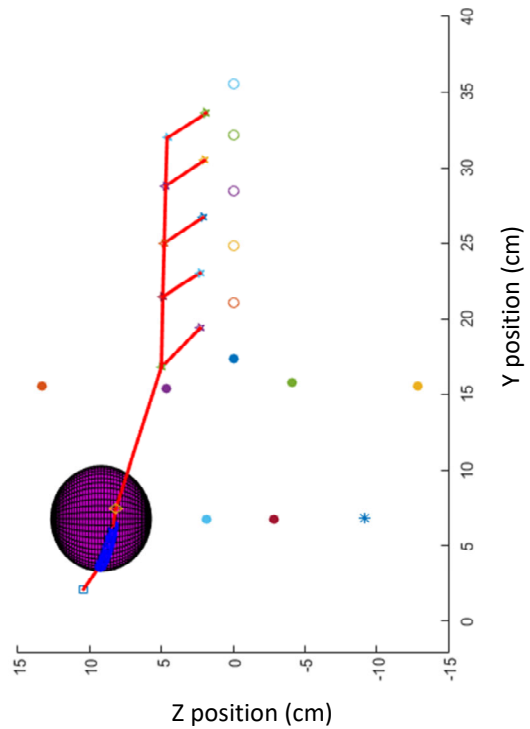
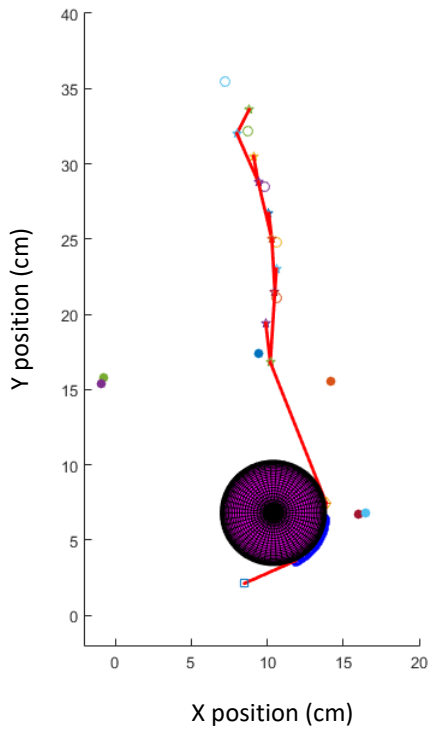
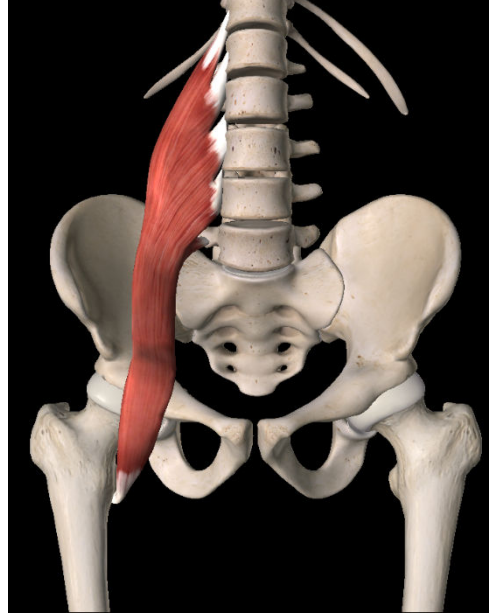


Figure 3.8: Sagittal view (left) and frontal view (right) of psoas major with an anatomical representation (top) and the model 3D point representation (bottom) with spherical warping object and wrapping points in anatomical position (right side only displayed).

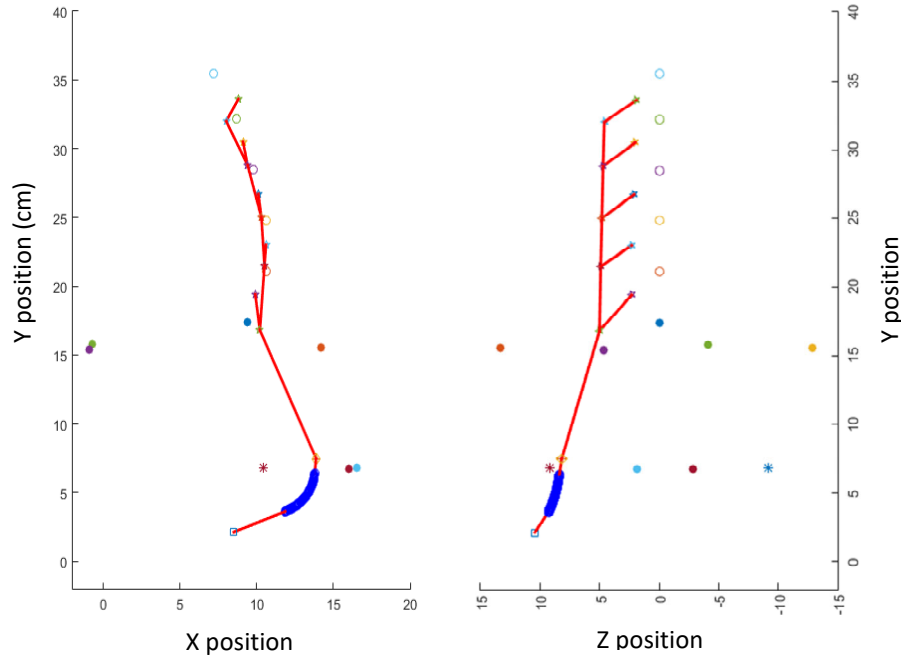


Figure 3.9: Sagittal view (left) and frontal view (right) of psoas major with spherical warping points in anatomical position (right side muscle displayed).

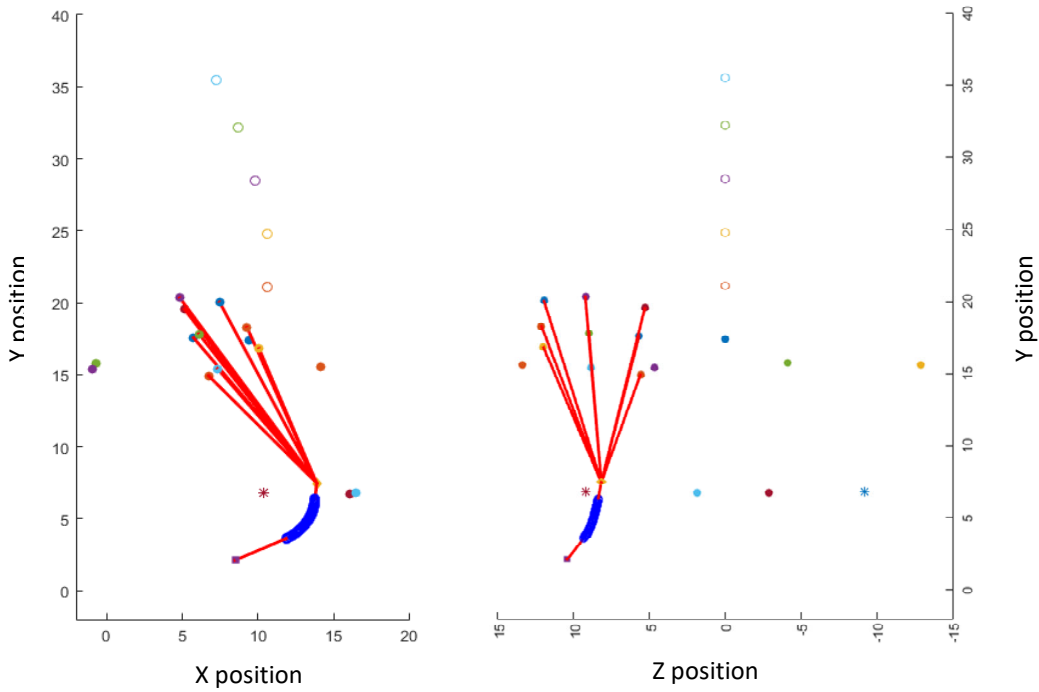


Figure 3.10: Iliacus with its 6 proximal segments on the ilium passing through the common psoas and iliacus via point prior to wrapping around the hip/pelvis sphere and attaching to the lesser trochanter of the femur (right side only displayed).

3.2.2.1.2 Gluteus Maximus

The earlier attempts to model GMAX have been over simplified with a single muscle path and element (Dostal & Andrews 1981). Several researchers have better represented this muscle with enhanced the complexity of GMAX modelling assumptions by adding more segments (Arnold et al. 2010), or addition via points for more complex muscles paths (Blemker & Delp 2005) and this approach builds on the enhancement of muscle complexity – straight line assumptions are not biological for this muscle. As shown in Figure 3.11 the GMax is a robust muscle and large in overall size – this characteristic require consideration from the straight-line assumptions of previous work. Examining the effects of ROM on GMAX, there were clearly issues in the flexion range as the muscle force continued to increase due to passive resistance, however the moment was decreasing (Figure 3.12). This was a non-physiological change in higher degrees of flexion as the moment arm was decreasing to unrealistically small lengths with hip flexion because there were no via points or wrapping geodesics to maintain anatomical relationships. A series of wrapping spheres were added to model to allow gluteus maximus inferior sections to wrap around the contours of the bony pelvis and the deeper layers of the muscle. The corrected lengths are shown in Figure 3.13. Semitendinosus and semimembranosus served as reference points to identify the placement of the sphere. A small sphere simulated the size and shape of the ischial tuberosities, and sacrotuberous ligament to enhance the anatomical relationships of this muscle.

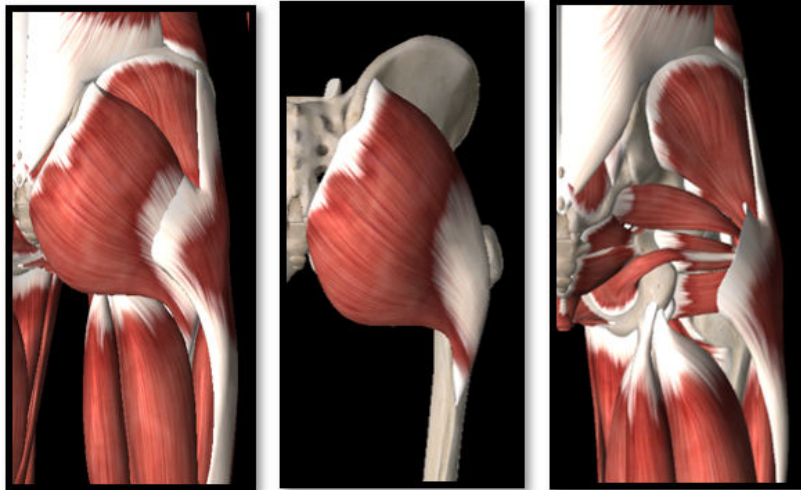


Figure 3.11: Gluteus maximus as it passes posterior to the hamstring group and ischial tuberosity.

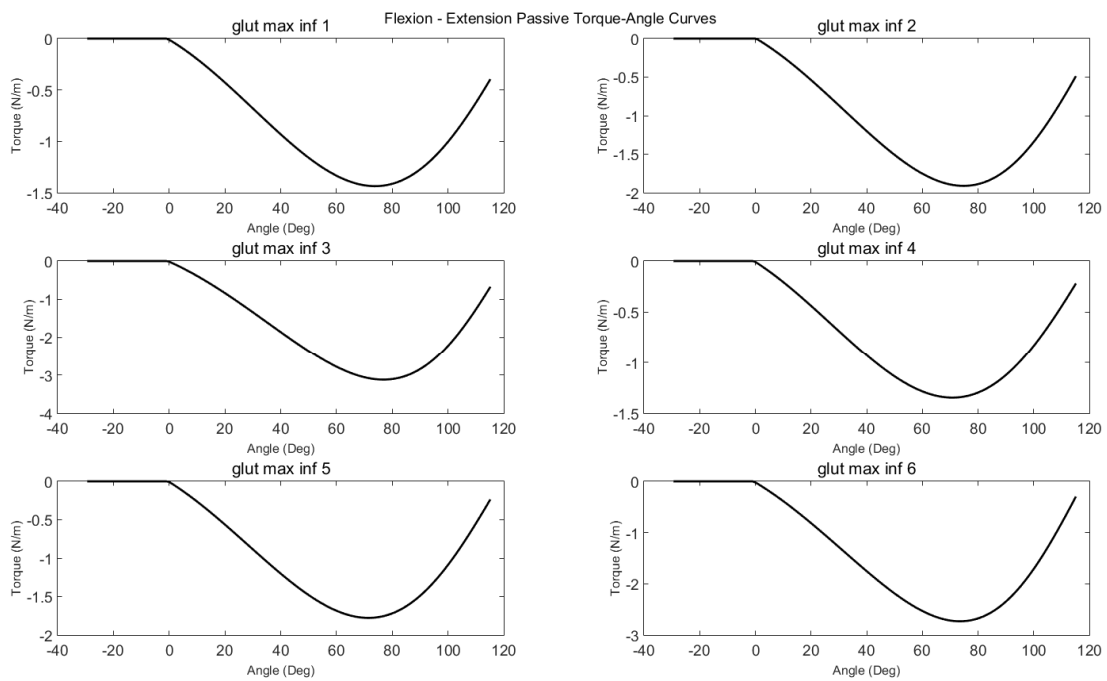


Figure 3.12: Gluteus maximus inferior reduces its moment arm to non-physiological amounts above ~70 degrees. (Extension is negative – flexion is positive, moments are calculated in flexion-extension plane.)

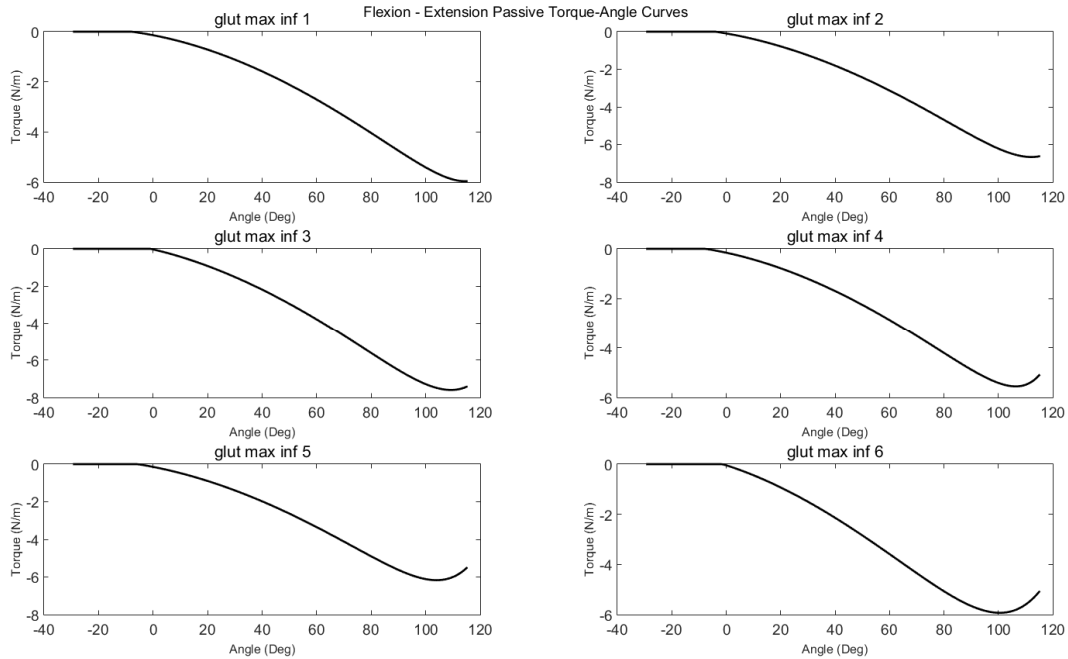


Figure 3.13: Gluteus maximus inferior was wrapped to provide realistic anatomical muscle mapping. (Extension is negative – flexion is positive, moments are calculated in flexion-extension plane.)

3.2.2.1.3 The Hamstrings.

Semitendinosus, semimembranosus and biceps femoris form the hamstrings group. They each have respective attachments on the posterior aspect of ischial tuberosity and arduous muscle paths at the distal end wrapping around the knee. These are modelled with via points to maintain anatomical relationships and preserve biomechanical function. At high levels of flexion, the straight-line path at the proximal end of the muscles violate reasonable assumptions of anatomy at the hip joint. The bony pelvis and ligamentous structures provide contours by which these two muscles navigate around – not through. Therefore, a geodesic wrapping sphere was used to wrap these three muscles when they are presumed to interact with the underlying boney and ligamentous anatomy of the ischial tuberosity and pelvis. The effects of these changes illustrated in Figures 3.15 – 3.17.

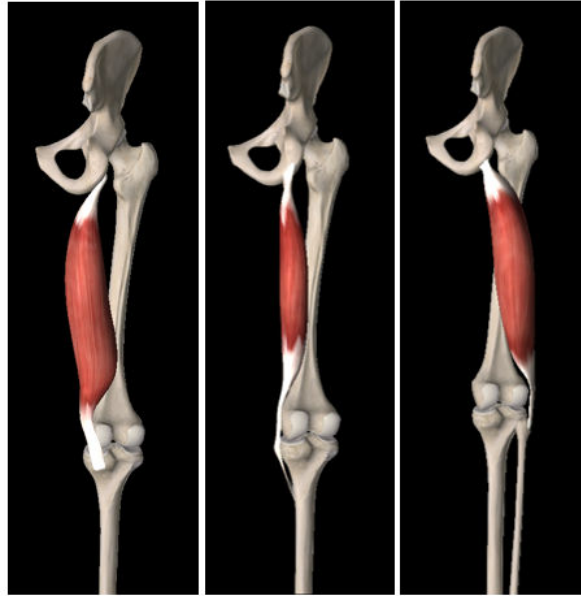


Figure 3.14: Semimembranosus (left), Semitendinosus (middle) and Biceps Femoris Long Head (right) each muscle was wrapped around the inferior margin of a sphere which represented the ischial tuberosity, the bony pelvis and the extensive ligamentous structures present in vivo.

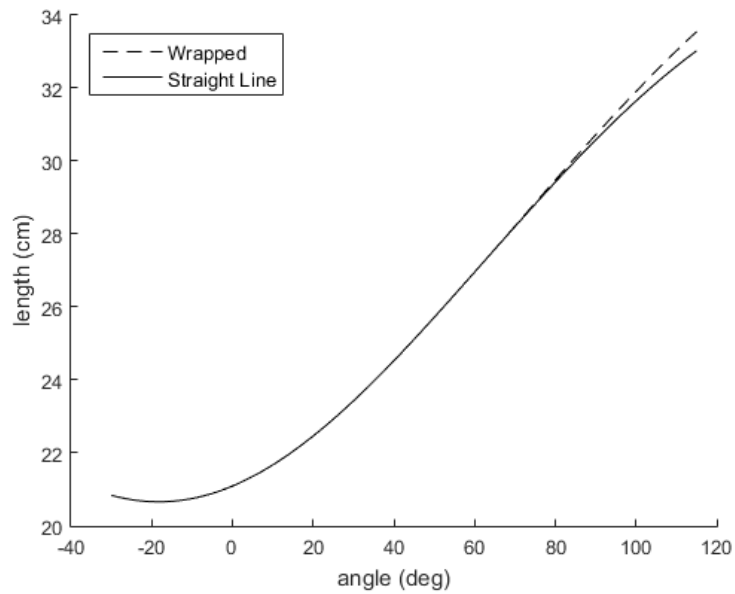


Figure 3.15: The effect of wrapping on changes in length for semimembranosus. Wrapping begins at 45 degrees of hip flexion and continues until terminal flexion.

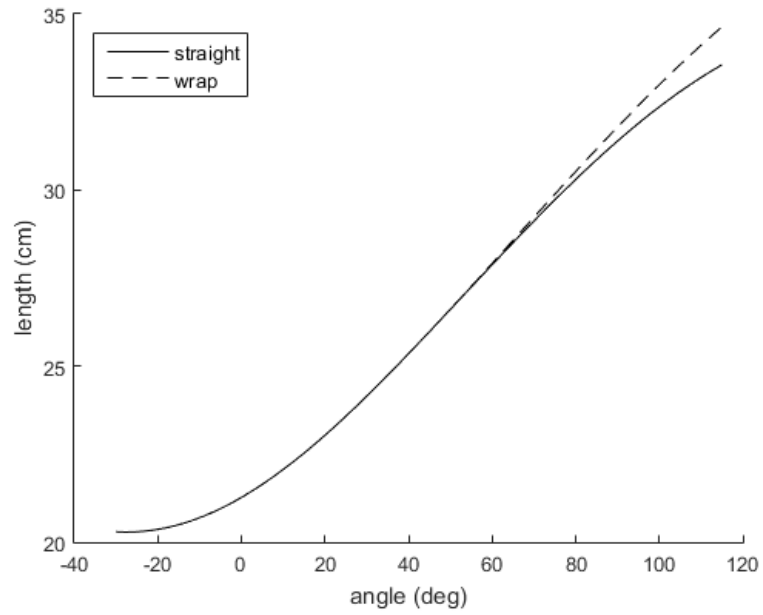


Figure 3.16: The effect of wrapping on changes in length for semitendinosus. Wrapping begins at 45 degrees of hip flexion and continues until terminal flexion.

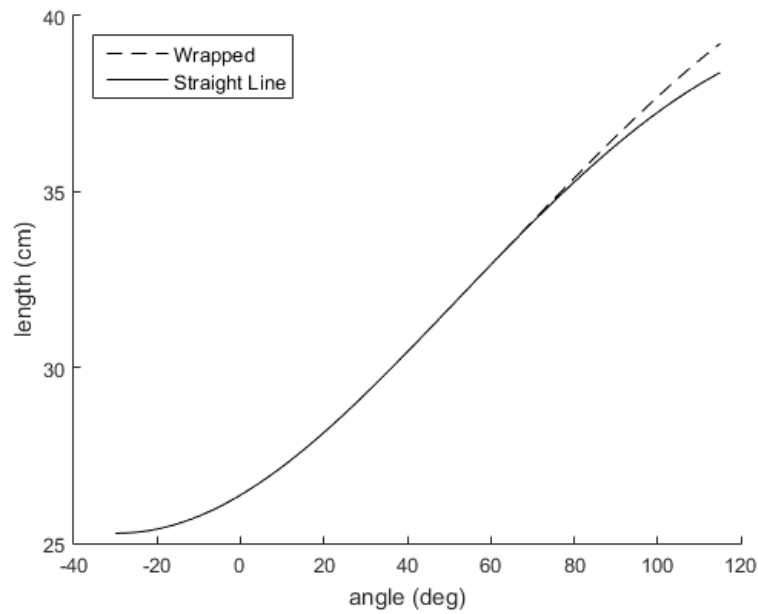


Figure 3.17: The effect of wrapping on changes in length for biceps femoris. Wrapping begins at 59 degrees of hip flexion and continues until terminal flexion.

3.2.2.2 Modified Muscle Rest Lengths & Sensitivity Testing

Initial evaluation the model performance during simulated movements identified critical errors in the original TLEM with respect to muscle lengths. Unfortunately, several groups have used this data set and no corrections were reported in the literature that this author was able to identify. Typically, these issues are considered less important because optimization procedures are used rather than a biologically driven approaches such as the approach used here. No current dataset exists which has experimentally defined optimal muscle length relationships for the hip muscles. The approach used here was similar to the initial development of the Spine model – all muscles were set to anatomical length as a default “optimal muscle rest length”. When re-examining the functional range of motion nearly all muscles were brought the physiological operating range within a physiologically appropriate range based on muscle mechanics. However, some sections of some muscles were still operating beyond a physiological range (these will be discussed by muscle in the following subsections). While some Researchers (Modenese 2016) have provide initial attempts to establish muscle parameters from both subject specific imaging and scaling factors from available datasets these are typically done by groups interested in gait and therefore only validated in relatively small ranges of motion required during gait (for example: -34 to 39 degrees of flexion/extension, -15 to 9 degrees of abduction/adduction). In this analysis muscle segments were observed over a full physiological range from 30 degrees of extension to 115 degrees of flexion, as well as 40 degrees of abduction and 40 degrees of adduction, to test the operational range this model will operate within. The objective of the optimal length correction was to maintain the muscle length within the physiological range of ~0.5 to ~1.6 rest lengths and with a preferred goal of ~0.8 to ~1.3 rest

lengths. Hence, modification of the muscle optimal length was required to enhance the biofidelity of the HSM. This assumption will need to be addressed in the ongoing development of the model; however, for the time being it will provide a more feasible solution for rest lengths.

3.2.2.2.1 Adductor Magnus

In this muscle the anatomical position was nearly “shortest” length the muscle would achieve. Adduction would only slightly shorten this muscle and extension would shorten it to a point and then lengthen it once again and clearly flexion and abduction would significantly lengthen the muscle. Illustrated in Table 3.6 are the muscle parameters modified in this work. Examples of the modifications which prevent violations in muscle function are illustrated in Figures 3.18 and 3.19, the adjusted length to a physiological range for those muscle still operating outside the expected physiological range. Note the non-physiological length predictions from the TLEM data set and the initial and secondary attempts to address these issues. Increments no smaller than 1 cm were used to adjust the optimal length within the ideal operational zone. This has rendered new “estimated optimal rest length” measures which are used in this model and reported in Table 3.6.

3.2.2.2.2 Iliacus

Setting muscle length to anatomical length provided little to no passive resistance contribution from iliacus. This is most improbable and therefore muscle rest lengths for this muscle were re-estimated based on the muscle length at 30 degrees of flexion, or the edge barrier of the neutral zone. Except for iliacus medial sections 2 and 3 which were better represented at rest lengths calculated with the hip in 15 degrees of hip flexion and anatomical position, respectively. This provided muscle lengths which contributed to passive resistance in

hip extension with more appropriate physiological behaviour (see Figure 3.20). The assumption here is that these muscles contribute to passive resistance during hip extension. Like adductor magnus the goal of these physiological estimates was to improve the physiological representation of the muscle function. This analysis was done in conjunction with the next chapter – inherently justifying the assumptions used here with experimental data.

Table 3.6: Modified muscle parameters from the TLEM data set based on physiological muscle length operating range over a physiological range of motion.

Muscle	TLEM OptLen	TLEM TenLen	Anatomical Length	Flex/Ext Range	Ab/Ad Range	Estimated Optimal Rest Length
Ad_Mag_Dist_1	10.8	4.2	24.8	28.8	26.8	28.8
Ad_Mag_Dist_2	10.8	4.2	25.2	29.2	-	25.2
Ad_Mag_Dist_3	10.8	4.2	26.3	28.3	-	26.3
Ad_Mag_Mid_1	10.4	0	14.4	19.4	-	19.4
Ad_Mag_Mid_2	10.4	0	14.4	19.4	-	19.4
Ad_Mag_Mid_3	10.4	0	17.5	21.5	18.5	21.5
Ad_Mag_Mid_4	10.4	0	13.3	20.3	19.3	19.8
Ad_Mag_Mid_5	10.4	0	20.9	23.9	21.9	22.9
Ad_Mag_Mid_6	10.4	0	21.0	24.0	21	23.0
Ad_Mag_Prox_1	10.7	0	11.1	-	-	11.1
Ad_Mag_Prox_2	10.7	0	10.8	-	-	10.8
Ad_Mag_Prox_3	10.7	0	12.8	-	-	12.8
Ad_Mag_Prox_4	10.7	0	15.0	-	-	15.0

Note: (1) A nil finding (-) reflects that the anatomical length was sufficiently represented within the operating range of the muscle over that particular plane of motion.

(2) Given that the flexion/extension plane of motion was most dominate for the adductor magus the rest lengths were selected based on this dominate range of motion with the exception of Adductor Magnus Middle section 5 which was deemed to become too short in the adduction range plane when using the flexion/extension value of 23.9 cm thus 22.9 was selected as a compromise between the adduction/abduction value at 21.9. A similar compromise was achieved for Adductor Magnus Middle section 6. See Figures XX and xx for details.

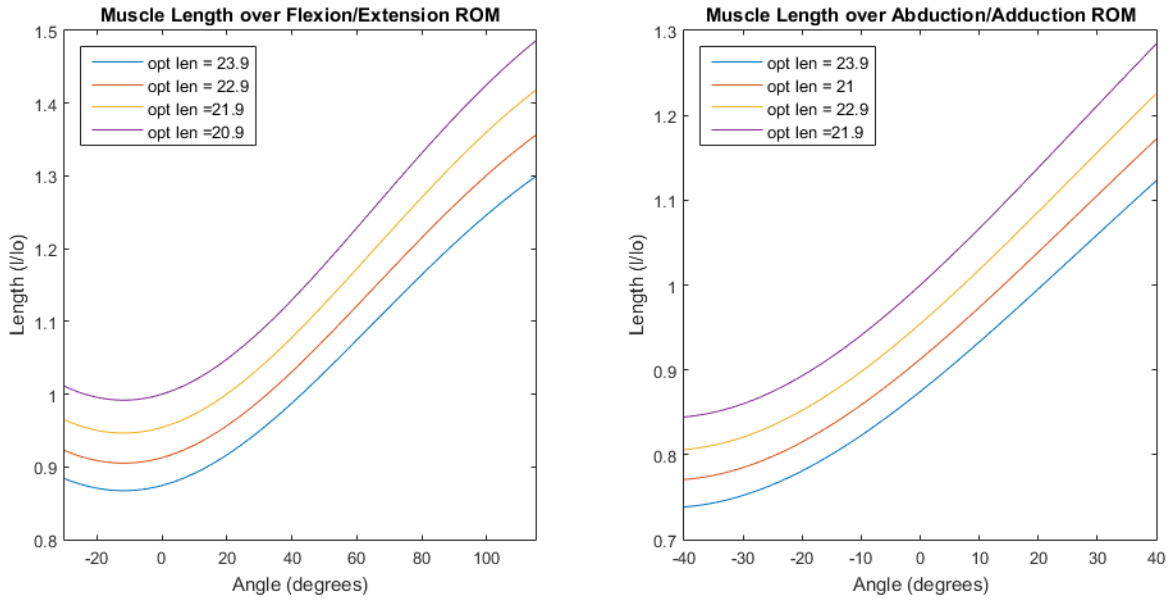


Figure 3.18: Adjusted physiological optimal muscle length to achieve more appropriate operating ranges for the force-length and PEC equations for Adductor Magnus Middle section 5. Here a compromise is struck between the flexion/extension plane and the abduction/adduction plane, selecting 22.9 cm as the optimal rest length.

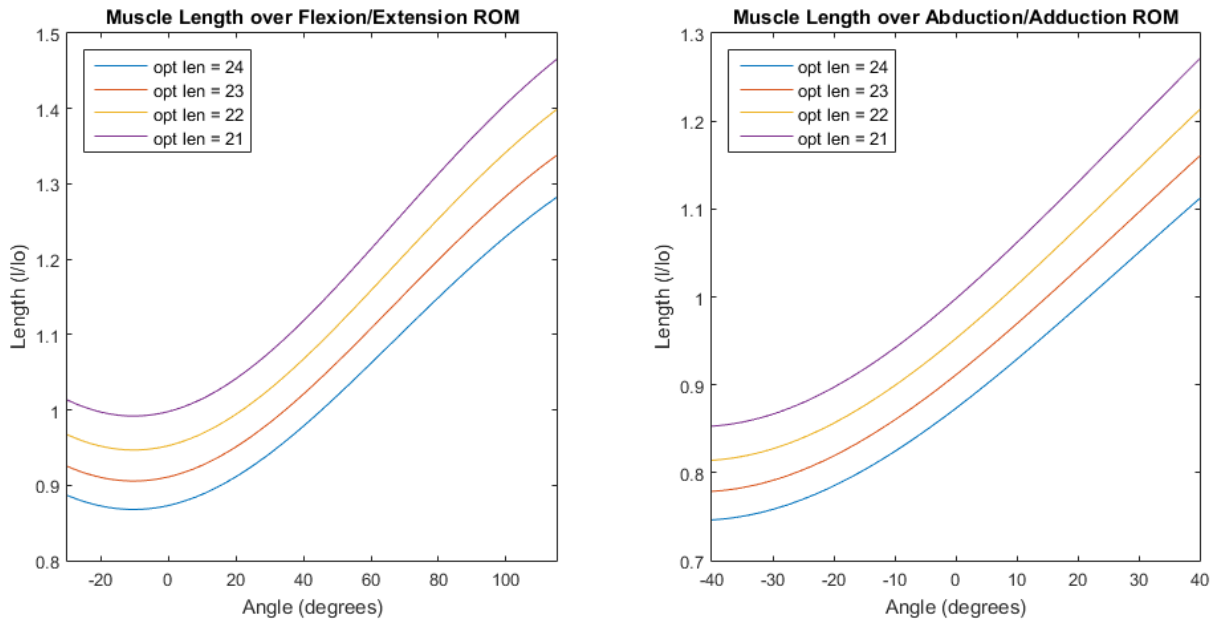


Figure 3.19: Adjusted physiological optimal muscle length to achieve more appropriate operating ranges for the force-length and PEC equations for Adductor Magnus Middle section 6. Here a compromise is struck between the flexion/extension plane and the abduction/adduction plane, selecting 23 cm as the optimal rest length.

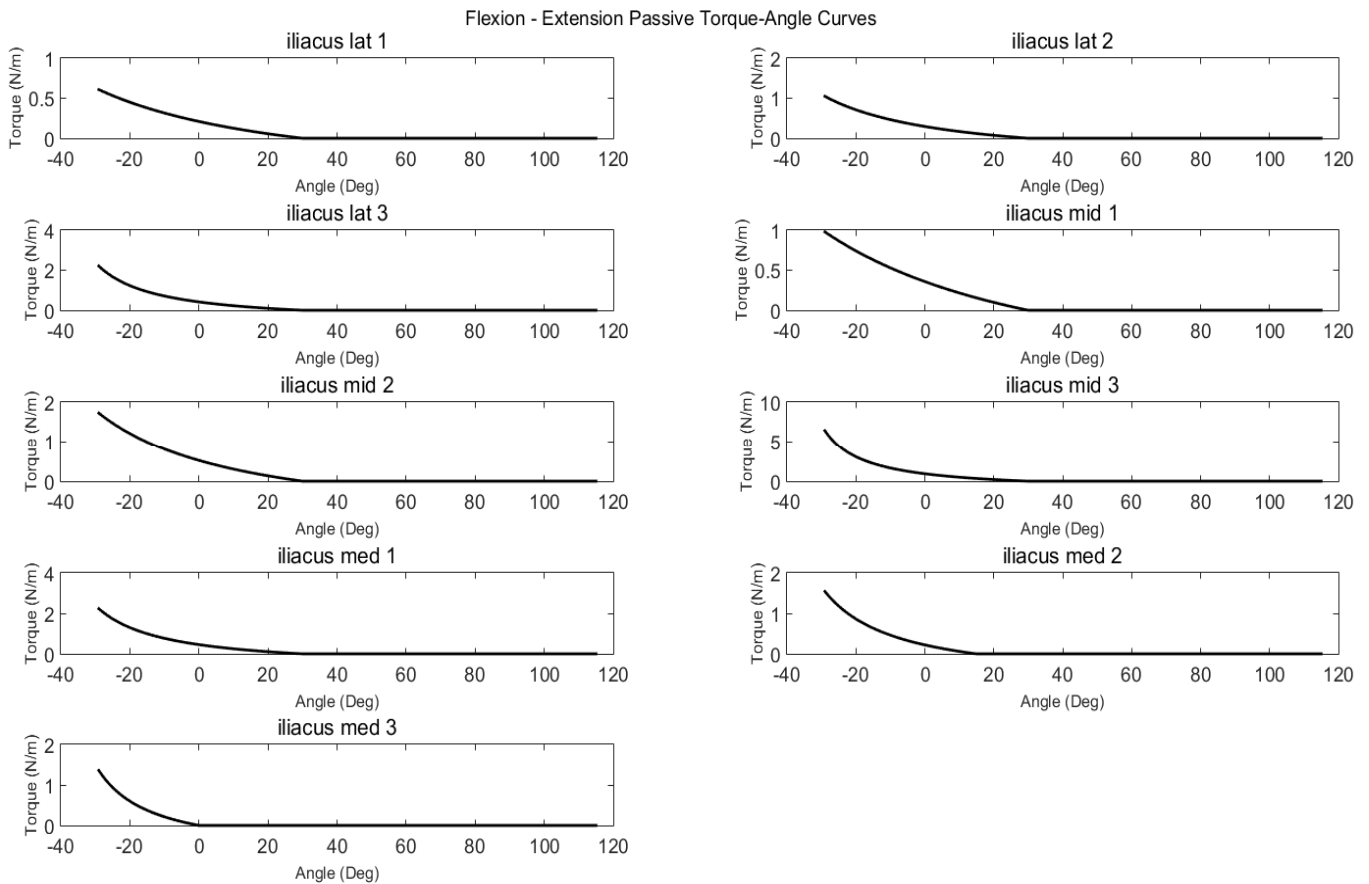


Figure 3.20: Passive resistive moment created by sections iliacus. (Extension is negative – flexion is positive, moments are calculated in flexion-extension plane.)

3.2.3 Ligament Parameters

Ligament attachments sites based on the HSM meshed coordinate system are shown in Table 3.5. The ligaments of the hip were modified with respect to their slack length (or rest length). Based on the experimental data as well as the TLEM data (i.e. the fixation position of the cadaveric specimen) the rest length, which was initially arbitrarily set to anatomical position was adjust to 30 degrees of flexion. This essentially shorten the rest lengths of ligaments and allowed them to contribute to passive joint resistance in a more meaningful way that matched the end-range motion of the joint.

Table 3.7: HSM ligament attachments

Ligament	#/ SEG	Origin (cm)			Seg.	Insertion (cm)			Seg.
		X	Y	Z		X	Y	Z	
ALL	1	12	19.2	0	L5	12.4	22.2	0	L4
PLL	1	8.6	20.2	0	L5	8.7	22.3	0	L4
LIG. FLAVUM	1	7.9	20.9	0	L5	8	22.6	0	L4
INTERTRANSVERSE	1	7.6	20.4	3.6	L5	7.4	23.4	3.6	L4
LAT FACET CAP	1	8	21.4	2	L5	7.2	22.1	2	L4
MED FACET CAP	1	7.2	22	2.4	L5	7.2	22	1.6	L4
INTERSPINUS	1	4.6	20.8	0	L5	3.6	22	0	L4
	2	6	21	0	L5	4.7	21.8	0	L4
	3	6.6	21.2	0	L5	4.7	21.8	0	L4
SUPRASPINUS	1	3.6	20.4	0	L5	3.6	22.3	0	L4
LUMBODORSAL	1	5.4	21	6.2	Pelvis	0.2	34	1.5	RC
ILIOFEMORAL (ANT)	1	12.40	9.90	10.30	Pelvis	9.19	3.37	11.10	Femur
ILIOFEMORAL (LAT)	1	11.60	10.10	11.20	Pelvis	9.19	3.37	11.10	Femur
PUBOFEMORAL	1	13.10	6.20	5.60	Pelvis	9.25	5.68	14.50	Femur
ISHIOFEMORAL	1	7.50	5.50	9.20	Pelvis	7.90	7.02	11.69	Femur

*Ligaments with a Z = 0 value do not have a right and left ligament.

3.2.3 Kinematics

The joint kinematics drive the positional changes in skeletal geometry and attachment points. The spine model will be discussed first, followed by the addition of the hip, ultimately forming the HSM. The spine model geometry is referenced from the midpoint between the hip joint centers (symmetry is assumed) which serves as the local origin. In this case the pelvis is considered to be fixed and the spine angles are calculated from this immovable base. Each spinal segment is then rotated based on a percent contribution of the total rotation of the lumbar spine measured from T12-L1 to the sacrum (eq. 3.1). The contribution of rotation by each segment was described by McGill (1986) as linear synchrony, since it was found to be equally acceptable as cubic and quadratic functions to describe the segmental spine movement. Rotations from kinematic inputs drive the rotation of clouds of data points, associated with anatomical structures and landmarks, in 3D around joint centers. The result is time series data of anatomical

points which can then be used to calculate muscle lengths and velocities, as well as changes in ligament length.

The hip model maintains the same origin and premise as the spine for rotational displacement – the pelvis is fixed, and the femur moves about the hip joint center. Clouds of points represent muscle and ligament attachment sites as well as via points, and these will be rotated as predicted from the experimental kinematic data. A very simple knee hinge joint will also be used to allow for tracking the lower limb bi-articular muscles such as the hamstring group and rectus femoris.

Equation 3.1: Vertebral Rotation

$$R(i) = \alpha(i) * Rt$$

$R(i)$: Rotation of the i th vertebra (rad)

i : the lumbar segmental level (L1, L2, L3, L4, L5)

$\alpha(i)$: % of total rotation assigned to the respective i th segmental level

Rt : total orthopedic rotation of the lumbar spine

3.2.4 Muscle Activation

Muscle activation is used to drive the Hill-Type EMG model, and this provides the foundation for the EMG to force relationship. The critical issue here is to ensure the neurological control pattern is adequately captured with the activation profiles from the EMG signals. This requires the appropriate electrode location and a sufficient number of channels to fully represent the control strategies. Then the electromyographic signals are filtered, FWR, and linear enveloped prior to being entering in the model.

3.2.5 Calculation of Muscle and Ligament Lengths and Velocities

Vertebral rotation is captured and recorded as described above throughout the movement trial. The distances between the muscle and ligament attachment sites in the absolute-inertial reference frames represent the muscle and ligament lengths. Central difference finite differentiation is used for the muscles and ligament length calculations when the muscle and ligaments are in a straight line. When an arc is a more appropriate representation of the muscle path, Equation 3.2 is used to calculate the length of the muscle. (Note: Appendix E demonstrates the congruency between the McGill model previously written in Visual Basic and the current HSM model recoded and updated in MATLAB.)

Equation 3.2: Lengths of muscle which follow an arced path

$$\lambda = [(p * ARCSIN(\frac{\zeta}{(r * p)}) * r) - Lt]$$

λ : Real muscle length (m)

p : Coefficient based on muscle being a simple arc or 'S' shaped

ζ : Linear distance between origin and insertion (m)

r : Radius of curvature of arc to represent muscle line (m)

Lt : Tendon Length

3.2.6 Calculation of Muscle Force

The Hill-type model is used to calculate muscle force (eq. 3.3). Normalized EMG corrected by length (eq. 3.5) and velocity (eq. 3.4) parameters and passive tissue contributions provides muscle force data. Similarly, ligament force is calculated from force-displacement curves (Figure 3.21). The main obstacle for this modelling approach is a clearly defined rest length for both

muscles and ligaments. Several approaches in the literature including that by Horsman (Horsman et al. 2007) to define whole muscle rest length based on the scaling factors of a muscle sarcomere do not seem to provide reasonable estimates. This is the major limitation to this model. However, a pragmatic approach has been used here to circumvent this issue by setting the hip muscles and ligaments to their rest length in the anatomical position though some of these had to be refined and adjusted. The anatomical position is not necessarily the functional rest length of a muscle. Refinement of some rest lengths have been made here and will continue to evolve in the future with more data to enhance the biofidelity. The approach to set rest length at anatomical position was initially used in the spine model, and later refined through experimentation (McGill, 2016; Personal Communication, Unpublished Data) this same evolution and enhancement will be applied to the hip as the model continues to be refined and used address different research questions.

Equation 3.3-1: Muscle Force

$$F(mus) = G * \left[\left(\frac{EMG}{EMG\ max} \right)^{\frac{1}{1.3}} * P_o * \Omega * \delta + Fpec \right]$$

$F(mus)$: Muscle Force (N)

G : gain or error term

EMG : EMG amplitude (arbitrary units)

$EMGmax$: MVC EMG amplitude (arbitrary units)

P_o : Maximum isometric force (N)

Ω : Coefficient for velocity modulation (unitless)

δ : Coefficient for length modulation (unitless)

$Fpec$: Force due to passive elasticity (N)

Equation 3.3-2: Passive muscle force-velocity parameter

$$\Omega = \frac{(P_o * b - V * a)}{(V + b)}$$

Concentric Contractions

Ω : Coefficient for velocity modulation

P_o : Maximum isometric force (N)

a, b : Coefficients

V : muscle velocity in rest lengths per second

$$\frac{a}{P_o} = \frac{b}{V_{max}}$$

V_{max} : Maximum velocity at which force can be produced

$$\Omega = 1 - 1.6V$$

eccentric contractions (0 to -0.125 L_o/s)

$$\Omega = 1.2$$

eccentric contractions (< -0.125 L_o/s)

Equation 3.3-3: Active length modulation coefficient

$$\delta = SIN \left(\pi * \left(\frac{L}{L_o} \right) - 0.5 \right)$$

δ : Coefficient for length modulation

L/L_o : Muscle length normalized to rest length

Equation 3.3-4: Passive muscle force-length parameter (Passive Elastic Component - PEC)

$$F_{pec} = \frac{x_{sec} * \left(\frac{L}{L_0}\right) * B * C}{1 - \frac{\left(\frac{L}{L_0}\right) - 1}{0.7}}$$

F_{pec} : Force due to passive elasticity

x_{sec} : cross sectional area

L/L₀ : Muscle length normalized to rest length

B and C : coefficients

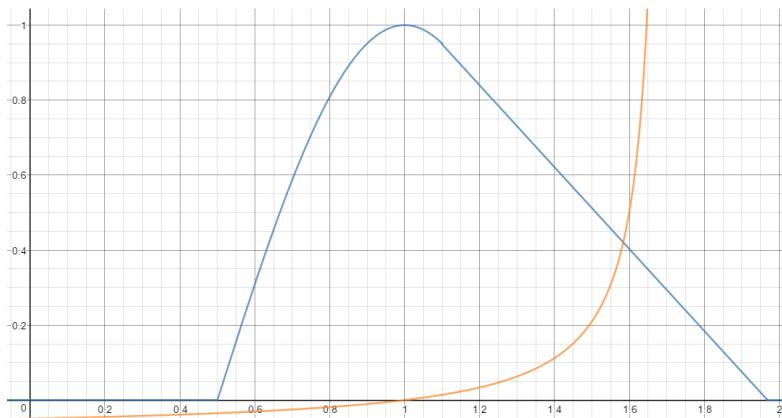


Figure 3.21: Active (Blue) and passive (orange) muscle force-length modulation. Active dynamics are a piece wise equation and PEC operates above rest lengths of 1.

Equation 3.3-5: Determination of the moment, disc compression and shear from a muscle

force:

$$M_m = (r_i F_j \cos K) - (r_j F_i \sin K)$$

M_m : muscle moment about L4/L5 (Nm)

r_i : horizontal component moment arm (m)

r_j : vertical component moment arm (m)
 F_i : horizontal component force vector (N)
 F_j : vertical component force vector (N)

$$M_c = F_m \cos((A_m + K) - A_d)$$

$$M_s = F_m \sin((A_m + K) - A_d)$$

M_c : disc compression due to muscle force (N)
 M_s : disc shear due to muscle force (N)
 A_m : absolute angle of muscle (rad)
 A_d : absolute angle of disc (rad)

3.2.7 Calculation of Ligament Force

Ligaments are visco-elastic structures which function to restrict and guide joint motion (Solomonow 2004). However, they have been modelled as linear non-visco-elastic elements (Yettram & Jackman 1982; Schultz et al. 1973). Two separate methods have been employed to evaluate ligament force in this model. The spine used its current approach from the original model and the hip took on a new approach mainly due to the availability of data. Both approaches are described below in detail.

3.2.7.1 Spine Ligaments

Anderson (Andersson 1983) developed an equations for ligament behaviour for ligamentum flavum, based on the work of Nachemson and Morris in 1954; interspinous and supraspinous ligaments, using data from Walters & Moris in 1963; and the lumbodorsal fascia based on Bazergui and colleges (1978) data. In this model, Andersson's basic equation for ligament force was enhanced to account for cross sectional area (CSA) as shown in Equation 3.5-5 with the phi term as a correction factor. As mentioned above the spinal ligaments were assumed to have

similar properties to those of supraspinous and interspinous ligaments, and the coefficients for the spinal ligaments are shown in Table 3.8. In addition, the angle at which the ligament engages in force production during forward flexion of the L4-L5 segment is shown in Table 3.9. Once the force is calculated the line of pull vector is computed and the passive moment is estimated based on the perpendicular from the rotating joint center.

Equation 3.8: Ligament Force (spine)

$$F(lig) = (a * \phi * (exp\beta\xi)) + P$$

$F(lig)$: Ligament Force (N)

a, β : coefficients

ϕ : correction for cross-section ($0.006 * \text{area mm}^2$)

ξ : Percent strain

P : ligament pre-tension (N)

Table 3.8: Input parameters for ligament force calculations

Ligament	alpha	beta	P	phi
Supra/Interspin.	2.3296*	0.27215	0.0	1.0
Ligament Flav.	1.1994*	0.06420	1.5	1.0
LDF	0.5381*	0.17843	/	1.0
PLL	2.3269	0.27215	0.0	0.177
ALL	2.3269	0.27215	0.0	0.1
Intertransverse	2.3269	0.27215	0.0	0.006
Articular	2.3269	0.27215	0.0	0.174
Supraspinatous	2.3269	0.27215	0.0	0.18
Interspinatous	2.3269	0.27215	0.0	0.78

* from Andersson 1983

**Table recreated from McGill Thesis 1986

Table 3.9: Point of application (degree of flexion) when ligaments start to strain

Ligament	CSA (mm ²)	Degree of flexion where strain occurs
Lig. Flav.	130	0
LDF	/	14
PLL	30	14
ALL	17	/
Intertranseverse	1	14
Articular	29	14
Supraspinatous	30	14
Interspinatous	130	14

**Table recreated from McGill Thesis 1986

3.2.7.2 Hip Ligaments

Ligament anatomical coordinates (Table 3.7) were available from the TLEM (Horsman et al. 2007) and the parameters of the of the ligaments were adopted from previous research (Hewitt et al. 2002). This data provided the basis of using a previously described method (shown in eq. 3.9) to evaluate ligament force (Barrett & Callaghan 2018). Incorporating the knowledge

form these three sources allowed this hip joint model to be the first to include ligament modeling into the joint load model (Figure 3.22).

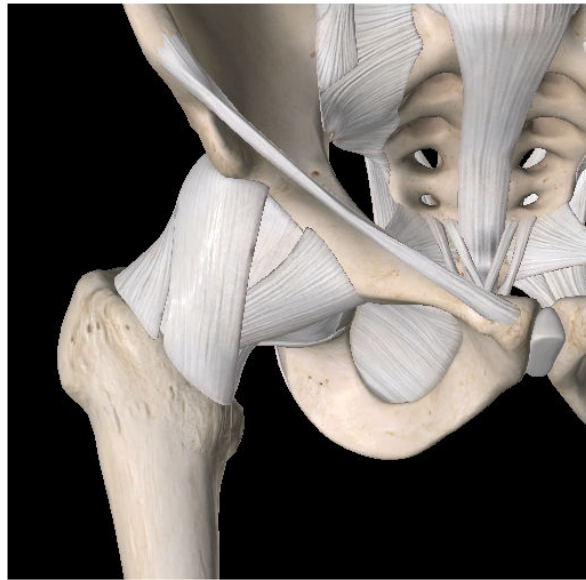


Figure 3.22: Hip ligaments and capsule.

Equation 3.9: Ligament Force (hip)

$$F(\xi(t)) = \frac{k\sigma}{\sqrt{2\pi}} \exp\left(-\frac{(\mu + \xi(t))^2}{2\sigma^2}\right) + \frac{k(\mu + \xi(t))}{2} \left[\operatorname{erf}\left(\frac{\mu + \xi(t)}{\sqrt{2}\sigma}\right) + 1 \right]$$

Where,

- $F(\xi(t))$ = Ligament Force (N) at a given length ($\xi(t)$)
- $\xi(t)$ = length change
- k, σ, μ = coefficients

And,

$$\operatorname{erf}(x) = \frac{2}{\sqrt{\pi}} \int_0^x e^{-t^2} dt$$

e = error term from matlab
 x = length change

Below are paired Figures (Figures 3.23-3.25, inferior iliofemoral; Figures 3.23, 3.26-3.27, superior iliofemoral; Figures 3.28-3.30 ischiofemoral) which were used to extract the raw data from the ligament parameters in the Hewitt and colleagues (2002) work and using the Barrett and Callaghan (2018) equation to inform the model parameters in this work. Contact with the Hewitt and colleagues failed to provide the original data set and the best that could be provided was original data from the Tables in the original paper. The approach taken here was to recreate 2 or 3 critical inflection points so that the curve could be recreated with the Barrett and Callaghan (2018) equation.

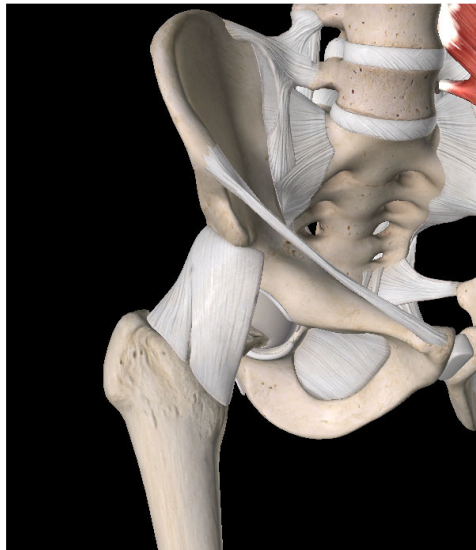


Figure 3.23: Anatomical illustration of the iliofemoral ligament.

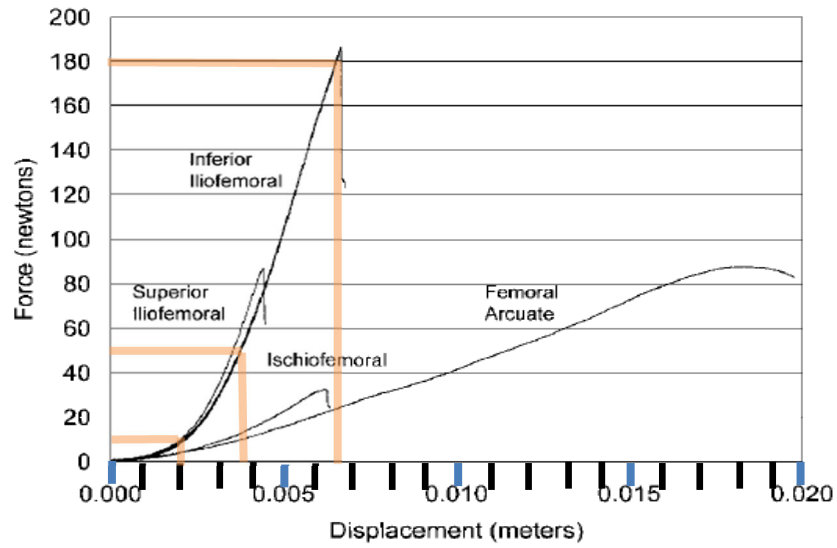


Figure 3.24: Experimental data from Hewitt 2002. Orange lines indicate key target points in the curve to identify the inferior iliofemoral ligament characteristics.

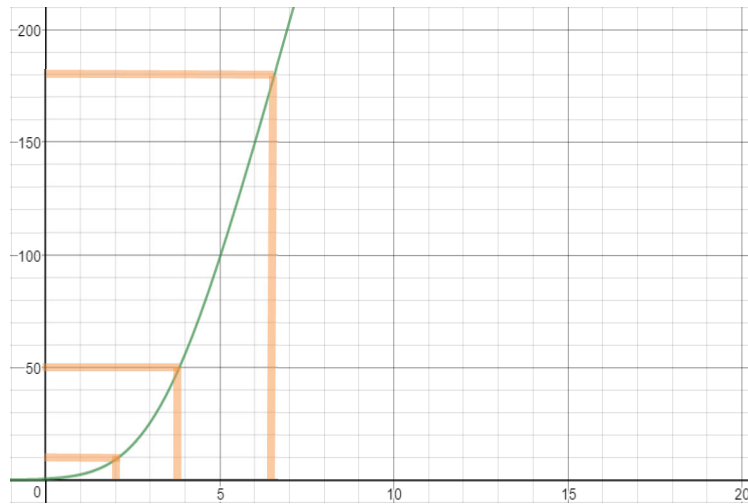


Figure 3.25: Model estimated force-displacement curve for inferior iliofemoral ligament. Coefficients in the Barrett equations are as follows: $K=55$, $s=1.5$ and $m=-3.3$.

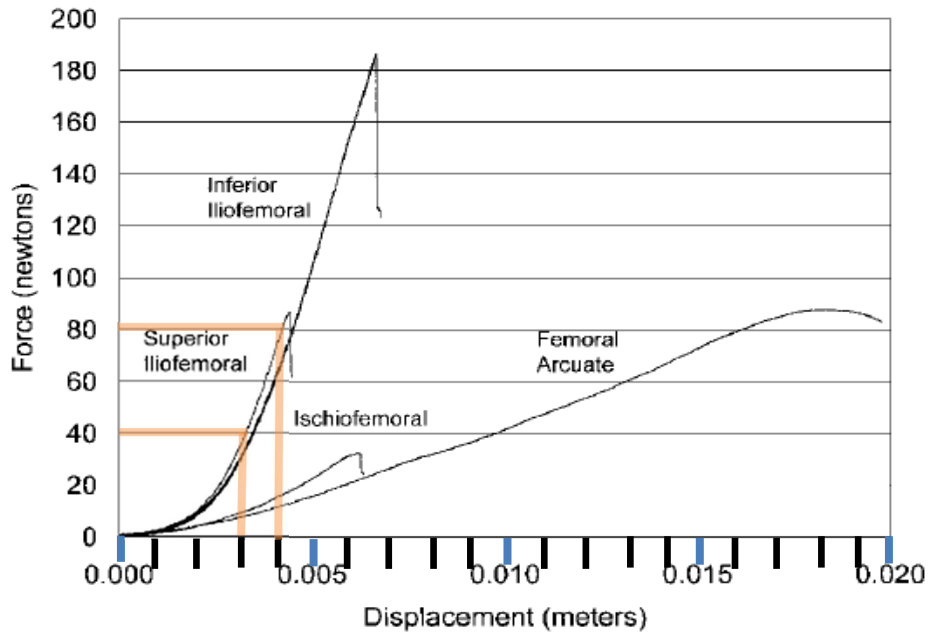


Figure 3.26: Experimental data from Hewitt 2002. Orange lines indicate key target points in the curve to identify the superior iliofemoral ligament characteristics.

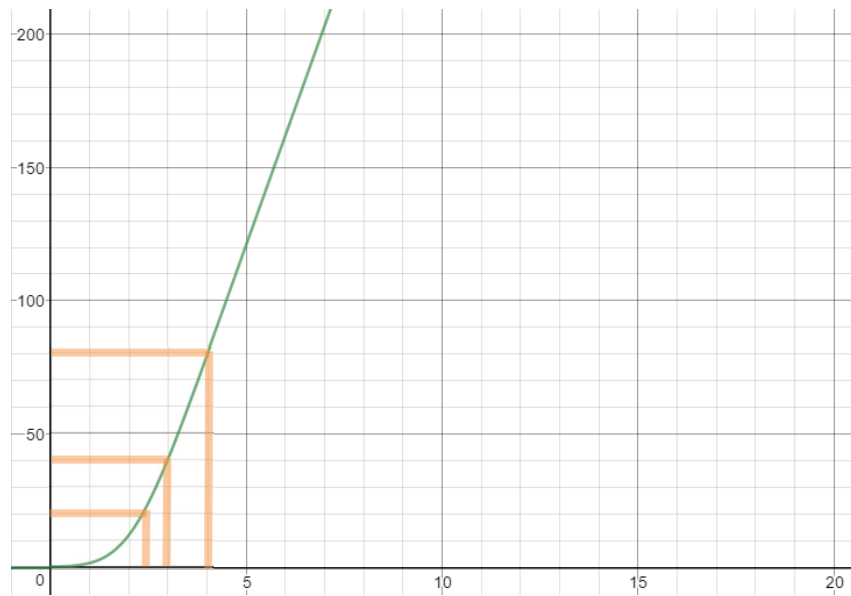


Figure 3.27: Model estimated force-displacement curve for superior iliofemoral ligament. Coefficients in the Barrett equations are as follows: $K=41$, $s=0.8$ and $m=-2.05$.



Figure 3.28: Anatomical illustration of the ischiofemoral ligament.

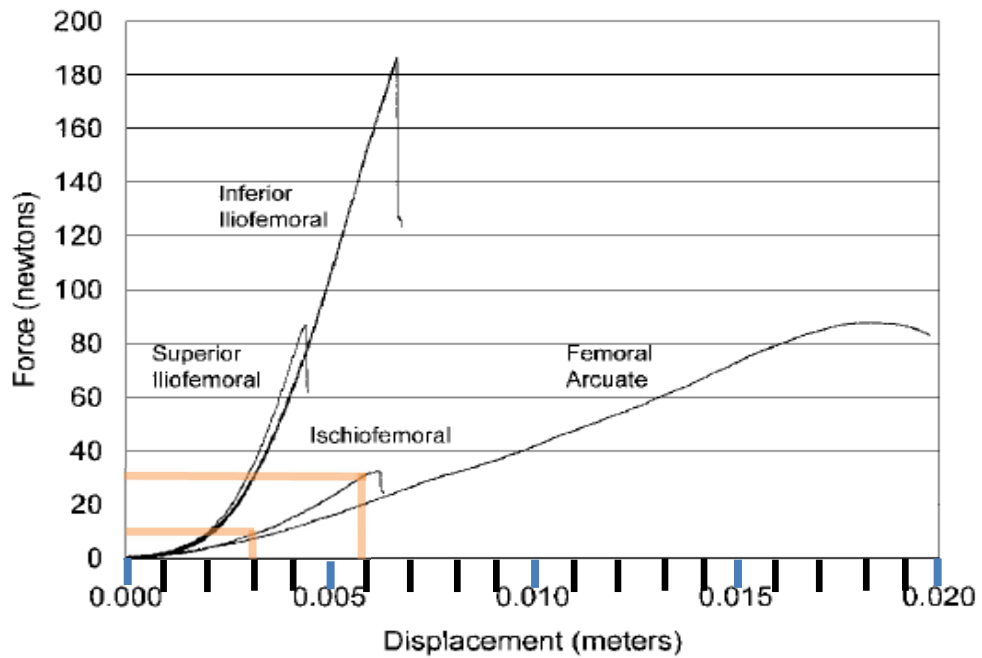


Figure 3.29: Experimental data from Hewitt 2002. Orange lines indicate key target points in the curve to identify the ischiofemoral ligament characteristics.

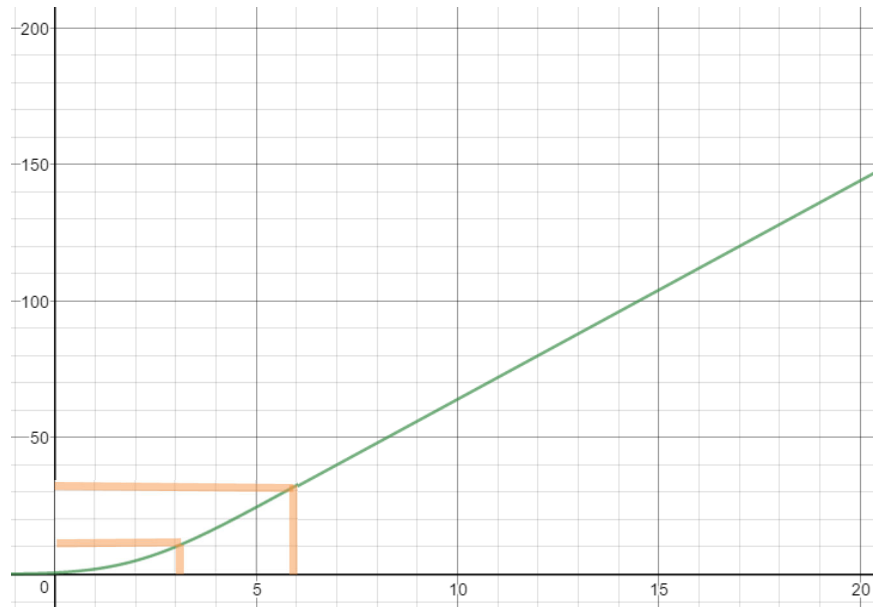


Figure 3.30: Model estimated force-displacement curve for ischiofemoral ligament. Coefficients in the Barrett equations are as follows: $K=8$, $s=1.5$ and $m=-2.0$.

The pubofemoral ligament. The pubofemoral ligament is absent from a stress-strain/force-displacement in the literature. Here it has been assumed to have similar behaviour to the iliofemoral ligament. This is based on the evidence of Hidaka et al. (2014) who observed the strain (%) for iliofemoral and pubofemoral were similar 3.48% and 3.28%, respectively at their maximal physiological strain. In contrast, the maximal strain for ischiofemoral ligament was 7.83%. This is perhaps a good indication of why the force-displacement behaviour of ischiofemoral ligament is so different in comparison to superior and inferior iliofemoral ligaments.



Figure 3.31: Anatomical illustration of the pubofemoral ligament.

3.3 Model Tuning – EMG driven model and Inverse Dynamics

Tuning the EMG driven model via the use of a gain factor is a critical step to provide for the accurate interpretation of the model results. This is a scaling factor that accommodates individual variabilities in traits such as muscle stress, size, etc., but it allows the model to converge on an estimated moment that equals the inverse dynamics estimation. This final step in the analysis of the model calculations will account for missing details, unknown entities and biological variances not accounted for in the HSM. When estimating muscle force from Eq.3-3.1 a gain factor is required since this is not a direct measure of muscle force. In this way the model can be corrected for individual variances and experimental assumptions (including electrode placement, as an example). A reference voluntary contraction (RVC) is used when a relatively large moment is created so that the initially predicted EMG driven moment can be “tuned” to the inverse dynamics predicted moment (Figure 3.30). A Least Squares Difference (LSD) (Eq. 3.10) is used to generate this value about the flexion/extension orthopedic joint axes in the current studies but could be tuned to any of the axes or even a resultant moment of all three summed axes. This gain

factor is then applied to all trials in order to tune the muscle force predictions of the EMG driven model. Two reference postures were examined in this thesis. A standing posture traditionally used to determine the gain for the lumbar spine, and a semi-squat posture for the hip estimates were used to calculate the gain for the hip and spine independently – the trial with the most congruency between model estimates was used to calculate the gain. Acceptable gain factors used here were consistent with laboratory standards when using the spine model which are between 0.5 and 1.5 (these cut-off values are based on long standing laboratory standards).

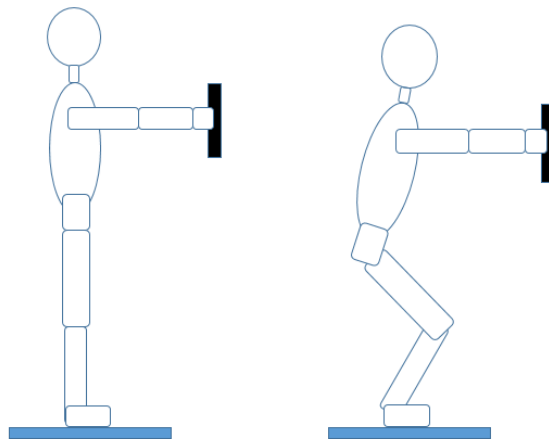


Figure 3.32: Reference voluntary contraction (RVC) positions for evaluating and tuning the model. Position one (left) standing erect with the weight held in front and position 2 (right) standing in a semi-squat position.

Equation 3.10: Least Squares Difference for calculating a gain factor.

$$G = \frac{\sum(M_{LSM} * M_{EMG})}{\sum(M_{EMG} * M_{EMG})}$$

where,

G = gain applied to the EMG model

M_{LSM} = Moment from Linked Segment Model

M_{EMG} = Moment from EMG driven Model

3.4 Results

The model showed very good congruency with the ID data during the RVC trials for most subjects. Examples of model congruency between the HSM and ID during the reference trials are shown in Figures 3.33-3.35. These Figures show the raw calculations used to calculate the HSM gain (additional examples of HSM performance are shown in Appendix E and G). In Figure 3.33 the first posture in Figure 3.32 was used since it yielded the best match. In contrast, Figures 3.34 and 3.35 the subject moves in and out of posture 2, the semi squat position, and there is an appreciation of the model performance and sensitivity to the changing position and load as the participant moves into and out of the testing position. Tables 3.10 and 3.11 provide the summary data from each subject's gain calculation for females and males, respectively. Acceptable gains range between 0.5 and 1.5 based on previous experience with the spine model. Gains outside the range were omitted and subject's joint loads were not used in the group analysis.

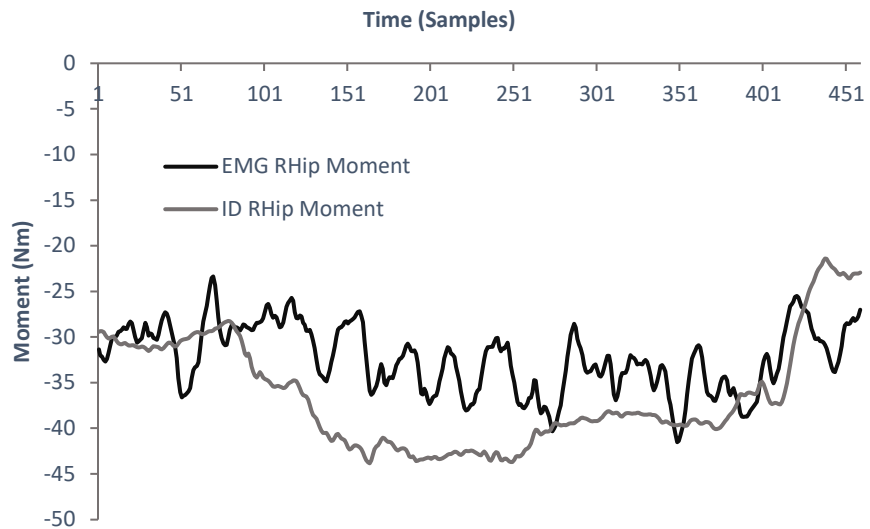


Figure 3.33: Right hip moment data comparing the HSM and ID (subject 13 in the ACL study, right hip gain of 1.12). This data is used in the model to calculate the tuning factor by which the HSM is adjusted to the ID prediction during the RVC trial. In this trial the data collection captured the posture demonstrated in position 1 in Figure 3.32.

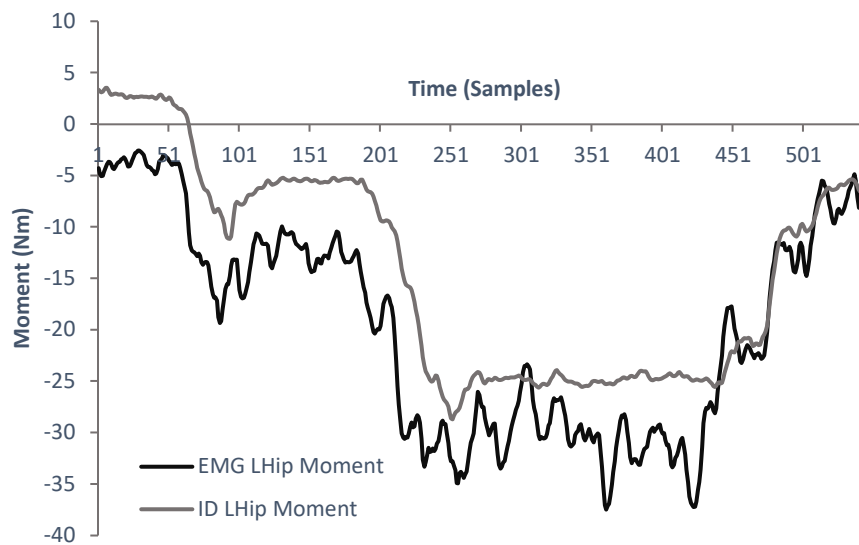


Figure 3.34: Left hip moment data comparing the HSM and ID (subject 13 from the ACL study, left hip gain of 0.94). This data is used in the model to calculate the tuning factor by which the HSM is adjusted to the ID prediction during the RVC trial. In this RVC trial the participant moves into and out of the posture in position 2 in Figure 3.32.

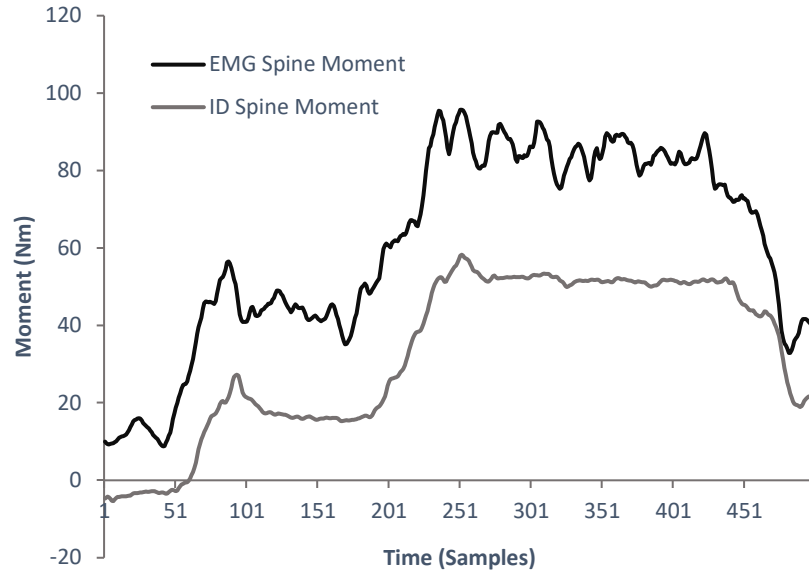


Figure 3.35: Lumbar spine moment data comparing the HSM and ID (subject 13 of the ACL study with a lumbar spine gain of 0.72). This data is used in the model to calculate the tuning factor by which the HSM is adjusted to the ID prediction during the RVC trial. In this RVC trial the participant moves into and out of the posture in position 2 in Figure 3.32.

Table 3.10: Muscle gains for study 3: ACL injury risk.

Subject ID	Right Hip	Left Hip	Spine
S01	0.71	0.53	0.83
S02	0.97	1.00	0.94
S03	1.01	1.01	0.68
S04	0.99	1.31	0.58
S05	1.17	1.35	1.26
S06	0.62	0.75	1.02
S07	1.06	0.95	0.55
S08	0.61	0.63	0.71
S09	1.19	1.32	0.70
S10	0.51	0.79	0.77
S11	0.69	0.69	0.50
S12	0.79	0.58	1.35
S13	1.12	0.94	0.72
S14	1.29	0.99	0.62
S15	1.20	1.12	0.91
S16	0.52	0.72	0.99
S17	0.85	0.80	0.82
S18	0.82	0.79	0.84

Table 3.11: Muscle gains for study 4: HRA.

Subject ID	Right Hip	Left Hip	Spine
S01	0.55	0.88	1.05
S02	---	---	---
S03	---	---	---
S04	---	---	---
S05	1.04	0.80	1.26
S06	0.85	1.19	1.34
S07	1.50	0.94	1.07
S08	1.43	1.09	1.04
S09	1.22	0.99	---
S10	0.92	---	1.40
S11	0.62	0.79	0.54
S12	0.93	0.83	0.85
S13	0.77	0.80	1.37
S14	0.99	1.38	1.09
S15	0.87	1.62	1.36
S16	1.05	0.88	1.17
S17	0.63	0.94	0.97
S19	0.97	1.33	1.42

3.5 The Integrated Hip-Spine Model Validation

There are many different ways to validate a biological model. This model, through its, respective parts, has achieved various stages of verification and validation along its development. The existing spine model has been assessed with various tests of validity as much as such a complicated approach can be. As has the data set for the lower limb anatomical parameters with its previous uses in biomechanical modelling. Validation in parts, suggests that the combination of two valid components ought to approach a valid model. Now, with the combination of both the spine and lower limb models this is the overarching approach to validation. Moreover, this current model has several updates as describe in section 3.2 and its various sub-sections to

enhance the model's capabilities. With these improvements in mind the model is iteratively validated as part of its implementation process. Consider the model overview in Figure 3.1 the HSM is gained, or tested against, the inverse dynamics model. In doing this the model is 'tested' for each subject to ensure a reasonable load estimation in the calibration task (RVC trial). In this way the gain factor is an indication of model performance. As an extension of this logic the HSM can be tested or evaluated relative to its predictions with ID. The mean (SD) gains in for the females were 0.89 (0.25), 0.90 (0.25), and 0.82 (0.23) for the right hip, left hip and spine, respectively; and for the males 0.96 (0.27), 1.03 (0.26) and 1.14 (0.25), respectively. Further validation testing such a model sensitivity as well as performance with respect to additional moments (lateral bend and twist in the spine and abduction/adduction and medial and lateral rotation at the hip) will enhance the models' abilities and validation in future experiments under an expanding repertoire of measurable tasks. For now, this is a trade-off, the model will continue to be refined but in its current form it's more than sufficient to address specific research questions as those posed in the following chapters. The complex model will show what elements are critical, and which should deserve more clarification, together with those that have less influence on the results and can be ignored.

3.6 Discussion

The Hip-Spine Model is a unique and novel investigative instrument for analysis of complex biomechanical interactions between the hip and spine. There are some risks to combining two anatomical data sets, however there is more to gain. Scaling is one of the major considerations when combining two data sets. First, the spine model data set has been developed and improved upon with respect to its anatomical detail for 37 years as described above in detail. Regarding

the hip model, the proposed data set has been adopted by many models including the London Lower Limb Model which was a published validation of the data set (Modenese et al. 2011b). The wide use and adoption of the Horsman et al. (2007) data set by open access modeling platforms provides a tremendous amount of credibility for its choice as the hip model data inputs. The benefits of combining these data appear to outweigh the potential negatives. First, human cadaver specimens ought to be used sparingly and only when necessary. In addition, the availability of a young and healthy cadaver, such as the one used by Horsman, are rare. Second, each of these data sets have been gathered and refined with extremely sophisticated data acquisition instruments, not readily available at the University. Last, and most importantly, these model inputs have been tested and proven to be of utility in the scientific community. They were gathered with sophisticated technology and instrumentation and proven to be robust through several studies and applications of each respective model. As such, rather than simply reproducing others work, the next logical step is to build upon what is known and create new knowledge. With that said, several enhancements and improvements have been incorporated into the HSM that improve upon both pre-existing data sets as a direct result of combining these two pre-existing data sets. For example, the psoas muscle now undergoes length changes and anatomical positioning that was not possible with the spine model alone. In the same way the TLEM now has a psoas muscle that responds to spine posture and muscle length changes. Likewise, the TLEM now has more accurate muscle parameters with wrapping and length estimation improvements more closely matching the anatomical function of psoas, iliacus, as well as the gluteal and hamstring muscle groups.

Further refinements and improvements make this model unique in comparison to others and enhancing the contribution of the model development section of this thesis. For example, in the hip, there were occasions which required wrapping spheres to ensure the anatomical and functional relationships were maintained as the model was pushed to its full range of motion. These spheres augmented the length of the muscle parts and these improvements resulted in longer muscle paths which were incorporated into the model calculations of muscle force. The wrapping spheres did not affect muscle force directly since the force vector was considered at the most proximal muscle segment applying force to the rigid segment (i.e. the bone). In this way the wrapping spheres only influenced muscle force indirectly through altering muscle length, though they have a profound effect on joint load as they are highly influential to moment arm length and therefore joint moment. By testing passive ROM profiles and taking this model to higher demands than previously tested offered the opportunity for serendipitous discovery of the model limitations and anatomical assumptions which is another major contribution of this thesis.

One major limitation of the HSM is the lack of available data to build a unique female model. The majority of anatomical data is on males and therefore the biological models build with this data are focused on males. While addressing this gap in the literature is beyond the scope of this thesis the intension to address this in the future will add to the scientific community in a meaningful way. This will in the current stages remain a future ambition of model development.

Future examination of the model will investigate EMG-assisted optimization approaches and compare them to the currently proposed method. There is some uncertainty of the best

approach for establishing the criterion measure for adjusting the muscle gain. Three options exist, including satisfying the hip or spine moment and then setting the gain, or some combination of a weighted hip and spine gain. These approaches will be considered and examined in the further development and testing of the model as the model is subjected to more subjects and tests in more situations.

This ambitious model development has the advantage of facilitating sensitivity analysis of the many subcomponents together with providing insight into how hips influence spine mechanics and vice-versa. But the trade-off lies in the number of assumptions that must be made. Only future analysis will reveal these trade-offs. The development of this model in its current state, including overcoming deficits in the previous datasets (TLEM), is a significant achievement and more insights into hip and spine function as well as the interaction between these joints will be enhanced by this undertaking. Furthermore, at the very least we now have a vehicle to take us along this journey to probe, provoke and investigate the relationship between the hips and spine.

4.0 Study 2: Passive Moment-Angle Curves and Joint Rotational Stiffness of the Hip in the sagittal and frontal planes: Implications for modelling and model evaluation, sex comparisons, and injury mechanisms.

4.1 Introduction

Biomechanical investigation of the hip often considers modelling approaches to estimate tissue loading due to the practical limitations in obtaining these measures in vivo. The passive tissue contribution to joint loading is often neglected in lower limb models under the assumption that the passive tissue contribution to total joint load is negligible. This assumption is mainly driven by the predominance of gait related lower limb modelling applications. In a broader range of human movement, which involves large amplitude ranges of motion (ROM), bolstering the analysis of passive tissue properties is needed to capture end-range stiffness. This knowledge will enhance the biofidelity of passive tissue properties in modelling approaches.

Establishing changes in muscle lengths over the hip range of joint motion, as an example, is an important parameter in the EMG-to-force estimation. Hence, there is a potential to enhance the understanding and the confidence in model predictions of the passive and active force estimates with the improved accuracy of optimal muscle length estimations. In addition, to the potential contribution to modelling, examining passive tissue characteristics in the hip is a worthy endeavour in its own right and can be further enhanced with comparisons between the sexes in vivo. This information may then lead to improvements in the estimation of load distribution and

may provide insights into normal mechanics and injury mechanisms through a range of human movement.

Examining regional interdependency in joint mechanics has led to new discoveries and deeper understanding of injury mechanism. Movement requires careful control of the available degrees of freedom at each joint with joint stiffness but complexity increases when the joints along the linkage increase. For example, stiffness in the foot is associated with a higher arch height (Williams et al. 2004), which in turn has been linked to the subgrouping of lower limb injuries among runners (Williams et al. 2001). There are also examples of this at the hip. Both patellofemoral pain (Roach et al. 2014) and patients experiencing back pain (Roach et al. 2015) have been reported to have decreased hip ROM on average. Moreover, postoperative success after hip replacement surgery was highly dependent on the restoration of hip mobility (Davis et al. 2007). On the other hand, compromise in the ability to control hip mobility also leads to other injuries like those observed at the knee, such as, ACL injuries (Hewett et al. 2005) and patellofemoral syndrome (Powers 2003). It appears that the synergies between joints in the kinetic and kinematic chains rely on an optimum of mobility and stability to achieve skilled movement within the margin of safety afforded by the joint and tissue capacities. Further understanding will be obtained with understanding of the passive contribution to joint rotational stiffness (JRS) at the hip.

Few studies have examined passive hip moments in vivo (Vrahas et al. 1990; Yoon & Mansour 1982), even fewer have examined more than simply sagittal plane motion, and fewer still have compared males and females. Early work in this area neglected to measure the end

range of motion. Yoon & Mansour (1982) tested hip ROM until the passive resistance of the hip overcame passive resistance in the inactivated spine creating spine motion. This limited their analysis to $\sim 12^\circ$ of extension and $\sim 55^\circ$ of flexion at the hip. However, understanding how hip mechanics are linked with regional mechanisms such as how back pain might be provoked by hip endrange mechanics will be critical.

The global objectives of this study were to investigate passive joint loading. A rubric referred to as a 'passive ROM profile' was utilised to describe the passive hip joint characteristics and facilitate comparisons between groups. A schematic representation of a moment-angle curve illustrates the outcomes variables of interest, which make up the 'passive ROM profile' and serve to guide the investigation (i.e., peak moment, peak angle, neutral zone barrier, neutral zone width; see Figure 4.1). The specific objectives of this study were the following: (1) Describe the hip moment-angle curves in the sagittal and frontal planes as well as passive hip joint rotational stiffness (JRS). (2) Compare male and female passive ROM profiles. (3) Evaluate the model performance estimating moment-angle curves for the average male. A series of research questions follows from these objectives:

1. Do the passive moment-angle curves appropriately reflect passive tissue behaviour?
2. Do differences exist between male and female passive ROM profiles?
3. Does the Hip-Spine Model (HSM) sufficiently predict the total passive hip moment?

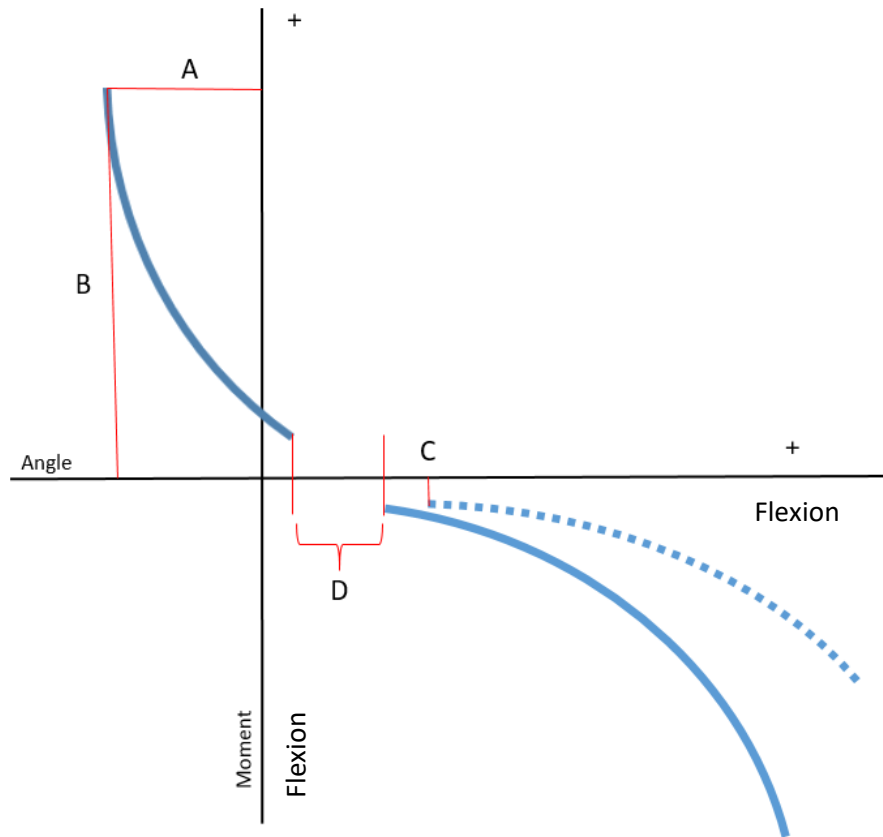


Figure 4.1: Schematic diagram of the passive ROM profile characteristics on a generic extension-flexion moment-angle curve. (A) Peak Moment; (B) Peak Angle; (C) Neutral Zone Barrier (NZB) ; (D) Neutral Zone Width (NZW). Note: Not included on the curve is the exponential curve fit $M=ae^{b\theta}$.

These questions probe the mechanical properties of the passive tissues. Each of these research questions leads to a series of hypotheses which are listed below:

1. An exponentially fitted curve will predict the passive ROM for each plane of motion and direction for both males and females.
2. The passive ROM profile will differ for males and females.
 - a. Males will have a larger peak moment in all planes of motion and direction.

- b. Females will have a larger angle at peak moment in all planes of motion and direction.
- c. Females will have a larger angle at the NZB.
- d. Therefore, females will also have a wider NZW.

*Note: Some research questions are not amenable to a testable statistic, their analysis will rely on descriptives of behaviour to assess differences and similarities.

4.2 Methods

Participants partook in a series of passive resistance trials in the sagittal and frontal plane while recording three-dimensional (3D) body segment kinematics and force measures were taken while monitoring muscle activity. Moment arm measures were also taken for each direction of motion from the point of force application (leg strap) to the greater trochanter (GT).

4.2.1 Participants

Fifteen healthy young females (20.6 (1.2) years of age with an average height of 166.7 (5.7) cm, and average weight of 65.0 (10.8) kg) and 17 healthy young males (20.9 (2.0) years of age with an average height of 177.9 (6.8) cm, and average weight of 79.3 (9.8) kg) participated in this study. Participants were given a verbal and written explanation of the experimental procedures and set-up prior to providing written informed consent approved by the University of Research Ethics (ORE) Board. Participants were absent of low back and lower limb pain and injury and had no history of trauma or damage to the soft tissues nor surgery in any of these areas. By chance, all participants were right leg dominant when asked, “which leg would you used to kick a soccer ball.”

4.2.2 Data Collection Procedures & Equipment

Participants were first prepared for electrode placement by shaving, abrading the skin with Nuprep® and cleaning with a 50/50 ethanol/water solution. The electrodes were placed bilaterally over the muscle bellies of Adductor Longus (AL), Biceps Femoris (BF), Gluteus Medius (GMed), Tensor Fascia Latae (TFL) and Rectus Femoris (RF). A bipolar electrode configuration was achieved using Ag-AgCl (Meditrace 130 Ag/AgCL electrodes, Covidien, MA, USA) self-adhesive electrodes. EMG was collected using 32 channels which were differentially amplified (CMRR of 115dB at 60Hz; input impedance: 10MΩ; Model AMT-8, Bortec Biomedical, Calgary, Canada) and then passed through an A/D converter sampled at 2160 Hz (16 bit, 64 channels with an input impedance of 1 MΩ and a common sampling rate) and collected on a Vicon Antec® Intel® Core™ 2 Duo PC using Vicon Nexus 1.8.5 software. EMG was required to ensure passive stiffness was recorded without the influence of muscle activation.

Next, maximal voluntary contractions (MVCs) were performed for physiologic normalization of each muscle (or muscle group for GMed and TFL) with the experimenter providing external resistance to a coached maximal exertion. Once the MVCs were completed the participants were prepared for motion capture using 10 mm diameter reflective markers and marker-clusters. The Nexus software was also used to collect kinematic data from the reflective markers, sampled at 60 Hz from eight optoelectronic cameras. The data was then saved and stored for processing and analysis. First, Visual 3D was used to calculate joint angles and then in MATLAB (version R2015a) using custom-written programs for EMG analysis and post-processing calculations and analysis. A general layout of the experimental data collection set-up is illustrated in Figure 4.2.

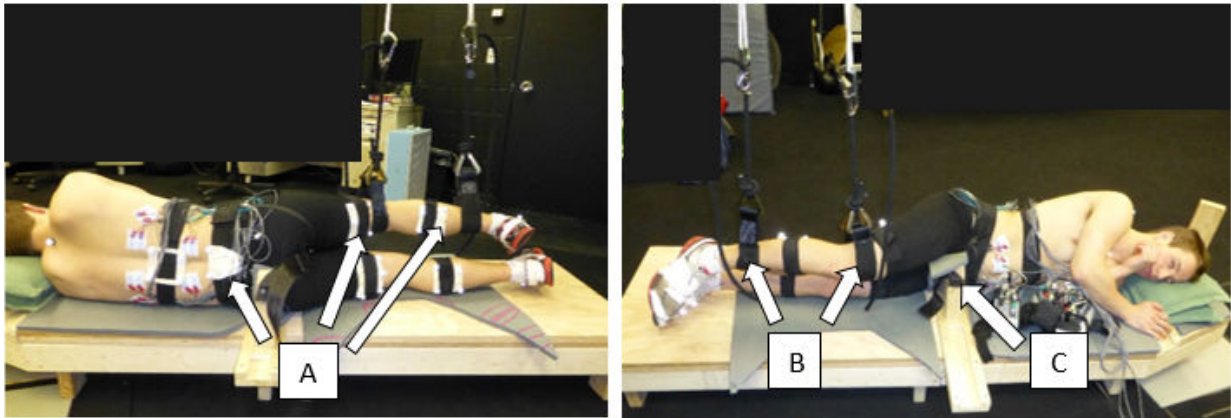


Figure 4.2: Experimental set-up, (A) Kinematic clusters, (B) Suspension Straps in-line with adjustable connectors and suspension ropes, (C) Pelvic restraint(s).

A schematic of the hip stiffness apparatus is shown in Figures 4.3 and 4.4 for the sagittal and frontal planes of motion, respectively. Two suspension ropes were hung from the ceiling, at the top end, and each was attached to a separate sling harness, at the bottom end. The slings supported the weight of the thigh and shank, independently. The height of the ceiling attachment to the participant leg was approximately 270-280 cm. The floor jig was covered in foam, and had two pelvic braces with a strap connecting them, to secure the torso and pelvis during testing. When measuring the frontal plane motion the floor jig was equipped with a removable lower body segment to allow the freedom of movement in the testing leg as well as the reposition of the left leg to remove any potential for collision during testing.

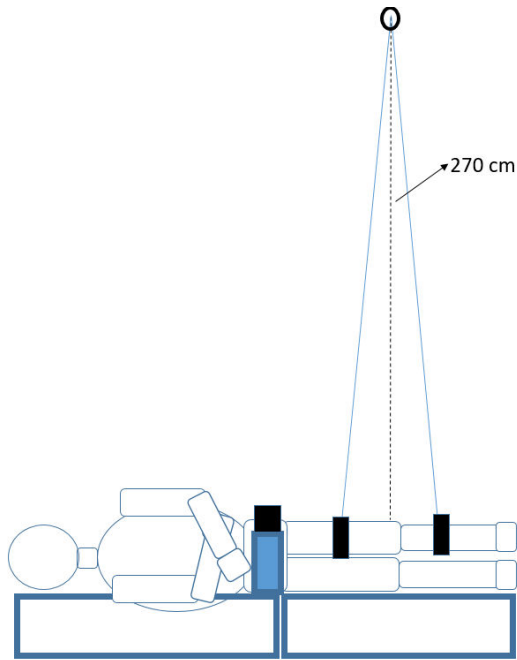


Figure 4.3: Experimental set-up for measuring sagittal motion (flexion and extension) moment-angle curves.

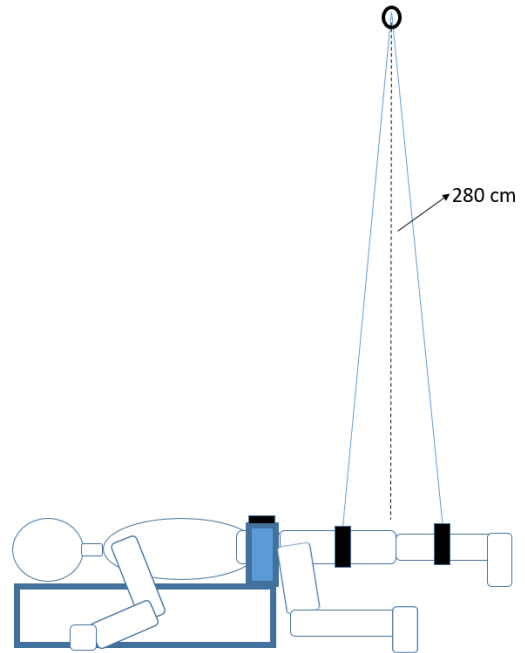


Figure 4.4: Experimental set-up for measuring frontal plane motion (abduction and adduction) moment-angle curves.

Two planes of motion at the hip, sagittal and frontal, were measured bi-directionally, with two conditions for hip flexion (straight leg and knee bent). The hip was pulled passive through the range of motion by the investigator at a slow and constant rate of 5-15°/sec. Passive hip resistance trials followed a series of light exercises (measured as part of studies in chapter 5 and 6) which served to provide a light tissue warm-up prior to testing passive hip stiffness. Each passive motion task (flexion straight leg (FSL), flexion knee bent (FKB), extension (Ext), abduction (Abd), adduction (Add) was performed a minimum of three times. Additional trials were collected if required if for example, monitored muscle activity was observed, or the knee buckled into flexion during the hip flexion straight leg condition due to “tight hamstrings”. There were never more than 6 trials required to complete three acceptable collections. A load cell (Transducer

Techniques™, Temecula, CA, USA) was used to collect the passive resistive force of the hip. The load cell was placed in-line with a leg strap and attached to rope which was pulled in a perpendicular direction to the leg. The load cell was calibrated in the laboratory with known weights after each testing session. The following sections describe the techniques used to measure each condition.

4.2.2.1 Hip Flexion Straight Leg (FSL)

Participants were set-up, side-lying in the passive hip testing apparatus (Figure 4.3) with the right leg suspended from the ceiling. The pulling rope was connected to the leg strap on the shank and held in-line with the load cell. The strap placed on the shank was measured to the greater trochanter and recorded for later moment calculations (Figure 4.5). In the rare occasion, if the knee buckled under tension of the hamstrings and posterior soft tissues the trial was repeated.

4.2.2.2 Hip Flexion Knee Bent (FKB)

Participants were set-up, side-lying in the passive hip testing apparatus (Figure 4.3) with the right leg suspended from the ceiling. The pulling rope was connected to the leg strap on the thigh and held in-line with the load cell. The strap placed on the thigh was measured to the greater trochanter and recorded for later moment calculations. The shank was not restrained allowing the hamstrings and posterior soft tissues to flex the knee without resistance allowing the hip to experience a full range of flexion (Figure 4.5).

4.2.2.3 Hip Extension (Ext)

Participants were set-up, side-lying in the passive hip testing apparatus (Figure 4.5) with the right leg suspended from the ceiling. The pulling rope was connected to the leg strap on the thigh and held in-line with the load cell. The distance from the greater trochanter to the point of

application (the thigh strap) was measured and recorded for later moment calculations. The shank was unrestrained during passive hip extension (see Figure 4.5).

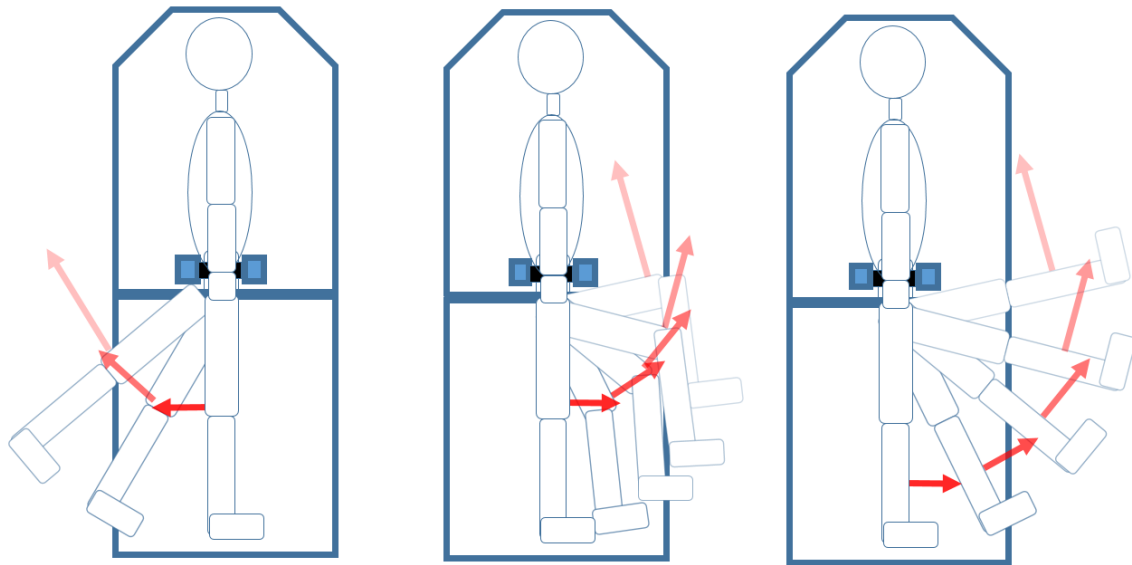


Figure 4.5: Schematic diagram of flexion and extension procedures for measuring angle-moment curves. Left – Extension, Middle – Flexion (Knee Bent), Right – Flexion (Straight Leg).

4.2.2.4 Hip Abduction (Abd) & Adduction (Add)

Participants were set-up, lying prone in the passive hip testing apparatus (Figure 4.6) with the right leg suspended from the ceiling. The pulling rope was connected to the leg strap on the shank and held in-line with the load cell. The strap was placed on the leg, just inferior to the knee joint on the shank, and the distance from the greater trochanter to the point of application (the leg strap) was measured and recorded for later moment calculations. The shank was not restrained. However, the knee was typically lockout at 0° due to the weight of the segments and the carefully adjusted sling heights and anatomical constraints in the knee; it remained in anatomical position during the passive pulls.

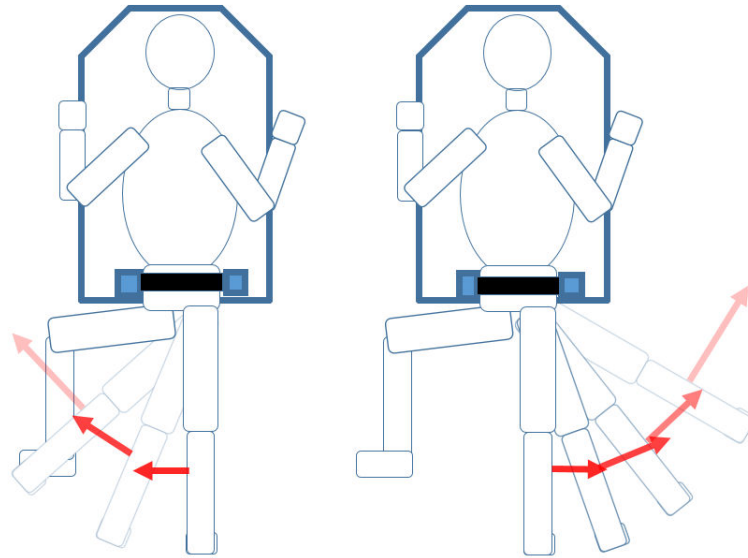


Figure 4.6: Schematic diagram of adduction (left) and abduction (right) procedures for measuring angle-moment curves.

4.2.3 Data Analysis

Load cell data and kinematic data were both filtered using a lowpass Butterworth first order digital filter at 2Hz (dual pass, effectively producing a second order zero lag filter). Several frequencies were reviewed to minimise noise and while maintaining peak magnitudes in the signals (see Appendix F) but ultimately a 2Hz cutoff was selected to maintain the physiological interpretation of the data while minimising noise and error.

To make comparisons between groups the data were analysed with individual means of the three trials collected and then group means were calculated from the individual means. Means were used to minimise random errors in the stiffness profiles of the data, yet still represented the individual physiological patterns in the data (Appendix D). The mean for each subject was used to calculate the mean of each group (male and female) and the fitted exponential curves were fitted to the group means. Finally, to evaluate the model performance with the group mean

angle-moment data the model was virtually moved in the identical range of motion as the mean passive ROM for the male subjects.

4.2.4 Statistical Analysis

Independent samples T-test were used to evaluate differences in peak moment, peak hip angle, neutral zone barriers (NZB), and the neutral zone width (NZW). All T-test comparisons were first analysed for equality of variances using Levene's Test, and the appropriate statistic (adjusted or not) were analysed with respect to the F-statistic and significance of $p < 0.5$.

4.2 Results

4.3.1 Hip passive ROM profile.

The data are presented in several forms, to best represent the behaviour of the passive resistive moment. First, Figure 4.7 displays the torque-angle data by subject. Considering the variability of initial angle, peak angle and peak moment individual behaviour on the torque-angle curves follow the expected characteristics for all subjects, planes of motion and direction.

The next series of plots shown in Figure 4.8-10 illustrate how the data were fitted to an exponential curve. A non-linear least squares exponential equation was fit to the mean data plot. The details of the coefficients and goodness of fit are seen in Table 4.1. The exponential equation was as follows:

(eq. 4.1)

$$M = ae^{b\theta}$$

Where, M , is the joint rotational moment (Nm), and, a and b are the coefficients. Next, the passive moment-angle resistance behaviour are shown with mean and standard deviation curves in Figures 4.11 to 4.15. In order to compare across groups and individuals and to control for ROM differences, when considering sex differences, the moment-angle curves were normalised by angle to %ROM. The individual data for moment-ROM data is presented in Figure 4.16 followed by the mean and standard deviation (for moment only since data are normalised to angle) in Figure 4.17 and the fitted exponential curves are shown in Figure 4.18. Exponential curves were also fit the moment-ROM data and the coefficients and goodness of fit for both moment-angle data fitted to the mean and moment-ROM data fitted to the individual trials at in Tables 4.2 and 4.3. The moment-ROM data was evaluated fitting the exponential equation to the group data as a whole as well as the mean data for the group (Figure 4.19). Finally, the passive joint rotational stiffness curves are shown in Figure 4.20. The equation used to derive the stiffness curves was the eq 4.1 by taking its derivative, which created the second equation:

(eq. 4.2)

$$k = abe^{b\theta}$$

Where, k , is the joint rotation stiffness. Peak passive joint rotational stiffness (PJRS) for FSL was more than three times higher than for FKB. While Add had the highest PJRS and FKB had the least.

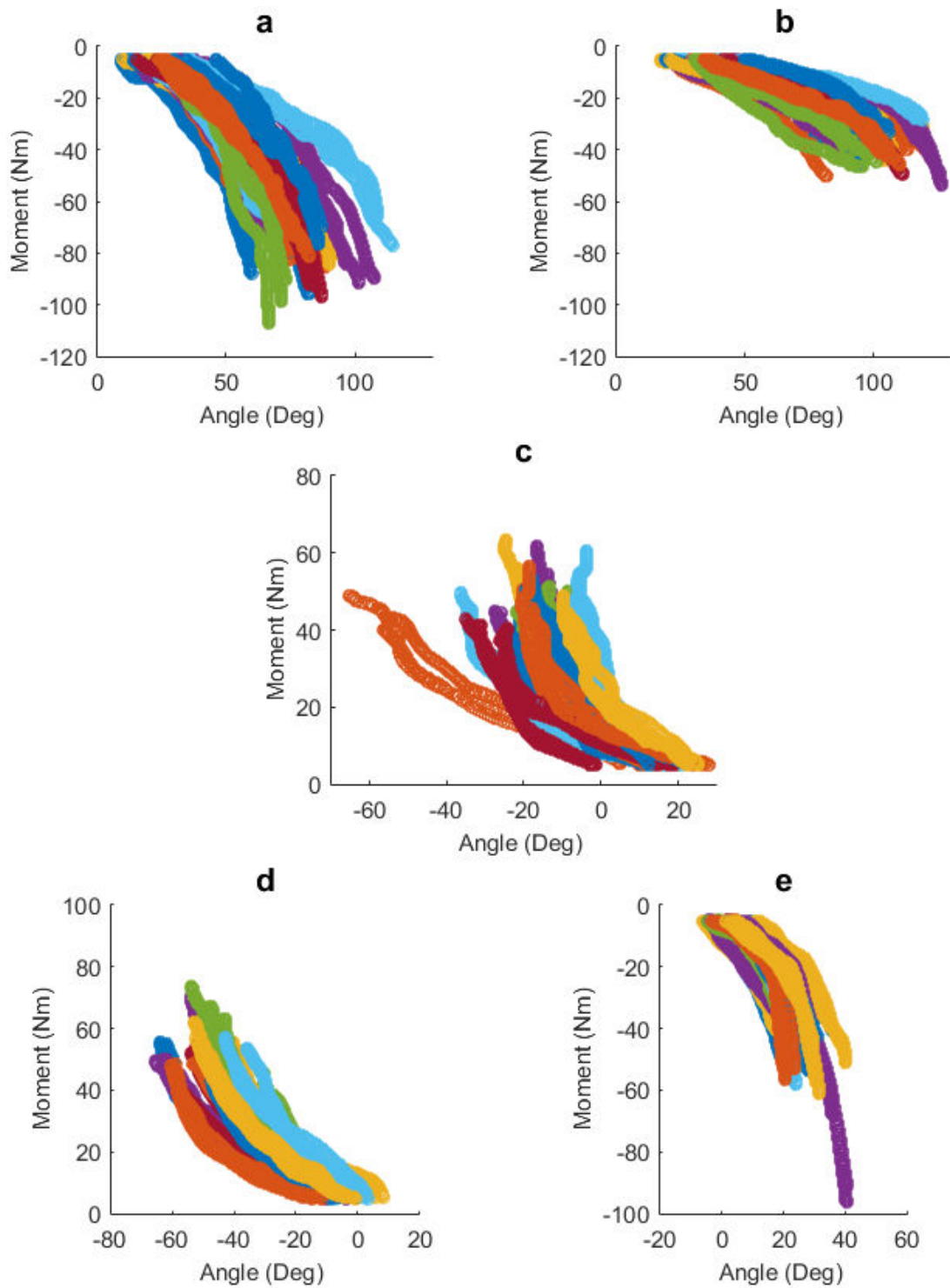


Figure 4.7: Subjects' mean torque-angle plots for (a) FSL, (b) FKB, (c) Ext, (d) Abd, (e) Add.

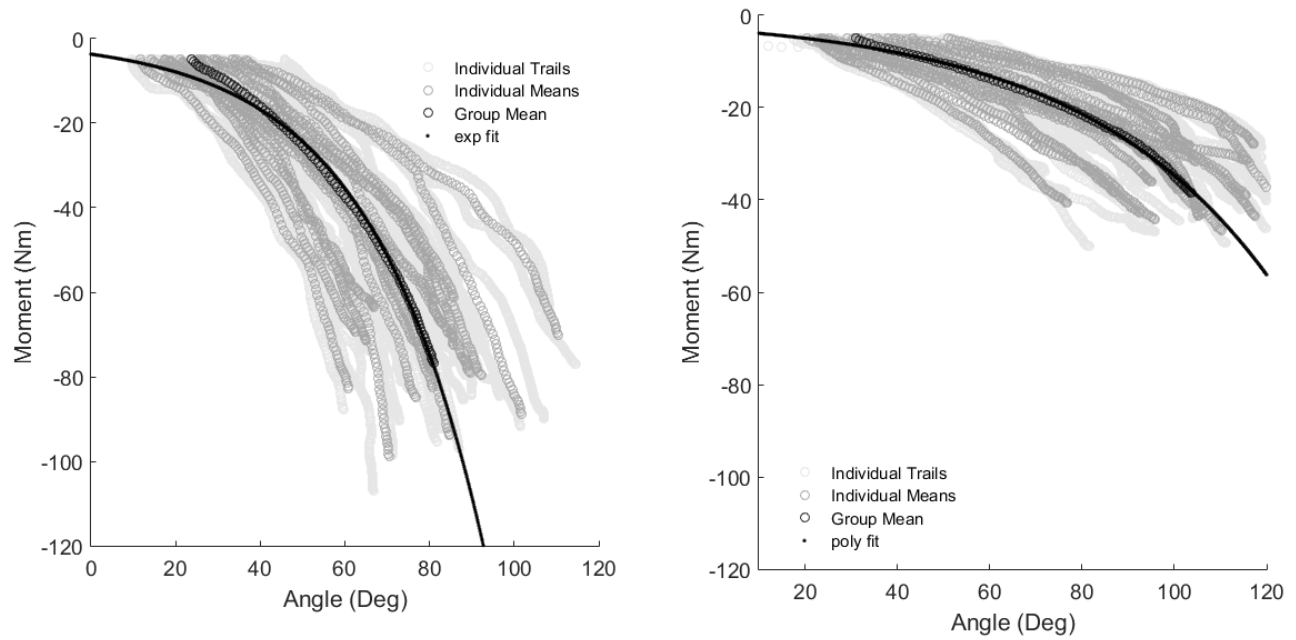


Figure 4.8: Passive hip resistance trials flexion straight leg (left) and flexion knee bent (right), individual means, and group means with a fitted exponential for the group mean.

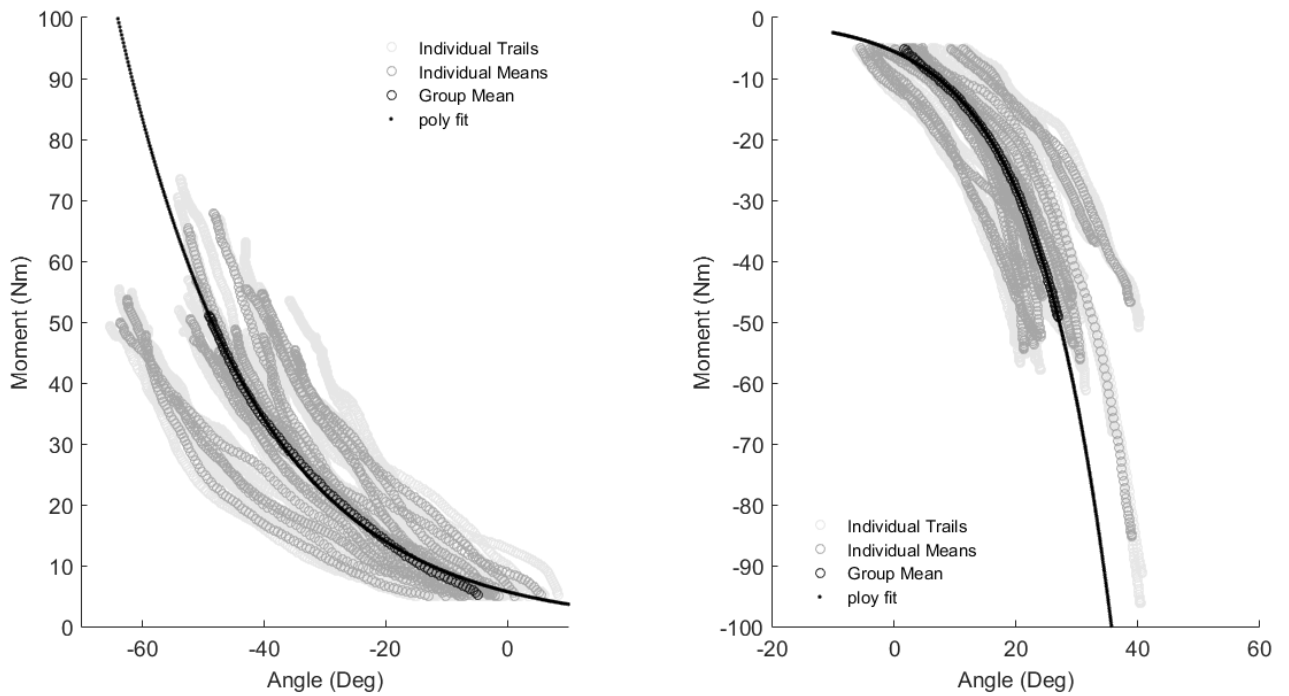


Figure 4.9: Passive hip resistance trials, abduction (left) and adduction (right), individual means, and group means with a fitted exponential for the group mean.

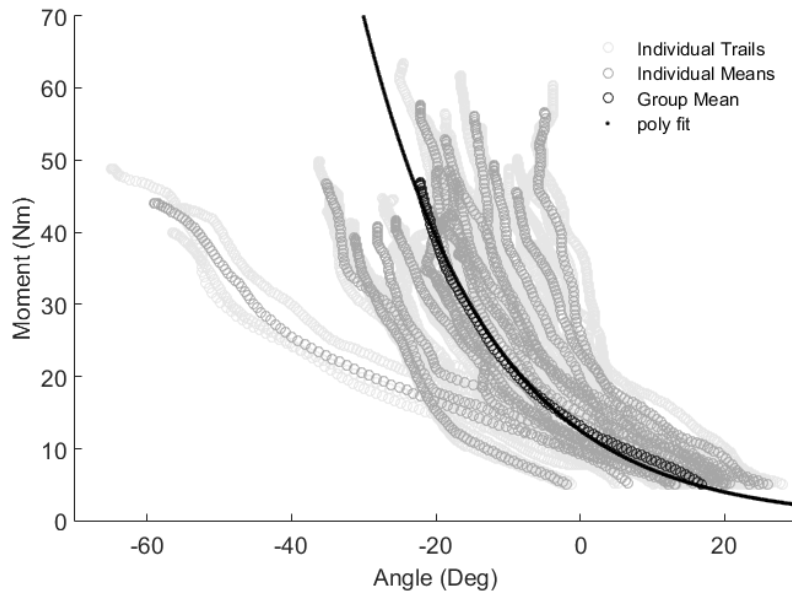


Figure 4.10: Passive hip resistance extension trials, individual means, and group means with a fitted exponential for the group mean.

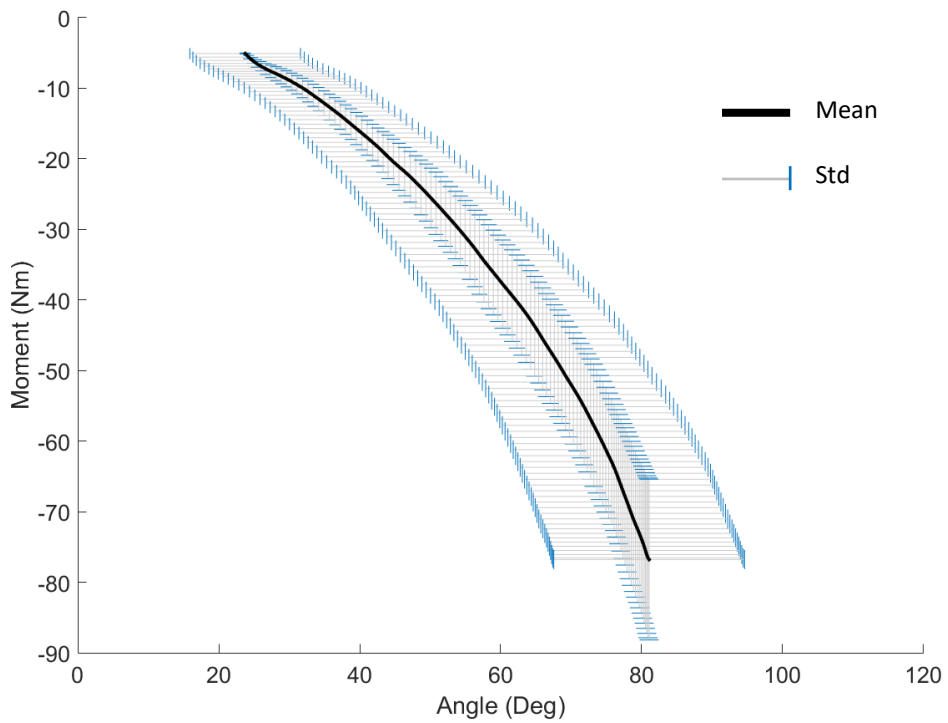


Figure 4.11: Mean male angle-moment curve for Flexion-Straight Leg and one standard deviation (Std) for both angle and moment data.

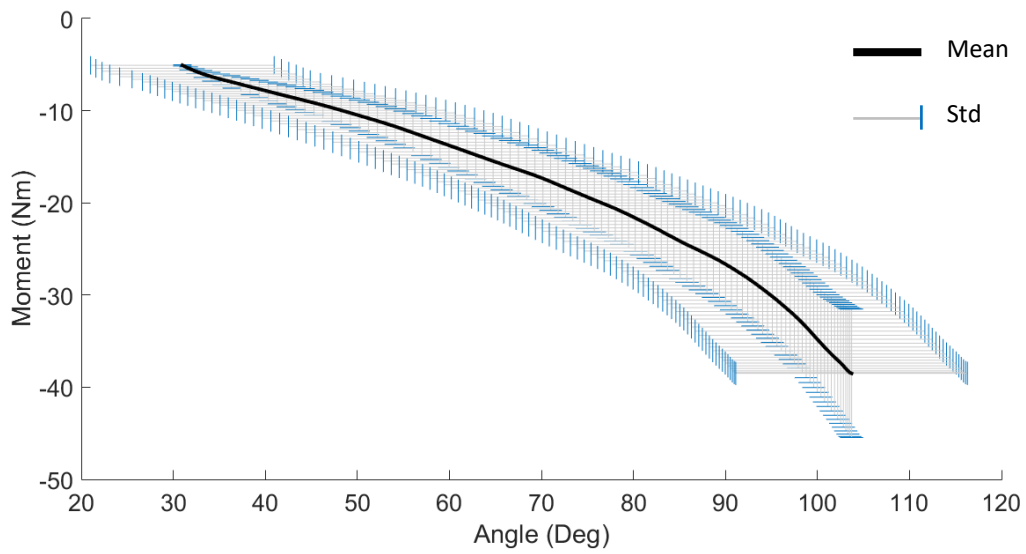


Figure 4.12: Mean male angle-moment curve for Flexion-Knee Bent and one standard deviation (Std) for both angle and moment data.

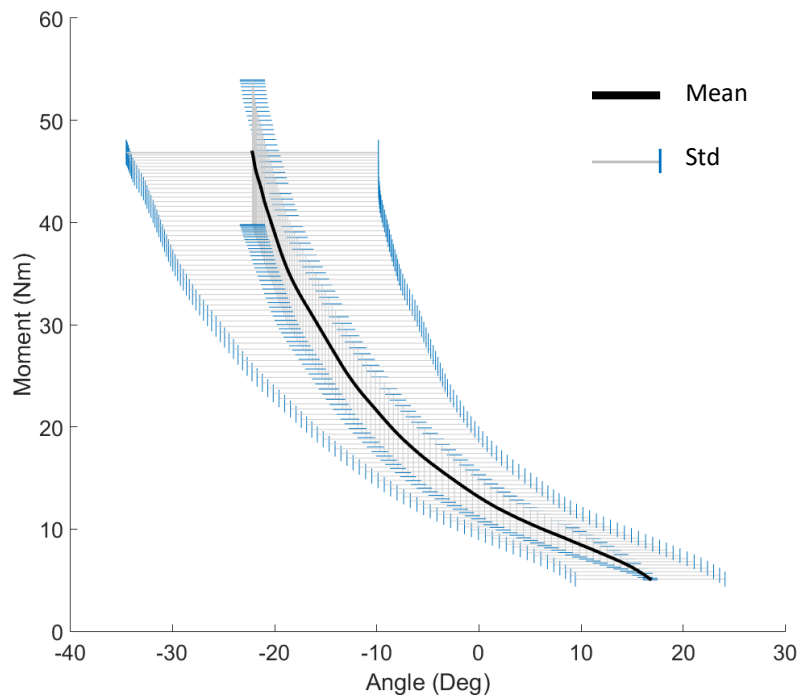


Figure 4.13: Mean male angle-moment curve for Extension and one standard deviation (Std) for both angle and moment data.

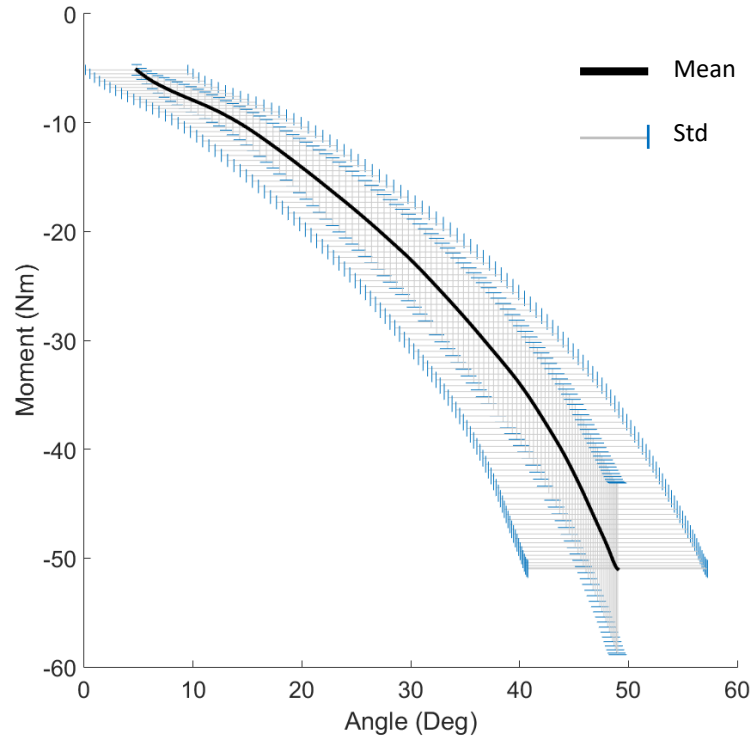


Figure 4.14: Mean male angle-moment curve for Extension and one standard deviation (Std) for both angle and moment data.

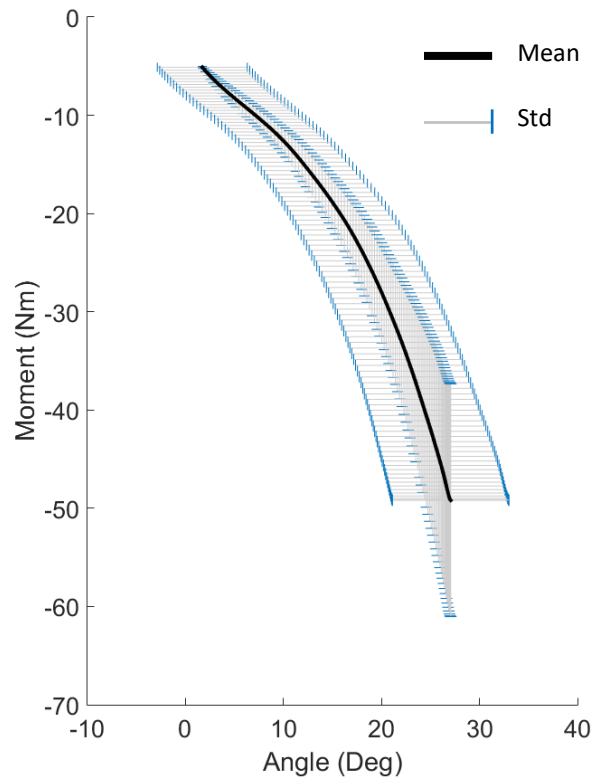


Figure 4.15: Mean male angle-moment curve for Extension and standard deviation (Std) for both angle and moment data.

Table 4.1: Equations of curve fit and goodness of fit measures for mean angle-moment data (males).

	Exponential Coefficients ($M=ae^{b\theta}$)		sse	R ²	rmse
	<i>a</i>	<i>b</i>			
Flexion – Straight Leg	-3.7976	0.0372	237.8109	0.9954	1.5499
Flexion – Knee Bent	-3.1057	0.0241	25.2350	0.9975	0.5049
Extension	12.5522	0.0572	103.8286	0.9942	1.0541
Abduction	5.6952	0.0447	42.4679	0.9980	0.6550
Adduction	-5.5518	0.0809	6.9356	0.9996	0.2647

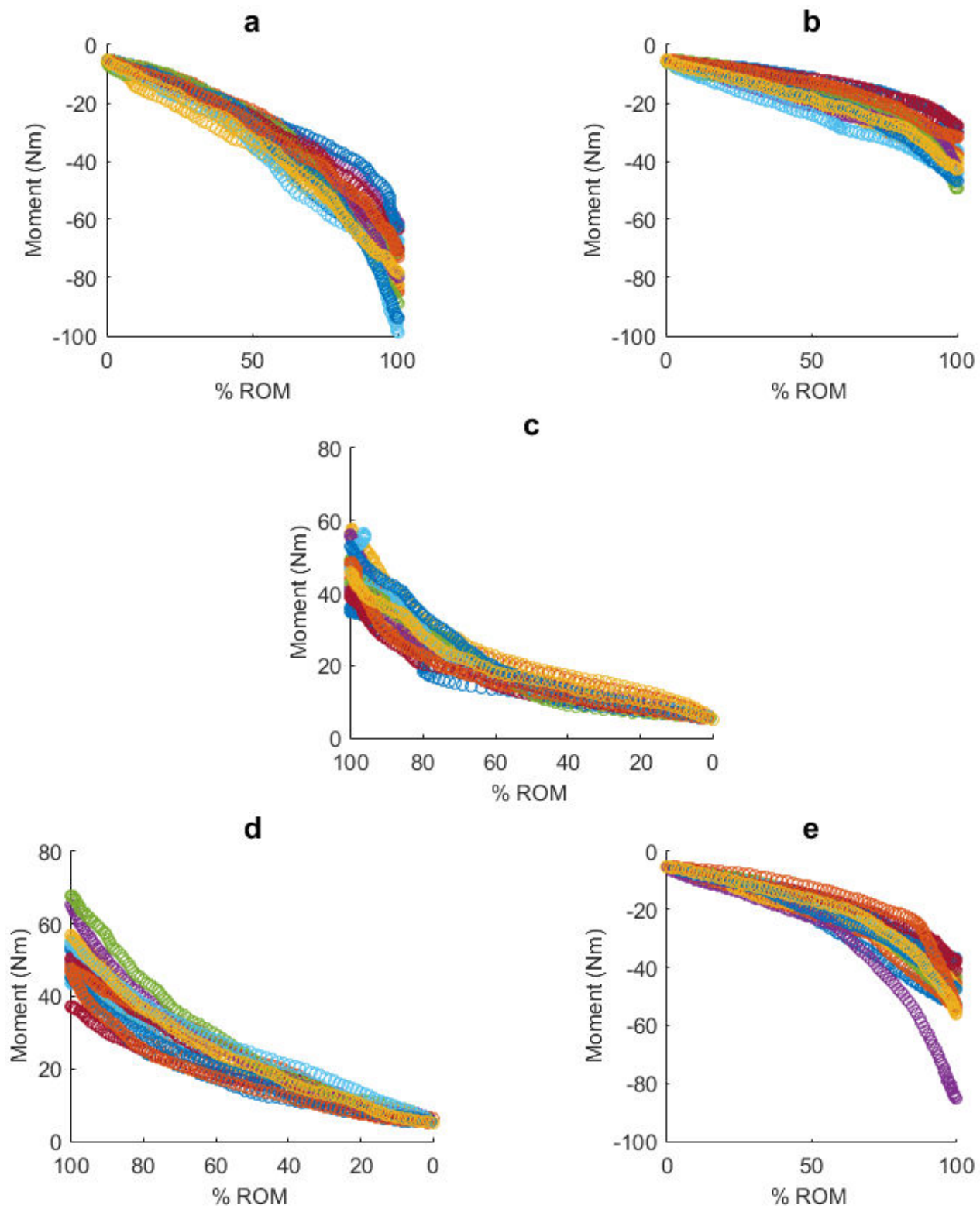


Figure 4.16: Subjects' mean torque-ROM plots for (a) FSL, (b) FKB, (c) Ext, (d) Abd, (e) Add.

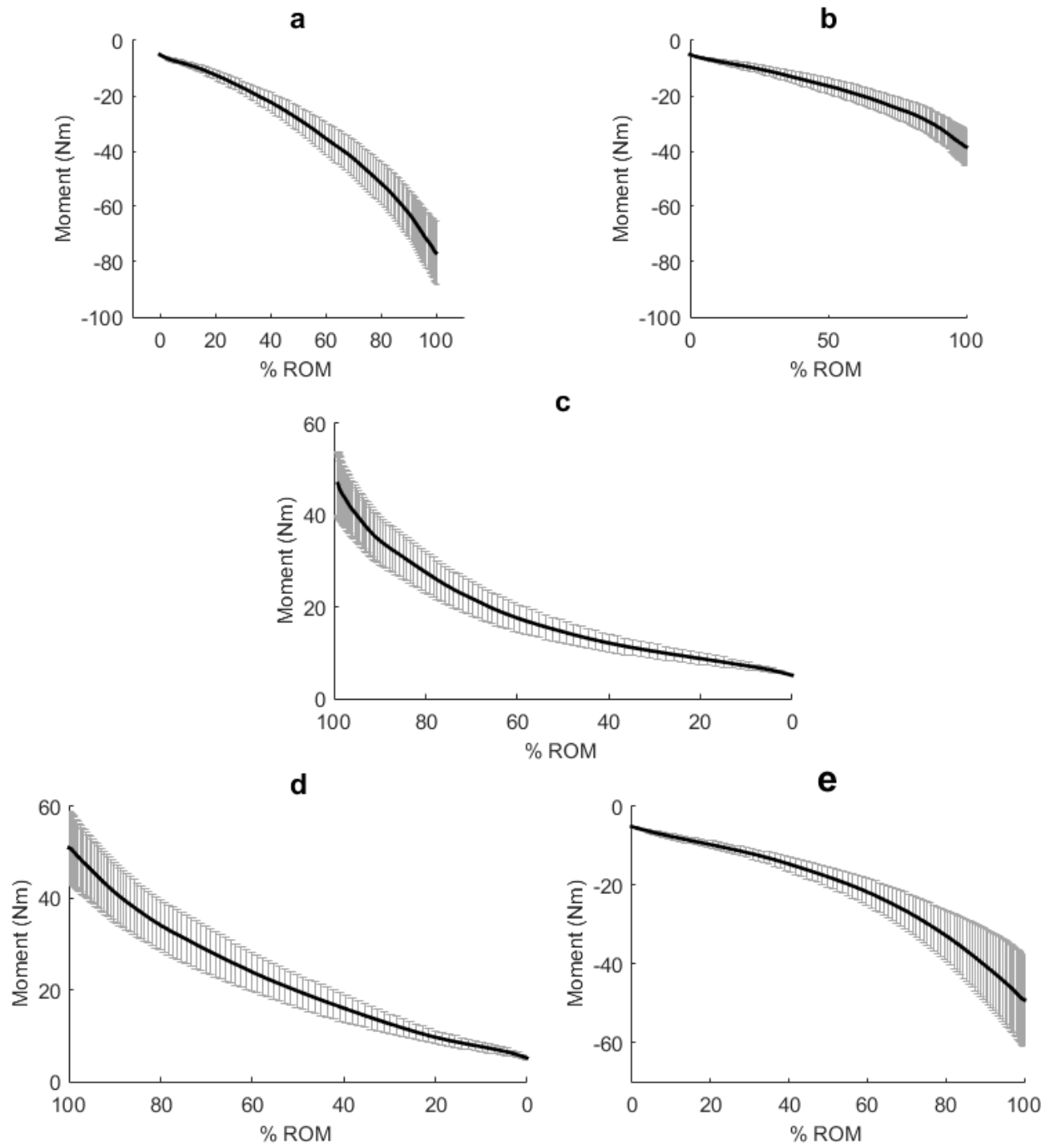


Figure 4.17: Mean male ROM-moment curve (black) with one standard deviation (Std) for moment data (grey ticks) for (a) FSL, (b) FKB, (c) Ext, (d) Abd, (e) Add.

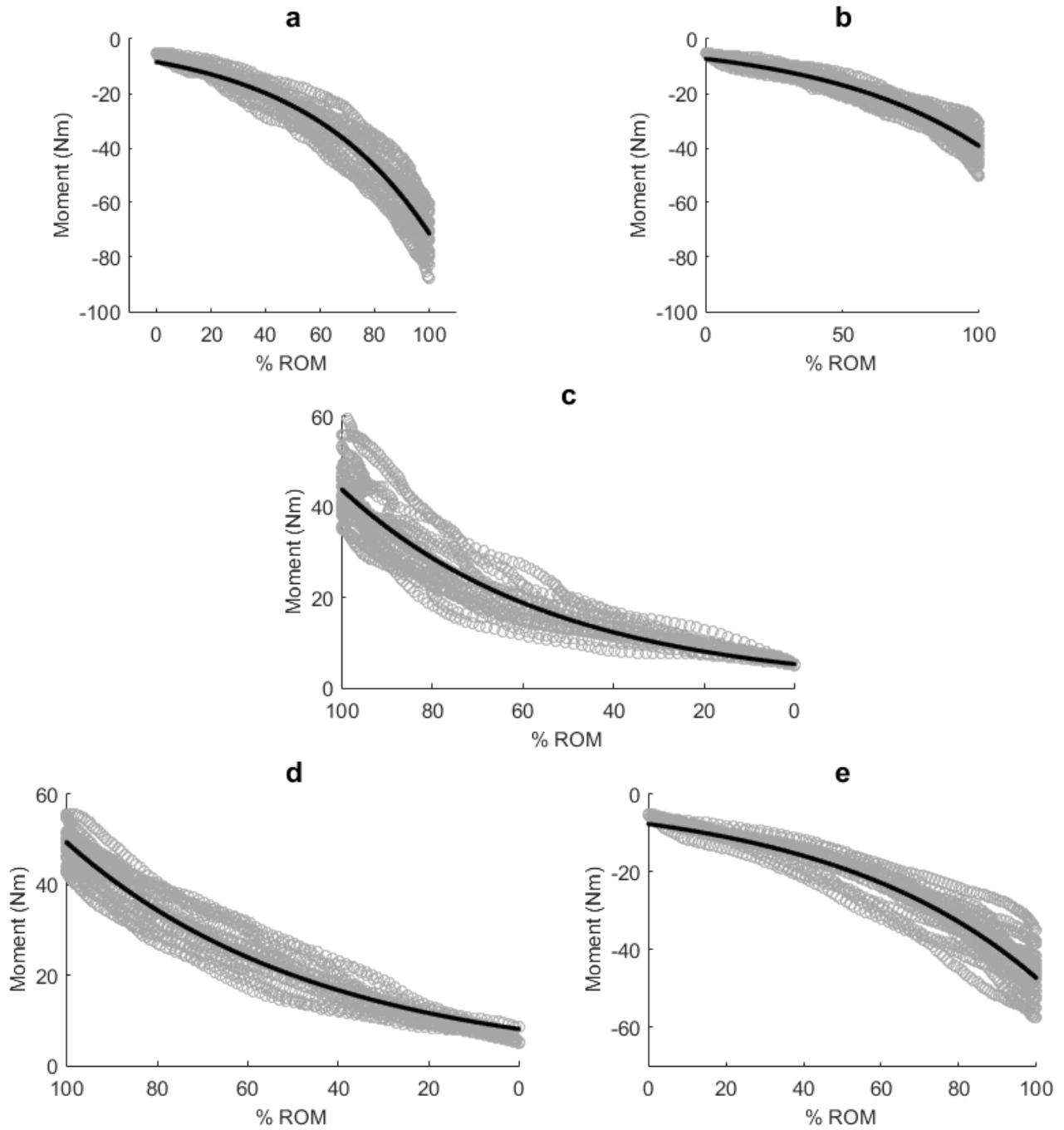


Figure 4.18: Torque-ROM curves with exponential curves fitted (black) to the individual trials (light grey) for (a) FSL, (b) FKB, (c) Ext, (d) Abd, (e) Add.

Table 4.2: Coefficients and goodness of fit measures for mean moment-ROM data (males).

	Exponential Coefficients ($M=ae^{b\theta}$)		sse	R ²	rmse
	<i>a</i>	<i>b</i>			
Flexion – Straight Leg	-3.7976	0.0372	237.8	0.9954	1.5499
Flexion – Knee Bent	-3.1057	0.0241	25.2	0.9975	0.5049
Extension	12.5522	0.0572	103.8	0.9942	1.0541
Abduction	5.6952	0.0447	42.4	0.9980	0.6550
Adduction	-5.5518	0.0809	6.9	0.9996	0.2647

Table 4.3: Coefficients and goodness of fit measures for moment-ROM curves of each trial (females).

	Exponential Coefficients ($M=ae^{b\theta}$)		sse	R ²	rmse
	<i>a</i>	<i>b</i>			
Flexion – Straight Leg	-8.4942	0.0213	55061.8	0.9223	6.03
Flexion – Knee Bent	-7.3281	0.0168	16717.8	0.9167	3.12
Extension	43.8502	0.0212	42968.6	0.8670	5.01
Abduction	8.1027	0.0181	22937.3	0.9344	3.6571
Adduction	-7.6689	0.0182	33834.9	0.8971	4.4417

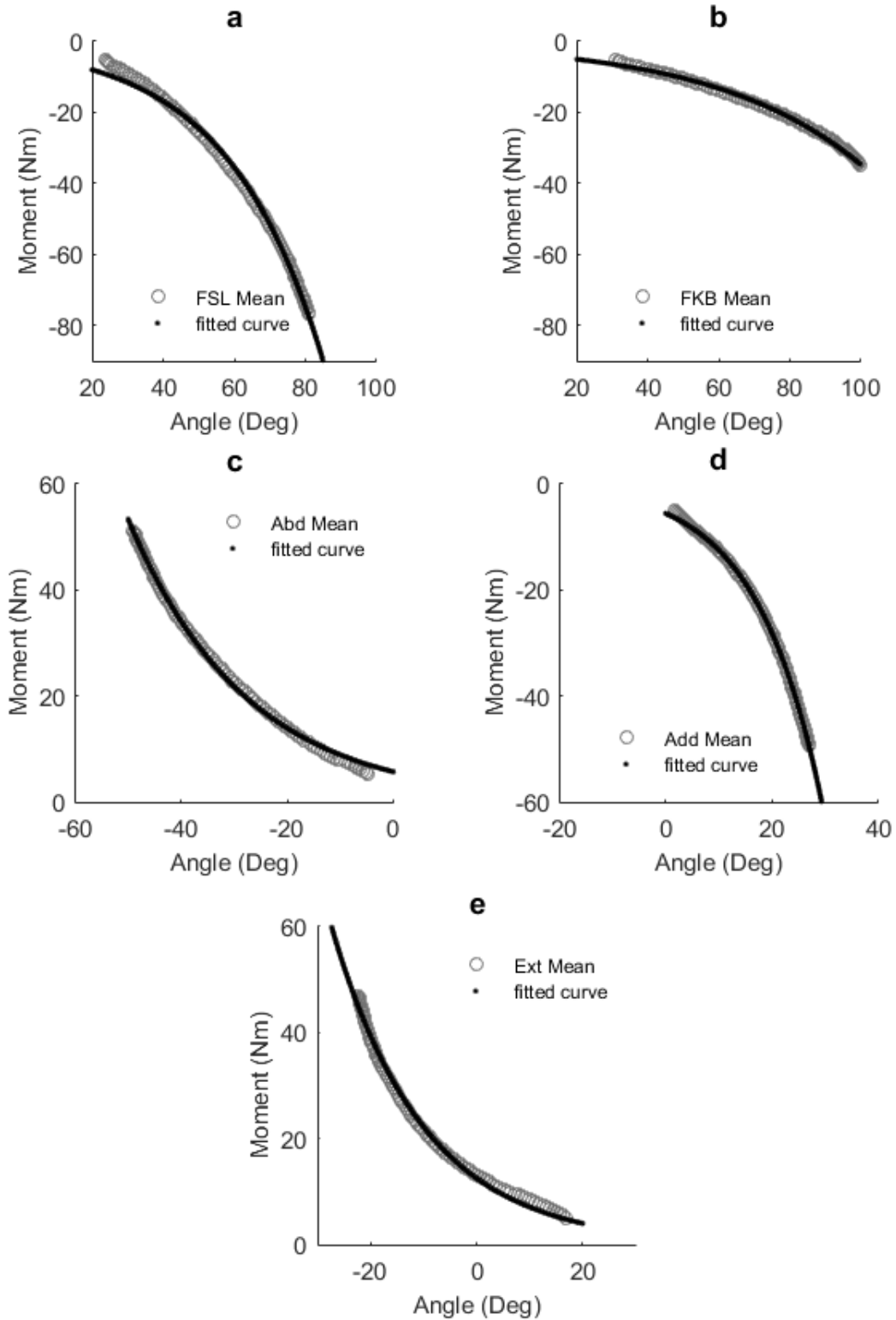


Figure 4.19: Angle-moment plots for males with fitted curves to the exponential function $M=ae^{b\theta}$. Subplots are defined as (a) Flexion – straight leg; (b) Flexion – bent knee; (c) Abduction; (d) Adduction; (e) Extension curves with mean experimental data (grey) and fitted curve (black).

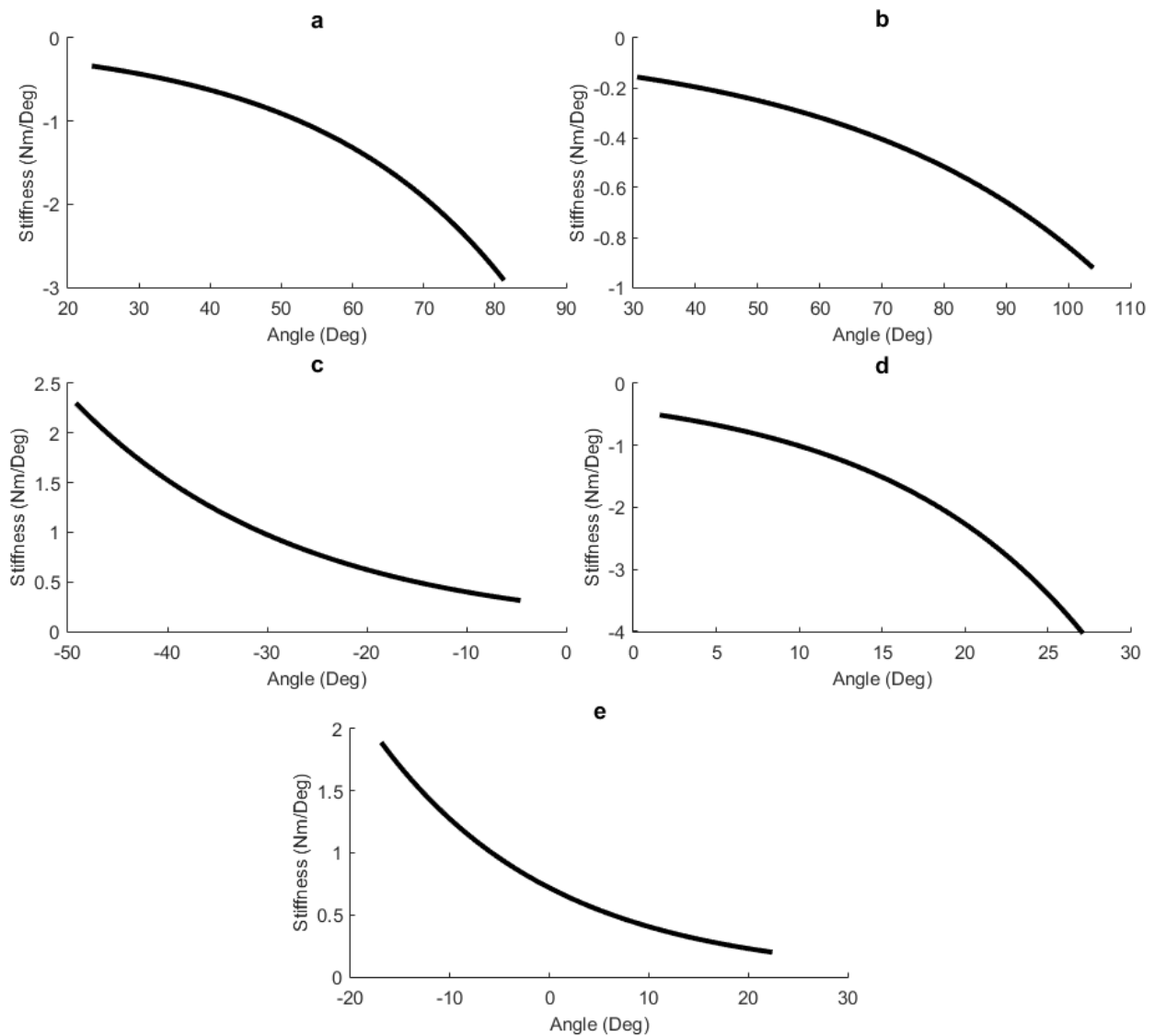


Figure 4.20: Passive hip joint rotational stiffness ($k=abe^{b\theta}$), subplots are defined as (a) Flexion – straight leg; (b) Flexion – bent knee; (c) Abduction; (d) Adduction; (e) Extension (males).

4.3.2 Compare male and female passive ROM profile

Overall, comparisons of the ‘passive ROM profile’ differed significantly between males and females. Comparisons of peak passive angle and neutral zone boundaries demonstrated differences between sexes as shown in Tables 4.1 and 4.2, respectively. Levene’s test was not

significant for any comparison, and therefore an equal variance was assumed for all comparisons. Females had higher peak angles in both flexion conditions (straight leg and knee bent); while peak extension and abduction were similar between sexes, and peak abduction angle was also greater in females. Only extension and adduction borders of the neutral zone differed between sexes. Males extension neutral zone was more biased to flexion ($\sim 17^\circ$) compared to females at ($\sim 6^\circ$). Similarly, females' adduction neutral zone border was shifted towards adduction at $\sim 10^\circ$ compared to males who were more neutral on average at $\sim 2^\circ$. Comparisons of neutral zone widths are displayed in Table 4.3. Levene's test was significant for comparisons between FSL-EXT and ABD-ADD. Therefore, the adjusted t-test statistics were evaluated base on the assumptions the variances were different for these comparisons. Males had considerably tighter neutral zones in FKB-EXT of approximately $\sim 60\%$ smaller ($t=-2.872$, $p < 0.01$) and ABD-ADD of approximately 44% smaller ($t=5.437$, $p < 0.01$) and strong trends of a smaller neutral zone in FSL-EXT approximately 54% smaller on average ($t=-1.855$, $p=0.076$). Interestingly there were no gender differences for any range of motion with respect to peak moment (Table 4.7). Male and female mean and standard deviations are graphically displayed in Figures 4.21-4.25 with side-by-side comparisons over the moment-angle curves. The ability of the fitted exponential curve to capture the behaviour of the passive hip resistance is shown in Figure 4.26. Table 4.8 provides the coefficients and goodness of fit values for the female data. Finally, Figure 4.27 provides a comparison of the male and female passive hip stiffness (PHS) with the stiffness-angle curves. The group trends show males have higher PHS at a given angle. The end range of hip extension appears to be the exception to this general observation.

Table 4.4: Comparison of neutral zone angle widths for passive resistance of the hip between sexes.

	Sex	Mean (Deg)	Std	t-test	p-value
NZ_FSL_EXT*	Male	6.90	6.32	-1.855	0.076
	Female	12.47	9.99		
NZ_FKB_EXT	Male	14.16	7.09	-2.872	0.007
	Female	23.36	10.86		
NZ_ABD_ADD*	Male	-6.50	2.89	5.437	<0.001
	Female	-14.73	5.19		

**Levene's Test of Homogeneity of Variances were significant, and the adjusted t-test statistic was evaluated.*

Table 4.5: Comparison of peak hip angle for passive resistance between sexes.

	Sex	Mean (Deg)	Std	t-test	p-value
FSL_max	Male	81.08	13.46	-4.894	<0.001
	Female	103.35	12.12		
FKB_max	Male	103.71	12.61	-2.185	0.037
	Female	112.26	8.94		
EXT_max	Male	-22.31	12.05	0.243	0.810
	Female	-23.17	6.82		
ABD_max	Male	-49.02	8.18	1.081	0.288
	Female	-52.84	11.66		
ADD_max	Male	26.98	5.79	-4.823	<0.001
	Female	38.56	7.75		

Note: Levene's Test for Equality of Variances was non-significant in all comparisons.

Table 4.6: Comparison of hip angle neutral zone barrier for passive resistance between sexes.

	Sex	Mean (Deg)	Std	t-test	p-value
FSL_min	Male	23.72	7.51	1.675	0.104
	Female	18.65	9.60		
FKB_min	Male	30.99	8.43	0.420	0.677
	Female	29.55	10.95		
EXT_min	Male	16.83	6.85	4.615	<0.001
	Female	6.19	6.10		
ABD_min	Male	-4.82	4.54	-0.101	0.920
	Female	-4.61	7.18		
ADD_min	Male	1.68	4.45	-4.846	<0.001
	Female	10.12	5.40		

Note: Levene's Test for Equality of Variances was non-significant in all comparisons.

Table 4.7: Comparison of peak hip moment for passive resistance between sexes.

	Sex	Mean (Deg)	Std	t-test	p-value
FSL_max	Male	76.8	10.96	1.371	0.18
	Female	71.82	9.30		
FKB_max	Male	38.49	6.61	0.804	0.427
	Female	36.37	8.30		
EXT_max*	Male	46.71	6.38	0.156	0.878
	Female	46.22	10.59		
ABD_max	Male	50.99	7.56	-0.218	0.829
	Female	51.63	8.93		
ADD_max	Male	49.08	11.21	1.631	0.113
	Female	43.62	6.88		

*Levene's Test of Homogeneity of Variances were significant and the adjusted t-test statistic was evaluated.

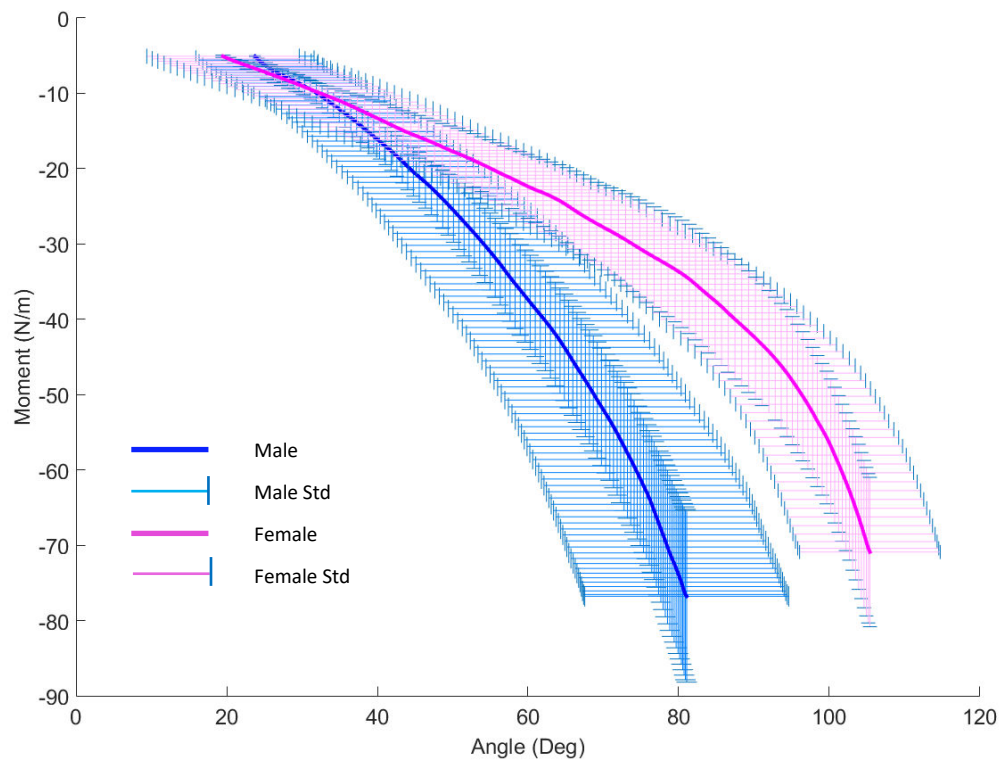


Figure 4.21: Mean male (blue) and female (magenta) angle-moment curves for hip flexion straight leg (FSL) with one standard deviation for angle (horizontal) and moment (vertical).

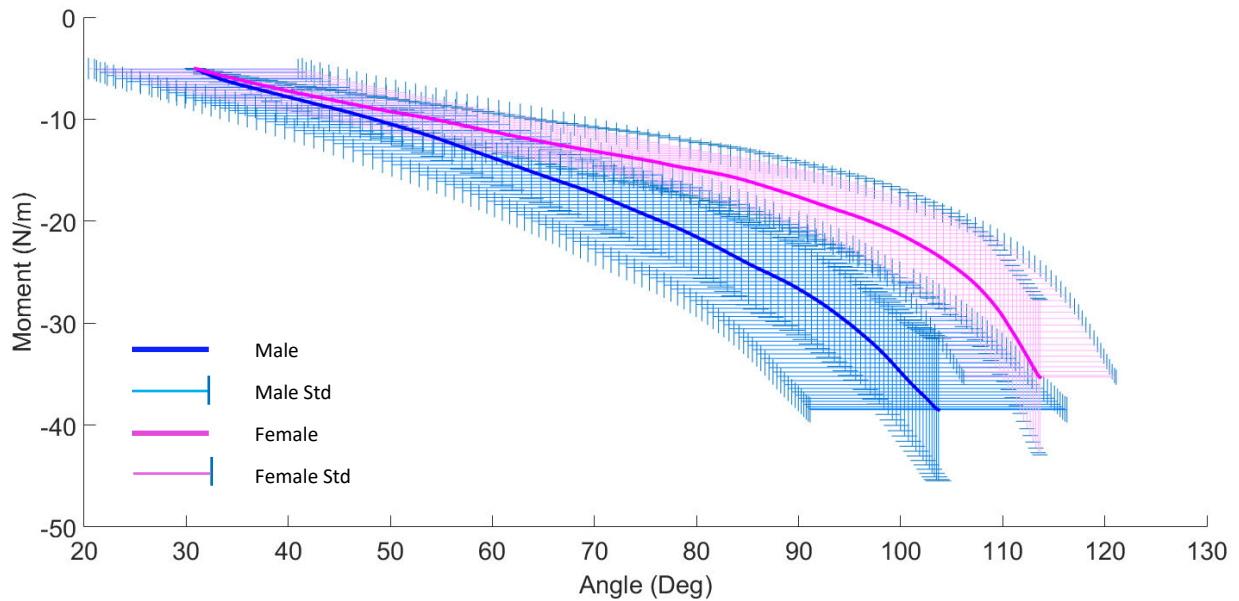


Figure 4.22: Mean male (blue) and female (magenta) angle-moment curves for hip flexion – knee bent (FKB) with one standard deviation for angle (horizontal) and moment (vertical).

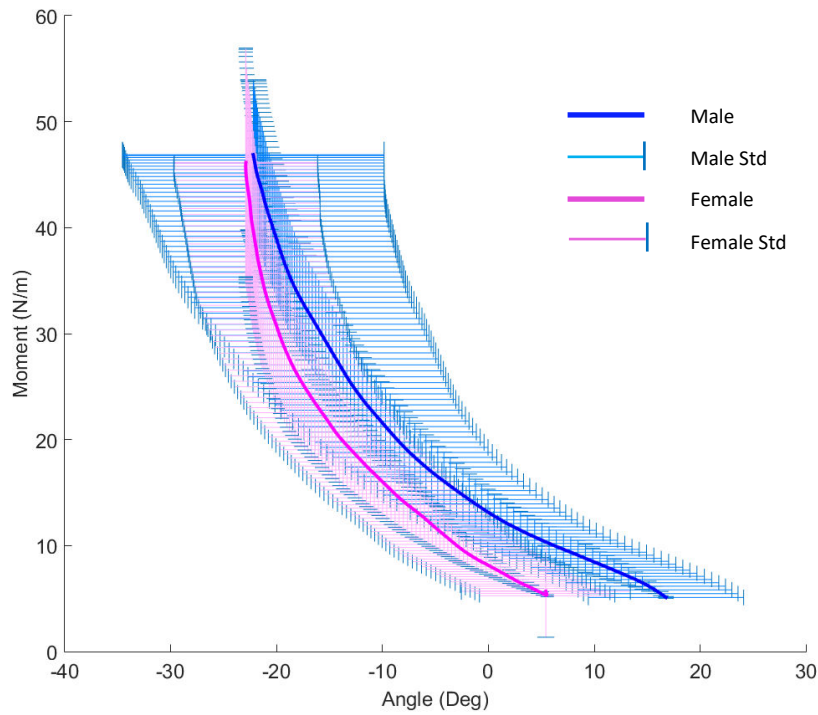


Figure 4.23: Mean male (blue) and female (magenta) angle-moment curves for hip extension (Ext) with one standard deviation for angle (horizontal) and moment (vertical).

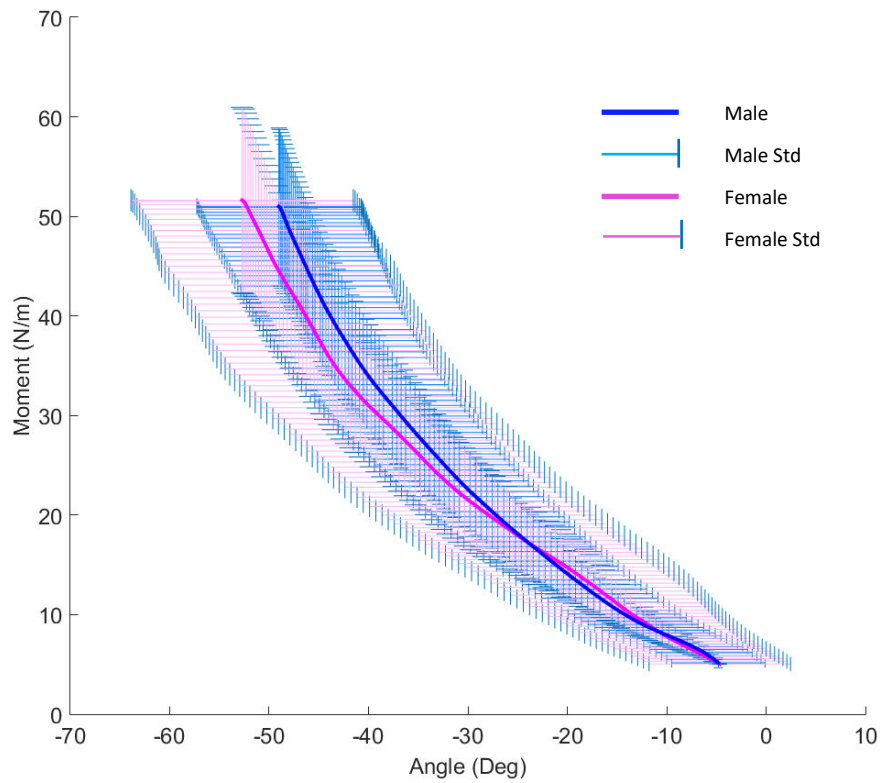


Figure 4.24: Mean male (blue) and female (magenta) angle-moment curves for hip abduction (ABD) with one standard deviation for angle (horizontal) and moment (vertical).

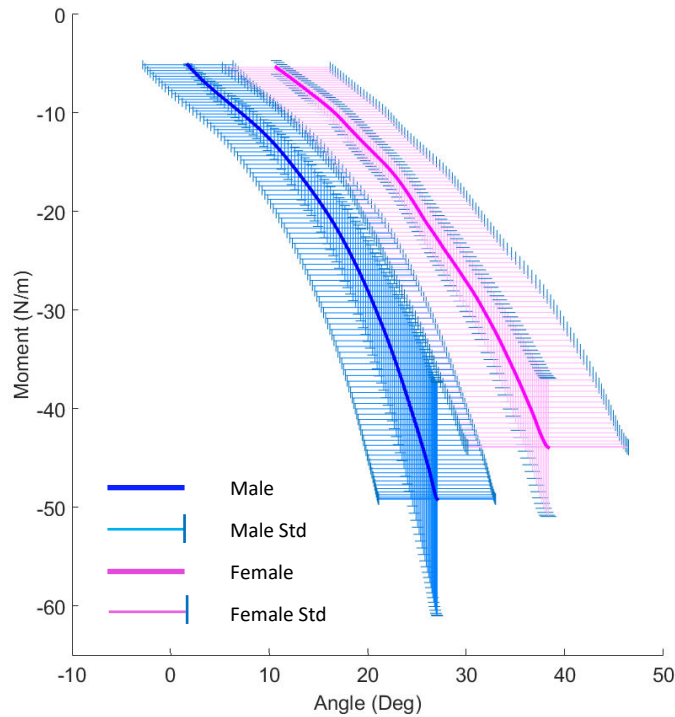


Figure 4.25: Mean male (blue) and female (magenta) angle-moment curves for hip adduction (ADD) with one standard deviation for angle (horizontal) and moment (vertical).

Table 4.8: Equations of curve fit and goodness of fit measures for mean angle-moment data (females).

	Exponential Coefficients ($M=ae^{b\theta}$)		sse	R ²	rmse
	a	b			
Flexion – Straight Leg	-4.4625	0.0256	305.8058	0.9915	1.7575
Flexion – Knee Bent	-2.8181	0.0212	211.5914	0.9700	1.4619
Extension	7.1127	0.0771	304.8217	0.9812	0.9810
Abduction	6.1726	0.0404	78.6805	0.9962	0.8915
Adduction	-3.5614	0.0665	77.0765	0.9945	0.8824

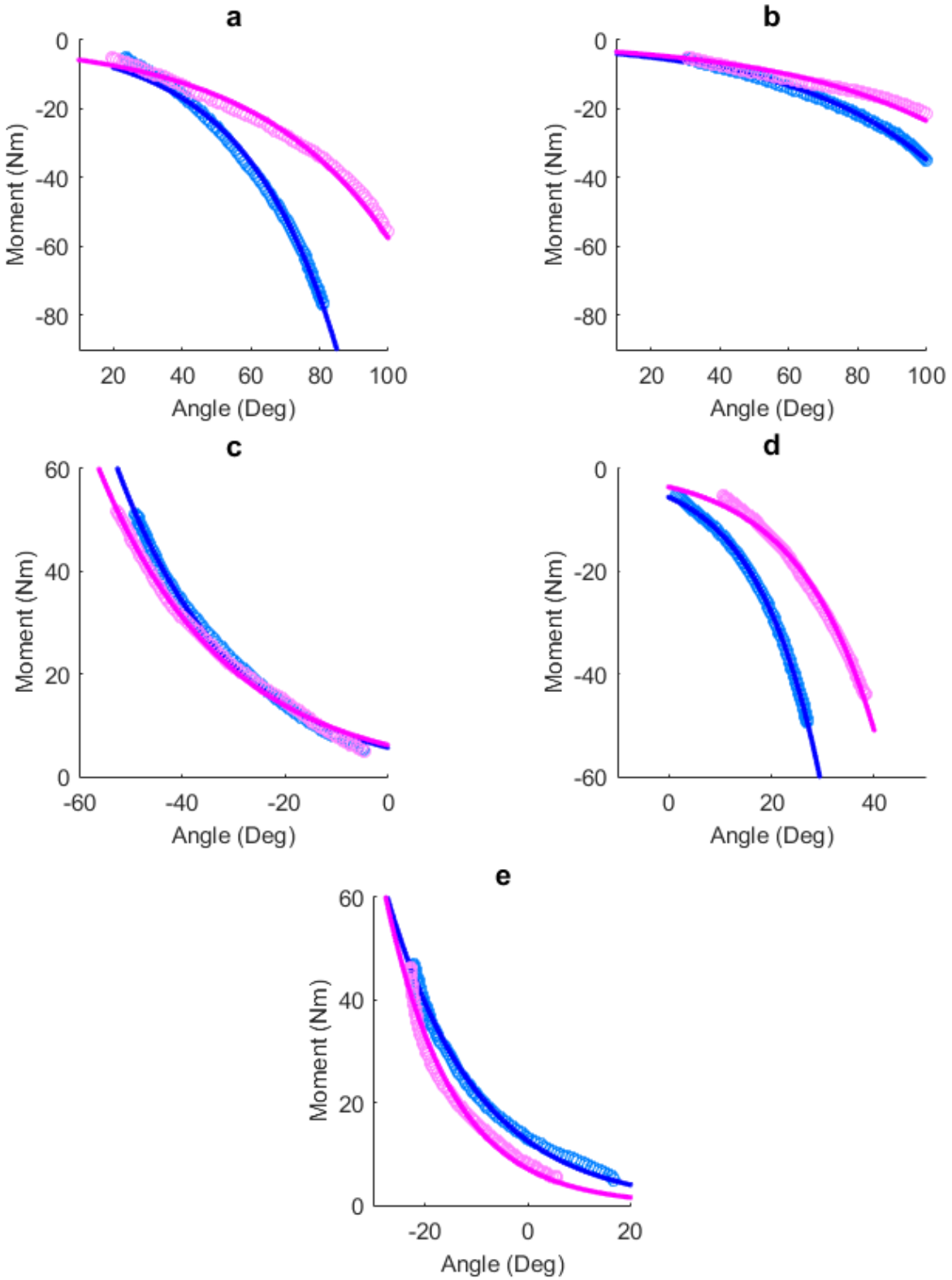


Figure 4.26: Female (magenta) and male (blue) moment-angle curves for (a) Flexion – straight leg; (b) Flexion – bent knee; (c) Abduction; (d) Adduction; (e) Extension curves with mean experimental data (light) and fitted curve (dark).

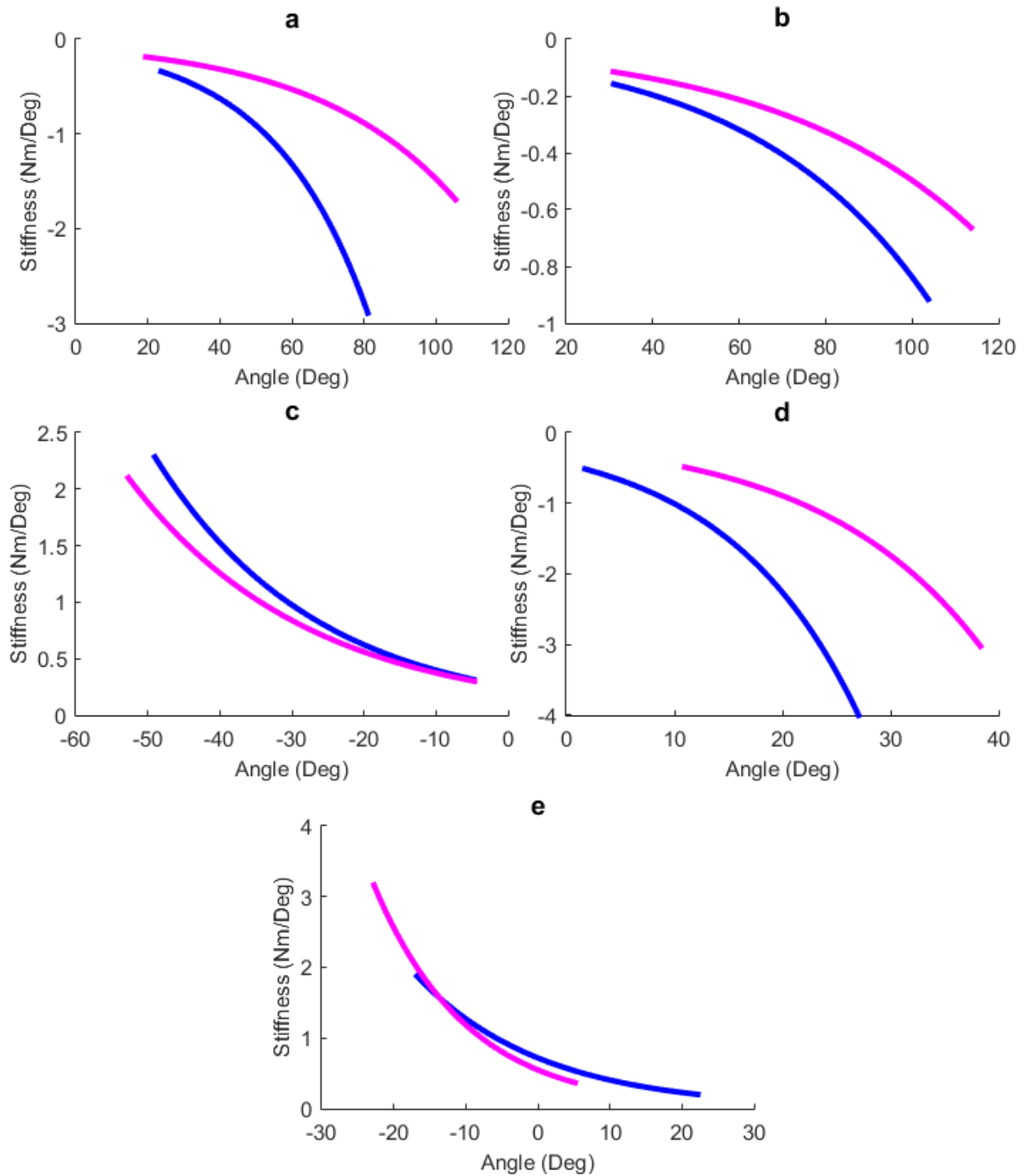


Figure 4.27: Comparison of female (magenta) and male (blue) passive hip joint rotational stiffness $k=abe^{b\theta}$. Subplots are defined as (a) Flexion – straight leg; (b) Flexion – bent knee; (c) Abduction; (d) Adduction; (e) Extension.

4.3.3 Evaluate the model performance estimating angle-moment curves.

The experimental data was evaluated in relation to the HSM predicted moment-angle curve. In general, the predicted HSM passive resistive moment captured the passive tissue resistance behaviour in the experimental data extremely well. Figures 4.28 and 4.29 demonstrate the predicted model performance with the moment-angle curves for the average male subject for the sagittal and frontal planes, respectively. In the sagittal plane, the model was sensitive to the knee flexion angle during both the FSL and FKB trials. This provides confidence in the constituent components of the HSM.

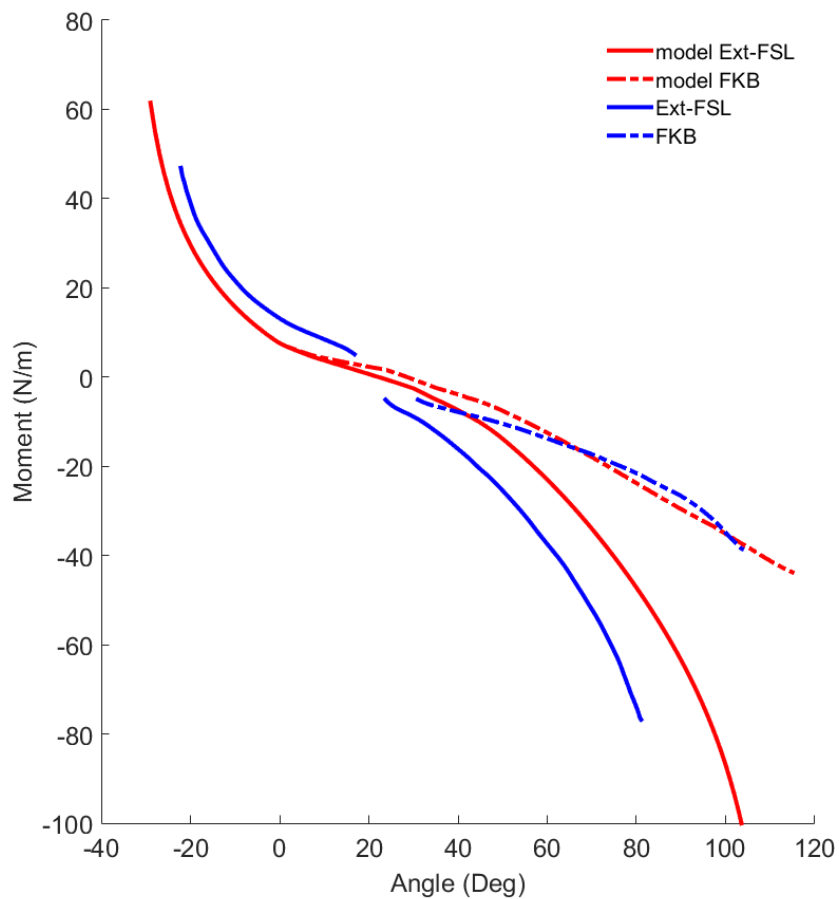


Figure 4.28: Experimental data (blue) and model predicted (red) passive hip angle-moment curves for extension to flexion straight leg (solid line) and knee bent (dash line).

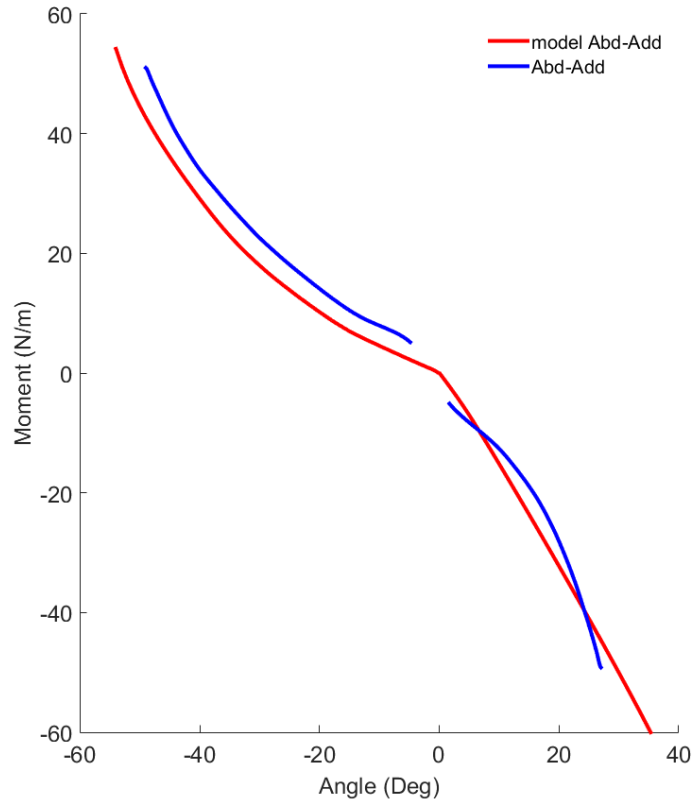


Figure 4.29: Experimental (blue) and model predicted (red) passive hip angle-moment curves for abduction and adduction.

4.4 Discussion

The main objective of this study was to characterise the moment-angle behaviour of the passive tissues of the hip in both the sagittal and frontal planes. Many of these observations lent themselves to descriptive analysis rather than statistical methods. However, there are areas in this analysis where statistical approaches were appropriate for comparison.

4.4.1 Hip passive ROM profile

The variance of responses obscured the ability of the fitted curves to represent the underlying tissue behaviour characteristics. Attempts were made to fit both exponential curves as well as polynomial curves. However, the experimental curve fitting approach was desired for several

reasons. Namely, this approach has been used extensively in the past (Yoon & Mansour 1982; S. McGill et al. 1994; S. M. McGill et al. 1994; Lee & Munn 2000) and allows the curve to continue the trend line behaviour beyond the experimental data range without fear of inflection points in the curve where the curve may no longer represent a physiological phenomenon. This is also a precaution when taking the derivative the moment-angle curve for joint rotational stiffness estimates. The first attempt to quantify group trends of the data using both curve fitting approaches (exponential and polynomial) failed to capture the individual's tissue behaviour accurately. To correct the ability of the fitted curves to represent the group data equations were fit to the group mean rather than the cluster of individual data. The data were normalised to trial length, from determined onset, when the moment exceeded 5Nm, to the peak moment, forming the end of the trial. The average for each individual was then calculated and each individual's mean was used to create a group (gender) mean. (Note: In one subject only two trials were deemed acceptable for extension, in another subject, a trial flexion trial was omitted – the curve of a single trial was not representative of the other two trials. Their data was omitted under the assumption of a collection error.) In this way, each subject was equally represented in the group mean. Ultimately, an exponential fit was selected, as the only difference when using a 3rd order polynomial was the ability to capture the toe region of the curve. However, the steep fall off below 5 Nm was likely non-physiological in the polynomial fit making it less desirable for a generalised fit (the exponential and polynomial comparisons are shown in the appendix to this section for completeness). The exponential curves fitted to group means were also extremely well suited to describe the curve behaviour as evidenced by the high R-squared and low RMSE values. Exponential curves have been widely used in the past to capture passive stiffness as well

as calculate joint rotational stiffness. This is due to the exponential characteristics of the passive tissues in vitro.

Similar results were observed with the moment-ROM data. Since the data were normalised, the fitted curves were calculated with respect to the entire data set rather than the group mean. The goodness of fit data more accurately represented the group data rather than the data fit to each trial (Table 4.2 and 4.3). When evaluating the moment-ROM curves the variation in data decreases compared to the moment-angle curves. This suggests that while absolute ROM in degrees may vary between individuals the behaviour when normalised to ROM is consistent (Figure 4.18). This being novel work, it is believed that presenting both moment-angle and moment-ROM data is desirable for future applications and comparisons.

4.4.2 Compare male and female passive ROM profile

Several differences exist between male and female passive hip ROM profiles. Males had smaller neutral zones (Table 4.4), and less ROM in flexion, extension and adduction (Table 4.5). Passive hip resistance begins at higher flexion angles for extension and more abducted angles for adduction. In other words, males have less total ROM in the hip and a smaller area of minimal passive resistance (or NZ) as defined here (less than ~5 Nm of resistance). Similarities exist between the peak moment at end range. Both males and females tested with similar end-range passive moment, though it took females more degrees of motion to achieve that moment. This is best shown in the comparison Figures 4.21 to 4.25, and in Figure 4.26 where the exponential curves are compared for males and females. The female data is equally well captured by its own exponential curve fit, as demonstrated by the R-squared and RMSE data (Table 4.8). Lastly, the

joint rotational stiffness curves, while following a similar pattern, show a distinct difference between males and females. Males have higher joint rotational stiffness at lower angles of motion. Moreover, with the exception of end-range extension, males demonstrate higher peak joint rotational stiffness.

No study, to this author's knowledge, has compared male and female passive hip moment-angle and joint rotational stiffness in either the sagittal or frontal planes. Of particular interest to this comparison is the potential for revealing the underlying injury mechanism given the overwhelming discrepancy in prevalence between the sexes in injuries like non-contact ACL strain/tear (Ford et al. 2000; Hewett, Myer, et al. 2006b). The dynamic control of the hip or better yet, the kinetic chain, requires ongoing feedback to balance the applied forces, moments, and stiffness required for controlled movement. The question of injury mechanism in ACL injuries will be more directly investigated in the next section of this thesis. However, it is worth mentioning the potential contribution of increased joint compliance in females compared to males since the hypothesis of increased ACL injury is turning towards a control strategy deficit at the hip. A lack of hip control, which is comprised of both active and passive components, could contribute to dynamic valgus during a landing activity and predispose one to an ACL injury. Based on these results it would appear as though females would require superior active control strategies to their male counterpart given the potential deficit in joint compliance. More on this later, for now it is important to note the significant differences in passive hip profiles between men and women.

4.4.3 Evaluate the model performance estimating angle-moment curves.

The HSM allows for the understanding of the distribution of load among the various tissues. The HSM model was highly congruent with mean male and able to predict differences in both the frontal and sagittal planes, and even with changes to knee flexion during hip flexion. As mentioned above this enhances the confidence of the model constituents and allows for the examination of synergies and mechanics in more detail. For example, comparing the hamstrings group during the FSL and FKB the effects of the knee flexion to shorten the hamstrings and therefore create a reduction in the passive resistive torque is substantial (Figure 4.30). The model provides a method to probe the mechanical interplay of, for example, bi-articulate muscles which is otherwise difficult or impossible to quantify.

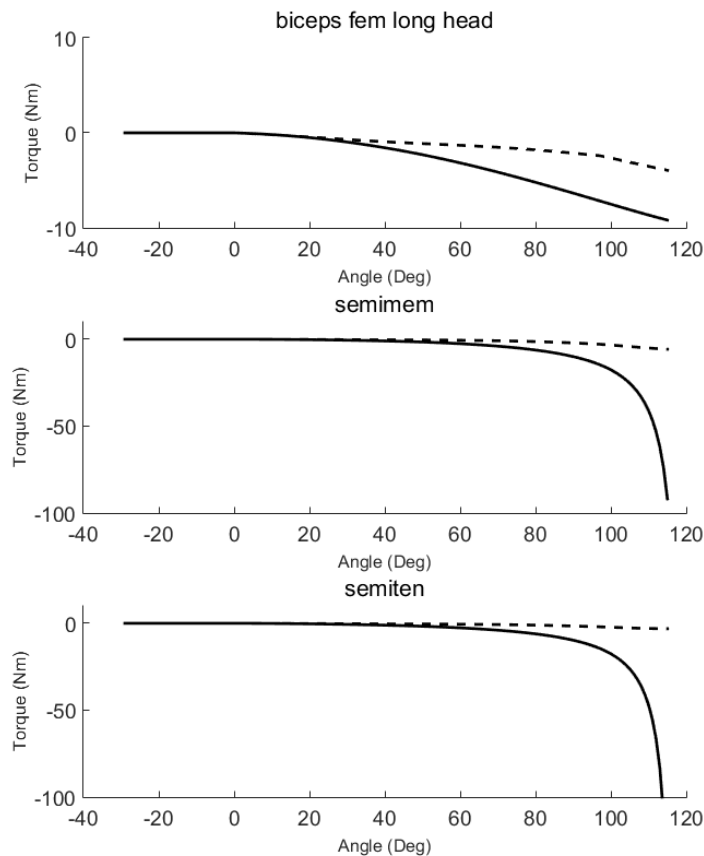


Figure 4.30: Flexion - extension passive torque-angle curves with both FSL (solid line) and FKB (dash-line) respective contribution from Biceps Femoris, Semitendinosus, and Semimembranosus. The change in knee angle effects the muscle length enough to greatly reduce the predicted hamstring contribution to total hip moment.

4.4.4 General Discussion

Vrahas and colleagues (1990) examined 15 males' passive hip resistance and found results were insensitive to rates of pull from the examiner implying viscosity is not an important consideration. Not only is this important when interpreting this study but it is also important when comparing between studies. Their results were similar to the current study considering they were near ~20 Nm at 60 degrees of hip flexion, with a trend line suggesting an exponential increase following this point. Yoon and Mansour (1982) measured ~45 Nm at ~60 degrees of hip flexion. This places this study within the variance of previous work. Moreover, both of these studies noted similar decreases with knee flexion at end range of flexion to this study. It should also be noted that these examples are taken from "representative" individual of the group and not a mean curve as presented in this study. However, the congruency between studies does provide confidence that the current data is consistent with the literature. This bolsters confidence in the methods used here for the frontal plane since no data is available in the literature for comparison. The exponential equations of this study provide moment-angle estimates over the full range of motion and can be more readily compared between future studies.

The association between hip mechanics and ACL injuries is thought to contribute to the increased prevalence of ACL injury among females. These non-contact ACL injuries are associated with dynamic valgus during landing and athletic cutting manoeuvres (i.e. abrupt directional changes) in sports like basketball or soccer, for example. One of the few studies to examine passive hip stiffness (or more accurately described as passive hip resistance) in males and females assessed the cross section of volleyball players (males and females), basketball and futsal (only

males) and evaluated the position of the hip passive resistance (PHPR) to gravity (Araújo et al. 2013). These results were similar to the data presented here, in that the hip resistance was greater in males than in females and males achieve less overall ROM during the testing procedure. These authors also indicated the potential of injury related to impaired control during landings or athletic cutting movements leading to dynamic valgus. Investigations of injury mechanisms, comparing male and female hip mechanics, should consider the potential of passive hip joint laxity when considering differences in male and female normal mechanics.

No study is without limitations and this study is no exception. Analysis was limited to a single hip and symmetry between sides is inherently assumed. In fact, there is known asymmetry that is documented in the pelvis and also highly dependent on ethnicity (Kurki 2017). However, the purpose of this work was not to quantify hip asymmetry but to analyze moment-angle behaviour, compare males and females, and evaluate model predictions of passive hip resistance. To this end, the evaluation of a single hip is justified. Next the apparatus (aka hip stiffness testing jig) does apply some force in the plane of action of the moment-angle curve. However, the attachment point (see Figure 4.3 and 4.4) of the ropes, located in the ceiling, minimised the vector cosine and therefore the potential of the apparatus to causing a significant amount of force in the horizontal plane. Lastly, the assumption of the GT as the axis of rotation for the moment arm calculation neglects the anatomical variability of, for example, the femoral neck angle. Since the length of the moment arm is substantially greater than this potential error source, it can be assumed that the error is minimal and therefore has a negligible effect on the results.

4.5 Conclusion

Several important contributions to the understanding of hip mechanics and hip modelling arose from this study. (1) Passive hip moment-angle and moment-ROM curves were quantified in the sagittal and frontal planes, bi-directionally, for males and females. Exponential curves were successfully applied to the experimental data to represent both the moment-angle/moment-ROM data as well as the passive joint rotational stiffness. (2) Passive hip ROM profiles were compared between males and females. Males have smaller NZs and less total ROM as compared to females. The definitions of kinematic NZ (degrees relative to the reference frame) are not the same as the passive kinetic NZ defined as the range of elastic equilibrium. (3) The HSM as described in chapter 3 can successfully estimate passive tissue resistance, which allows for the examination of the contribution from the constituent components within the model.

5.0 Study 3: Analysis of hip and spine mechanics: Implications for the risk for Anterior Cruciate Ligament injury

5.1 Introduction

A critical element of injury prevention is understanding injury mechanism. As described in the conceptual model presented in chapter three (Figure 3.1), injury occurs when loading demands exceed tissue tolerance. Movement and motor patterns modulate tissue loading, thus influencing the opportunity to promote or avoid tissue overload and the resultant injury. Infinite combinations of motor patterns can produce the same joint movement and an infinite combination of joint movements can be achieved through the linkage to produce goal-oriented movement. For example, given a similar external loading condition, if the mechanism of injury is understood, there is a possibility of modulating tissue load through corrective movement and motor patterns thereby redistributing the load concentration and avoiding tissue injury or failure. This, in theory, would reduce injury risk by restoring the balance of capacity and demands.

Injury screening techniques for non-contact ACL injuries, including movement pattern observation, have been suggested to provide the appropriate identification of at risk groups (Myer et al. 2010b). Among the at-risk group was high level female athletes, participating in sports like basketball and soccer, where an increase prevalence of 2.5-7.5 times greater than their male counter parts at a similar level and exposure in the NCAA was seen (Arendt et al. 1999; Arendt & Dick 1995). When examining non-contact ACL injuries understanding hip function has proven to be quite valuable by providing insight into injury mechanism (Hewett & Myer 2011; Hewett et al. 2010; Reiman, Bolgia, et al. 2009). Recently, Myers, Hewett and colleagues identified

two major deficiencies in this population, one, a ‘neuromuscular’ pattern (Hewett et al. 2004) and two, a ‘biomechanical’ pattern (Myer et al. 2010a; Myer, Ford, et al. 2011; Myer et al. 2010b) both relating to predicting and influencing (Myer et al. 2007b) ACL injury. The next evolution of the understanding of these mechanisms is threefold: one, a more biologically driven, robust investigation of tissue loading available with the development of the aforementioned model in Chapter 3, and two, a more holistic examination of the kinetic chain including hip and spine mechanics; and three, a detailed evaluation of neuromuscular control strategy. Ultimately, the goal of this work is to improve understanding of at-risk behaviour that may lead to injury. A detailed understanding of the injury mechanism and how it affects joint mechanics will lead to superior prevention and management strategies. Only total joint load estimates have been evaluated thus far, and it is hypothesized that the use of more sophisticated modeling approaches will likely improve the precision of the understanding of ACL injury mechanisms with the possibility of improving rehabilitation and prevention techniques.

Specifically, the research questions and accompanying hypotheses were:

- (1) How do those with high and low knee valgus differ in joint angles, load, and EMG profiles?
 - i. It is hypothesised that comparing a sub-set of high and low valgus groups will have differences in joint angles, joint loads, tissue loads and EMG patterns (Table 5.1).

Table 5.1: Specific Research Questions and Hypothesis for the primary outcome measures.

Specific Questions	Related Hypotheses
Joint Angles: <ul style="list-style-type: none"> - Does flexion angle differ between valgus groups? 	Joint Angles: <ul style="list-style-type: none"> - Spine, Hip and Knee Flexion angles will be larger in the HVG.
Joint Loads: <ul style="list-style-type: none"> - Forces: Does AP shear differ between valgus groups? - Moments: Do moments in the spine, hip and knee differ between groups? 	Joint Loading: <ul style="list-style-type: none"> - Forces: Joint AP shear will be greater in the HVG. - Moments: Joint moments in the spine, hip and knee will differ between groups in all directions.
Motor Patterns (EMG): <ul style="list-style-type: none"> - Do peak EMG and iEMG hip abductor muscles (TFL, GMed, GMax) differ between the HVG and the LVG? - Do the QUAD peak and iEMG motor patterns differ for the HVG and the LVG 	Motor Patterns (EMG): <ul style="list-style-type: none"> - Hip abductor muscles (TFL, GMed, GMax) will be greater in the LVG for both peak and iEMG - QUAD activation will be higher in the HVL for both peak and iEMG

*Joint implies all joints in analysis, spine, hip, and knee.

In addition, as part of a secondary analysis, several research questions arose focusing on the interpretation of continuous data. These questions and hypotheses are listed here:

- (1) Does dominate knee valgus correlate to non-dominate knee joint valgus? Is it possible to predict knee valgus in the non-dominate knee from the dominate knee?
 - i. DKV in the dominate limb will correlate with the non-dominate limb.
 - ii. DKV can be predicted from the dominate limb to the non-dominate limb.
- (2) What are the strongest predictors (of those recorded) for high dynamic knee valgus?
 - i. No single variable will emerge as a single best predictor for DKN.
 - ii. The dominate (right) and non-dominate (left) will have a unique set of “best” predictors of DKV.

(3) Which muscles' activation pattern best predict dynamic knee valgus?

- i. The abductor group (GMed and TFL) and GMax will best predict DKV.

5.2 Methods

A cohort of young adult females participated in a laboratory-based study to investigate non-contact ACL injury risk. Participants performed jumping and landing tasks while biomechanical data was collected.

5.2.1 Study Design

A cross-sectional study design was used to evaluate the mechanics of two sub-groups, high and low valgus risk, during a drop vertical jump task (DVJ).

5.2.2 Participants

Eight-teen female participants ($n = 18$; age = 20.7 ± 1.3 years; height = 1.64 ± 0.05 m; mass = 56.2 ± 11.0 kg) were recruited from the university undergraduate population including both recreational and varsity athletes from a variety of sports (soccer, basketball, volleyball, rugby, and martial arts). Participants were included between the ages of 18-25 and generally healthy enough to participate in moderate exercise. Exclusion criteria included chronic or recurrent lower limb and/or back injury, current or chronic pain in the back or lower limb, any pathology related to balance impairment or other condition(s) limiting the participant's ability to participate in exercise.

5.2.3 Tasks

The drop vertical jump task was performed using a 31 cm high box and dropping on to two adjacent force plates. The participants stood upright with their feet shoulder width apart and

toes at the edge of the box. The participant was asked to “drop off the box” using both feet simultaneously and asked not to jump up, but rather simply jump forward towards the force plates. The landing absorption phase was timed with the counter movement effort of a maximum vertical jump. The participant’s feet had to land clearly onto each force plate and with a single contact from each foot, in other words, “sticking the landing” with both feet at the same time. Finally, they returned to a resting upright standing position with feet approximately shoulder width apart.

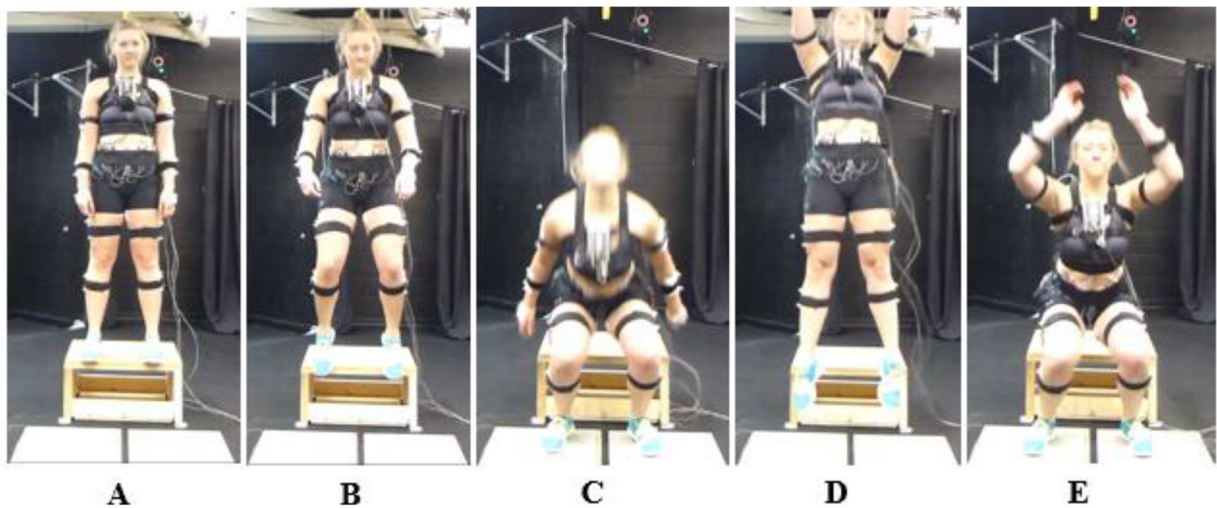


Figure 5.1: The drop vertical jump (DVJ) task is portrayed from start (A) to completion (E). The participant makes a small jump off the box (A-B), lands with one foot on each of the force plates (C), and performs a maximum vertical jump (D), and lands a second time with one foot on each force plate (E).

5.2.4 Procedures

Participants were scheduled for a 4-hour data collection. Each participant was familiarized with the laboratory and testing procedures. A full written information letter was provided and reviewed by each participant before signing an informed consent form. Participants were provided with water and washroom breaks as required.

Participants wore standard athletic shorts or their own tight-fitting athletic shorts and a rolled-up t-shirt or sports top. Prior to electrode placement the skin was abraded with Nuprep™ abrasive and wiped cleaned with ethanol to clean the skin. Ag-AgCl surface electrodes pairs were placed in bi-polar configurations with a center to center distance of 2.5 cm, parallel to the muscle fiber orientation. Electrodes were placed on six torso muscle bilaterally including: Rectus Abdominis (RA), External Oblique (EO), Internal Oblique (IO), Lower Erector Spinae (LES), Upper Erector Spinae (UES) and Latissimus Dorsi (LAT); as well as bilaterally over six hip muscles: Tensor Fascia Latae (TFL), Gluteus Medius (GMed), Gluteus Maximus (GMax), Rectus Femoris (QUAD), Adductor Longus (ADD), Semitendinosus (HAM). Each electrode was then held in place with Hypafix™ and the EMG amp was secured with clear tape.

Each participant performed maximal isometric contractions (MVCs) for each muscle (or muscle group) so the biological signals could be normalized. For the abdominal muscles five abdominal contractions (flexion, lateral bend right and left, and, twist right and left) in a semi-recumbent posture sitting on a plinth with hips and knees bent to approximately 90 degrees with the ankles held in place by one researcher and upper body restrained by the second researcher. The ES muscles were normalized with Biering Sorensen test and a modified Biering Sorensen test, (i) back extension and then (ii) back extension, gluteal squeeze and latissimus contraction. The LAT and GMax were evaluated during this test and their specific MVC tests – the highest contraction level was used for normalization. The ADD muscles were tested in a recumbent position with the hips and knees flexed with a foam block used to “squeeze” together as both ADD groups (right and left) were normalized with a single hip adduction contraction simultaneously. The QUAD muscle was normalized in the sitting position with the research

restraining knee extension. GMax and HAM muscle were normalized using (i) a hip extension and (ii) hip extension with knee flexion contraction while laying prone. Finally, the LAT muscles were resisted by the researcher in a standing position with the should flexed ~75-80 degrees and abducted horizontally ~45 degrees. All MVCs were coached with verbal motivation to produce maximal effort.

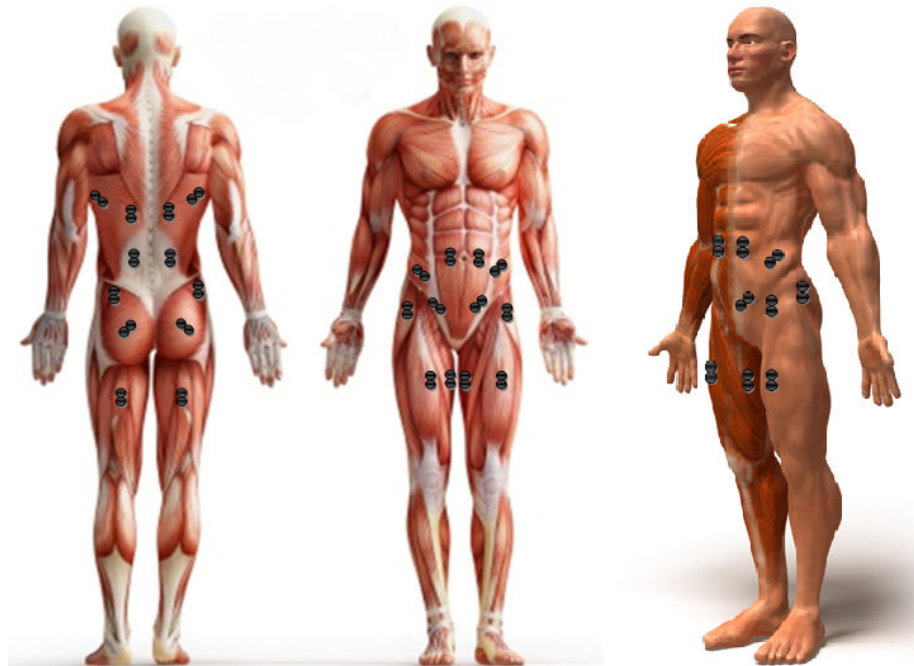


Figure 5.2: Twenty-Four EMG channels will be collected including 6 bilateral core muscles (Rectus Abdominis (RA), External Oblique (EO), Internal Oblique (IO), Lower Erector Spinae (LES), Upper Erector Spinae (UES), and Latissimus Dorsi (LD)) and 6 bilateral hip/leg muscles (Rectus Femoris (RF), Tensor Fascia Latae (TFL), Gluteus Medius (GMed), Gluteus Maximus (GMax), Biceps Femoris (BF), and Adductor Longus (ADD)).

Next the subjects performed a series of tasks in a block randomized order. Note that only the DVJ tasks are included in this analysis as this is the first step to evaluating underlying mechanisms and currently only the DVJ is used to assess injury risk. To avoid unnecessary complexity the other

task (i.e. single leg DVJ were omitted from this analysis. It is also important to note that all subjects performed the DVJ tasks first before a series of randomized secondary tasks. When performing the DVJ task participants were given a verbal description of the task as well as a visual demonstration. No performance criteria were included in the description. A maximum jump was requested, and verbal confirmation was requested when motivation or effort seemed less than maximum. The performance of each task was observed by a member of the research team to ensure the criteria of the task were met each time. Trials were repeated for the following reasons: jumping up off the box, landing off the force plate, landing on the same force plate, loss of balance, lack of maximum jump height, or, data collection capture error. Feedback was given to the participant and once again it only related to task requirements and not performance (i.e. the participant was asked to “stick the landing”, or “try that again and try to land with one foot on each force plate”). Deviation in task criteria or errors in data collection (EMG drop out, marker occlusion, etc) required an additional trail until three “good” attempts were collected. All trials both satisfactory and unsatisfactory were saved and examined as necessary in post-collection analysis. Data collection capture time was buffered on both sides of the task to ensure appropriate post-collection analysis including filtering kinematic and EMG signals (Howarth & Callaghan 2009).

Post collection the trials were evaluated in Visual 3D to quantify the knee excursion relative to a body fixed plane. The plane was created using the hip joint center (HJC) and the ankle joint center (AJC) and a third arbitrary point anterior to the hip joint center in the local hip coordinate system. These three points created a “hip ankle plane” which was used to evaluate knee valgus (Figure 5.3). Groups were created based on individual trials with the intention of capturing

'injurious events' rather than categorizing individuals since there was a great deal of movement variability (Figure 5.4).

5.2.5 Outcome Measures & Statistical Design

The primary outcome measures were to compare high and low valgus trails. ANOVA testing was used in IBM SPSS statistics 20® was used to evaluate the differences between groups. In addition to this primary goal, secondary analysis was done on the data using continuous data with the intension of informing further research. A Pearson Correlation analysis was used to address the question of does having one high valgus knee related to having two high valgus knees, and a simple regression was used to evaluate if it is possible to predict the predictive ability of their second knee moving into valgus based on one knee's valgus score. A stepwise multiple regression model was used to evaluate the best predictors of DKV. Confidence intervals, part and partial correlates and collinearity diagnostics were all evaluated including Durbin-Watson post-hoc analysis with the residuals to examine the potential for serial and auto-correlations. Heteroscedasticity was examined with scatter plots of the residuals and predictors, as well as histograms and normal probability plots. Also, the standardized Beta values were evaluated since the metrics used in the model are not similar qualities and therefore do not have similar variances, therefore normalizing the variance is required for meaningful comparisons. Also, as a general rule, the final model produced in the stepwise analysis was adopted since it provides the "best" predictor of the depend variable.

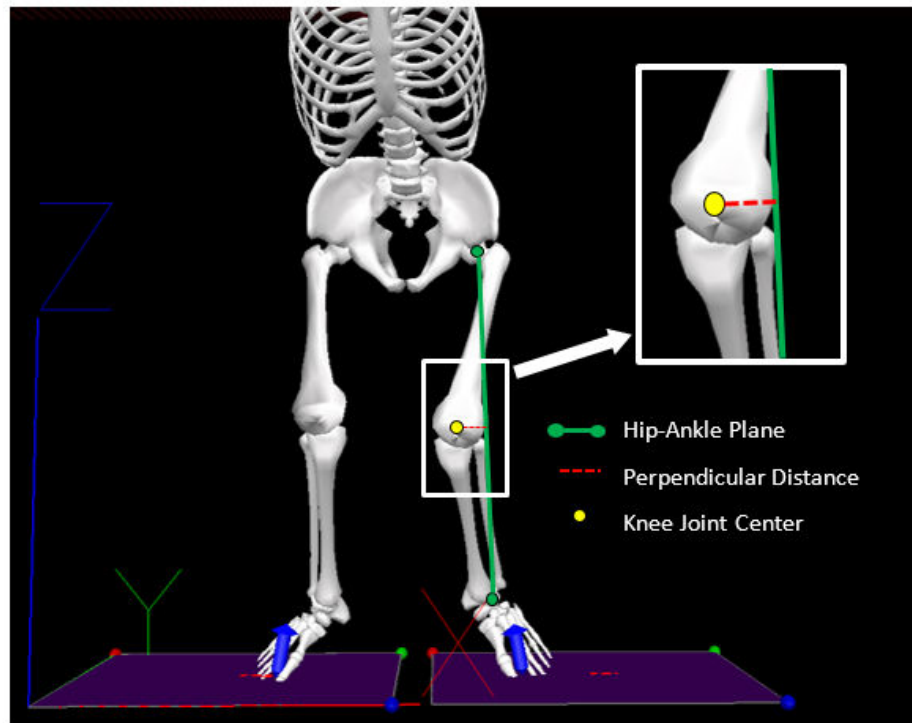
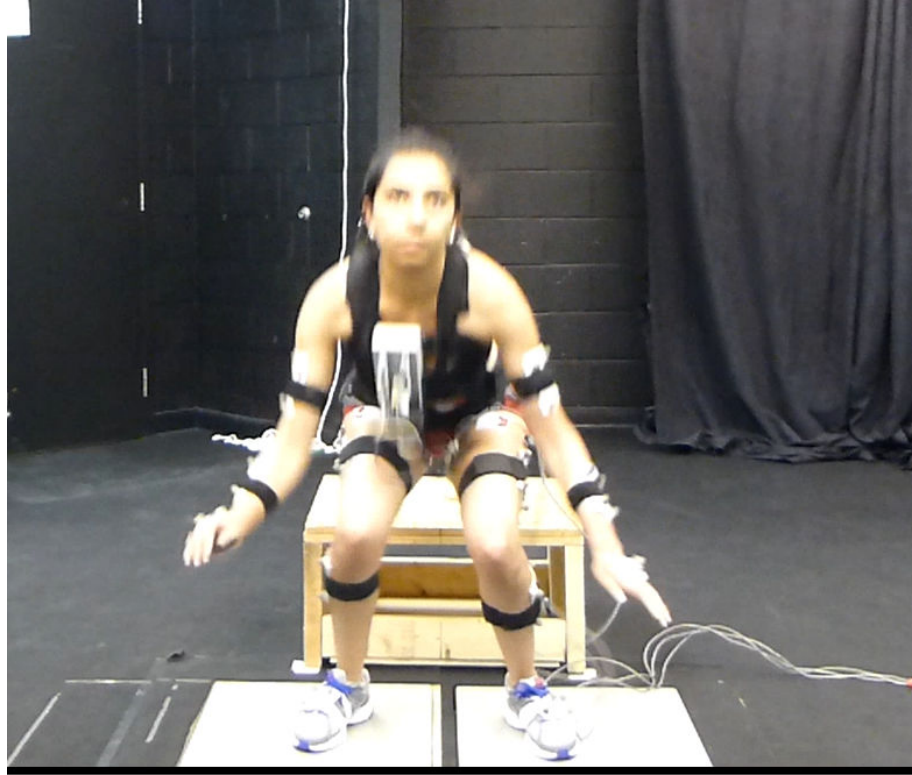


Figure 5.3: A subjected landing in DVJ (top). An accompanying schematic representation of the body fixed hip-ankle plane and the perpendicular medial knee displacement which quantifies the knee valgus measure (bottom).

5.3 Results

Upon examination of the data it became very clear that classification of a single subject as high, low or no valgus would not be possible due to the individual variability and the continuum of results. Illustrated in Figure 5.4 are the dynamic valgus measures across all 18 subjects and three trials. In light of the unexpected phenomenon, that individuals could be classified as both high and low valgus when comparing the right and left side, for example subjects 3, 4, 9, 10, and 13, and even when considering valgus on the same side, for example subjects 7 and 17, trials were evaluated independently. This allows the data to represent what changes with an at-risk trial rather than trying to identify an at-risk individual, who may display a variety of movement from trial to trail. The primary analysis the data has been divided categorically into 'Joint Angles', 'Joint Loads', and 'EMG Patterns' where groups of high and low valgus are compared. The secondary analysis follows with question specific sections.

5.3.1 Primary Analysis

5.3.1.1 Joint Angles

Spine motion data was compared with two groups, the Valgus Group (VG, n=42) and the No Valgus Group (NVG, n=20). The valgus group consisted of trials with both unilateral and bilateral valgus, whereas, the no valgus group had bilateral low valgus. These groups were created since either hip has the potential to effect spine motion. Time histories of spine flexion/extension motion during the first landing of the DVJ are shown in Figure 5.5. Peak spine flexion differed between the NVG and VG (peak means= 27.1 (7.4) and 32.4 (9.9), respectively, and $t= 2.1, p<0.05$).

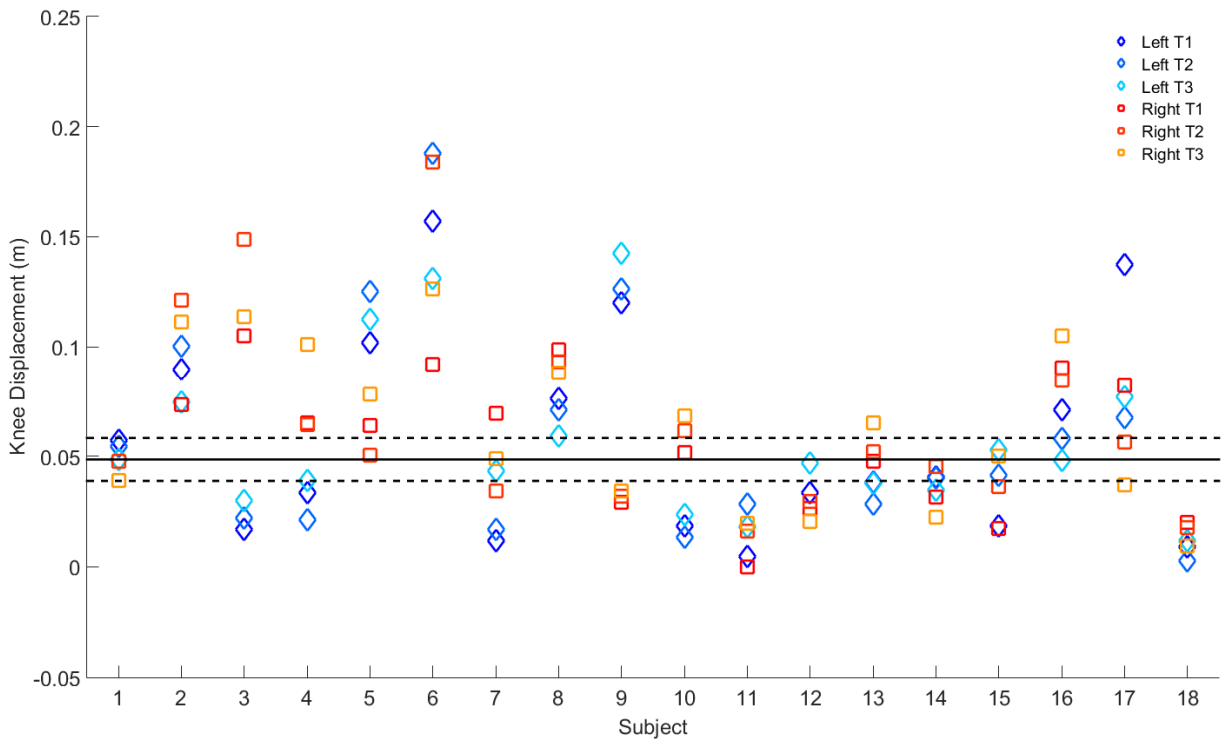


Figure 5.4: Knee displacement during the first landing of the DVJ task. Median (solid) and dashed ($\pm 20\%$) reveal the barrier between high and low valgus, which creates the comparison groups.

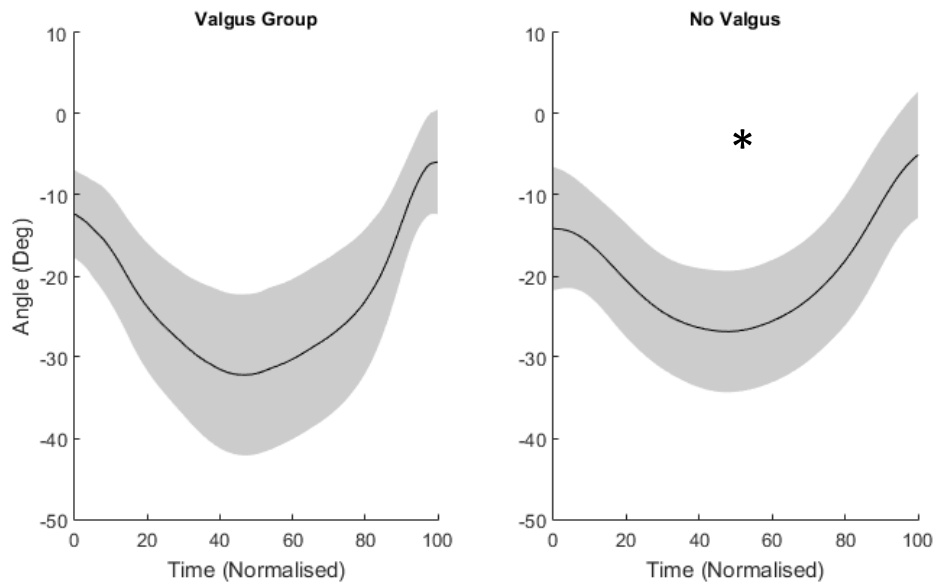


Figure 5.5: Mean and std of spine flexion-extension angles during first land for “valgus group” (Unilateral and Bilateral Valgus) vs the No Valgus group. *SSD in peak angles between valgus group and no valgus group.

Examining the hip and knee kinematic data the right and left sides were collapsed into two groups a Low Valgus Group (LVG, n=40) and a High Valgus Group (HVG, n=44). Time histories are shown in Figure 5.6 and mean peak angle for hip flexion angle for the LVG were 81.9 (11.7) and 95.0 (10.4) for the HVG, which were statistically significantly different ($t=-6.235$, $p<0.001$). Mean peak angle for the knee were also statistically significantly different ($t=2.281$, $p=0.025$) with means of 92.7 (9.9) and 98.0 (11.0), for the LVG and HVG, respectively.

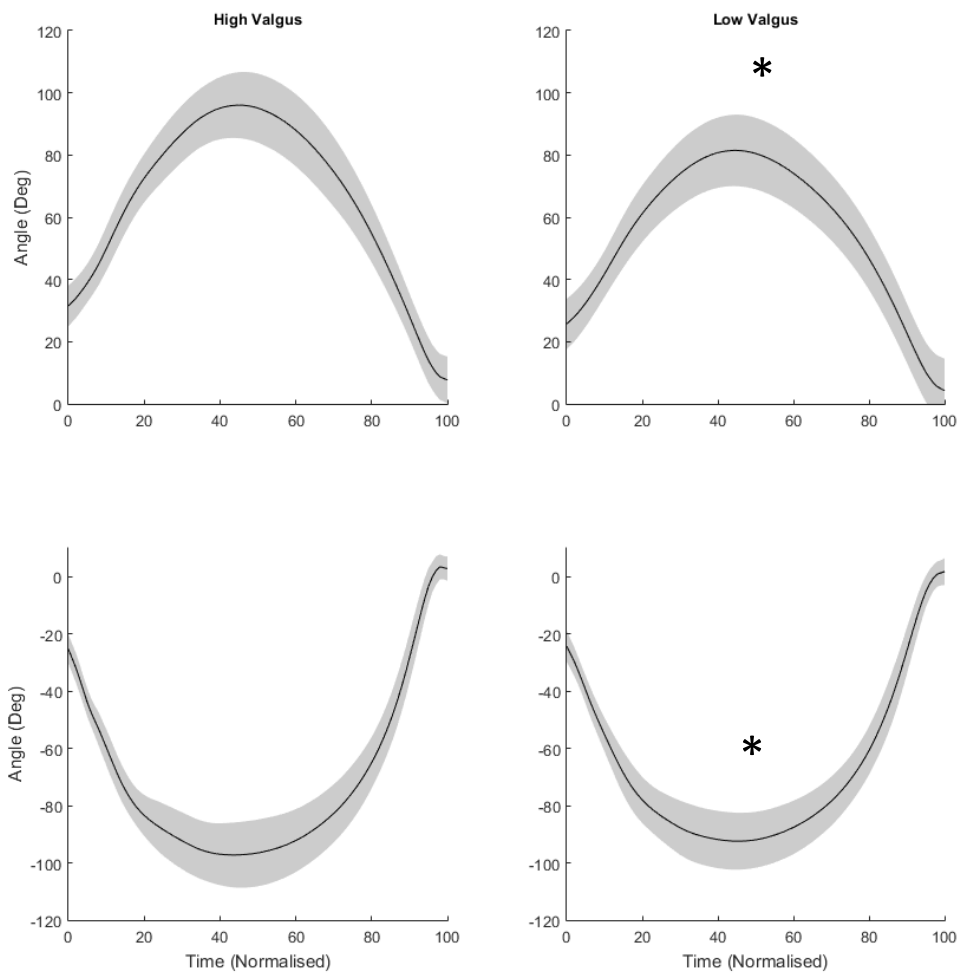


Figure 5.6: Time histories of the mean (black line) and standard deviation (shaded area) of hip (top), and knee (bottom) flexion-extension angles during first land for the high valgus group (HVG) and low valgus group (LVG), on left and right respectively. *SSD in peak angles between HVG and LVG.

Time histories of the hip and knee abduction-adduction angles are shown in Figure 5.7, and internal-external rotation in Figure 5.8. There were no differences in abduction-adduction or internal-external peak angles between groups for the hip or the knee.

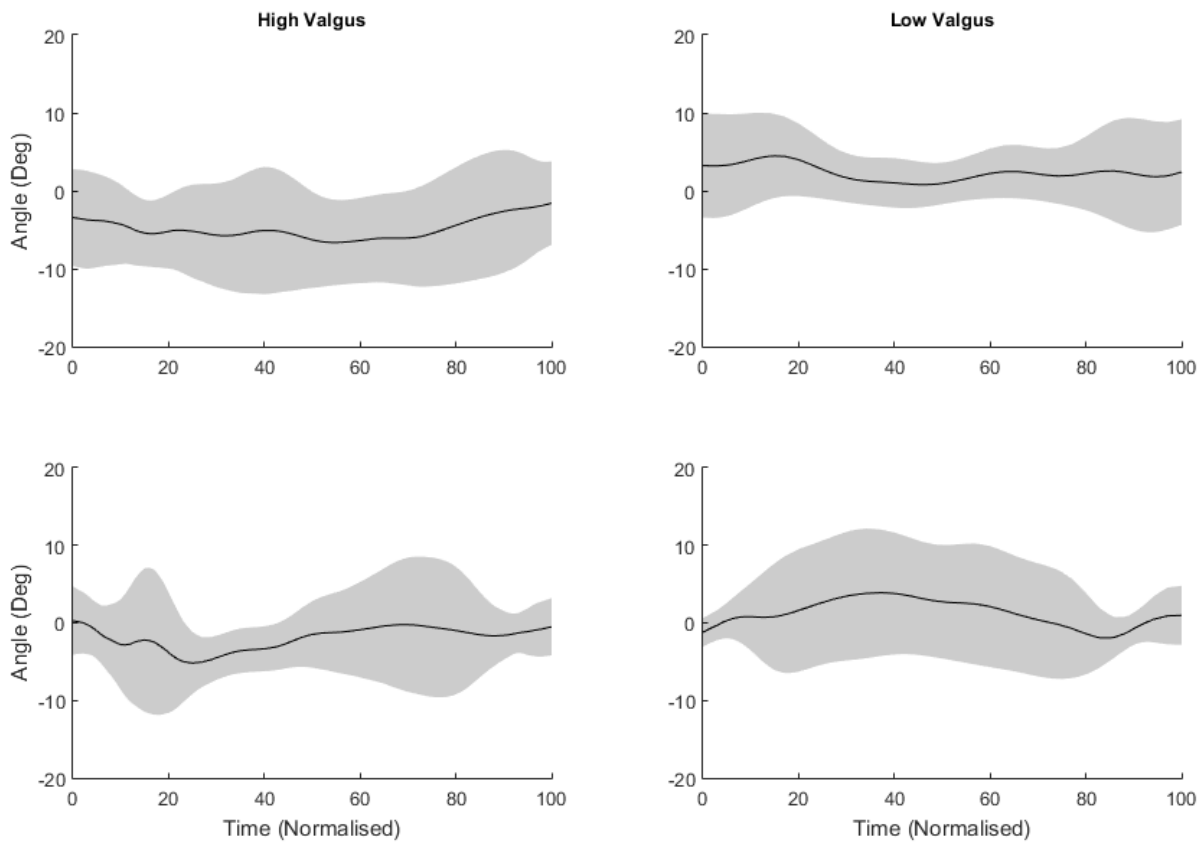


Figure 5.7: Time histories of the mean (black line) and standard deviation (shaded area) of hip (top), and knee (bottom) abduction-adduction angles during first land for the high valgus group (HVG) and low valgus group (LVG), on left and right respectively.

Further examination of the spine angles compared bilateral, unilateral and no valgus groups to assess the effects of single and double DKV. Time histories of the kinematic data from the three groups for the spine, hip and knee are illustrated in Figure 5.9. Lumbar mean peak flexion angles were 27.1 (7.4), 33.2 (11.0), and 31.7 (9.3), for the NVG, UVG, and BVG,

respectively. The differences in peak spine angle showed trends ($F=2.32$ $p=0.107$) towards less spine motion in the NVG. The peak hip flexion angle was 76.0 (11.9), 92.37 (9.8), and 99.0 (10.2), for the NVG, UVG, and BVG, respectively. The NVG had significantly less peak hip flexion than both the BVG and the UVG ($F=26.16$, $p<0.001$, pairwise comparisons Tukey HSD $p<0.001$, $p<0.001$). Finally, the knee behaviour was similar to the hip with the peak flexion angles for the knee were 89.9 (9.4), 96.4 (11.9), and 98.8 (10.9), for the NVG, UVG, and BVG, respectively. Similar to the hip the NVG had significantly less peak knee flexion ($F=3.91$, $p=0.025$) but this time only different from the BVG (Tukey's HSD, $p<0.05$).

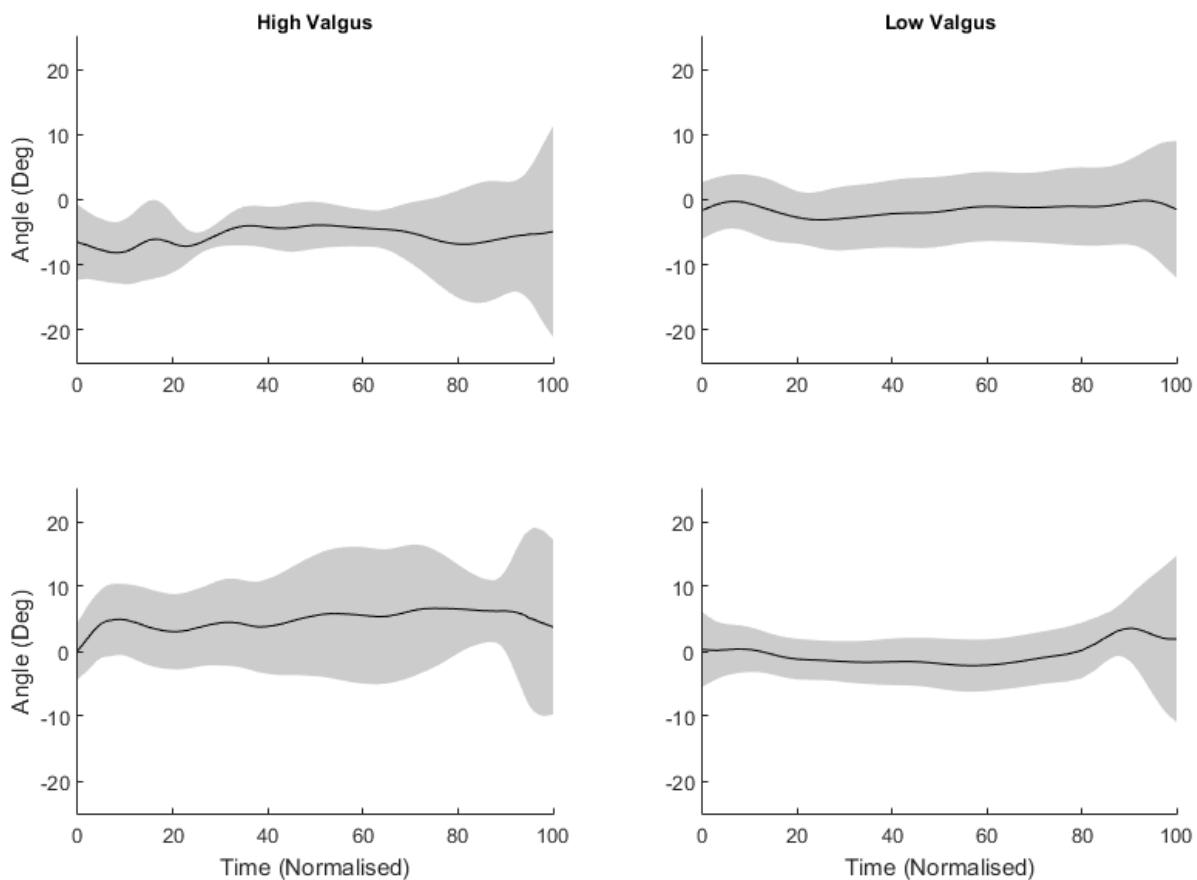


Figure 5.8: Time histories of the mean (black line) and standard deviation (shaded area) of hip (top), and knee (bottom) medial-lateral rotation angles during first land for the high valgus group (HVG) and low valgus group (LVG), on left and right respectively.

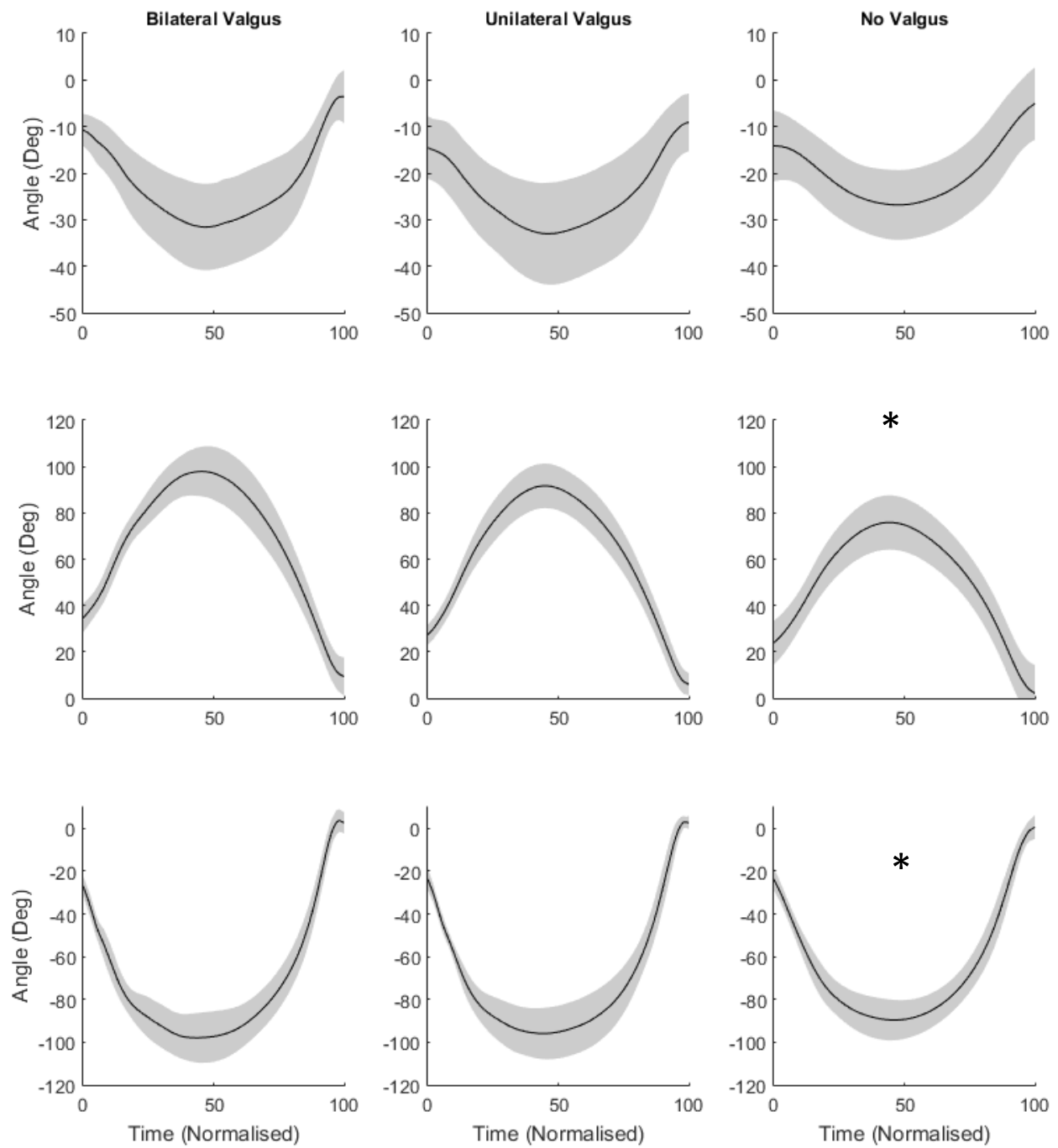


Figure 5.9: Time histories of the mean (black line) and standard deviation (shaded area) of spine (top), hip (middle) and knee (bottom) flexion-extension angles during first land for the bilateral valgus group (BVG, left), Unilateral Valgus Group (UVG, center), and No valgus group (NVG, right), on left and right respectively. *SSD in peak angles between NVG and the other two groups.

5.3.1.2 Joint Loads (Inverse Dynamics)

Forces. Illustrated in Figure 5.10 is the time histories for the ID force data for the spine, hip and knee. Examining peak force data from ID analysis and comparing the HVG and LVG, only peak AP shear there was a statistically significant difference ($t=-5.428$, $p<0.001$), between the HVG and the LVG with a mean peak shear of 505.3 (142.6) N, and 357.2 (102.2) N, respectively. No differences were observed in ML shear or compression forces. The hip findings were similar to the spine with a statistically significant difference ($F=-4.741$, $p<0.001$) between the HVG and LVG only in peak AP shear with mean peak shear values of 297.8 (91.7) N and 213.1 (69.1) N, respectively (Figure 5.10). Anterior shear in the knee was only trending a difference between HVG and LVG with mean peaks of 432.1 (64.6) and 403.1 (76.66) for the HVG and LVG, respectively (Figure 5.11). These findings are best summarised in Figures 5.12 and 5.13.

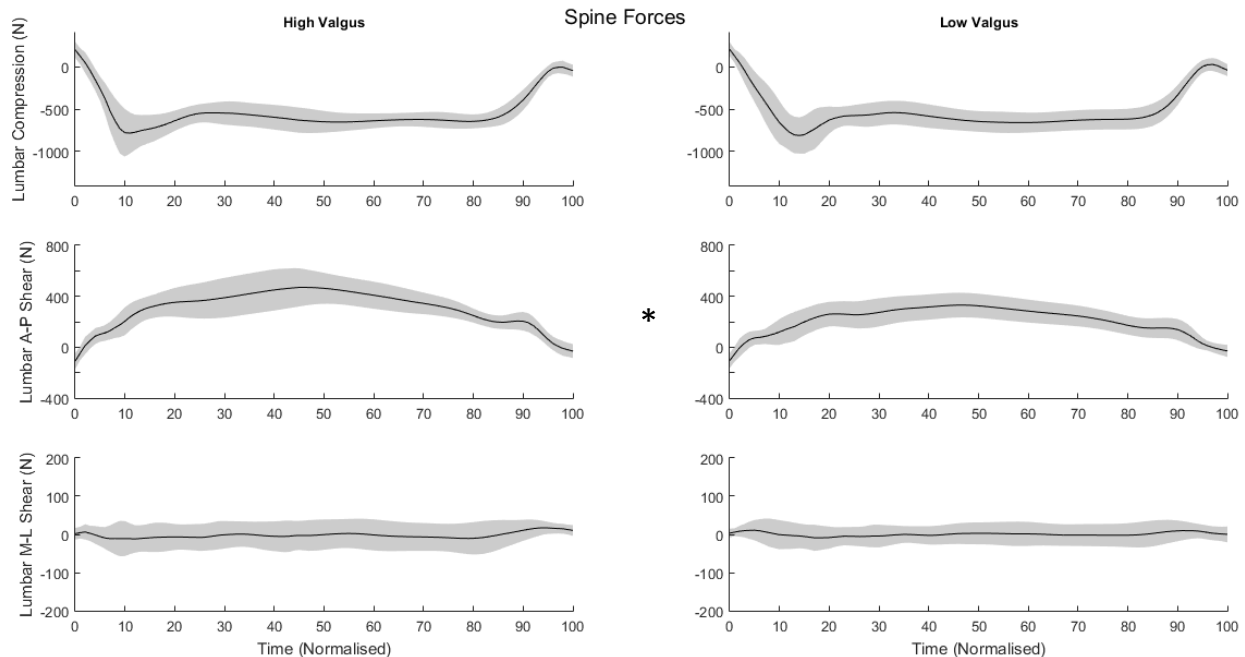


Figure 5.10: Comparisons of spine forces (inverse dynamics) between the high and low valgus groups. *SSD between LVG and HVG, $p<0.05$.

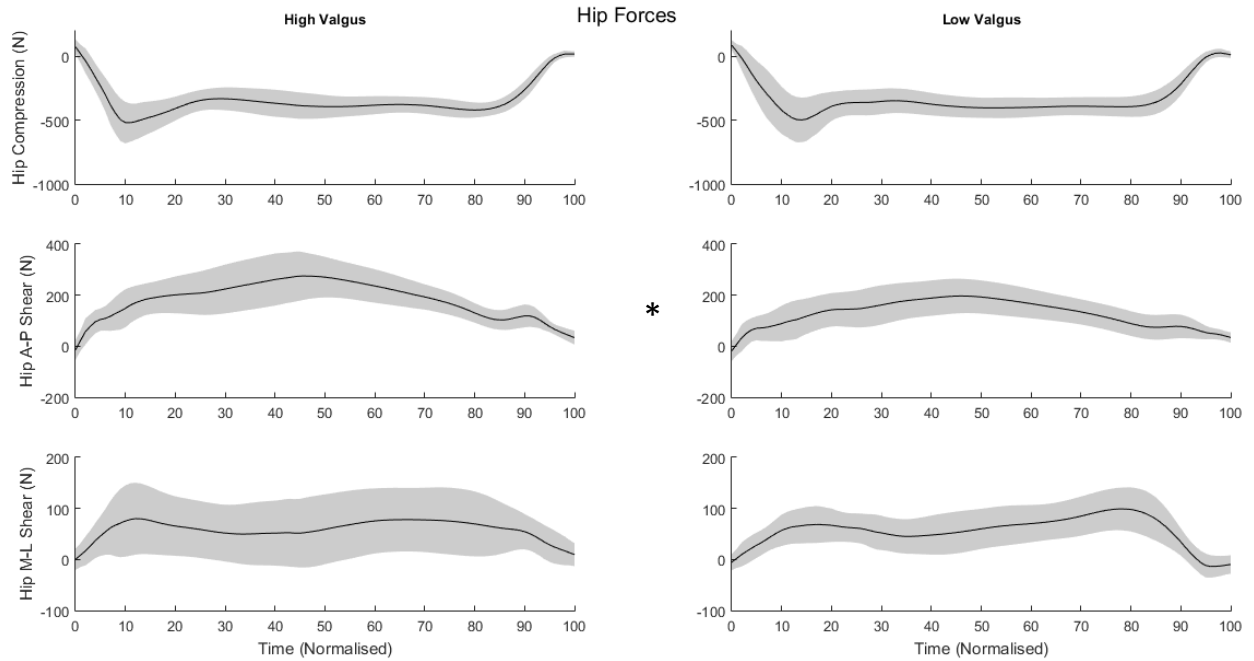


Figure 5.11: Comparisons of hip forces (inverse dynamics) between the HVG and the LVG. *SSD between LVG and HVG, $p < 0.05$.

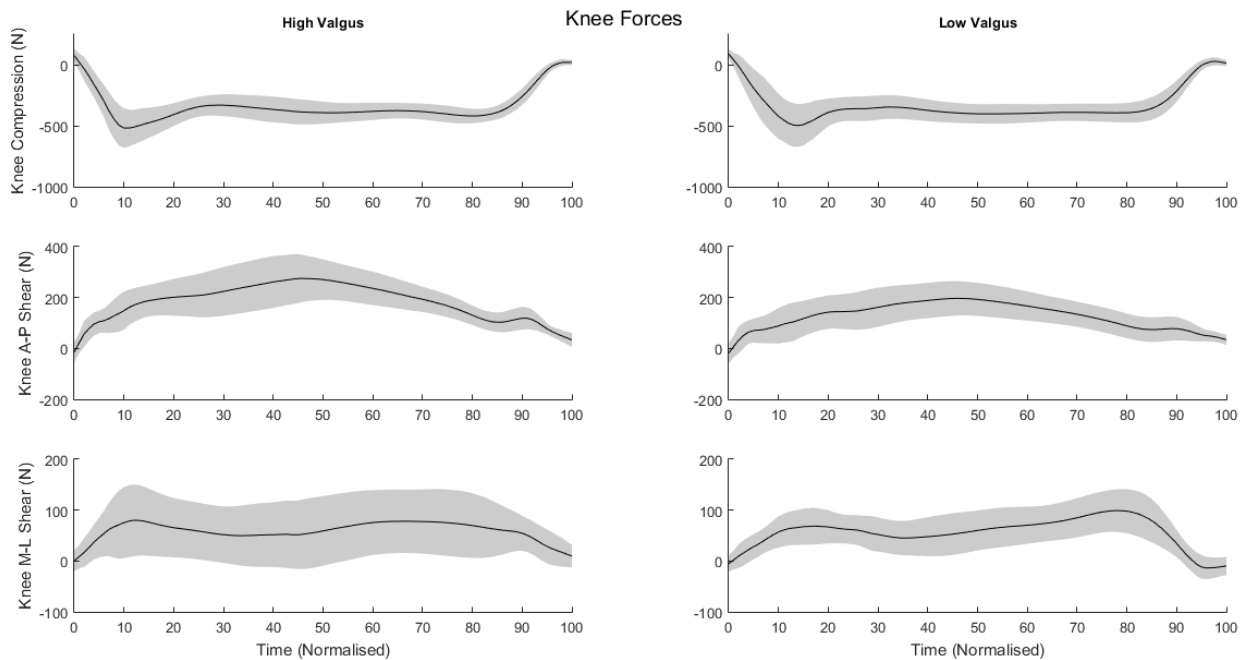


Figure 5.12: Comparisons of knee forces (inverse dynamics) between the HVG and the LVG. *SSD between LVG and HVG, $p < 0.05$.

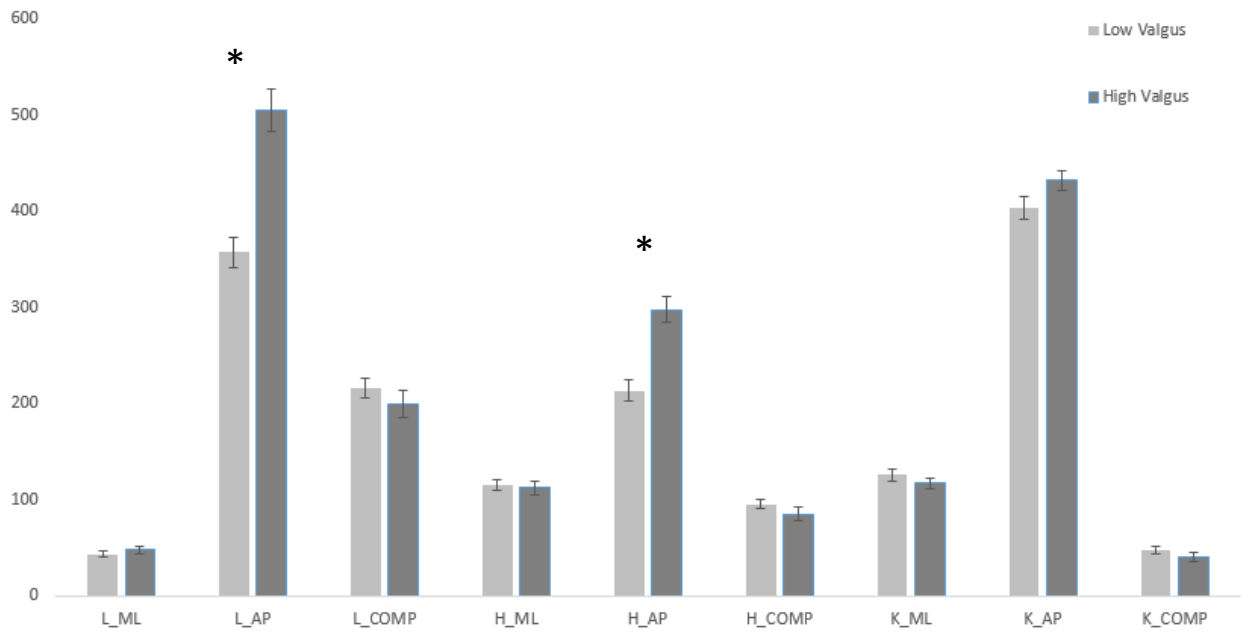


Figure 5.13: Histogram of the peak (maximum) inverse dynamics forces for the spine, hip and knee. *SSD between LVG and HVG, $p < 0.05$.

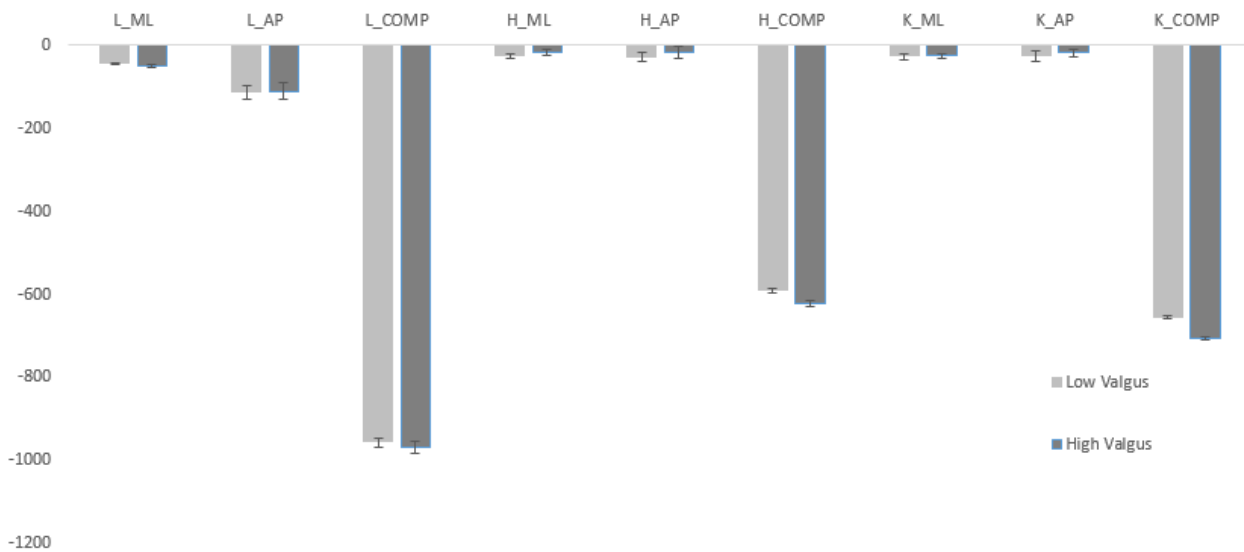


Figure 5.14: Histogram of the peak (minimum) inverse dynamics forces for the spine, hip and knee.

Moments. Time histories are shown for spine (Figure 5.15), hip (Figure 5.16), and knee (Figure 5.17) to provide an impression of the comparisons between the HVG and the LVG. While Figures 5.18 and 5.19 illustrate the histograms of peak maximum (positive) moments and peak minimum (negative) moments, respectively. **Peak Maximum Moments.** Lumbar spine flexion moment was more than 20% higher ($t=-3.097$, $p<0.01$) in the HVG (136.7 (52.4) Nm) compared to the LVG (107.8 (28.5) Nm). Peak hip moments in flexion-extension (61.4 (22.5) and 47.5 (15.0), $t=-3.296$, $p=0.001$), abduction-adduction (33.3 (8.6) Nm and 21.6 (7.5) Nm, $t=-5.298$, $p<0.001$), and internal external rotation (13.0 (8.6) Nm and 7.9 (4.4) Nm, $t=-3.394$, $p=0.001$) were all higher in the HVG compared to the LVG. Similar to the hip, knee moments in flexion-extension (122.7 (18.6) and 110.9(22.5) Nm, $t=-2.638$, $p=0.01$), abduction-adduction (25.0 (9.2) Nm, and 18.3 (4.7) Nm, $t=-4.060$, $p<0.001$), and internal external rotation (7.9 (3.9) Nm and 10.3 (3.5) Nm, $t=3.032$, $p=0.003$) were all higher in the HVG compared to the LVG with the exception of internal-external rotation moments which was smaller in the LVG. **Peak Minimum Moments.** Lumbar spine flexion moment was nearly 20% higher ($t=-4.364$, $p<0.001$) in the HVG (-176.8 (28.9) Nm) compared to the LVG (149.0 (29.6) Nm). Peak hip moments in flexion-extension (117.5 (22.9) and 102.6 (21.6), $t=-3.052$, $p=0.003$) for the HVG and LVG, respectively. Examining the abduction-adduction the HVG was statistically significantly lower than the LVG (21.8 (12.0) Nm and 28.4 (9.7) Nm, $t=-2.758$, $p<0.01$). Knee moments were only different between group for peak minimum internal-external rotation (3.5 (3.1) Nm and 1.2 (3.5) Nm, $t=4.076$, $p<0.001$) were all higher in the HVG compared to the LVG.

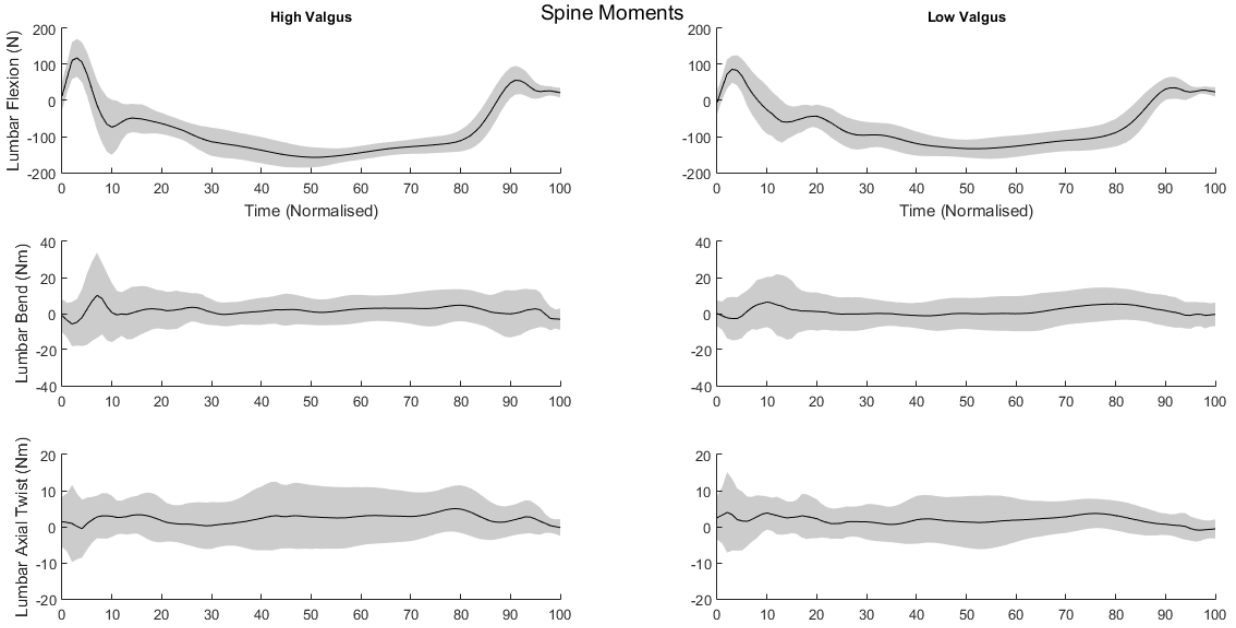


Figure 5.15: Lumbar spine moments for the DVJ first landing, initial contact to take-off, for the HVG (left) and LVG (right), with flexion across the top, lateral bend in the center, and axial twist along the bottom.

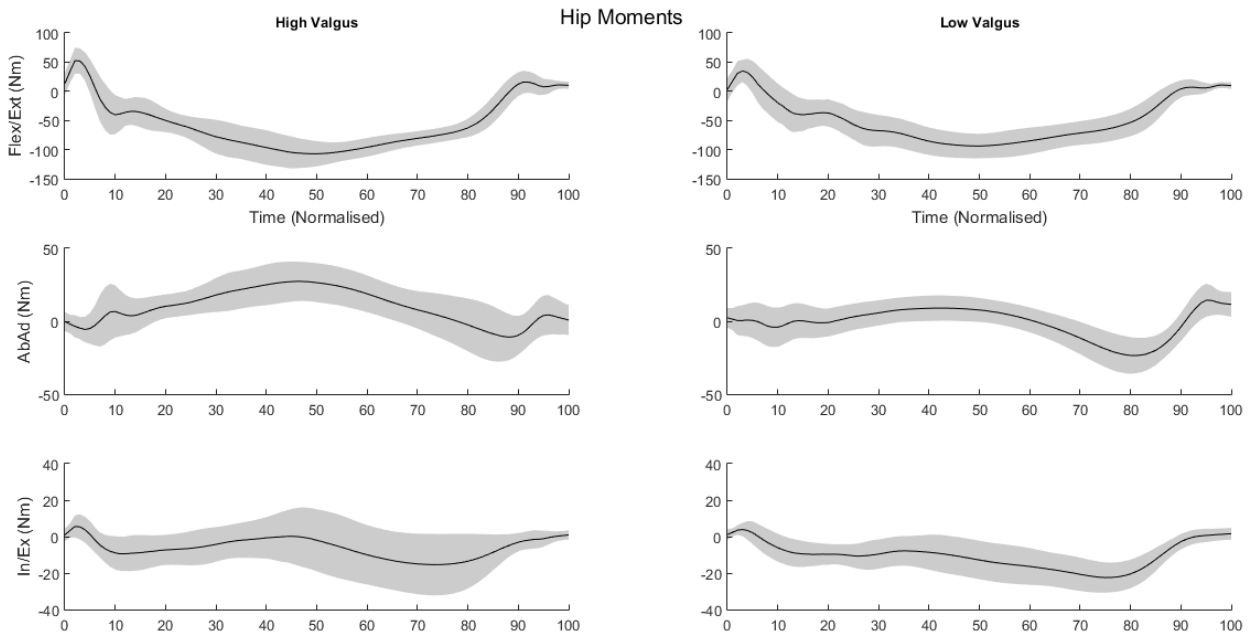


Figure 5.16: Hip moments for the DVJ first landing, initial contact to take-off, for the HVG (left) and LVG (right), with flexion across the top, abduction-adduction in the center, and medial-lateral torque along the bottom.

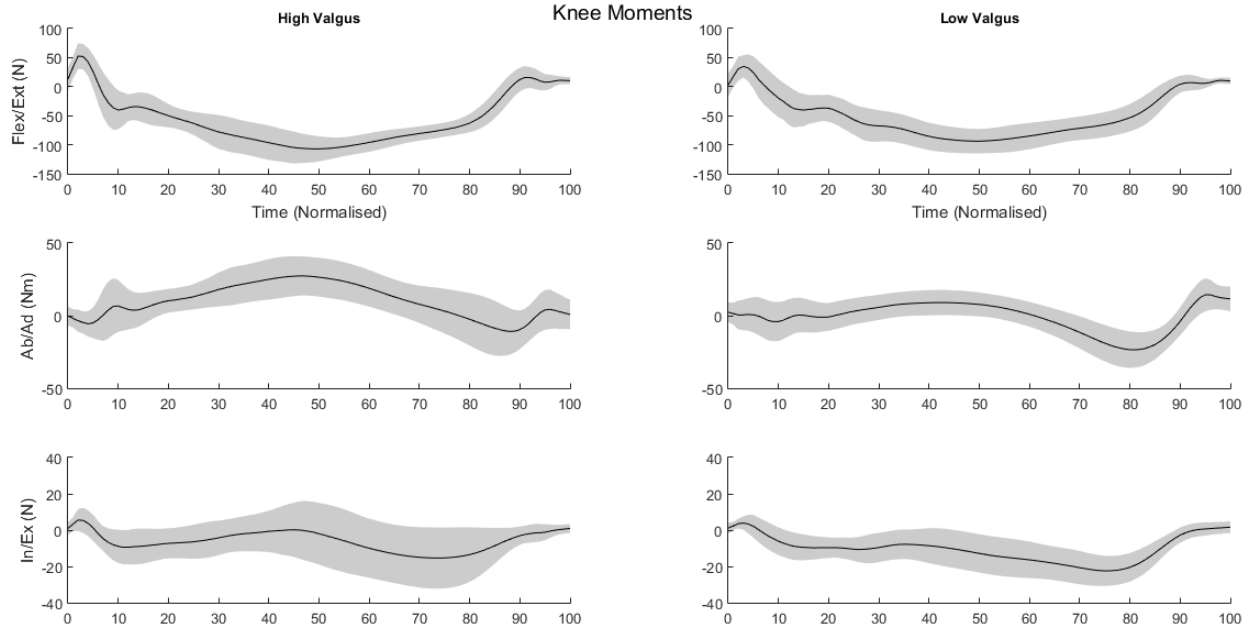


Figure 5.17: Knee moments for the DVJ first landing, initial contact to take-off, for the HVG (left) and LVG (right), with flexion across the top, abduction-adduction in the center, and medial-lateral torque along the bottom.

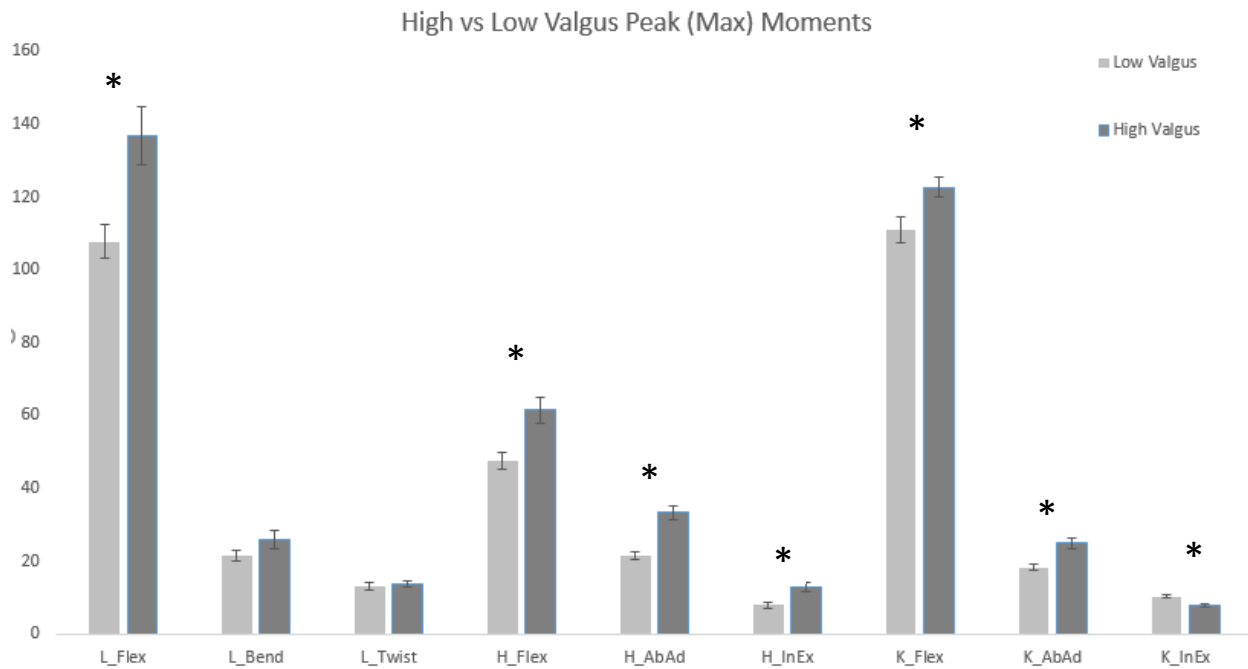


Figure 5.18: Peaks (max) moments for high and low valgus group means with standard error bars. * Indicates statically significantly different comparisons ($P \leq 0.01$). (L_Flex = Lumbar Spine Flexion/Extension Moment; H=Hip; K=Knee)

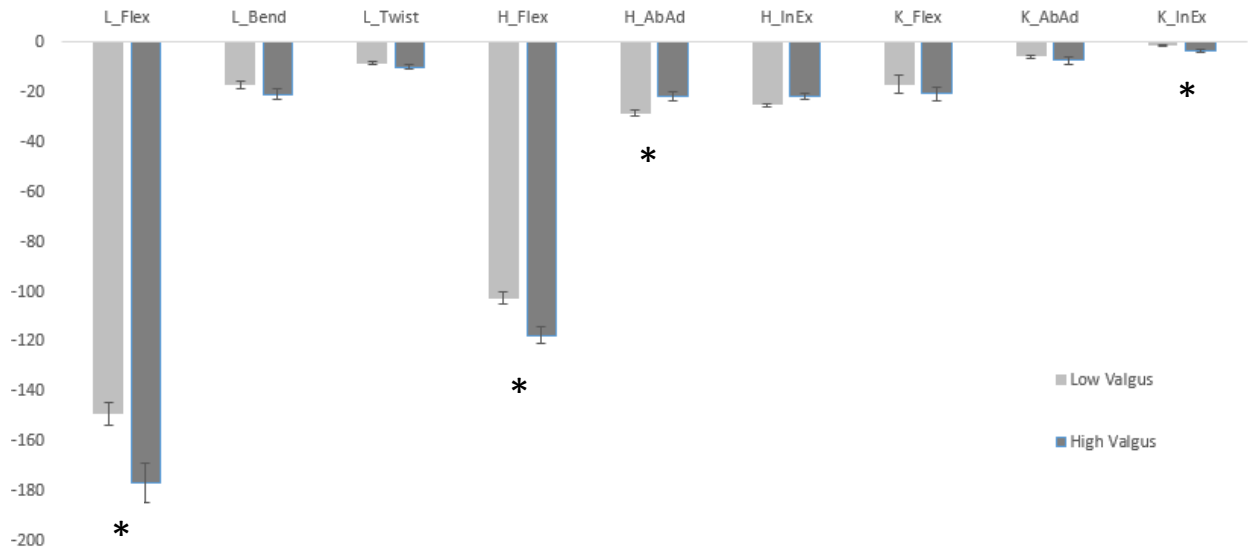


Figure 5.19: Figure xx: Peaks (min) moments for high and low valgus group means with standard error bars. * Indicates statically significantly different comparisons ($P \leq 0.01$). (L_Flex = Lumbar Spine Flexion/Extension Moment; H=Hip; K=Knee)

5.3.3 Joint Loads Estimates from the HSM

Spine. Illustrated in Figure 5.20 are the spine compression forces from the DVJ trails among the BVG, UVG, and NVG estimated from the HSM. The BVG had -3406 N of spine compression which was significantly more than the UVG with -2876 N and the -2533 N ($F = 5.894$, $p = 0.006$; pairwise comparisons $p = 0.032$; $p = 0.002$). The remaining spine forces were not significantly different between groups and the data is presented in Table 5.2. Spine flexion moments predicted by the HSM are illustrated in Figure 5.21. The BVG had a higher peak moment ($F = 3.950$, $p = 0.027$) than the NVG ($p < 0.01$) and only trending higher than the UVG (0.076).

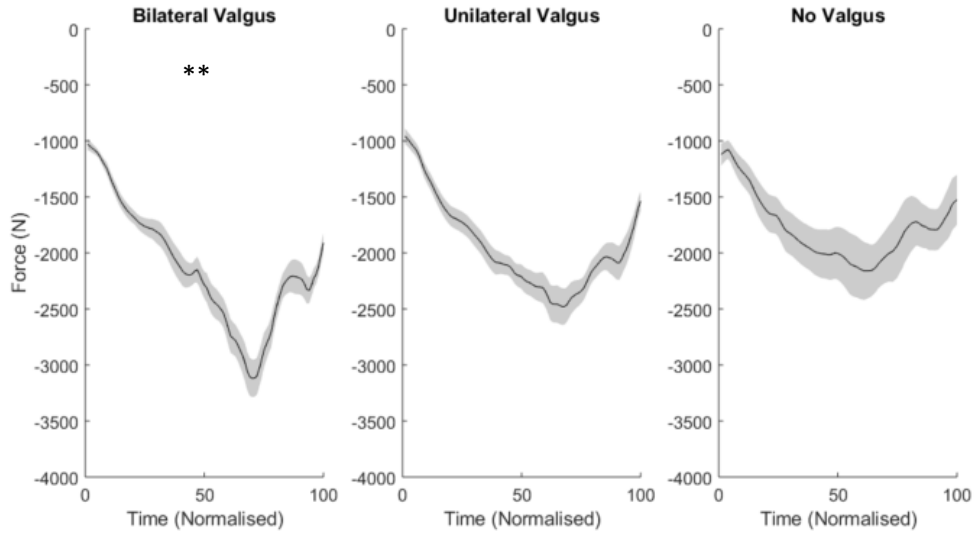


Figure 5.20: Mean lumbar spine compression force and StE (shaded area) for the DVJ trails comparing the high valgus bilateral, unilateral and no valgus groups. ** Indicates significantly different from both comparisons for peak minimum compression.

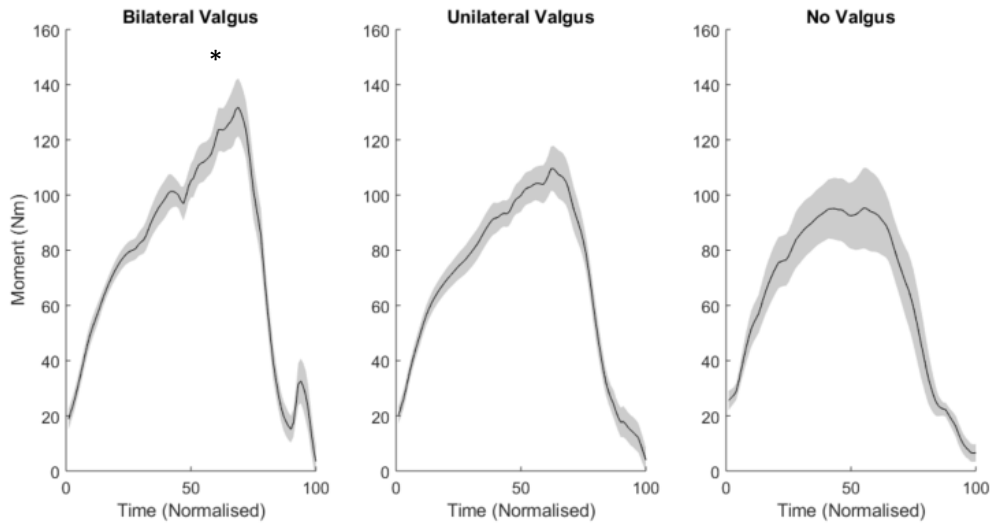


Figure 5.21: Mean lumbar spine flexion-extension moments and StE (shaded area) for bilateral valgus (left), unilateral valgus (middle) and no valgus (right) for the DVJ trails comparing the high valgus bilateral and unilateral with low (“No”) valgus groups. *Indicates significantly different from “No Valgus” comparison.

Hip. Illustrated in Figure 5.22 are the hip forces between HVG and LVG demonstrated several differences which are displayed in Table 5.3 with accompanying statistical results. To summarise the most important results the HVG had higher compression at 6479 (3891) N compared to LVG at 4465 (1523) which was significantly different ($t=3.177$, $p < 0.01$); and, the HVG also had lower minimum compression force at 22N (472) compared to LVG at 1051 (471) also significantly different ($t = 9.981$, <0.001). The LVG also had the highest posterior shear at -4170 (1399) compared to the HVG at -3119 (1042) which were significantly different ($t = -3.962$, $p < 0.001$). Furthermore, the HVG had lowest minimum medial shear force at -801 (282) compared to LVG -1042 (274), which was also significantly different ($t = -3.960$, $p < 0.001$); similarly the HVG had the lower peak medial shear force at -2300 (735) compared to the LVG -2981 (1409), which was significantly different ($t = -2.815$, $p < 0.01$). With respect to the hip moments minimum abduction moment was lower in the HVG -113 (56) Nm compared to the LVG which had minimum abduction moment of -192 (230) Nm (Figure 5.23). In addition the minimum external rotation moment was smallest in the HVG -66 (38) Nm compared to the LVG -113 (81) Nm, which was significantly different ($t = -3.427$, $p = 0.01$).

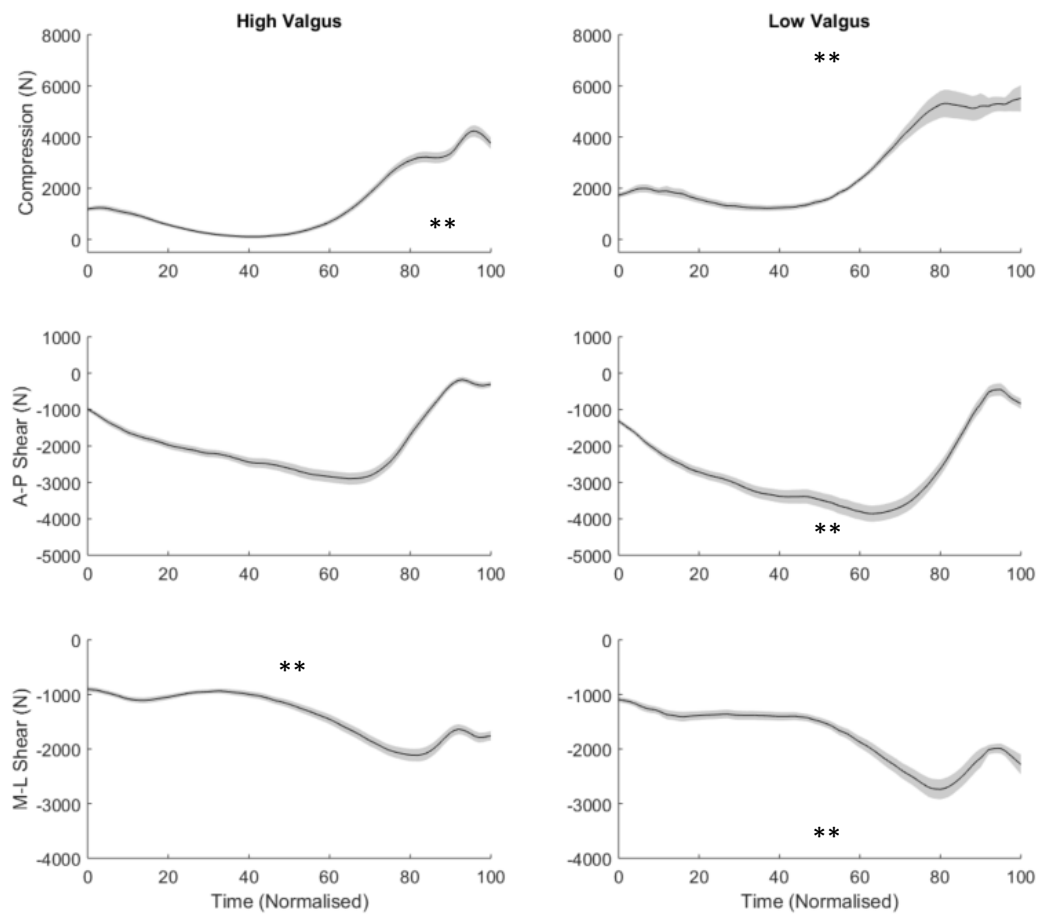


Figure 5.22: Mean hip spine forces (Compression (top), AP Shear (middle) and ML shear (bottom)) and StE (shaded area) for the DVJ trails comparing the high valgus bilateral and unilateral with low (“No”) valgus groups. Note: Left hip forces were normalised to the right side (ML shear Left *-1). * Significantly different ($p < 0.05$), ** significantly different ($p < 0.01$); * above the curve indicates peak max score difference, * below the line indicates peak min score difference.

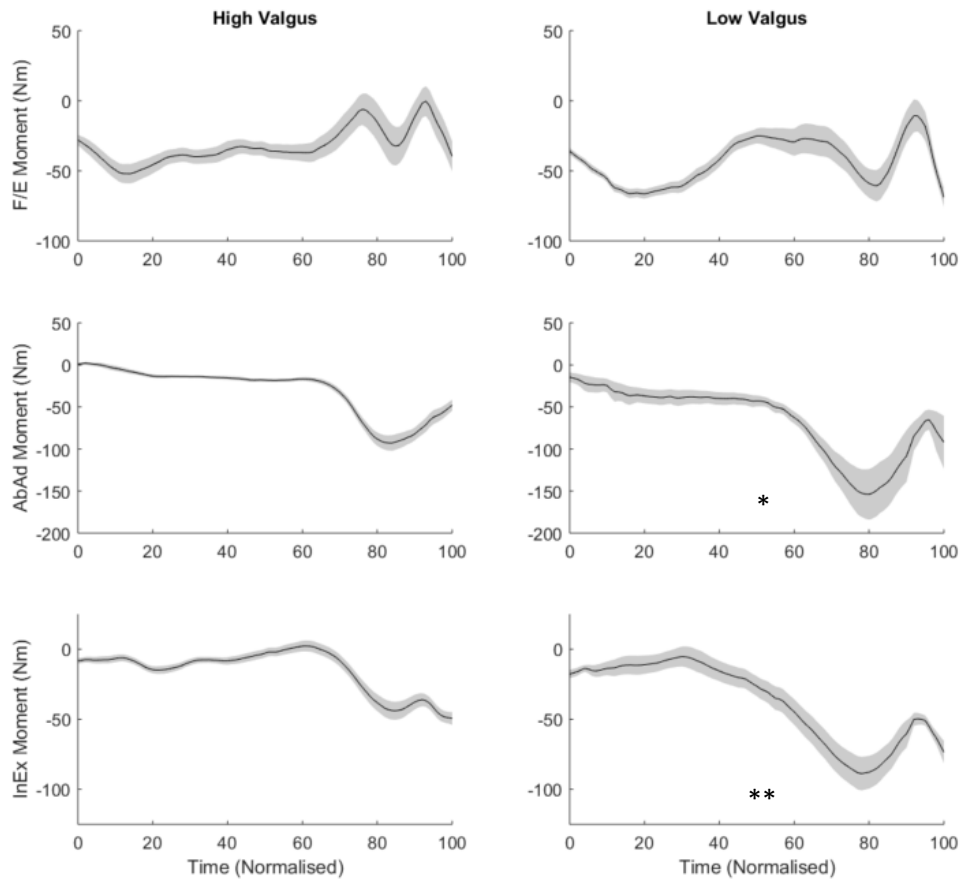


Figure 5.23: Mean hip moments (Flexion-Extension (top), Abduction-Adduction (middle) and Internal-External (bottom)) and StE (shaded area) for the DVJ trails comparing the high valgus bilateral and unilateral with low (“No”) valgus groups. Note: Left hip forces were normalised to the right side (ML shear Left *-1). * Significantly different ($p < 0.05$), ** significantly different ($p < 0.01$); *above the curve indicates peak max score difference, * below the line indicates peak min score difference.

Table 5.2: Mean (SD) of peak spine loads during DVJ first landing for bilateral, unilateral and no valgus.

Load	Bilateral Valgus	Unilateral Valgus	No Valgus
Max Compression (N)	-972 (148)	-934 (261)	-993(273)
Max AP Shear (N)	195 (72)	162 (53)	167 (67)
Max ML Shear (N)	31 (66)	4 (53)	-8 (31)
Max Flex-Ext Moment (Nm)	149 (25)*	124 (30)	108 (53)
Max Bend Moment (Nm)	17 (16)	13 (12)	7 (7)
Max Twist (Nm)	2 (6)	5 (10)	6 (13)
Min Compression (N)	-3406 (377)**	-2876 (562)	-2533 (934)
Min AP Shear (N)	50 (36)	38 (64)	68 (29)
Min ML Shear (N)	-205 (102)	-203 (140)	-166 (115)
Min Flex-Ext Moment (Nm)	-5 (19)	-6 (16)	1 (11)
Min Bend Moment (Nm)	-27 (14)	-32 (35)	-23 (20)
Min Twist (Nm)	-15 (10)	-14 (6)	-15 (7)

Bold indicates significant difference in omnibus test

* indicates significantly different in one pairwise comparison (highest vs lowest only)

** indicates significantly different in both pairwise comparisons

Table 5.3: Mean (SD) of peak hip loads during DVJ first landing for bilateral, unilateral and no valgus.

Load	High Valgus	Low Valgus	Statistics*
Max Compression (N)	6479 (3891)	4465 (1523)	t = 3.177, p < 0.01
Max AP Shear (N)	53 (487)	-269 (1048)	
Max ML Shear (N)	-801 (283)	-1042 (274)	t = -3.960, p < 0.001
Max Flexion-Extension Moment (Nm)	40 (45)	29 (67)	
Max Abduction-Adduction Moment (Nm)	9 (17)	-2 (43)	
Max Medial-Lateral Moment (Nm)	17 (20)	10 (39)	
Min Compression (N)	22 (472)	1051 (471)	t = 9.981, p < 0.001
Min AP Shear (N)	-3119 (1042)	-4170 (1399)	t = -3.962, p < 0.001
Min ML Shear (N)	-2300 (735)	-2981 (1409)	t = -2.815, p < 0.01
Min Flexion-Extension Moment (Nm)	-85 (80)	-109 (45)	
Min Abduction-Adduction Moment (Nm)	-113 (56)	-192 (230)	t = -2.201, p < 0.05
Min Medial-Lateral Moment (Nm)	-66 (38)	-113 (81)	t = -3.427, p = 0.01

* Only statistically significant tests reported

5.3.1.4 EMG Patterns

The final category of parameters to examine the differences between the HVG and LVG as part of the primary analysis were the EMG patterns during the DVJ. **Peak EMG.** Peak EMG during the DVJ trials on the first landing are shown in Table 5.4. TFL and GMAX were all statistically significantly higher in the HVG compared to the LVG with differences of 9%, and ~23% of MVC in

peak EMG, respectively. There were no differences in the ADD, HAM and QUAD neural patterns during the first landing. **iEMG (% Movement * %EMG)**. The results of the iEMG are displayed in Table 5.5. Similar to the peak EMG, the iEMG for the first landing of the DVJs there was a statistical significantly increase in TFL, GMAX, GMED, HAM and QUAD, by approximately 136 %, 144%, 128%, 133%, and 123% of the HVG, respectively. Only the ADD neural patterns were not different when held to the $p < 0.008$ standard.

Table 5.4: Peak EMG collapsed across right and left sides.

	Valgus Condition		Independent Samples t-Test		
	Low	High	t	df	Sig. (2-tailed)
	Mean (SD)	Mean (SD)			
TFL*	41.7 (16.8)	32.7 (11.7)	2.827	69.217	0.006
GMAX*	81.7 (42.3)	58.5 (27.0)	2.890	64.510	0.005
GMED	73.75 (24.9)	71.8 (35.2)	0.266	68	0.791
ADD	36.7 (19.1)	33.8 (19.4)	0.689	82	0.493
HAM	47.5 (26.5)	38.6 (22.3)	1.645	80	0.104
QUAD	141.3 (37.1)	125.2 (27.4)	2.218	65.241	0.030

*Indicates muscles which were statistically significantly different ($p < 0.008$).

Note: Levene's test of equal variance was applied and when required the adjusted values were used.

Table 5.5: iEMG (%Movement * %EMG) collapsed across right and left sides.

	Valgus Condition		Independent Samples t-Test		
	Low	High	t	df	Sig. (2-tailed)
	Mean (SD)	Mean (SD)			
TFL*	2175 (1131)	1597 (637)	2.852	60.209	0.006
GMAX*	3405 (1660)	2366 (931)	3.409	59.762	0.001
GMED*	3227 (826)	2520 (859)	3.204	57	0.002
ADD*	2463 (1458)	1848 (925)	2.284	64.894	0.026
HAM	2744 (1375)	2049 (1049)	2.569	72.896	0.012
QUAD*	8515 (2213)	6911 (1320)	3.864	56.501	<0.001

*Indicates muscles which were statistically significantly different (0.008).

Note: Levene's test of equal variance was applied and when required the adjusted values were used.

5.3.2 Secondary Analysis of Continuous Variable Data

This analysis addressed the question of the which variables relate to dynamic valgus when examining all cases of DVJ. Due to sample size limitations in this secondary analysis trials were entered independently to form a total of 54 cases. Since classification was not possible and this is secondary analysis deemed to inform further research it has been included here and should be considered in the context of this limitation.

5.3.2.1 Does one knee valgus score predict the other knee?

The relationship of one knee valgus score with the other knee was significantly, moderately correlated ($r = 0.420$, $p < 0.01$, $df = 54$). However, the predictive ability of one knee valgus score on the other knee valgus score accounted for less than 20% of the variability ($R^2 = 0.176$, $Adj R^2 = 0.160$, $SEE = 0.034$) though this predictive ability was significant ($F=11.122$,

p<0.01). The model predicts an increase in one valgus score by 1 mm would predict an increase in the other by 0.36mm (B = 0.364, SE = 0.109, standardize Beta = 0.420, t = 3.335, p < 0.01, 95% CI 0.145-0.584). Upon inspection the residual statics mean score is ~0.00 and homoscedasticity appears within normal limits (shown in appendix).

5.3.2.2 What is the overall strongest predictor of DKV?

To test the overall best predictors of dynamic knee valgus the biomechanical variables were entered into the stepwise regression model with case-wise/pairwise exclusions for missing data, separately for each side (dominate vs non-dominate or right vs left). For the right side a total of 8 models were evaluated using the stepwise approach and the results of the model estimates are shown in Table 5.6 with the corresponding statistical report in Table 5.7 and 5.8; and for the left side 6 models were evaluated with the results shown in Tables 5.9-5.11. In both analysis the predictive variables of DKV were hip and spine variables (Tables 5.6 and 5.9, for the right and left side, respectively).

Table 5.6: Multiple Regression Models for Right Knee Valgus using a stepwise approach.

Model	Variables Entered/ Removed		Model Summary			
	Variable Entered	Method	R	R ²	Adj R ²	Std Err of the Est
1	R_Hip_AbAd_Min	Stepwise (Criteria: Probability of F to enter <= 0.050, Probability of F to remove >=0.100).	.793	.628	.619	.033765
2	R_Hip_Flex_Max		.883	.779	.769	.0182325
3	R_Hip_AbAd_Mom_Max		.913	.834	.822	.0159970
4	LRA_Peak		.928	.862	.848	.0147777
5	RIO_iEMG		.949	.900	.888	.0127063
6	RLES_Peak		.967	.936	.925	.0103493
7	R_Knee_Flex_Min		.975	.950	.941	.0092126
8*	RLAT_Peak		.980	.961	.952	.0082778

*Durbin-Watson = 2.5 indicating no meaningful serial correlations (1.5-2.5 is considered safe).

Table 5.7: ANOVA results of the Right Knee Valgus stepwise multiple regression models.

		ANOVA				
Model	Variable	Sum of Squares	df	Mean Square	F	Sig.
1	Regression	.040	1	.04	72.624	<0.001 ^b
	Residual	.023	43	.001		
	Total	.063	44			
2	Regression	.049	2	.025	74.035	<0.001 ^c
	Residual	.014	42	.000		
	Total	.063	44			
3	Regression	.053	3	.018	68.634	<0.001 ^d
	Residual	.010	41	.000		
	Total	.063	44			
4	Regression	.054	4	.014	62.332	<0.001 ^e
	Residual	.009	40	.000		
	Total	.063	44			
5	Regression	.057	5	.011	70.471	<0.001 ^f
	Residual	.006	39	.000		
	Total	.063	44			
6	Regression	.059	6	.010	91.984	<0.001 ^g
	Residual	.004	38	.000		
	Total	.063	44			
7	Regression	.060	7	.009	101.064	<0.001 ^h
	Residual	.003	37	.000		
	Total	.063	44			
8	Regression	.061	8	.008	110.762	<0.001 ⁱ
	Residual	.002	36	.000		
	Total	.063	44			

Dependent Variable: Peak_MKD_R_a

Predictors: (Constant), R_Hip_AbAd_Min_b

Predictors: (Constant), R_Hip_AbAd_Min, R_Hip_Flex_Max_c

Predictors: (Constant), R_Hip_AbAd_Min, R_Hip_Flex_Max, R_Hip_AbAd_Mom_Max_d

Predictors: (Constant), R_Hip_AbAd_Min, R_Hip_Flex_Max, R_Hip_AbAd_Mom_Max, LRA_Peak_e

Predictors: (Constant), R_Hip_AbAd_Min, R_Hip_Flex_Max, R_Hip_AbAd_Mom_Max, LRA_Peak, RIO_iEMG_f

Predictors: (Constant), R_Hip_AbAd_Min, R_Hip_Flex_Max, R_Hip_AbAd_Mom_Max, LRA_Peak, RIO_iEMG, RLES_Peak_g

Predictors: (Constant), R_Hip_AbAd_Min, R_Hip_Flex_Max, R_Hip_AbAd_Mom_Max, LRA_Peak, RIO_iEMG, RLES_Peak, R_Knee_Flex_Min_h

Predictors: (Constant), R_Hip_AbAd_Min, R_Hip_Flex_Max, R_Hip_AbAd_Mom_Max, LRA_Peak, RIO_iEMG, RLES_Peak, R_Knee_Flex_Min, RLAT_Peak_i

Table 5.8: Multiple Regression model analysis of the Right DKV.

Model 8	Standardized Coefficients	t	Sig.	Correlations			Collinearity Statistics	
	Bata			Zero-order	Partial	Part	Tolerance	VIF
(Constant)		-5.031	<.001					
R_Hip_AbAd_Min	-.602	-11.319	<.001	-.793	-.884	-.373	.383	2.609
R_Hip_Flex_Max	.607	12.710	<.001	.626	.904	.419	.475	2.103
R_Hip_AbAd_Mom_Max	.224	4.745	<.001	.645	.620	.156	.489	2.046
LRA_Peak	-.331	-8.699	<.001	-.135	-.823	-.286	.748	1.336
RIO_iEMG	.352	8.664	<.001	.043	.822	-.285	.657	1.521
RLES_Peak	-.254	-6.044	<.001	.063	-.710	-.199	.614	1.629
R_Knee_Flex_Min	.199	3.877	<.001	-.509	.543	.128	.413	2.423
RLAT_Peak	.117	3.135	.003	.143	.463	.103	.774	1.293

Table 5.9: Multiple Regression Models for Left Knee Valgus using a stepwise approach.

Variables Entered/ Removed		Model Summary				
Model	Variable Entered	Method	R	R ²	Adj R ²	Std Err of the Est
1	L_Hip_AbAd_Min	Stepwise (Criteria: Probability of F to enter <= 0.050, Probability of F to remove >=0.100).	.759	.576	.560	.0232619
2	L_Hip_In_Ex_Min		.875	.766	.748	.0175870
3	L_Hip_Flex_Max		.943	.889	.876	.0123536
4	Spine_Flex_Min		.954	.911	.896	.0113290
5	L_Knee_InEx_Mom_Max		.970	.941	.928	.0094076
6	L_Knee_ID_ML_Shear_Min		.982	.965	.956	.0073730

*Durbin-Watson = 2.5 indicating no meaningful serial correlations (1.5-2.5 is considered safe).

Table 5.10: ANOVA results of the Left Knee Valgus stepwise multiple regression models.

Model Variable	ANOVA				
	Sum of Squares	df	Mean Square	F	Sig.
1 Regression	.020	1	.020	36.618	<0.001 ^b
Residual	.015	27	.001		
Total	.034	28			
2 Regression	.026	2	.013	42.649	<0.001 ^c
Residual	.008	26	.000		
Total	.034	28			
3 Regression	.031	3	.010	66.857	<0.001 ^d
Residual	.004	25	.000		
Total	.034	28			
4 Regression	.031	4	.008	61.055	<0.001 ^e
Residual	.003	24	.000		
Total	.034	28			
5 Regression	.032	5	.006	73.194	<0.001 ^f
Residual	.002	23	.00		
Total	.034	28			
6 Regression	.033	6	.006	101.876	<0.001 ^g
Residual	.001	22	.000		
Total	.034	28			

Dependent Variable: Peak_MKD_L_a

Predictors: (Constant), L_Hip_AbAd_Min_b

Predictors: (Constant), L_Hip_AbAd_Min, L_Hip_In_Ex_Min_c

Predictors: (Constant), L_Hip_AbAd_Min, L_Hip_In_Ex_Min,
L_Hip_Flex_Max_d

Predictors: (Constant), L_Hip_AbAd_Min, L_Hip_In_Ex_Min,
L_Hip_Flex_Max, Spine_Flex_Min_e

Predictors: (Constant), L_Hip_AbAd_Min, L_Hip_In_Ex_Min,
L_Hip_Flex_Max, Spine_Flex_Min, L_Knee_In_Ex_Mom_Max_f

Predictors: (Constant), L_Hip_AbAd_Min, L_Hip_In_Ex_Min,
L_Hip_Flex_Max, Spine_Flex_Min, L_Knee_In_Ex_Mom_Max,
L_Knee_ID_ML_Shear_Min_g

Table 5.11: Multiple Regression model analysis of the left DKV.

Model 8	Standardized Coefficients	t	Sig.	Correlations			Collinearity Statistics	
	Bata			Zero-order	Partial	Part	Tolerance	VIF
(Constant)		-9.778	<.001					
L_Hip_AbAd_Min	-.346	-6.754	<.001	-.759	-.821	-.268	.603	1.659
L_Hip_In_Ex_Min	-.242	-4.263	<.001	-.621	-.673	-.169	.489	2.046
L_Hip_Flex_Max	.372	8.094	<.001	.624	.865	.322	.748	1.337
Spine_Flex_Min	-.359	-6.486	<.001	-.333	-.810	-.258	.515	1.941
L_Knee_InEx_Mom_Max	.272	4.622	<.001	.508	.702	.184	.455	2.199
L_Knee_ID_ML_Shear_Min	.195	3.930	.001	.322	.642	.156	.639	1.565

5.3.2.3 What muscles best predict DKV?

To examine which muscle patterns best predict DKV the right and left knees were examined separately in two stepwise multiple regression analyses. To address these questions each trial was included in the analysis. Each hip's unilateral muscles and bilateral core muscles for iEMG and peak EMG were included into the stepwise multiple regression model.

The predictive ability of the left hip valgus score by left hip and core muscles was weak ($R^2 = 0.212$, $Adj R^2 = 0.191$, $SEE = 0.030$, $N = 40$), although the model research statistical significance ($F=10.232$, $p<0.01$). Based on the stepwise approach to multiple regression, only LTFL iEMG parameter was entered into the model and with a mere ~20% of the variance accounted for in the model muscle activity (iEMG and peak EMG) alone is a poor predictor of knee valgus. Note that the model was first attempted with GMed peak EMG and iEMG, but then attempted again with this muscle excluded since it was not a predictor. Due to drop out the increased the samples from $N=29$ to $N=40$ justified this exclusion since it was not a predictor in the original analysis.

Next, five models were created to predict right DKV. This time the model was statistically significantly strong ($R^2 = 0.578$, $Adj R^2 = 0.544$, $SEE = 0.0287$, $N = 41$, $F=16.894$, $p<0.001$) in the five iteration of the stepwise regression model. The final iteration settled on the three best predictors RGMED iEMG, RGMED peak EMG, and RGMAX iEMG. The model summaries are included in Table 5.12, due to the small sample size the adjusted R^2 value was improved with the removal of the RQUAD muscle iEMG, however it is worth noting this was also a significant predictor of valgus in the right hip in fact it was the best single predictor but this variability was capture when the other variables were added to the model.

Examining the effects of side dominance more closely with the iEMG values (Tables 5.13 and 5.14) it is apparent that neuromuscular control differs between sides. It seems neuromuscular patterns are more responsible for the differences between high and low valgus on the dominate side vs non-dominate side.

Table 5.12: Right Knee Stepwise Regression Analysis Model Summary

Model	Variable Entered	Variables Removed	R	R ²	Std. Error of the Estimate (SEE)	F	Sig.
1	RQUAD iEMG		0.303	0.285	0.0359972	16.914	<0.001
2	RGMED iEMG		0.402	0.371	0.0337657	12.775	<0.001
3	RGMED peak		0.528	0.490	0.0304015	13.797	<0.001
4	RGMAX iEMG		0.584	0.538	0.0289224	12.654	<0.001
5		RQUAD iEMG	0.578	0.544	0.0287457	16.894	<0.001

Table 5.13: iEMG (%Movement * %EMG) on the right side for Hi vs Low Valgus on the right knee.

	Valgus Condition		Independent Samples t-Test		
	Low	High	t	df	Sig. (2-tailed)
	Mean (SD)	Mean (SD)			
RTFL	2073 (1037)	1675 (657)	1.543	41	0.130
RGMAX	3595 (1575)	2137 (937)	3.795	41	<0.001*
RGMed	3334 (845)	2457 (811)	3.439	41	0.001*
RADD	2178 (765)	1923 (1106)	0.842	41	0.405
RHAM	2523 (943)	1774 (744)	2.578	39	0.014*
RQUAD	8121 (1896)	7740 (1628)	4.003	41	<0.001*

Table 5.14: iEMG (%Movement * %EMG) on the left side for Hi vs Low Valgus on the left knee.

	Valgus Condition		Independent Samples t-Test		
	Low	High	t	df	Sig. (2-tailed)
	Mean (SD)	Mean (SD)			
LTFL	2260 (1221)	1494 (613)	2.588	31.876	0.014*
LGMAX	3242 (1751)	2775 (794)	1.069	29.867	0.293
LGMed	3099 (813)	3288 (1268)	-0.458	23	0.651
LADD	2696 (1829)	1749 (629)	2.280	26.562	0.031
LHAM	2257 (1021)	1839 (726)	1.488	39	0.145
LQUAD	8170 (2253)	7189 (1197)	1.676	27.410	0.105

5.4 Discussion

The most profound findings in this study are the number of differences and the predominance of the spine and hip variables which differentiate the HVG and LVG. These have been overlooked in the previous studies of the knee. Specifically, the first hypothesis was supported, the spine, hip and knee all had increased flexion angles during the DVJ (Figures 5.5 and 5.6). This indicates the HVG which is essential frontal plane collapse at the knee joint also had decreased control in the sagittal plane at the spine, hip and knee. As expected with the increase in sagittal plane flexion angles increases in AP shear at the spine and hip were also predominate in the HVG, this hypothesis was also supported. Following this logic further with increased joint angles and differences in joint forces, moments would also differ between groups in all directions. This hypothesis was conditionally accepted with differences in spine peak (max and min) flexion/extension moments as well as maximum (flexion, medial, abduction) hip and knee moments in all three planes (Figure 5.19). In contrast the spine lateral bend and axial twist, hip lateral, and knee extension, and adduction moments were not statistically different; however, spine extension, hip extension adduction and knee external rotation moments were statistically different (Figure 5.19). Lastly, the hypothesis related to the isolated examination of the neuromuscular control strategy revealed in the EMG patterns was also accepted. Examining the peak EMG data the TFL and GMAX were the key differentiators in the control strategy of the hip muscles. Moreover, when examining the “work” the muscles were doing during the entire landing and propulsion event with the iEMG the TFL, GMAX, GMED, ADD, and QUAD patterns were all statistically different between HVG and LVG as well as biologically significant. The LVG generally had higher activation in all muscle groups indicating less coordinate control of the joints

when landing and jumping. Hence, several important differences were present between the HVG and LVG in kinematics, kinetics and neural control strategies. The complexity of the ACL injury problem and DKV should not be limited to a simple examination of the knee. In order to understand these mechanisms thoroughly a more complete examination of the linkage is required.

Equally impressive is the secondary results which suggest the most meaningful correlations are found once again among the spine and hip variables over the knee variables for predicting DKV. In both the dominate and non-dominate knees the top three regression model variables were related directly to the hip. The next variables were spine variables on both sides and then following these were knee variables (Figure 5.4 and 5.7). The next interesting results with neuromuscular patterns were the differences in the dominate and non-dominate sides. The non-dominate side was essentially unpredictable with respect to DKV while the dominate side was highly predictable neural control strategy related to GMED iEMG, GMAX peak and RGMAX iEMG, with the QUAD iEMG excluded from the final model but the strongest single predictor. This is hypothesized to relate to the lack of control capability or difference between the dominate and non-dominate sides (Figures 5.11 and 5.12). The collapse in the knee is best predicted by motions, postures and loads associated with the hip and spine.

There were of course limitations to this study as with any study. Testing the individuals with this robust analysis, 24 channels of EMG, full body kinematics and the in-depth processing and analysis is a time intense process. This led to a limitation in sample size. To overcome this limitation the assumption was made that the critical features of DKV would be represented on a

trial by trial basis rather than an individual basis. In this way only a HKV trial would be deemed “at-risk” and not the individual. Since anyone could, in theory, have a good or bad landing. However, this does challenge the conventional way of considering independence with respect to statistical analysis. There was also EMG drop out in some muscles more than others, for example, LGMED which limited the analysis of all data. There is no doubt a significant challenge when capturing this amount of data simultaneously. Lastly, we used a group of undergraduate females in the kinesiology department with a varied level of athletic ability. We were not able to capture a pool of varsity only female basketball and soccer players, however, this pool of participants would likely provide more generalized findings to a broader group of recreational female athletes. It is more likely the characteristics of the specific sport put the female athletes at higher risk rather than the physical characteristics of the athletes who play those particular sports.

In comparing the data presented here some interesting comparisons can be made with the literature. Early in the quantification of DKV during DVJ was a significant difference in female dominant and non-dominant sides. It is also noteworthy this phenomenon of difference in dominance was not present in males (Ford et al. 2000). In contrast, there were no obvious differences in DKV and leg dominance, however, this work did identify differences in control strategy faults leading to DKV. Further contrast with the literature in this area is the understanding and quantification of neuromuscular control. Neuromuscular control, in the context of ACL injury literature, has been quantified through strategies of neuromuscular control like movement patterns (Hewett et al. 2004) or exercise training programs (Hewett et al. 2016; Myer et al. 2007a). In this work, neuromuscular deficits were directly measured and evaluated, it is therefore not possible to compare the results of this study's neuromuscular deficits with

those inferred in the literature. This was one of the main motivations for the work of this thesis as the major gap in the literature provided great opportunity to shed light onto a neglected area of inquiry.

This study demonstrated a predominance of hip and spine biomechanical and neuromuscular control strategies. Spine and hip movement and motor patterns are able to predict and at least in part explain the phenomena of DKV or “valgus collapse” as it has been referred to in the literature (Quatman & Hewett 2009). It remains clear that neuromuscular control (motor patterns) should be a target for clinical intervention to control movement patterns, such as DKV. With this new knowledge perhaps more effective ‘neuromuscular training programs’ can be designed and implemented with the hopes of improving effectiveness over the current standard (Taylor et al. 2018).

5.5 Conclusions

In summary, the hip and spine function to control the distal linkage. This is consistent with the biomechanical principle that states proximal stiffness is required to optimize distal mobility and athleticism. Those participants who displayed DKV also displayed more spine and hip collapse in the sagittal plane, higher joint loading and divergent neuromuscular patterns. Clinical interventions should be designed to directly address these differences in order to better address the at-risk movement behaviour of DKV which is thought to be the main contributor to the high prevalence of ACL injuries in female athletes.

6.0 Study 5: Quantifying the demands and exposures in commonly used rehabilitation exercises - Towards the development of an atlas of exercises for clinical use

6.1 Introduction

A critical issue for the development of highly effective personalized programs is the progression of exercise intensity. Conforming to the most fundamental training principle - overload; considerations for the design and implementation of a progressive exercise program is essential. As the patient gains in desired variables such as strength or endurance the demands of the exercise must also progress to maintain the overload principle. In this population the tipping point between too much demand and not enough is a moving target as the patient recovers and tissues heal and pain sensitivity decreases. However, often overlooked in the rehabilitation and training field is the mechanical cost or demand analysis of the prescribed exercises themselves. Expertise in programming requires an understanding of not just increasing intensity but also the increasing or changing demands of the exercise on specific surrounding tissues and joints, many of which are sensitized and damaged. In other words, striking a balance between exercise demands and the patient's capacity is critical in the designing a successful progressive rehabilitation program.

Providing appropriate graded demands while optimizing exposure and maintaining the boundaries of the patient's capacity is the goal of effective rehabilitation program. To this end, there is a scattering of information on hip rehabilitation exercises from several different groups. Direct interpretation and comparison between groups is challenging due to different data collection techniques and analyzing approaches. A single database with standardized procedures would make for a very useful resource to understand the progressions of hip exercises along with detailed and accurate understanding of joint and tissue demands. As an example, consider a

classic exercise like "hip hikes" shown to target gluteus medius and minimus (hip abductors), perhaps thought to be an ideal hip exercises for abductor training (Bolgia & Uhl 2005). However, consider the repetitive bending of the spine required to perform this exercise such that this ideal muscle targeting exercise may be deemed completely inappropriate for some patient populations with motion intolerant low back pain. Thus, muscle activation as well as the resulting joint and tissue loading ought to be considered when designing exercise protocols. Providing a single source of the most commonly used exercises will enable clinicians to integrate the cost and benefit trade-offs of each exercise.

The purpose of this study is to quantify the demands and the exposure of commonly used rehabilitation exercises in order to inform clinical practice of: one, progressive activation strategies for targeted muscle groups and; two, joint kinematic and kinetic demands at the hip and spine; collectively in order to elucidate the requirements of popularized rehabilitation exercises. This information can then be used to develop clinical recommendations across the spectrum of hip and spine conditions. Characterizing and describing these exercises and creating an atlas or lookup table so that a clinician can choose an exercise based on what is tolerable, determined from a specific assessment of the disorder, thereby increasing the precision of exercise prescription for each individual's specific needs and capabilities.

The first phase of the Hip Rehabilitation Atlas (HRA) examined the "hip hinge squat" and five modifications to this exercise for comparison. It was hypothesized that muscle activation, joint movement demands, and joint loads will differ between squat sub-types. Specific hypotheses to each squat type are listed here:

1. Hip Hinge Squat (HHS)

- I. Will have moderate peak angles, forces and moments compared to the other sub-types of squats.
2. Bosu Ball Squat (BOSU)
 - I. Will have higher muscle activation than HHS in all muscle groups.
3. Adductor Ring Squat (ARS)
 - I. Will have a lower Abduction angle than HHS, BOSU, ABS.
 - II. Will have higher ADD activation than HHS.
 - III. Will have a higher adduction and medial rotation moment than all other sub-types.
4. Single Leg Squat (SLS):
 - I. Will have the lowest flexion and abduction angle.
 - II. Will have the highest muscle activation in all hip muscles (TLF, GMED, GMAX, ADD, HAM, QUAD).
 - III. Will have the highest joint compression and medial shear force as well as the highest extension and adduction moments and the lowest abduction.
5. Abductor Band Squat (ABS)
 - I. Will have higher GMAX activation than the HHS.

6.2 Methods

A group of healthy males performed a series of hip rehabilitation exercises for the purposes of quantifying muscle and joint loading demands. An anatomically detailed model driven with biological signals obtained from the individual enables tissue load estimates sensitive to the unique strategies employed with each repetition of each exercises in each person.

6.2.1 Participants

A healthy group of twenty males volunteered to participate in this study forming a sample of convenience. Participants were young and healthy (mean age of 21 (± 1.89) years; mean mass of 81.97 (± 15.00) kg; height of 1.78 (± 0.07) m) with no current (within the last six months) reports of any back or hip injury for which they had required treatment from a health professional. In addition, they were not experiencing any form of back, hip or lower limb pain or discomfort. Participants were excluded if they had any history of a major injury, surgery, or known congenital anomalies of the torso, pelvis hip or lower extremity. Participants were asked refrain from any form of moderate to high intensity exercise for a 48-hour period prior to their testing day.

6.2.2 Tasks and Apparatus

Participants were asked to perform a series of exercises after a short accommodation phase to refine the technique of each exercise. Each exercise was performed until three satisfactory trials were collected. A satisfactory trial was observed when the task was formed, balance was maintained, and accurate movement patterns and timing was performed as would be coached in a clinical setting. An illustration and description of the exercises can be found in Table 6.1.

The Bosu™ ball is a semi-domed rubber inflatable ball with a hard-rigid plastic on one side providing a platform for standing. In this study the Bosu™ ball was used with rubber inflatable side down and participants stood on the rigid plastic surface. The Bosu™ is shown in Figure 6.1. A Palates adductor ring was used to provide resistance to the adductor squeeze squat. It is a standard size and resistance (Figure 6.2). Finally, a green mini-band was used from Perform Better™ for the knee abduction squat (Figure 6.3).

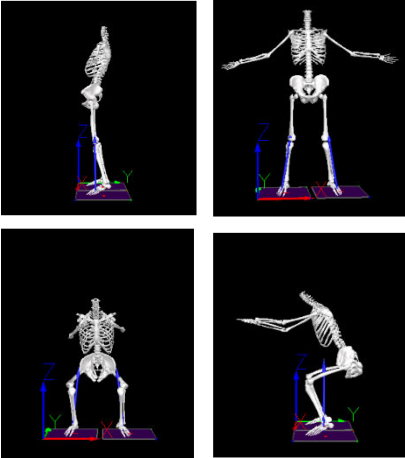
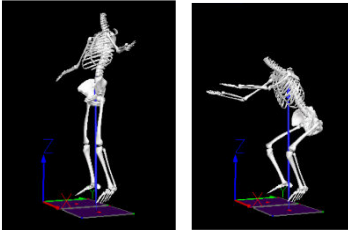
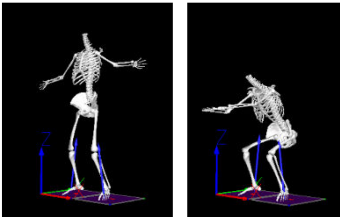
6.2.3 Procedure

Each participant was acquainted with the laboratory, testing procedures and exercises prior to signing informed consent documents which were approved by the office of research ethics. Participants wore their own tight-fitting shorts or a pair of laboratory bicycle shorts that permitted the use of surface EMG recordings and kinematic motion capture. Participants also removed their shirt during testing, so it did not obscure the reflective markers for motion capture. The subjects were then prepared for electromyographic (EMG) recordings. The skin was shaved, cleaned, and abrading with Nuprep to exfoliate the skin, alcohol was used to remove any residue and debris. Next, the EMG (Ag-AgCl) surface electrodes pairs were placed in bi-polar configurations with a center to center distance of 2.5 cm, parallel to the muscle fiber orientation. Electrodes were placed on six torso muscle bilaterally including: Rectus Abdominis (RA), External Oblique (EO), Internal Oblique (IO), Lower Erector Spinae (LES), Upper Erector Spinae (UES) and Latissimus Dorsi (LAT); as well as bilaterally over six hip muscles: Tensor Fascia Latae (TFL), Gluteus Medius (GMed), Gluteus Maximus (GMax), Rectus Femoris (QUAD), Adductor Longus (ADD), Semitendinosus (HAM). Each electrode was then held in place with Hypafix™ and the EMG amp was secured with clear tape (positioning is shown in Figure 6.4).



Figure 6.1: Bosu™ ball with a semi-domed rubber and firm plastic platform.

Table 6.1: Squat variations with illustrations and descriptions.

<p>1) Hip Hinge Squat (HHS)</p> 	<p>The hip hinge squat is a common rehabilitation pattern. The hip is used as the dominate joint sparing the spine and knees which only move to accommodate motion at the hip joint. The arms were used as a counterbalance and take from the side to the front as the hips move back and down during the squat. This technique formed the foundation for each modification and was adopted in each sub-category of squat technique. This would be most accurately referred to as the “Hip Hinge – Counter Movement Squat”.</p>
<p>2) Bosu Ball Squat (BOSU)</p> 	<p>A semi-domed “Bosu” ball with a rigid platform was used to perform a squat. The air filled dome provides an unStable surface (the rigid plastic surface) requiring the participant to balance and control the surface while squatting.</p>
<p>3) Adductor Ring Squat (ARS)</p> 	<p>A Pilates ring was placed just distal to the knee joint on the medial condyles of the tibia and the participants were asked to squeeze the ring while performing a hip hinge squat.</p>

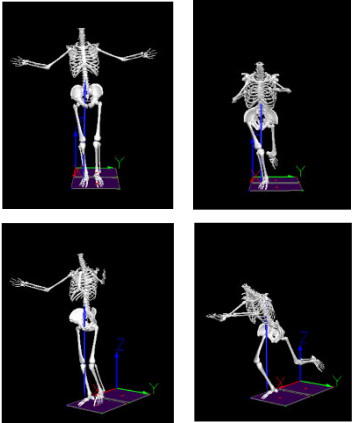
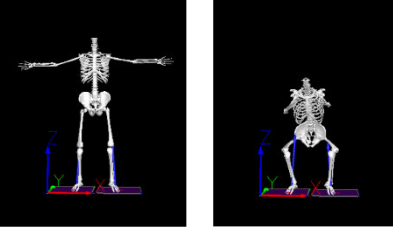
<p>4) Single Leg Squat (SLS)</p> 	<p>The single leg squat was performed on the right leg. The left leg was lifted and projected to the rear the hands again were used for counterbalance.</p>
<p>5) Abductor Band Squat (ABS)</p> 	<p>A mini band which forms a loop was placed immediately distal to the knee joint. The knees were abducted against the resistance of the band with a continued effort to abduct against the resistance during the squat.</p>



Figure 6.2: Pilates adductor ring with padded handles and ring structure.



Figure 6.3: Green Mini-Band from Perform Better™.

Each participant performed maximal isometric contractions (MVCs) for each muscle (or muscle group) so the biological signals could be normalized. For the abdominal muscles five abdominal contractions (flexion, lateral bend right and left, and, twist right and left) in a semi-recumbent posture sitting on a plinth with hips and knees bent to approximately 90 degrees with the ankles held in place by one researcher and upper body restrained by the second researcher. The ES muscles were normalized with Biering Sorensen test and a modified Biering Sorensen test, (i) back extension and then (ii) back extension, gluteal squeeze and latissimus contraction. The LAT and GMax were evaluated during this test and their specific MVC tests – the highest contraction level was used for normalization. The ADD muscles were tested in a recumbent position with the hips and knees flexed with a foam block used to “squeeze” together as both ADD groups (right and left) were normalized with a single hip adduction contraction simultaneously. The QUAD muscle was normalized in the sitting position with the research restraining knee extension. GMax and HAM muscle were normalized using (i) a hip extension and (ii) hip extension with knee flexion contraction while laying prone. Finally, the LAT muscles were resisted by the researcher in a standing position with the shoulder flexed ~75-80 degrees and abducted horizontally ~45 degrees. All MVCs were coached with verbal motivation to produce maximal effort. Finally, a quite reference collection was collected. The subject laid completely

relaxed, prone and then supine, while a short trial was collected for post processing purposes after the collection. Finally, the subjects performed a series of exercises outlined in Table 6.1. These exercises are commonly prescribed in clinical settings and are familiar to the researcher who has had experience in clinical setting prescribing these exercises.

Analysis of each exercise included EMG muscle activation patterns, kinematic joint angles and model driven joint loading (note: the data collection and processing steps are consistent throughout the thesis and are detailed in Appendix D). Combined, this analysis categorized this data into a number of different classification spectrums allowing clinicians to make customized rehabilitation programs tailored to the patient based on some combination of observed clinical objectives (i.e. activation profile, joint ROM, loading profile). For example, an elderly patient may want low joint load to prevent hip fracture, and moderate gluteal activation to enhance the performance of stair ascents. Yet, another patient may wish to maximize external rotation capacity without regard for joint loading due to the specific demands of an athletic endeavor. This atlas will inform rehabilitation programs and clinical decision making for hip and spine conditions beyond anything currently available to the clinician.

6.2.1. Statistical Analysis

One-way repeated measures ANOVA was used to evaluate the five squat types on several outcome variables defined in the hypotheses. Testing homogeneity of variance was done with Mauchly's test of Sphericity. If the differences in variance were significant then the Greenhouse-Geisser modification was used to account for the differences in variance. The presentation of squat type was randomised in a number generator using MATLAB to avoid issues with order

effects and learning. Pair-wise differences were evaluated when the ANOVA test indicated a difference within the groups and a Least-Significant-Difference was used to evaluate multiple comparisons. For the squat pattern types the right-side analysis includes all 5 sub-types. The left side purposely omits the SLS as all subjects performed this exercise on only the right side.

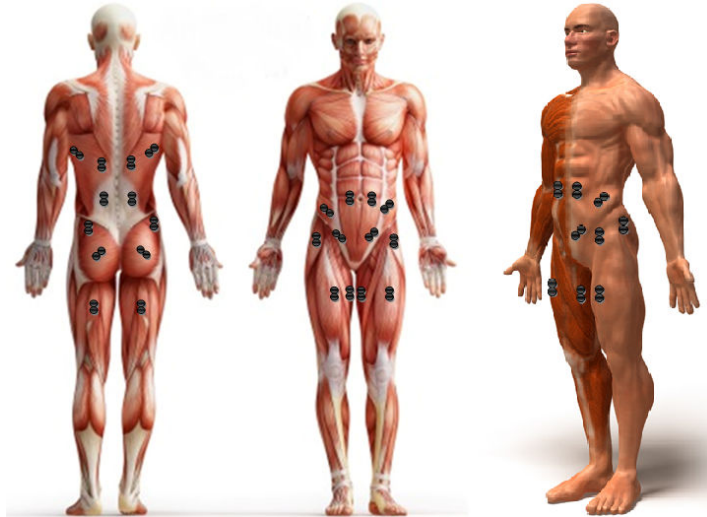


Figure 6.4: Twenty-Four EMG channels will be collected including 6 bilateral core muscles (Rectus Abdominis (RA), External Oblique (EO), Internal Oblique (IO), Lower Erector Spinae (LES), Upper Erector Spinae (UES), and Latissimus Dorsi (LD)) and 6 bilateral hip/leg muscles (Rectus Femoris (RF), Tensor Fascia Latae (TFL), Gluteus Medius (GMed), Gluteus Maximus (GMax), Biceps Femoris (BF), and Adductor Longus (ADD)).

6.3 Results

An overview of the results indicated that neuromuscular patterns and movement patterns alter joint and tissue loads. The result will be divided into the following sections: movement patterns, motor patterns and joint loads.

6.3.1 Movement Patterns

Hip hinge squats have a low kinematic demand on the spine. The mean (SD) angles during the hip hinge squat patterns are shown in Table 6.2. When comparing the peak spine flexion across

the five squat types showed significantly more spine peak flexion angle in the adductor ring squat compared to all other types (Table 6.3).

Table 6.2: Descriptive data for mean spine angle (degree) across five squat sub-types.

Squat Type	Spine Flex (deg)	Spine Bend (deg)	Spine Twist (deg)
HHS	-6.09 (7.9)	0.91 (1.9)	0.11 (1.1)
BOSU	-7.46 (7.4)	0.48 (2.2)	0.21 (1.3)
ARS	-10.64 (8.6)	0.35 (2.1)	0.35 (1.2)
SLS	-6.35 (7.4)	2.30 (1.9)	-0.07 (1.1)
ABS	-6.70 (7.61)	0.69 (2.0)	0.31 (1.3)

Table 6.3: Peak spine flexion angle during five squat types and statistical analysis.

Squat Type	Peak Flexion Angle (Deg) Mean (SD)	Repeated Measures ANOVA	Pairwise comparisons (ARS vs others)
HHS	-13.18 (9.1)	Mauchly's Test of Sphericity = 0.146, p=0.005 Greenhouse-Geisser F=5.257, df=2.407, p=0.007	0.005
BOSU	-14.99 (10.0)		0.036
ARS	-20.95 (12.8)		---
SLS	-13.73 (9.1)		0.013
ABS	-15.3 (8.8)		0.029

Hip angles differed between squat type. Peak flexion angles were 98.9 (10.9), 98.3 (8.6), 94.1 (11.6), 91.9 (7.7), and 97.3 (11.6), for the HHS, BOSU, ARS, SLS, ABS, respectively, for the

right hip. Mauchly's Test of Sphericity was not significant ($p=0.24$). The repeated measures ANOVA revealed a significant difference between groups ($F=6.004$, $p < 0.001$). Pair-wise comparisons with LSD showed that the HHS and BOSU were performed with more hip peak flexion than the ARS and SLS (1v3, $p < 0.01$; 1vs4 $p < 0.01$; 2v3 $p < 0.05$; 2v4 $p < 0.001$). The ARS version was also less flexion than the Abductor Squat ($p < 0.05$). For the left hip peak flexion angles were similar with values of 98.1 (11.9), 96.9 (9.8), 89.7 (17.1), and 92.3 (22.8), for the HHS, BOSU, ARS, and Abductor Band, respectively, for the right hip. Statistical significance was not reached likely due to the higher variability in the left hip peak flexion angle during the ARS, and Abductor Band.

The hip abduction angles also differed significantly between squat types. The right hip abduction angles of -18.9 (4.5), -17.4 (7.4), -13.4 (4.4), -6.9 (8.5), and -21.0 (7.9), for the HHS, BOSU, ARS, SLS, ABS, respectively. These were different overall according to the ANOVA test ($F=12.589$, $df=4$, $p<0.001$). The SLS had the lowest peak abduction angle compared to the HHS ($p < 0.001$), BOSU ($p < 0.001$), SLS (0.012), ABS (0.001); followed by the ARS compared to the HHS ($p < 0.001$), BOSU (0.045), and Abductor Band ($p < 0.01$). On the left side there was also observed differences with the ANOVA ($F=5.010$, $df=3$, $p = 0.005$). Similarly, the left hip peak abduction was smallest in the Adduction Ring squat 15.6 (4.2) degrees compared to the HHS at 20.5 (3.9) degrees ($p < 0.001$) and ABS at 21. 2 (6.5) degrees ($p < 0.01$).

There were no differences in the medial and lateral rotation across the hip angles which were all relatively neutral in position with peak external rotation angles of -0.8 (7.4), 0.11 (7.3), 1.9 (8.3), 1.0 (7.8), and 0.8 (6.6) for the HHS, BOSU, ARS, SLS, ABS, respectively, on for the right

hip. Similarly, for the left hip the peak external rotation values were relatively neutral at -0.7 (6.1), 0.3 (6.5), -3.1 (6.1), 0.1 (7.6), respectively, for the HHS, BOSU, ARS, SLS and ABS.

6.3.2 Motor Patterns

Examining the time histories for the neuromuscular patterns revealed peak EMG would be most appropriate measure for analysis given the discrete nature of the squat. Displayed in Figure 6.5 are the median of three trail peak EMG for each subject were used to calculate mean values with standard deviation (SD) for the group by squat type.

The right TFL revealed significantly higher peak activation level (Mauchly's Test = 0.038, $p < 0.001$; Greenhouse-Geisser $F = 4.738$, $df = 2.059$, $p = 0.016$) with pairwise comparisons showing the ARS produced higher values with a mean score of 20.2 (± 20.9) %EMG then the HHS ($p < 0.05$) and the ABS ($p = 0.05$), and only trending higher than the BOSU ($p = 0.063$). Similarly, the SLS produced higher peak activation levels at 21.6 (± 18.0) then the HHS ($p < 0.01$), BOSU ($p < 0.01$), and the ABS ($p = 0.01$). GMax on the right side showed a difference between conditions (Mauchly's Test = 0.460, $p = 0.385$; $F = 12.972$, $df = 4$, $p < 0.001$) and pairwise comparisons showing both the SLS and the ABS producing higher peak scores (29.6 (15.6) and 18.0 (12.6), respectively) than the HHS ($p < 0.001$, $p < 0.05$, respectively), BOSU ($p < 0.001$, $p < 0.05$, respectively) and the ARS ($p < 0.01$, $p < 0.05$, respectively). GMed (49.4 (25.8)) on the right side revealed a statistically significant difference between conditions (Mauchly's Test = 0.286, $p < 0.08$; $F = 18.540$, $df = 4$, $p < 0.001$) and pairwise comparisons showed that the SLS was different from all other sub-types (HHA 21.3 (26.4), $p < 0.001$; BOSU 20.7 (24.1), $p < 0.001$; ARS 20.4 (17.6), $p < 0.001$; ABS 21.3 (21.7),

p <0.001). The right ADD group was not significantly different across sub-types of squats (Mauchly's Test = 0.078, p < 0.001; Greenhouse-Geisser F = 0.989, df = 1.934, p = 0.066). Right HAM EMG was similar to GMED with an overall difference (Mauchly's Test = 0.058, p < 0.001; Greenhouse-Geisser F = 7.022, df = 2.474, p = 0.002) and only the SLS (17.8 (13.9)) was different than the other sub-types (HHA 9.8 (13.1), p = 0.004; BOSU 11.1 (12.2), p = 0.007; ARS 9.9 (9.2), p = 0.008; ABS 7.6 (9.7), p = 0.001). Finally, the right QUAD showed a general trend of progressive increases from HHS towards the SLS and ABS. Examining the results with statistical analysis showed a difference overall (Mauchly's Test = 0.376, p < 2.09; F = 4.127, df = 4, p < 0.005). Pairwise comparisons showed that the SLS (41.7 (26.7)) was significantly higher activation than the HHS (23.8 (20.6) p = 0.007) and the BOSU (30.6 (21.9) p = 0.041). Similarly, the ABD at a mean activation of 37.5 (27.2) was also different from the HHS (p = 0.020) but only trended different from BOSU (p = 0.061).

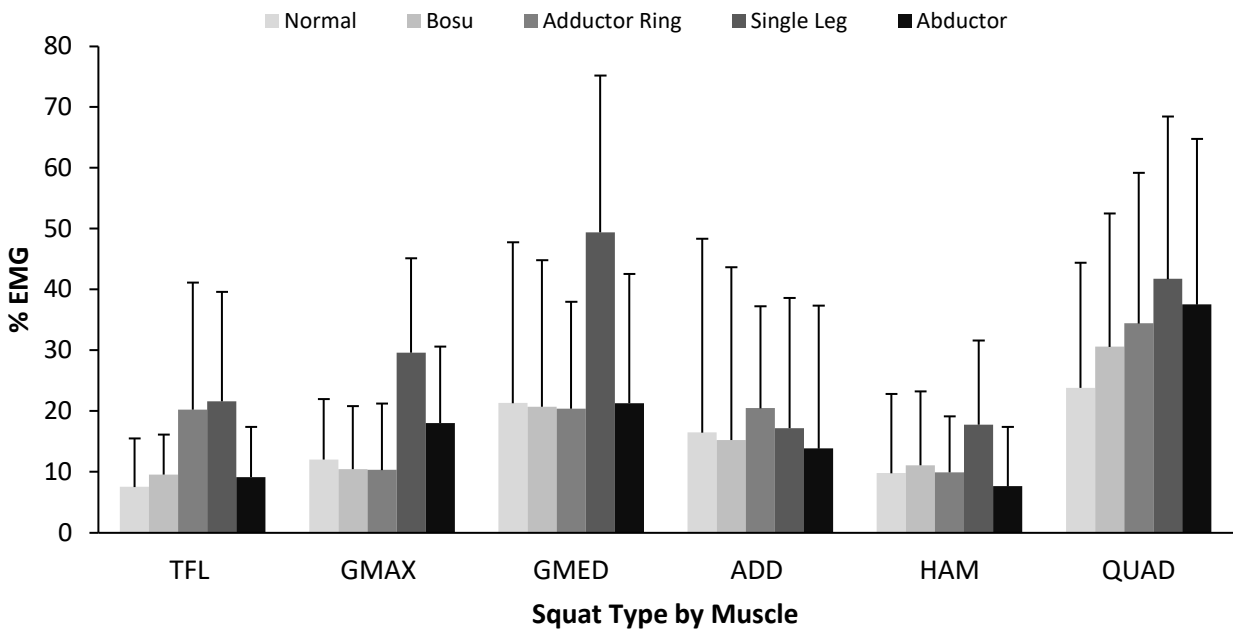


Figure 6.5: Mean and standard deviation (SD) bars for the median peak EMG values for each squat sub-type by neural driver.

6.3.3 Joint Loads

Examining the HSM estimated spine and hip loads during the squat sub-types demonstrated consistent loading profiles for the spine, with the exception of the lateral bend moment in the SLS, while migrating joint demands at the hip. Spine loads during the squat variations revealed no difference in peak compression (Table 6.4) peak anterior shear (Table 6.5), and peak flexion moment (Table 6.6). Spine lateral bend moment was statistically different in the SLS (Table 6.7); as would be expected with a single leg support.

Table 6.4: Spine compression peaks (minimum) estimated from HSM for five squat types.

Squat Type	Mean (SD) Compression (kN)	Repeated Measures ANOVA
HHS	-1.909 (0.790)	Mauchly's Test of Sphericity = 0.159 p= 0.007 Greenhouse-Geisser F=1.528, df=2.250, p=0.232
BOSU	-1.927 (0.770)	
ARS	-1.877 (0.685)	
SLS	-2.063 (0.751)	
ABS	-1.887 (0.753)	

Table 6.5: Spine AP shear peaks estimated from HSM for five squat types.

Squat Type	Mean (SD) AP Shear (N)	Repeated Measures ANOVA
HHS	109.8 (41.6)	Mauchly's Test of Sphericity = 0.188 p = 0.015 Greenhouse-Geisser F= 0.706, df=2.627, p=0.537
BOSU	107.7 (29.0)	
ARS	113.0 (23.7)	
SLS	117.7 (40.1)	
ABS	116.7 (35.1)	

Table 6.6: Spine Flexion Moment peaks estimated from HSM for five squat types.

Squat Type	Mean (SD) Flexion Moment (Nm)	Repeated Measures ANOVA
HHS	100.5 (46.6)	Mauchly's Test of Sphericity = 0.217, p = 0.027 F=0.765, df=4.474, p=0.498
BOSU	98.4 (42.9)	
ARS	93.3 (38.0)	
SLS	101.8 (40.8)	
ABS	98.0 (44.3)	

Table 6.7: Spine Lateral Bend Moment peaks estimated from HSM for five squat types.

Squat Type	Mean (SD) Flexion Moment (Nm)	Repeated Measures ANOVA	Pairwise comparisons (SLS vs others)
HHS	-17.0 (10.0)	Mauchly's Test of Sphericity = 0.545, p = 0.584 F=11.783, df=4, p<0.001	<.001
BOSU	-19.3 (9.6)		<.001
ARS	-18.7 (11.5)		.001
SLS	-28.0 (12.6)		---
ABS	-19.4 (10.2)		.001

Hip loads, both forces and moments, differed between squat sub-types in many directions and squat-types. Peak compression force of the right hip during the SLS was approximately double that of the other squat variations (Table 6.8). Peak anterior shear force showed several important differences. Namely, the HSS was less than all types except the BOSU, which was only a trending difference; at the other end the SLS and ARS were higher than all other sub-types (Table 6.9). While medial shear force was significantly higher once again in the SLS by approximately 40% (Table 6.10). Peak hip extension moment for SLS was significantly higher and nearly double the other sub-types (Table 6.11). The peak adduction moment in the SLS was approximately three times greater than all sub-types and significantly different from the comparisons (Table 6.12). The peak medial rotation moment was significantly greater in the ARS version compared to the BOSU and SLS, while showing strong trends of a higher magnitude over the HHS and ABS. On the other hand, the SLS was significantly lower than all other comparison squat-types (Table 6.13). Finally, in the medial-lateral plane: peak medial rotation moment was significantly greater in the ARS sub-type (Table 6.14); and the SLS was significantly higher than all other comparisons with many additional differences with sub-types demonstrated in Table 6.15.

Table 6.8: Right Hip compression peaks estimated from HSM for five squat types.

Squat Type	Mean (SD) Compression (kN)	Repeated Measures ANOVA	Pairwise comparisons (SLS vs others)
HHS	1.224 (1.1)	Mauchly's Test of Sphericity = 0.120, p = 0.002	<0.001
BOSU	1.209 (0.6)		<0.001
ARS	1.301 (0.5)		<0.001
SLS	2.505 (0.9)	Greenhouse-Geisser F=16.665, df=2.437, p < 0.001	---
ABS	1.332 (0.8)		0.001

Table 6.9: Right Hip AP Shear peaks estimated from HSM for five squat types.

Squat Type	Mean (SD) AP Shear (kN)	Repeated Measures ANOVA	Pairwise comparisons (HHS vs others)	Pairwise comparisons (SLS vs others)	Pairwise comparisons (ARS vs others)
HHS	-1.680 (0.83)	Mauchly's Test of Sphericity = 0.218, p = 0.027	---	.000	.002
BOSU	-1.909 (1.02)		0.062	.001	.074
ARS	-2.267 (0.98)		0.002	.280	
SLS	-2.410 (1.08)	Greenhouse- Geisser F= 7.265, df=2.138, p=0.002	<0.001	---	.280
ABS	-2.024 (1.11)		0.69	.023	.028

Table 6.10: Right Hip ML shear peaks estimated from HSM for five squat types.

Squat Type	Mean (SD) ML Shear (kN)	Repeated Measures ANOVA	Pairwise comparisons (SLS vs others)
HHS	-1.394 (0.80)	Mauchly's Test of Sphericity = 0.122, p = 0.002	0.003
BOSU	-1.309 (0.68)		0.002
ARS	-1.452 (0.44)		0.005
SLS	-2.010 (0.87)	Greenhouse-Geisser F=7.788, df=2.223, p=0.001	---
ABS	-1.476 (0.63)		0.018

Table 6.11: Right hip peak extension moment estimated from HSM for five squat types.

Squat Type	Mean (SD) Extension Moment (Nm)	Repeated Measures ANOVA	Pairwise comparisons (SLS vs others)
HHS	-52.3 (30.9)	Mauchly's Test of Sphericity = 0.103, p =0.001	<.001
BOSU	-53.8 (34.1)		<.001
ARS	-55.33 (33.9)		<.001
SLS	-102.5 (52.9)	Greenhouse-Geisser F= 12.861, df=1.974, p<0.001	---
ABS	-64.0 (30.3)		.012

Table 6.12: Right hip Abduction rotation moment peaks estimated from HSM for five squat types.

Squat Type	Mean (SD) Moment (Nm)	Repeated Measures ANOVA	Pairwise comparisons (SLS vs others)
HHS	-27.0 (19.2)	Mauchly's Test of Sphericity = 0.166, p = 0.009 Greenhouse-Geisser F=17.698, df=2.189, p<0.001	<.001
BOSU	-27.2 (24.0)		<.001
ARS	-26.8 (20.1)		<.001
SLS	-75.3 (31.5)		---
ABS	-30.9 (21.3)		.001

Table 6.13: Right hip adduction moment peaks estimated from HSM for five squat types.

Squat Type	Mean (SD) Moment (Nm)	Repeated Measures ANOVA	Pairwise comparisons (ARS vs others)	Pairwise comparisons (SLS vs others)
HHS	12.3 (26.2)	Mauchly's Test of Sphericity = 0.165, p = 0.008 Greenhouse-Geisser F=6.712, df=2.161, p=0.003	.055	.043
BOSU	13.2 (18.2)		.043	.002
ARS	26.6 (25.8)		---	.001
SLS	2.3 (19.1)		.001	---
ABS	13.6 (24.7)		.051	.007

Table 6.14: Right hip medial rotation moment peaks estimated from HSM for five squat types.

Squat Type	Mean (SD) Moment (Nm)	Repeated Measures ANOVA	Pairwise comparisons (ARS vs others)
HHS	11.2 (25.3)	Mauchly's Test of Sphericity = 0.066, $p < 0.001$ Greenhouse-Geisser F=5.131, df=2.387, $p=0.008$.011
BOSU	13.3 (28.7)		.034
ARS	28.7 (26.4)		---
SLS	7.2 (22.0)		.010
ABS	9.3 (25.1)		.010

Table 6.15: Right hip lateral rotation moment peaks estimated from HSM for five squat types.

Squat Type	Mean (SD) Moment (Nm)	Repeated Measures ANOVA	Pairwise comparisons (HHS vs others)	Pairwise comparisons (BOSU vs others)	Pairwise comparisons (ARS vs others)	Pairwise comparisons (SLS vs others)
HHS	-25.5 (8.3)	Mauchly's Test of Sphericity = 0.083, $p < 0.001$ Greenhouse- Geisser F=16.866, df=1.910, $p < 0.001$	---	.018	.003	<.001
BOSU	-19.4 (6.3)		.018	---	.316	<.001
ARS	-17.7 (8.0)		.003	.316	---	<.001
SLS	-45.3 (20.5)		<.001	.000	<.001	---
ABS	-27.4 (12.3)		.556	.031	.008	.009

6.4 Discussion

The primary result of this study demonstrates that variations of an exercise influence joint angles, muscle activation patterns and joint loads. Specifically, during the squat exercises tested here, variation in demands on the spine were relatively low while much more variation existed at the hip. The range of motion in the spine were low, with small peak angles and minimal deviation from neutral postures. Hip demands were not so straight forward with several differences of note between exercises. The neuromuscular demands limited the depth of squat during the SLS (reduced hip flexion angle). The SLS was also performed with less abduction angle as the mass needed to be stacked over the support limb. Thus, the motor patterns at the hip were consistent with the hypotheses, the SLS had increased demand on all muscles with the exception of the adductors which were similarly activated among all exercises. GMAX was higher in activation during the SLS and the ABS. Interestingly, TFL activation was also high during the ARS implying a higher demand of co-contraction than was expected. Finally, examining the loading profiles the spine again was very conservative with joint loads well below previously established guidelines based on laboratory standards (3400 N of compression and 500 N of anterior shear, McGill 2016). Once again, however, the lessons on the hip are more variable with each exercise variation. The SLS had higher compression, anterior and medial shear as hypothesized. The extension moment was also higher for SLS, in fact, nearly double the comparison squats (6.10). The adduction demand showed the SLS to be the highest indicating the high demands for balance and control. While the ARS was a demanding variation creating a relatively higher abduction moment compared to the other sub-types. Finally, the medial

rotation moment was the highest in ARS as predicted. Summarised below are the results referenced to each specific hypothesis:

1. Hip Hinge Squat (HHS)
 - I. The HHS will have moderate peak angles, forces and moments compared to the other sub-types of squats – **Accepted**.
2. Bosu Ball Squat (BOSU)
 - I. The BOSU will have higher muscle activation than HHS in all muscle groups.
3. Adductor Ring Squat (ARS)
 - I. ARS will have a lower Abduction angle than HHS, BOSU, ABS – **Accepted**.
 - II. ARS will have higher ADD activation than HHS – **Rejected**.
 - III. ARS will have a higher adduction and medial rotation moment than all other sub-types – **Accepted**.
4. Single Leg Squat (SLS):
 - I. SLS will have the lowest flexion and abduction angle – **Accepted**.
 - II. SLS will have the highest muscle activation in all hip muscles (TLF, GMED, GMAX, ADD, HAM, QUAD) - **Accepted** conditionally.
 - III. The SLS will have the highest joint compression and medial shear force as well as the highest extension and abduction moments and the lowest abduction - **Accepted** Conditionally.
5. Abductor Band Squat (ABS)
 - I. ABS will have higher GMAX activation than the HHS – **Accepted**.

The objective was to rank exercises for movement, load, and muscle activation to guide prescription. The data supports the notion that clinicians can preferentially activate lateral hip abductors when performing single leg squats justifying its consideration for those patients requiring a preferential hip abduction activation strategy. However, the resultant higher levels of joint loads may be contraindicated for some. Reviewing the influence of squat type on spine load suggests some consideration for biological relevance. The higher demands of a SLS on the spine versus the comparisons might have relevant contraindication in some clinical sub-sets. When examine loading patterns across all sub-types the HHS and ABS versions were often ranked lower (although only trends) this could have biological significance. Both of these techniques are taught to patients with back pain in order to reduce symptoms of low back pain associated with ADLs, such as, getting in or out of a chair. In this population the biological relevance of a 50% less lateral bend moment (or more in some clusters of the population) may make the difference in whether pain is triggered – or not. Statistical significance matters little to the patient struggling to tune the technique to eliminate pain. Thus, providing clinicians with this robust analysis of motions, motor patterns, and loads may facilitate higher efficacy with improved guidance for clinical decision making.

This study is not without limitation. The sample size is small with many comparisons with is consideration when examining the results. However, this type of detailed analysis is extensive and extremely costly with respect to time and resources. The population studied was healthy young males. Extrapolating to the capabilities of all patient populations may be difficult. However, this is the first step towards a broadly described atlas of motion, activation patterns

and joint loads – more specific details on patient populations can be updated in the future to enhance the application of this work to a wider distribution of patients and conditions.

The hip rehab atlas will develop in time as other look up Tables for rehabilitation exercises have, for example in the spine (McGill 2016). This author is not aware of any other comprehensive work that offers detailed description of motions, postures, and loads in one resource. Several studies have reported isolated motor patterns during hip rehabilitation but lack description of joint and muscle demands. In conclusion, success in progressing rehabilitation exercises require an understanding of tolerance and ensuring the dose of demands is below this biological tipping point. This data offers guidance to the clinician to arrange tolerable progressions of exercise. Future work will expand the atlas for usage with different patients, and different protocols considering goals such as enhancing strength, or endurance, or motor control, to name a few. This long-term goal is to enhance precision medicine, with precision assessment and precision intervention for more effective rehabilitation practices in a patient centered, individualised medicine framework.

7.0 Global Discussion of the Thesis: Hip-Spine Mechanics

This thesis addressed the gap in the current knowledge of the relationships between hip and spine mechanics aided with the development of an anatomically detailed, biologically driven, HSM. The range of investigation included a continuum from injury mechanisms to rehabilitation through to elements of performance enhancement. An examination of passive hip stiffness revealed differences between males and females, particularly in neutral zone characteristics and end-range of motion was discovered. The model predicted the behaviour of male passive hip stiffness when compared to experimental data with reasonably good success. Examining the mechanisms underlying ACL injury risk in females revealed that hip and spine variables differed in motion and motor patterns between the DKV groups. The differences in DKV provide insight into injury risk and patterns associated with injurious movement behaviours through the linkage. Finally, the issue of selecting appropriate rehabilitation exercises was assisted with an examination of neuromuscular, kinematic and kinetic patterns and their consequences. The model development enabled the probing of several issues that recognized individual differences are important and that addressing them will lead to enhanced MSK assessment and treatment outcomes.

The development of the unique HSM, sensitive to individual movement and motor control strategies was important and essential to enhance understanding of the interactions between hip and spine function. No longer can one expect to understand the function of the spine in isolation. Several important contributions were made in this section of the thesis. By simply adding the models together the enhanced anatomical function of the psoas major is now achievable since this muscle cross and interacts with both joints. The model is the first to add

ligaments to hip modeling joint loads. This is an important step for mapping stress distributions accurately across passive and active components of the joint. In addition, the model has been tested and validated with experimental passive angle-motion data to provide confidence in the model performance. Geodesics were also added to the model to provide more accurate model predictions at the full range of motion – as previous models were only tested in limited range tasks like walking. Similarly, muscle parameters (rest length) were improved to deal with muscle length changes throughout the range of motion. These were major enhancements to the current model from previous versions as this model can now accurately estimate 3D joint kinetics through a full range of flexion-extension and adduction-abduction ROM. Moreover, the model was used with subject data and in the process of using the model it is validated through verification initially with comparisons with a linked segment model and then tuned to match the RVC to enhance model output accuracy. This process of evaluating the gain provides reassurance that the model is sufficiently accurate in estimating joint load as the desired gain is 1.0 the closer the gain to 1.0 the more confidence in the ability of the model to represent the individual's anatomy, with mean gains between 0.82 and 1.14 across all three joints (spine, and right and left hip) for both males and females. Therefore, the conclusion can be made that the HSM performed very well for the majority of subjects, both males and females. These contributions and modelling enhancements are significant advancements and contributions directly resulting from this work.

Looking towards the future the ground is now prepared to investigate issues with gender and ethnicity (and other potential sub-groups) that influence differential rates of orthopaedic disease and injury. Eventually, the development of scaling factors for the model state variables and will enhance predictions and provide insights into patterns of dysfunction that cluster groups

of people, and specific sports, and specific occupations. For example, the examination of hip and spine function in search for mechanisms which assist in the understanding of ACL injury risk revealed a number of statistically and biologically significant factors that dichotomised knee valgus groups. This knowledge will lead to the development of more precise intervention strategies and rehabilitation approaches to address these mechanisms which contribute to ACL injury risk. Finally, analysis utilizing the HSM to assess variables linked with exercise technique highlighted the importance in being sensitive to individual differences and movement strategies. People are different. Their injury patterns form clusters around their mechanics. This thesis has appreciation for the notion that precise prescription of exercise progressions is justifiable once the individual differences are recognised.

More work in the future is needed to refine many assumptions in the model. However, the model had given some direction as to where the efforts need to be directed. Creating passive stiffness tuning to the individual, adding muscle and joint stiffness predictions, and even accounting for asymmetries identified in a clinical examination to model parameters would enhance the adaptability of the model to a wider range of individuals. Not to mention an option for a virtual female pelvis with all the associated anatomy. These advancements will develop in time with more access to these base parameters and the pursuit of experimental data to support the further development and refinement of the model.

The contributions from the three, primarily experimental, studies are significant and worth mentioning in some detail. The passive angle-moment study was the first attempt to evaluate bi-planar passive motion at the hip in vivo and it was done in males and females. Normative data

now exists for passive ROM and this data has been used to validate the current modelling approach. Next, the ACL injury mechanism study was a major step forward to reveal mechanisms behind the differences in DKV among females who are at risk for ACL injuries. Identifying the motor patterns and resulting EMG driven force profiles which differentiate HVG and LVG has the potential to lead to more precise interventions and control strategies to prevent injury and enhance performance. Finally, the evaluation of rehabilitation strategy and the modification of exercises will lead to the enhancement and refinement of exercise prescription leading to the development of more individualised care for improved patient outcomes. All of these contributions are highlighted by the ability to capture new information from the utilization of the newly developed HSM. The model pulls together movement, neural control, and posture while estimated the resulting joint loads providing an enhanced understanding of the function or disfunction of the system for the first time all at once.

In conclusion, the development of the model and respective themes of this study support the notion that individualised medicine for MSK disorders, specifically those related to the hip and spine, is not only possible but a worthwhile pursuit. Directing interventions to the mechanism of injury through matched intervention strategies form rehabilitation beyond recovery and on to performance is the overarching goal of this work. This will goal will lead to the improvement in precision medicine for hip and spine disorders.

References

- Al-Eisa, E. et al., 2006. Effects of Pelvic Skeletal Asymmetry on Trunk Movement. *Spine*, 31(3), pp.71–79.
- Anderson, A.E., Ellis, B.J. & Weiss, J. a, 2007. Verification, validation and sensitivity studies in computational biomechanics. *Computer methods in biomechanics and biomedical engineering*, 10(3), pp.171–84. Available at: <http://www.pubmedcentral.nih.gov/articlerender.fcgi?artid=3361760&tool=pmcentrez&endertype=abstract> [Accessed May 21, 2013].
- Andersson, G.B., Ortengren, R. & Schultz, a, 1980. Analysis and measurement of the loads on the lumbar spine during work at a table. *Journal of biomechanics*, 13(6), pp.513–20. Available at: <http://www.ncbi.nlm.nih.gov/pubmed/7400179>.
- Andersson, G.B.J., 1983. Loads on the Lumbar Spine: In vivo Measurements and Biomechanical Analysis. In D. A. Winter et al., eds. *Biomechanics*. Champaign, Illinois: Human Kinetics.
- Arab, A.M. et al., 2011. Altered muscular activation during prone hip extension in women with and without low back pain. *Chiropractic & manual therapies*, 19(1), p.18. Available at: <http://www.ncbi.nlm.nih.gov/pubmed/21838925> [Accessed August 23, 2011].
- Arab, A.M. & Nourbakhsh, M.R., 2010. The relationship between hip abductor muscle strength and iliotibial band tightness in individuals with low back pain. *Chiropractic & osteopathy*, 18, p.1. Available at: <http://www.pubmedcentral.nih.gov/articlerender.fcgi?artid=2821316&tool=pmcentrez&endertype=abstract>.
- Araújo, V.L. et al., 2013. Characterization of hip passive stiffness of volleyball, basketball and futsal young athletes. *Physical Therapy in Sport*, 14(4), pp.227–231. Available at: <http://dx.doi.org/10.1016/j.ptsp.2012.10.002>.
- Arendt, E. & Dick, R., 1995. Knee Injury Patterns Among Men and Women in Collegiate Basketball and Soccer: NCAA Data and Review of Literature. *The American Journal of Sports Medicine*, 23(6), pp.694–701.
- Arendt, E.A., Agel, J. & Dick, R., 1999. Anterior Cruciate Ligament Injury Patterns Among Collegiate Men and Women. , 34(2), pp.86–92.
- van Arkel, R.J., Amis, A.A. & Jeffers, J.R.T., 2015. The envelope of passive motion allowed by the capsular ligaments of the hip. *Journal of Biomechanics*, 48(14), pp.3803–3809. Available at: <http://dx.doi.org/10.1016/j.jbiomech.2015.09.002>.
- Arnold, A. et al., 2000. Accuracy of Muscle Moment Arms Estimated from MRI-Based Musculoskeletal Models of the Lower Extremity. *Computer Aided Surgery*, 5, pp.108–119.
- Arnold, E.M. et al., 2010. A model of the lower limb for analysis of human movement. *Annals of biomedical engineering*, 38(2), pp.269–79. Available at: <http://www.pubmedcentral.nih.gov/articlerender.fcgi?artid=2903973&tool=pmcentrez&endertype=abstract> [Accessed November 5, 2012].

- Arokoski, J. et al., 1999. Back and Hip Extensor Muscle Function During Therapeutic Exercises. *Arch Phys Med Rehabil*, 80(July), pp.842–850.
- Aronld, E.M. et al., 2010. A Model of the Lower Limb for Analysis of Human Movement. *Annals of Biomedical Engineering*, 38(2), pp.269–279.
- Bahler, A.S., 1968. Modeling of Mammalian Skeletal Muscle. *IEEE transactions on bio-medical engineering*, 15(4), pp.249–57.
- Barash, H.L., Galante, J.O. & Lambert, C.N., 1970. Spondylolisthesis and Tight Hamstrings. *The Journal of Bone and Joint Surgery*, 52–A(7), pp.1319–28.
- Barrett, J.M. & Callaghan, J.P., 2018. A procedure for determining parameters of a simplified ligament model. *Journal of Biomechanics*, 66, pp.175–179. Available at: <https://doi.org/10.1016/j.jbiomech.2017.10.037>.
- Bell, a. L., Pedersen, D.R. & Brand, R. a., 1990. A Comparison of the Accuracy of Several Hip Center. *J Biomech*, 23(November), pp.6–8.
- Ben-Galim, P. et al., 2007. Hip-spine syndrome: the effect of total hip replacement surgery on low back pain in severe osteoarthritis of the hip. *Spine*, 32(19), pp.2099–102. Available at: <http://www.ncbi.nlm.nih.gov/pubmed/17762811>.
- Bergmark, A., 1989. Stability of the lumbar spine. *Acta Orthopaedica*, 60(s230), pp.1–54. Available at: <http://informahealthcare.com/doi/abs/10.3109/17453678909154177>.
- Blemker, S.S. & Delp, S.L., 2005. Three-Dimensional Representation of Complex Muscle Architectures and Geometries. *Annals of biomedical engineering*, 33(5), pp.661–673. Available at: <http://link.springer.com/10.1007/s10439-005-7385-0> <http://www.ncbi.nlm.nih.gov/pubmed/1614337>.
- Bolgia, L.A. & Uhl, T.L., 2005. Electromyographic Analysis of Hip Rehabilitation Exercises in a Group of Healthy Subjects. *Journal of Orthopaedic & Sports Physical Therapy*, 35, pp.487–494.
- Bonneau, N., Gagey, O. & Tardieu, C., 2012. Biomechanics of the human hip joint. *Computer Methods in Biomechanics and Biomedical Engineering*, 15(S1).
- Brand, R. a et al., 1982. A model of lower extremity muscular anatomy. *Journal of biomechanical engineering*, 104(4), pp.304–10. Available at: <http://www.ncbi.nlm.nih.gov/pubmed/7154650>.
- Brand, R. a et al., 1994. Comparison of hip force calculations and measurements in the same patient. *The Journal of arthroplasty*, 9(1), pp.45–51. Available at: <http://www.ncbi.nlm.nih.gov/pubmed/8163975>.
- Bresler, E. & Frankel, J.B., 1950. The forces and moments in the leg during level walking. *Journal of Applied Mechanics*, 72, pp.27–36.
- Brown, J.M.M. et al., 2007. Muscles within muscles: Coordination of 19 muscle segments within three shoulder muscles during isometric motor tasks. *Journal of electromyography and*

- kinesiology* : official journal of the International Society of Electrophysiological Kinesiology, 17(1), pp.57–73. Available at: <http://www.ncbi.nlm.nih.gov/pubmed/16458022> [Accessed July 23, 2011].
- Brown, S.H. & Gerling, M.E., 2012. Importance of sarcomere length when determining muscle physiological cross-sectional area: A spine example. *Proceedings of the Institution of Mechanical Engineers, Part H: Journal of Engineering in Medicine*, 226(5), pp.384–388. Available at: <http://pih.sagepub.com/lookup/doi/10.1177/0954411912441325> [Accessed June 24, 2013].
- Brown, S.H.M. & McGill, S.M., 2005. Muscle force-stiffness characteristics influence joint stability: a spine example. *Clinical biomechanics (Bristol, Avon)*, 20(9), pp.917–22. Available at: <http://www.ncbi.nlm.nih.gov/pubmed/16055250>.
- Bruno, P.A. & Bagust, J., 2006. An investigation into the within-subject and between-subject consistency of motor patterns used during prone hip extension in subjects without low back pain §. *Writing*.
- Buchanan, T.S. et al., 2004. Neuromusculoskeletal Modeling : Estimation of Muscle Forces and Joint Moments and Movements From Measurements of Neural Command. *Biomedical Engineering*, pp.367–395.
- Bullock-Saxton, J., Janda, V. & Bullock, M., 1993. Reflex activation of gluteal muscles in walking. *Spine*, 18(6), pp.704–708.
- Callaghan, J.P., Patla, A.E. & McGill, S.M., 1999. Low back three-dimensional joint forces , kinematics , and kinetics during walking. *Data Processing*, 14, pp.203–216.
- Cambridge, E.D.J. et al., 2012. Progressive hip rehabilitation: the effects of resistance band placement on gluteal activation during two common exercises. *Clinical biomechanics (Bristol, Avon)*, 27(7), pp.719–24. Available at: <http://www.ncbi.nlm.nih.gov/pubmed/22464817> [Accessed May 22, 2013].
- Cassidy, J.D., Carroll, L. & Cote, P., 1998. The Saskatchewan health and back pain survey. The prevalence of low back pain and related disability in Saskatchewan adults. *Spine*, 23(17), pp.1860–7.
- Cavagna, G.A., Saibene, F.P. & Margaria, R., 1964. Mechanical work in running. *Journal of Applied Physiology*, 19(2), pp.249–56.
- Chaffin, D.B., 1969. A computerized biomechanical model-development of and use in studying gross body actions. *Journal of biomechanics*, 2(4), pp.429–41. Available at: <http://www.ncbi.nlm.nih.gov/pubmed/16335142>.
- Chapman, A.E. & Harrower, P.T., 1977. Linear approximation of muscle mechanics in isometric contraction. *Biological Cybernetics*, 27(1), pp.1–7.
- Cholewicki, J. & McGill, S.M., 1994. EMG assisted optimization: A hybrid approach for estimating muscle forces in an indeterminate biomechanical model. *Journal of Biomechanics*, 27(10), pp.1287–89.

- Cholewicki, J. & McGill, S.M., 1996. Mechanical stability of the in vivo lumbar spine: implications for injury and chronic low back pain. *Clinical Biomechanics*, 11(1), pp.1–15.
- Cholewicki, J. & McGill, S.M., 1996. Mechanical stability of the in vivo lumbar spine: implications for injury and chronic low back pain. *Clinical biomechanics*, 11(1), pp.1–15.
- Cholewicki, J., McGill, S.M. & Norman, R.W., 1995. Comparison of muscle forces and joint load from an optimization and EMG assisted lumbar spine model: Towards development of a hybrid approach. *Journal of Biomechanics*, 28(3), pp.321–331.
- Clark, T. & Hawkins, D., 2010. Are fixed limb inertial models valid for dynamic simulations of human movement? *Journal of biomechanics*, 43(14), pp.2695–701. Available at: <http://www.ncbi.nlm.nih.gov/pubmed/20673667> [Accessed November 21, 2012].
- Cools, A.M. et al., 2007. Rehabilitation of Scapular Muscle Balance Which Exercises to Prescribe ? *American Journal of Sports Medicine*, 35(10), pp.1744–1751.
- Cools, A.M. et al., 2002. Scapular Muscle Recruitment Pattern : Electromyographic Response of the Trapezius Muscle to Sudden Shoulder. *Journal of Orthopaedic & Sports Physical Therapy*, 32(5), pp.221–229.
- Cools, A.M. et al., 2003. The American Journal of Sports Medicine Scapular Muscle Recruitment Patterns : Trapezius Muscle Latency with and without. *Sports Medicine*, 31(4).
- Cote, P., Cassidy, J.D. & Carroll, L., 1998. The Saskatchewan Health and Back Pain Survey. The prevalence of neck pain and related disability in Saskatchewan adults. *Spine*, 23(15), pp.1689–98.
- Crowninshield, R.D. et al., 1978. A biomechanical investigation of the human hip. *Journal of biomechanics*, 11(1–2), pp.75–85. Available at: <http://www.ncbi.nlm.nih.gov/pubmed/22519928>.
- Dagenais, S., Caro, J. & Haldeman, S., 2008. A systematic review of low back pain cost of illness studies in the United States and internationally. *Internal Medicine*, 8, pp.8–20.
- Davis, K.E. et al., 2007. The Importance of Range of Motion after Total Hip Arthroplasty. , 1246(465), pp.180–184.
- Delleman, N.J. & Drost, M.R., 1992. Lecture Value of biomechanical macromodels as suitable tools for the prevention of work-related low back problems. *Clinical Biomechanics*, 7, pp.138–148.
- Delp, S.L. et al., 1990. An Interactiv Gaphics-Based Model of the Lower Extremity to Study Orthopaedic Surgical Procedures. *IEEE Transactions on Biomedical Engineering*, 37(8), pp.757–67.
- Delp, S.L. et al., 2007. OpenSim: open-source software to create and analyze dynamic simulations of movement. *IEEE transactions on bio-medical engineering*, 54(11), pp.1940–50. Available at: <http://www.ncbi.nlm.nih.gov/pubmed/18018689>.
- Delp, S.L. & Maloney, W., 1993. Effects of hip center location on the moment-generating

- capacity of the muscles. *Journal of biomechanics*, 26(4–5), pp.485–99. Available at: <http://www.ncbi.nlm.nih.gov/pubmed/8478351>.
- Deyo, R.A., Mirza, S.K. & Martin, B.I., 2006. Back Pain Prevalence and Visit Rates. *Spine*, 31(23), pp.2724–2727.
- Van Dillen, L.R. et al., 2008. Hip Rotation Range of Motion in People with and without Low Back Pain Who Participate in Rotation-Related Sports. *Physical Therapy in Sport*, 9(2), pp.72–81.
- Van Dillen, L.R., Maluf, K.S. & Sahrman, S. a, 2009. Further examination of modifying patient-preferred movement and alignment strategies in patients with low back pain during symptomatic tests. *Manual therapy*, 14(1), pp.52–60. Available at: <http://www.pubmedcentral.nih.gov/articlerender.fcgi?artid=2659590&tool=pmcentrez&rendertype=abstract> [Accessed July 17, 2012].
- Dillen, L.R. Van, Maluf, K.S. & Sahrman, S.A., 2007. Further examination of modifying patient-preferred movement and alignment strategies in patients with low back pain during symptomatic tests \$. *Manual Therapy*, (2).
- Distefano, L.J. et al., 2009. Gluteal muscle activation during common therapeutic exercises. *The Journal of orthopaedic and sports physical therapy*, 39(7), pp.532–40. Available at: <http://www.ncbi.nlm.nih.gov/pubmed/19574661>.
- Dostal, W.F. & Andrews, J.G., 1981. A Three-dimensional biomechanical model of the hip musculature. *Journal of Biomechanics*, 14(11), pp.803–812.
- Dostal, W.F. & Andrews, J.G., 1981. A three-dimensional biomechanical model of the hip musculature. *Journal of Biomechanics*, 14(11), pp.803–812.
- Dreyfuss, H., 1966. *Anthropometric data: Standing 50thile American Adult Male*. Whitney Library of Design, New York.
- Ellison, J.B., Rose, S.J. & Sahrman, S. a, 1990. Patterns of hip rotation range of motion: a comparison between healthy subjects and patients with low back pain. *Physical therapy*, 70(9), pp.537–41. Available at: <http://www.ncbi.nlm.nih.gov/pubmed/2144050>.
- Ellison, J.B., Rose, S.J. & Sahrman, S.A., 1990. Patterns of Hip Rotation Range of Motion: A Comparison Between Healthy Subjects and Patients with Low Back Pain. *Physical therapy*, 70(9).
- English, a W., Wolf, S.L. & Segal, R.L., 1993. Compartmentalization of muscles and their motor nuclei: the partitioning hypothesis. *Physical therapy*, 73(12), pp.857–67. Available at: <http://www.ncbi.nlm.nih.gov/pubmed/8248294>.
- Erdemir, A. et al., 2007. Model-based estimation of muscle forces exerted during movements. *Clinical biomechanics*, 22, pp.131–154.
- Ford, K.R., Myer, G.D. & Hewett, T.E., 2000. Valgus Knee Motion during Landing in High School Female and Male Basketball Players. *Medicine & Science in Sports & Exercise*, 35(10), pp.1745–1750.

- Freeman, S., Mascia, A. & McGill, S., 2013. Arthroгенic neuromusculature inhibition: a foundational investigation of existence in the hip joint. *Clinical biomechanics (Bristol, Avon)*, 28(2), pp.171–7. Available at: <http://www.ncbi.nlm.nih.gov/pubmed/23261019> [Accessed June 4, 2013].
- Gagnon, D., Larivière, C. & Loisel, P., 2001. Comparative ability of EMG, optimization, and hybrid modelling approaches to predict trunk muscle forces and lumbar spine loading during dynamic sagittal plane lifting. *Clinical biomechanics (Bristol, Avon)*, 16(5), pp.359–72. Available at: <http://www.ncbi.nlm.nih.gov/pubmed/11390042>.
- Garrick, J.G. & Requa, R.K., 1993. Ballet injuries. An analysis of epidemiology and financial outcome. *The American journal of sports medicine*, 21(4), pp.586–90. Available at: <http://www.ncbi.nlm.nih.gov/pubmed/8368421>.
- Gianotti, S.M. et al., 2009. Incidence of anterior cruciate ligament injury and other knee ligament injuries : A national population-based study. *Journal of Science and Medicine in Sport*, 12, pp.622–627.
- Gombatto, S.P. et al., 2007. Patterns of lumbar region movement during trunk lateral bending in 2 subgroups of people with low back pain. *Physical therapy*, 87(4), pp.441–54. Available at: <http://www.ncbi.nlm.nih.gov/pubmed/17374634> [Accessed July 17, 2012].
- Gordon, B.Y.A.M., Huxley, A.F. & Julian, F.J., 1966. The variation in isometric tenon with sarcomere length in vertebrate muscle fibers. *Journal of Physiology*, 184, pp.170–192.
- Graven-Nielsen, T., 2006. Fundamentals of muscle pain, referred pain, and deep tissue hyperalgesia. *Scandinavian journal of rheumatology.*, 122(Suppl 122), pp.1–43. Available at: <http://www.ncbi.nlm.nih.gov/pubmed/16997767> [Accessed June 16, 2013].
- Graven-Nielsen, T., Svensson, P. & Arendt-Nielsen, L., 1997. Effects of experimental muscle pain on muscle activity and co-ordination during static and dynamic motor function. *Electroencephalography and clinical neurophysiology*, 105(2), pp.156–64.
- Green, J.P., Grenier, S.G. & McGill, S.M., 2002. Low-back stiffness is altered with warm-up and bench rest : implications for athletes. *Medicine & Science in Sports*, 34(7), pp.1076–81.
- Grenier, S.G. & McGill, S.M., 2007. Quantification of lumbar stability using two different abdominal activation strategies. *Arch Phys Med Rehabil*, 88, pp.54–62.
- Grenier, S.G. & McGill, S.M., 2007. Quantification of lumbar stability by using 2 different abdominal activation strategies. *Archives of physical medicine and rehabilitation*, 88(1), pp.54–62. Available at: <http://www.ncbi.nlm.nih.gov/pubmed/17207676>.
- Guimaraes, a C. et al., 1994. Effects of muscle length on the EMG-force relationship of the cat soleus muscle studied using non-periodic stimulation of ventral root filaments. *The Journal of experimental biology*, 193, pp.49–64. Available at: <http://www.ncbi.nlm.nih.gov/pubmed/7964399>.
- Haugstad, G.K. et al., 2006. Posture, movement patterns, and body awareness in women with chronic pelvic pain. *Journal of psychosomatic research*, 61(5), pp.637–44. Available at:

- <http://www.ncbi.nlm.nih.gov/pubmed/17084141> [Accessed July 17, 2012].
- Van der Helm, F.C. & Veenbaas, R., 1991. Modelling the mechanical effect of muscles with large attachment sites: application to the shoulder mechanism. *Journal of biomechanics*, 24(12), pp.1151–63. Available at: <http://www.ncbi.nlm.nih.gov/pubmed/1769980>.
- Henninger, H.B. et al., 2010. Validation of computational models in biomechanics. *Proceedings of the Institution of Mechanical Engineers, Part H: Journal of Engineering in Medicine*, 224(7), pp.801–812. Available at: <http://pih.sagepub.com/lookup/doi/10.1243/09544119JEIM649> [Accessed May 30, 2013].
- Hewett, T.E. et al., 2005. Biomechanical measures of neuromuscular control and valgus loading of the knee predict anterior cruciate ligament injury risk in female athletes: a prospective study. *The American journal of sports medicine*, 33(4), pp.492–501. Available at: <http://www.ncbi.nlm.nih.gov/pubmed/15722287> [Accessed March 22, 2012].
- Hewett, T.E. et al., 2010. Invited Clinical Commentary - Understanding and preventing ACL injuries: Considerations - Update 2010 correspondence. *North American Journal of Sports Therapy*, 5(4), pp.234–251.
- Hewett, T.E. et al., 2016. Utilization of ACL Injury Biomechanical and Neuromuscular Risk Profile Analysis to Determine the Effectiveness of Neuromuscular Training. *The American Journal of Sports Medicine*, pp.3146–3151. Available at: <http://www.ncbi.nlm.nih.gov/pubmed/27474385> <http://ajs.sagepub.com/lookup/doi/10.1177/0363546516656373>.
- Hewett, T.E., Ford, K.R. & Myer, G.D., 2006. Anterior cruciate ligament injuries in female athletes: Part 2, a meta-analysis of neuromuscular interventions aimed at injury prevention. *The American journal of sports medicine*, 34(3), pp.490–8. Available at: <http://www.ncbi.nlm.nih.gov/pubmed/16382007>.
- Hewett, T.E. & Myer, G.D., 2011. The mechanistic connection between the trunk, hip, knee, and anterior cruciate ligament injury. *Exercise and sport sciences reviews*, 39(4), pp.161–6. Available at: <http://www.ncbi.nlm.nih.gov/pubmed/21799427>.
- Hewett, T.E., Myer, G.D. & Ford, K.R., 2006a. Anterior cruciate ligament injuries in female athletes: Part 1, mechanisms and risk factors. *The American journal of sports medicine*, 34(2), pp.299–311. Available at: <http://www.ncbi.nlm.nih.gov/pubmed/16423913> [Accessed March 6, 2012].
- Hewett, T.E., Myer, G.D. & Ford, K.R., 2006b. Anterior cruciate ligament injuries in female athletes: Part 1, mechanisms and risk factors. *The American journal of sports medicine*, 34(2), pp.299–311. Available at: <http://www.ncbi.nlm.nih.gov/pubmed/16423913>.
- Hewett, T.E., Myer, G.D. & Ford, K.R., 2004. Decrease in neuromuscular control about the knee with maturation in female athletes. *The Journal of bone and joint surgery. American volume*, 86–A(8), pp.1601–8. Available at: <http://www.ncbi.nlm.nih.gov/pubmed/15292405>.

- Hewett, T.E., Myer, G.D. & Ford, K.R., 2004. Decrease in Neuromuscular Control About the Knee with Maturation in Female Athletes. *The Journal of Bone*, 86–A(8), pp.1601–8.
- Hewitt, J.D. et al., 2002. The mechanical properties of the human hip capsule ligaments. *Journal of Arthroplasty*, 17(1), pp.82–89.
- Hill, A. V., 1938. The Heat of Shortening and the Dynamic Constants of Muscle. *Proceedings of the Royal Society B: Biological Sciences*, 126(843), pp.136–195.
- Hof, A.L., 1984. EMG and muscle force: An introduction. *Human Movement Science*, 3, pp.119–153.
- Hof, A.L. & van den Berg, J., 1977. Linearity between the weighted sum of the EMGs of the human triceps surae and the total torque. *Journal of biomechanics*, 10(9), pp.529–39. Available at: <http://www.ncbi.nlm.nih.gov/pubmed/914876>.
- Hof, A.L. & Van den Berg, J., 1981a. EMG to Force Processing I: An Electrical Analogue of the Hill Muscle Model. *Journal of Biomechanics*, 14(11), pp.747–758.
- Hof, A.L. & Van den Berg, J., 1981b. EMG to force processing II: Estimation of parameters of the Hill muscle model for the human triceps surae by means of a calfergometer. *Journal of biomechanics*, 14(11), pp.759–70. Available at: <http://www.ncbi.nlm.nih.gov/pubmed/7334036>.
- Hof, A.L. & Van den Berg, J., 1981c. EMG to force processing III: Estimation of model parameters for the human triceps surae muscle and assessment of the accuracy by means of a torque plate. *Journal of biomechanics*, 14(11), pp.771–85. Available at: <http://www.ncbi.nlm.nih.gov/pubmed/7334037>.
- Hof, A.L. & Van den Berg, J., 1981d. EMG to force processing IV: Eccentric-concentric contractions on a spring-flywheel set up. *Journal of biomechanics*, 14(11), pp.787–92. Available at: <http://www.ncbi.nlm.nih.gov/pubmed/7334038>.
- Hoffman, S.L. et al., 2011. Effect of classification-specific treatment on lumbopelvic motion during hip rotation in people with low back pain. *Manual therapy*, 16(4), pp.344–50. Available at: <http://www.ncbi.nlm.nih.gov/pubmed/21256073> [Accessed July 17, 2012].
- Holtermann, a et al., 2009. Selective activation of neuromuscular compartments within the human trapezius muscle. *Journal of electromyography and kinesiology : official journal of the International Society of Electrophysiological Kinesiology*, 19(5), pp.896–902. Available at: <http://www.ncbi.nlm.nih.gov/pubmed/18585928> [Accessed July 23, 2011].
- Holtermann, a et al., 2010. The use of EMG biofeedback for learning of selective activation of intra-muscular parts within the serratus anterior muscle: a novel approach for rehabilitation of scapular muscle imbalance. *Journal of electromyography and kinesiology : official journal of the International Society of Electrophysiological Kinesiology*, 20(2), pp.359–65. Available at: <http://www.ncbi.nlm.nih.gov/pubmed/19342256> [Accessed September 2, 2011].
- Hootman, J.M., Dick, R. & Agel, J., 2007. Epidemiology of Collegiate Injuries for 15 Sports:

- Prevention and Recommendations for Injury Prevention Initiatives. *Journal of Athletic Training*, 42(2), pp.311–319.
- Horsman, K.M.D. et al., 2007. Morphological muscle and joint parameters for musculoskeletal modelling of the lower extremity. *Clinical biomechanics (Bristol, Avon)*, 22(2), pp.239–47. Available at: <http://www.ncbi.nlm.nih.gov/pubmed/17134801> [Accessed November 1, 2012].
- Howarth, S.J. & Callaghan, J.P., 2009. The rule of 1 s for padding kinematic data prior to digital filtering : Influence of sampling and filter cutoff frequencies. *Journal of Electromyography and Kinesiology*, 19(5), pp.875–881. Available at: <http://dx.doi.org/10.1016/j.jelekin.2008.03.010>.
- Hungerford, B., Gilleard, W. & Hodges, P., 2003. Evidence of altered lumbopelvic muscle recruitment in the presence of sacroiliac joint pain. *Spine*, 28(14), pp.1593–600. Available at: <http://www.ncbi.nlm.nih.gov/pubmed/12865851>.
- Ikeda, D.M. & McGill, S.M., 2012. Can Altering Motions, Postures, and Loads Provide Immediate Low Back Pain Relief. , 37(23), pp.1469–1475.
- Ikeda, D.M. & McGill, S.M., 2012. Can altering motions, postures, and loads provide immediate low back pain relief: a study of 4 cases investigating spine load, posture, and stability. *Spine*, 37(23), pp.E1469-75. Available at: <http://www.ncbi.nlm.nih.gov/pubmed/22872216> [Accessed October 29, 2012].
- Jacobs, C. a et al., 2009. Electromyographic analysis of hip abductor exercises performed by a sample of total hip arthroplasty patients. *The Journal of arthroplasty*, 24(7), pp.1130–6. Available at: <http://www.ncbi.nlm.nih.gov/pubmed/18757169> [Accessed October 18, 2010].
- Jensen, R.H. & Davy, D.T., 1975. An investigation of muscle lines of action about the hip: a centroid line approach vs the straight line approach. *Journal of biomechanics*, 8(2), pp.103–10. Available at: <http://www.ncbi.nlm.nih.gov/pubmed/1150676>.
- Johnson, G.R. et al., 1996. Modelling the muscles of the scapula morphometric and coordinate data and functional implications. *Journal of biomechanics*, 29(8), pp.1039–51. Available at: <http://www.ncbi.nlm.nih.gov/pubmed/8817371>.
- Jones, E.J. et al., 2008. Cross-sectional area and muscular strength: A brief review. *Sports Medicine*, 38(12), pp.987–994.
- Kankaanpää, M. et al., 1998. Back and hip extensor fatigability in chronic low back pain patients and controls. *Archives of physical medicine and rehabilitation*, 79(4), pp.412–7. Available at: <http://www.ncbi.nlm.nih.gov/pubmed/9552107>.
- Kavicic, N., Grenier, S. & McGill, S.M., 2004a. Determining the Stabilizing Role of Individual Torso Muscles During Rehabilitation Exercises. *Spine*, 29(11), pp.1254–1265.
- Kavicic, N., Grenier, S. & McGill, S.M., 2004b. Quantifying Tissue Loads and Spine Stability While Performing Commonly Prescribed Low Back Stabilization Exercises. *Spine*, 29(20), pp.2319–

2329.

- Khalil, T. et al., 1992. Stretching in the rehabilitation of low-back pain patients. *Spine*, 17(3), pp.311–7.
- Khan, T. et al., 2018. ACL and meniscal injuries increase the risk of primary total knee replacement for osteoarthritis : a matched case – control study using the Clinical Practice Research Datalink (CPRD). *British journal of sports medicine*, pp.1–5.
- Klein Horsman, M.D. et al., 2007. Morphological muscle and joint parameters for musculoskeletal modelling of the lower extremity. *Clinical biomechanics (Bristol, Avon)*, 22(2), pp.239–47. Available at: <http://www.ncbi.nlm.nih.gov/pubmed/17134801> [Accessed May 26, 2013].
- Krause, D. et al., 2009. Electromyographic Analysis of the Gluteus Medius in Five Weight-Bearing Exercises. *Journal of Strength and Conditioning Research*, 23(9), pp.2689–94.
- Kujalal, U.M. et al., 1994. Baseline strength pain in a . dolescent athletes and nonathletes. *Scandinavian Journal of Medicine & Science in Sports*, 4(8), pp.200–5.
- Kumar, S., 2001. Theories of musculoskeletal injury causation. *Ergonomics*, 44(1), pp.17–47.
- Kurki, H.K., 2017. Bilateral Asymmetry in the Human Pelvis. *The Anatomical Record*, 300(September), pp.653–665.
- Lamoth, C.J.C. et al., 2002. Pelvis-thorax coordination in the transverse plane during walking in persons with nonspecific low back pain. *Spine*, 27(4), pp.E92-9. Available at: <http://www.ncbi.nlm.nih.gov/pubmed/11840116>.
- Larivi, C. & Gagnon, D., 1999. The L5 / S1 joint moment sensitivity to measurement errors in dynamic 3D multisegment lifting models. , 18, pp.573–587.
- Lee, B. & McGill, S., 2016. The effect of core training on distal limb performance during ballistic strike manoeuvres. *Journal of Sports Sciences*, 00(00), pp.1–13. Available at: <https://www.tandfonline.com/doi/full/10.1080/02640414.2016.1236207>.
- Lee, B. & McGill, S., 2015. The Effect of Long Term Isometric Training on Core/Torso Stiffness. *Journal of strength and conditioning research / National Strength & Conditioning Association*, 29(6), pp.1515–1526. Available at: <http://www.ncbi.nlm.nih.gov/pubmed/25807026>.
- Lee, R.Y.W. & Munn, J., 2000. Passive moment about the hip in straight leg raising. *Clinical Biomechanics*, 15(5), pp.330–334.
- Leinonen, V. et al., 2000. Back and hip extensor activities during trunk flexion/extension: effects of low back pain and rehabilitation. *Archives of physical medicine and rehabilitation*, 81(1), pp.32–7. Available at: <http://www.ncbi.nlm.nih.gov/pubmed/10638873>.
- Lenaerts, G. et al., 2008. Subject-specific hip geometry affects predicted hip joint contact forces during gait. *Journal of biomechanics*, 41(6), pp.1243–52. Available at: <http://www.ncbi.nlm.nih.gov/pubmed/18346745> [Accessed July 17, 2012].

- Lewis, C.L. & Sahrman, S. a, 2009. Muscle activation and movement patterns during prone hip extension exercise in women. *Journal of athletic training*, 44(3), pp.238–48. Available at: <http://www.ncbi.nlm.nih.gov/pubmed/19478835>.
- Lewis, C.L., Sahrman, S. a & Moran, D.W., 2007. Anterior hip joint force increases with hip extension, decreased gluteal force, or decreased iliopsoas force. *Journal of biomechanics*, 40(16), pp.3725–31. Available at: <http://www.pubmedcentral.nih.gov/articlerender.fcgi?artid=2580726&tool=pmcentrez&rendertype=abstract> [Accessed November 2, 2012].
- Lewis, C.L., Sahrman, S. a & Moran, D.W., 2010. Effect of hip angle on anterior hip joint force during gait. *Gait & posture*, 32(4), pp.603–7. Available at: <http://www.pubmedcentral.nih.gov/articlerender.fcgi?artid=3063362&tool=pmcentrez&rendertype=abstract> [Accessed July 17, 2012].
- Li, K. & Zhang, X., 2009. Can Relative Strength Between the Back and Knees Differentiate Lifting Strategy ? *Human Factors*, 51(6), pp.785–796.
- Lohmander, L.S. et al., 2004. High Prevalence of Knee Osteoarthritis , Pain , and Functional Limitations in Female Soccer Players Twelve Years After Anterior Cruciate Ligament Injury. *Arthritis and rheumatism*, 50(10), pp.3145–3152.
- de Looze, M.P., Kingma, I. & Bussmann, J.B.J., 1992. Validation of a dynamic linked segment model to calculate joint momemts in lifting. *Clinical biomechanics (Bristol, Avon)*, 7, pp.161–169.
- Lu, T.-W. & Chang, C.-F., 2012. Biomechanics of human movement and its clinical applications. *The Kaohsiung journal of medical sciences*, 28(2 Suppl), pp.S13-25. Available at: <http://www.ncbi.nlm.nih.gov/pubmed/22301008> [Accessed July 17, 2012].
- Lu, T.W. et al., 1998. Validation of a lower limb model with in vivo femoral forces telemetered from two subjects. *Journal of biomechanics*, 31(1), pp.63–9. Available at: <http://www.ncbi.nlm.nih.gov/pubmed/9596539>.
- Lubbe, N.V.A.N.D.E.R. et al., 2004. Comparison of Manual Therapy and Exercise Therapy in Osteoarthritis of the Hip : A Randomized Clinical Trial. *Rheumatology*, 51(5), pp.722–729.
- Lund, T. et al., 2002. Three-Dimensional Motion Patterns During Active Bending in Patients with Chronic Low Back Pain. , 27(17), pp.1865–1874.
- Luo, W., Stanhope, S.J. & Sheehan, F.T., 2009. Using two palpable measurements improves the subject-specific femoral modeling. *Journal of biomechanics*, 42(12), pp.2000–5. Available at: <http://www.pubmedcentral.nih.gov/articlerender.fcgi?artid=2727693&tool=pmcentrez&rendertype=abstract> [Accessed July 17, 2012].
- Luomajoki, H., Kool, J., Bruin, E.D. De, et al., 2008. Movement control tests of the low back ; evaluation of the difference between patients with low back pain and healthy controls. *BMC Musculoskeletal Disorders*, 12(Mc), pp.1–12.

- Luomajoki, H., Kool, J., de Bruin, E.D., et al., 2008. Movement control tests of the low back; evaluation of the difference between patients with low back pain and healthy controls. *BMC musculoskeletal disorders*, 9(Mc), p.170. Available at: <http://www.pubmedcentral.nih.gov/articlerender.fcgi?artid=2635372&tool=pmcentrez&rendertype=abstract> [Accessed July 17, 2012].
- Manchikanti, L. et al., 2009. Comprehensive review of epidemiology, scope, and impact of spinal pain. *Pain physician*, 12(4), pp.E35-70. Available at: <http://www.ncbi.nlm.nih.gov/pubmed/19668291>.
- Marras, W.S. & Sommerich, C.M., 1991a. A Three-dimensional motion model of loads on the lumbar spine: I. Model structure. *Human factors*, 33(2), pp.123–137.
- Marras, W.S. & Sommerich, C.M., 1991b. A three-dimensional motion model of loads on the lumbar spine: II. Model validation. *Human factors*, 33(2), pp.139–49. Available at: <http://www.ncbi.nlm.nih.gov/pubmed/1860701>.
- Marshall, P.W.M., Cashman, A. & Cheema, B.S., 2011. A randomized controlled trial for the effect of passive stretching on measures of hamstring extensibility, passive stiffness, strength, and stretch tolerance. *Journal of Science and Medicine in Sport*, 14(6), pp.535–540. Available at: <http://dx.doi.org/10.1016/j.jsams.2011.05.003>.
- Marshall, P.W.M., Patel, H. & Callaghan, J.P., 2011. Gluteus medius strength, endurance, and co-activation in the development of low back pain during prolonged standing. *Human movement science*, 30(1), pp.63–73. Available at: <http://www.ncbi.nlm.nih.gov/pubmed/21227522> [Accessed July 15, 2012].
- Matsuyama, Y. et al., 2004. Hip-spine syndrome: total sagittal alignment of the spine and clinical symptoms in patients with bilateral congenital hip dislocation. *Spine*, 29(21), pp.2432–7. Available at: <http://www.ncbi.nlm.nih.gov/pubmed/15507807>.
- McAndrew, D., Gorelick, M. & Brown, J.M.M., 2006. Muscles within muscles: A mechanomyographic analysis of muscle segment contractile properties within human gluteus maximus. *Journal of Musculoskeletal Research*, 10(1), pp.23–35.
- McCurdy, K. et al., 2010. Comparison of lower extremity EMG between the 2-leg squat and modified single-leg squat in female athletes. *Journal of sport rehabilitation*, 19(1), pp.57–70. Available at: <http://www.ncbi.nlm.nih.gov/pubmed/20231745>.
- McGill, S., Seguin, J. & Bennett, G., 1994. Passive stiffness of the lumbar torso in flexion, extension, lateral bending, and axial rotation: Effect of belt wearing and breath holding. *Spine*, 19(6), pp.696–704.
- McGill, S.M., 1998. Low back exercises : Evidence for improving exercise regimens. *Source*.
- McGill, S.M. et al., 2010. Evidence of a double peak in muscle activation to enhance strike speed and force: An example with elite mixed martial arts fighters. *Journal of Strength & Conditioning Research*, 24(216), pp.348–357.
- McGill, S.M., 2004. Linking latest knowledge of injury mechanisms and spine function to the

- prevention of low back disorders. *Journal of Electromyography and Kinesiology*, 14, pp.43–47.
- McGill, S.M., 2007. *Low Back Disorders: Evidence-Based Prevention and Rehabilitation* 2nd ed., Champaign, Illinois: Human Kinetics.
- McGill, S.M., 2001. Low Back Stability : From Formal Description to Issues for Performance and Rehabilitation.
- McGill, S.M. et al., 1994. Passive stiffness of the human neck in flexion, extension, and lateral bending. *Clinical Biomechanics*, 9(3), pp.193–198.
- McGill, S.M., 1997. The biomechanics of low back injury: Implications on current practice in industry and the clinic. *Journal of Biomechanics*, 30(5), pp.465–475.
- McGill, S.M. & Cholewicki, J., 2001. Biomechanical Basis for Stability : An Explanation to Enhance Clinical Utility. *Journal of Orthopaedic & Sports Physical Therapy*, 31(2), pp.96–100.
- McGill, S.M. & Karpowicz, A., 2009. Exercises for Spine Stabilization : Motion / Motor Patterns , Stability Progressions , and Clinical Technique. *Arch Phys Med Rehabil*, 90(1), pp.118–126. Available at: <http://dx.doi.org/10.1016/j.apmr.2008.06.026>.
- McGill, S.M. & Norman, R.W., 1986. Partitioning of the L4-L5 Dynamic Moment into Disc, Ligamentous, and Muscular Components During Lifting. *Spine*, 11(7), pp.666–78.
- McGill, S.M. & Norman, R.W., 1986. Partitioning of the L4-L5 Dynamic Moment into Disc, Ligamentous, and Muscular Components During Lifting. *Biomechanics*.
- Miyamoto, N., Hirata, K. & Kanehisa, H., 2015. Effects of hamstring stretching on passive muscle stiffness vary between hip flexion and knee extension maneuvers. *Scandinavian Journal of Medicine and Science in Sports*, pp.1–8.
- Modenese, L., Phillips, a T.M. & Bull, a M.J., 2011a. An open source lower limb model: Hip joint validation. *Journal of biomechanics*, 44(12), pp.2185–2193. Available at: <http://www.ncbi.nlm.nih.gov/pubmed/21742331> [Accessed July 22, 2011].
- Modenese, L., Phillips, a T.M. & Bull, a M.J., 2011b. An open source lower limb model: Hip joint validation. *Journal of biomechanics*, 44(12), pp.2185–93. Available at: <http://www.ncbi.nlm.nih.gov/pubmed/21742331> [Accessed November 9, 2012].
- Moore, K.L. & Dalley, A.F., 2006. *Clinically Oriented Anatomy* Fifth., Baltimore: Lippincott Williams & Wilkins.
- Moreside, J.M. & McGill, S.M., 2011. Quantifying normal 3D hip ROM in healthy young adult males with clinical and laboratory tools: Hip mobility restrictions appear to be plane-specific. *Clinical Biomechanics*, 26(8), pp.824–829. Available at: <http://dx.doi.org/10.1016/j.clinbiomech.2011.03.015>.
- Morris, J.M., Lucas, D.B. & Bresler, M.S., 1961. Role of the Trunk in Stability of the Spine. *The Journal of bone and joint surgery. American volume*, 43(3), pp.327–51.

- Murphy, D.R. et al., 2006. Interexaminer reliability of the hip extension test for suspected impaired motor control of the lumbar spine. *Journal of Manipulative and Physiological Therapeutics*, 29(5), pp.374–7.
- Myer, G.D. et al., 2014. Biomechanics laboratory-based prediction algorithm to identify female athletes with high knee loads that increase risk of ACL injury. *British journal of sports medicine*, 45(4), pp.245–252.
- Myer, G.D. et al., 2010a. Clinical correlates to laboratory measures for use in non-contact anterior cruciate ligament injury risk prediction algorithm. *Clinical biomechanics (Bristol, Avon)*, 25(7), pp.693–9. Available at: <http://www.pubmedcentral.nih.gov/articlerender.fcgi?artid=2900517&tool=pmcentrez&endertype=abstract> [Accessed April 27, 2012].
- Myer, G.D. et al., 2010b. Development and validation of a clinic-based prediction tool to identify female athletes at high risk for anterior cruciate ligament injury. *The American journal of sports medicine*, 38(10), pp.2025–33. Available at: <http://www.ncbi.nlm.nih.gov/pubmed/20595554> [Accessed March 15, 2012].
- Myer, G.D. et al., 2007a. Differential neuromuscular training effects on ACL injury risk factors in "high-risk" versus "low-risk" athletes. *BMC musculoskeletal disorders*, 8, p.39. Available at: <http://www.pubmedcentral.nih.gov/articlerender.fcgi?artid=1871588&tool=pmcentrez&endertype=abstract>.
- Myer, G.D. et al., 2007b. Differential neuromuscular training effects on ACL injury risk factors in "high-risk" versus "low-risk" athletes. *BMC musculoskeletal disorders*, 8, p.39. Available at: <http://www.pubmedcentral.nih.gov/articlerender.fcgi?artid=1871588&tool=pmcentrez&endertype=abstract> [Accessed June 5, 2013].
- Myer, G.D., Brent, J.L., et al., 2011. Real-Time Assessment and Neuromuscular Training Feedback Techniques to Prevent Anterior Cruciate Ligament Injury in Female Athletes. *Strength and Conditioning Journal*, 33(3), pp.21–35.
- Myer, G.D., Ford, K.R., et al., 2011. Three-dimensional motion analysis validation of a clinic-based nomogram designed to identify high ACL injury risk in female athletes. *The Physician and sportsmedicine*, 39(1), pp.19–28. Available at: <http://www.ncbi.nlm.nih.gov/pubmed/21378483>.
- Myers, C.A. et al., 2011. Role of the Acetabular Labrum and the Iliofemoral Ligament in Hip Stability: An in Vitro Biplane Fluoroscopy Study. *American Journal of Sports Medicine*, 39(1_suppl), p.85S–91S.
- Nadler, S. et al., 2001. Relationship Between Hip Muscle Imbalance and Occurrence of Low Back Pain in Collegiate Athletes. *American Journal of Physical Medicine & Rehabilitation*, 80(8), pp.572–577.
- Nadler, S.F. et al., 2002. Hip muscle imbalance and low back pain in athletes: influence of core

- strengthening. *Medicine and science in sports and exercise*, 34(1), pp.9–16. Available at: <http://www.ncbi.nlm.nih.gov/pubmed/11782641>.
- Nadler, S.F. et al., 2000. The Relationship Between Lower Extremity Injury , Low Back Pain , and Hip Muscle Strength in Male and Female Collegiate Athletes. *Measurement*, pp.89–97.
- Nelson-wong, E. et al., 2008. Gluteus medius muscle activation patterns as a predictor of low back pain during standing. *Clinical biomechanics*.
- Nourbakhsh, M.R. & Arab, A.M., 2002. Relationship between mechanical factors and incidence of low back pain. *The Journal of orthopaedic and sports physical therapy*, 32(9), pp.447–60. Available at: <http://www.ncbi.nlm.nih.gov/pubmed/12322811>.
- Offierski, C.M. & MacNab, I., 1983. Hip-spine syndrome. *Spine*, 8, pp.316–21.
- Oliver, G.D. et al., 2010. Muscle activation of different core exercises. *Journal of Strength and Conditioning Research*, 0(0), pp.1–6.
- Page, P., Frank, C.C. & Lardner, R., 2010. Pathomechanics of musculoskeletal pain and muscle imbalances. In *Assessment and Treatment of Muscle Imbalances: The Janda Approach*. Champaign, Illinois, pp. 43–55.
- Pereira, B.P. et al., 2004. Properties of the two neuromuscular compartments in a split bipennate muscle. *Journal of orthopaedic research : official publication of the Orthopaedic Research Society*, 22(6), pp.1325–30. Available at: <http://www.ncbi.nlm.nih.gov/pubmed/15475216> [Accessed November 23, 2011].
- Piazza, S.J., Okita, N. & Cavanagh, P.R., 2001. Accuracy of the functional method of hip joint center location: effects of limited motion and varied implementation. *Journal of biomechanics*, 34(7), pp.967–73. Available at: <http://www.ncbi.nlm.nih.gov/pubmed/11410180>.
- Pirouzi, S. et al., 2006. Low Back Pain Patients Demonstrate Increased Hip Extensor Muscle Activity During Standardized Submaximal Rotation Efforts. *Spine*, 31(26), pp.999–1005.
- Powers, C.M., 2010. The Influence of Abnormal Hip Mechanics on Knee Injury: A Biomechanical Perspective. *Journal of Orthopaedic & Sports Physical Therapy*, 40(2), pp.42–51.
- Powers, C.M., 2003. The Influence of Altered Lower-Extremity Kinematics on Patellofemoral Joint Dysfunction : A Theoretical Perspective COMMENTARY. *Journal of Orthopaedic & Sports Physical Therapy*, pp.639–646.
- Quatman, C.E. & Hewett, T.E., 2009. The anterior cruciate ligament injury controversy : is ““ valgus collapse ”” a sex-specific mechanism ? *British journal of sports medicine*, 43, pp.328–335.
- Reid, D.A. & McNair, P.J., 2004. Passive force, angle, and stiffness changes after stretching of hamstring muscles. *Medicine and Science in Sports and Exercise*, 36(11), pp.1944–1948.
- Reiman, M.P., Bolgla, L.A. & Lorenz, D., 2009. Hip Function’ s Influence on Knee Dysfunction : A Proximal Link to a Distal Problem. *Physical Therapy*, pp.33–46.

- Reiman, M.P., Weisbach, P.C. & Glynn, P.E., 2009. The Hip ' s Influence on Low Back Pain : A Distal Link to a Proximal Problem Hip – Spine Syndrome. *Physical Therapy*, pp.24–32.
- Roach, S.M. et al., 2015. PASSIVE HIP RANGE OF MOTION IS REDUCED IN ACTIVE SUBJECTS WITH CHRONIC LOW BACK PAIN COMPARED TO CONTROLS. , 10(1), pp.13–20.
- Roach, S.M. et al., 2014. PATELLOFEMORAL PAIN SUBJECTS EXHIBIT DECREASED PASSIVE HIP RANGE OF MOTION COMPARED TO CONTROLS. , 9(4), pp.468–475.
- Safran, M.R. et al., 2013. In vitro analysis of peri-articular soft tissues passive constraining effect on hip kinematics and joint stability. *Knee Surgery, Sports Traumatology, Arthroscopy*, 21, pp.1655–1663.
- Sahrmann, S.A., 2001. *Diagnosis and Treatment of Movement Impairment Syndroms*, Missouri: Mosby, Inc.
- Sakamoto, A.C.L. et al., 2009. Muscular activation patterns during active prone hip extension exercises. *Journal of Electromyography and Kinesiology*, 19, pp.105–112.
- Saunders, W. a et al., 1979. Degenerative joint disease in the hip and spine. *Rheumatology and rehabilitation*, 18(3), pp.137–41. Available at: <http://www.ncbi.nlm.nih.gov/pubmed/493800>.
- Scheys, L. et al., 2011. Level of subject-specific detail in musculoskeletal models affects hip moment arm length calculation during gait in pediatric subjects with increased femoral anteversion. *Journal of biomechanics*, 44(7), pp.1346–53. Available at: <http://www.ncbi.nlm.nih.gov/pubmed/21295307> [Accessed July 17, 2012].
- Schmitz, R.J., Riemann, B.L. & Thompson, T., 2002. Gluteus Medius Activity During Isometric Closed-Chain Hip Rotation. *Instrumentation*, pp.179–189.
- Scholtes, S. a, Gombatto, S.P. & Van Dillen, L.R., 2009. Differences in lumbopelvic motion between people with and people without low back pain during two lower limb movement tests. *Clinical biomechanics (Bristol, Avon)*, 24(1), pp.7–12. Available at: <http://www.pubmedcentral.nih.gov/articlerender.fcgi?artid=2643272&tool=pmcentrez&rendertype=abstract> [Accessed July 15, 2012].
- Schultz, A.B. et al., 1973. Analog studies of forces in the human in the human spine: Mechanical properties and motion segment behaviour. *Journal of Biomechanics*, 6, pp.373–383.
- Schultz, A.B. et al., 1982. Analysis and measurement of lumbar trunk loads in tasks involving bends and twists. *Journal of Biomechanics*, 15(9), pp.669–75.
- Schwartz, M.H. & Rozumalski, A., 2005. A new method for estimating joint parameters from motion data. *Journal of Biomechanics*, 38, pp.107–116.
- Shum, G.L.K., Crosbie, J. & Lee, R.Y.W., 2010. Back pain is associated with changes in loading pattern throughout forward and backward bending. *Spine*, 35(25), pp.E1472-8. Available at: <http://www.ncbi.nlm.nih.gov/pubmed/21102275>.
- Shum, G.L.K., Crosbie, J. & Lee, R.Y.W., 2005a. Effect of low back pain on the kinematics and

- joint coordination of the lumbar spine and hip during sit-to-stand and stand-to-sit. *Spine*, 30(17), pp.1998–2004. Available at: <http://www.ncbi.nlm.nih.gov/pubmed/16135992>.
- Shum, G.L.K., Crosbie, J. & Lee, R.Y.W., 2005b. Symptomatic and asymptomatic movement coordination of the lumbar spine and hip during an everyday activity. *Spine*, 30(23), pp.E697-702. Available at: <http://www.ncbi.nlm.nih.gov/pubmed/16319739>.
- Sigward, S.M., Havens, K.L. & Powers, C.M., 2011. Knee Separation Distance and Lower Extremity Kinematics During a Drop Land: Implications for Clinical Screening. *Journal of Athletic Training*, 46(5), pp.471–475.
- Sjolie, A.N., 2004. Low-back pain in adolescents is associated with poor hip mobility and high body mass index. *Scandinavian Journal of Medicine & Science in Sports*, pp.168–175.
- Solomonow, M., 2004. Ligaments : a source of work-related musculoskeletal disorders. *Journal of Electromyography and Kinesiology*, 14(1), pp.49–60.
- T, C. & M, S., 1997. Ovid : Low back loads over a variety of abdominal exercises : se ... Low back loads over a variety of abdominal exercises : searching for the safest abdominal challenge Ovid : Low back loads over a variety of abdominal exercises : se ... *Medicine & Science in Sports & Exercise*, 29(June), pp.804–811.
- Tafazzoli, F. & Lamontagne, M., 1996. Mechanical behaviour of hamstrings muscles in low-back pain patients and control subjects. *Clinical biomechanics (Bristol, Avon)*, 11(1), pp.16–24.
- Taylor, J.B. et al., 2018. Hip biomechanics differ in responders and non-responders to an ACL injury prevention program. *Knee Surgery, Sports Traumatology, Arthroscopy*, 0(0), p.0. Available at: <http://dx.doi.org/10.1007/s00167-018-5158-1>.
- Thys, H., Faraggiana, T. & Margaria, R., 1972. Utilization of muscle elasticity in exercise. *Journal of Applied Physiology*, 32(4), pp.491–4.
- Vad, V.B., 2004. Low Back Pain in Professional Golfers: The Role of Associated Hip and Low Back Range-of-Motion Deficits. *American Journal of Sports Medicine*, 32(2), pp.494–497. Available at: <http://journal.ajsm.org/cgi/doi/10.1177/0363546503261729> [Accessed May 17, 2011].
- Vleeming, A. et al., 1996. The Function of the Long Dorsal Sacroiliac Ligament: Its Implication for Understanding Low Back Pain. *Spine*, 21(5), pp.556–62.
- Vleeming, A. et al., 1995. The Posterior Layer of the Thoracolumbar Fascia. *Spine*, 20(7), pp.753–58.
- Vogt, L. & Banzer, W., 1997. Dynamic testing of the motor stereotype in prone hip extension from neutral position. *Clinical Biomechanics*, 12(2), pp.122–127.
- Vrahas, M.S. et al., 1990. Contribution of passive tissues to the intersegmental moments at the hip. *Journal of Biomechanics*, 23(4), pp.357–362.
- Wickham, J.B. & Brown, J.M., 1998. Muscles within muscles: the neuromotor control of intramuscular segments. *European journal of applied physiology and occupational physiology*,

- 78(3), pp.219–25. Available at: <http://www.ncbi.nlm.nih.gov/pubmed/9720999>.
- Wickham, J.B. & Brown, J.M.M., 2011. The Function of Neuromuscular Compartments in Human Shoulder Muscles. *Journal of neurophysiology*. Available at: <http://www.ncbi.nlm.nih.gov/pubmed/21975455> [Accessed November 16, 2011].
- Williams, D.S. et al., 2004. High-arched runners exhibit increased leg stiffness compared to low-arched runners. , 19, pp.263–269.
- Williams, D.S., McClay, I.S. & Hamill, J., 2001. Arch structure and injury patterns in runners. , 16, pp.341–347.
- Williams, J.M., Haq, I. & Lee, R.Y., 2010. Is pain the cause of altered biomechanical functions in back pain sufferers? *Human movement science*, 29(2), pp.311–25. Available at: <http://www.ncbi.nlm.nih.gov/pubmed/20153909> [Accessed July 17, 2012].
- van Wingerden, J.P. et al., 1993. A functional-anatomical approach to the spine-pelvis mechanism: interaction between the biceps femoris muscle and the sacrotuberous ligament. *European Spine Journal*, 2, pp.140–44.
- Winter, D.A., 2009. *Biomechanics and Motor Control of Human Movement* 4th ed., Hoboken, New Jersey: John Wiley & Sons, Inc.
- Wong, T.K.T. & Lee, R.Y.W., 2004. Effects of low back pain on the relationship between the movements of the lumbar spine and hip. *Human Movement Science*, 23, pp.21–34.
- Wong, T.K.T. & Lee, R.Y.W., 2002. Relationship between the movements of the lumbar spine and hip. *Human Movement Science*, 21, pp.481–494.
- Yerys, S. et al., 2002. Effect of Mobilization of the Anterior Hip Capsule on Gluteus Maximus Strength. *Test*, 10(4), pp.218–224.
- Yettram, A.L. & Jackman, M.J., 1982. Structural analysis for the forces in the human spinal column and its musculature. *Journal of biomechanical engineering*, 4, pp.118–24.
- Yoon, Y.S. & Mansour, J.M., 1982. The passive elastic moment at the hip. *Journal of biomechanics*, 15(12), pp.905–10. Available at: <http://www.ncbi.nlm.nih.gov/pubmed/7166551>.
- Yoshimoto, H. et al., 2005. Spinopelvic alignment in patients with osteoarthritis of the hip: a radiographic comparison to patients with low back pain. *Spine*, 30(14), pp.1650–7. Available at: <http://www.ncbi.nlm.nih.gov/pubmed/16025036>.

Appendix A: Hip Anatomy Parameters

The following is taken directly from Horseman and colleges (Horsman et al. 2007).

Table 1: Attachment sites with respect to the global frame for each muscle and muscle section (with the leg in the original fixated position).

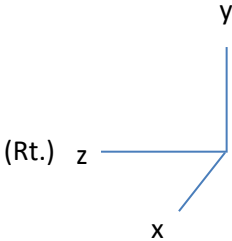
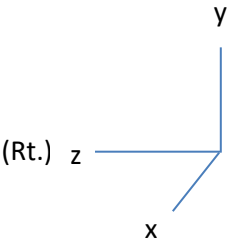
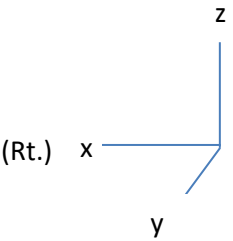
Muscle (part)	Elem. #	Origin				Segm.	e(cm)	Insert.				e(cm)
		X(cm)	Y(cm)	Z(cm)	X(cm)			Y(cm)	Z(cm)	Segm		
Add. brev. (prox.)	1	4.62	-1.30	-6.92	Pelvis	0.06	-1.85	-8.34	1.81	Femur	0.08	
	2	5.07	-1.32	-7.12	Pelvis		-1.32	-9.52	1.92	Femur		
Add. brev. (mid.)	3	4.57	-1.82	-7.61	Pelvis	0.06	-0.96	-10.75	1.99	Femur	0.08	
	4	4.93	-1.84	-7.78	Pelvis		-0.68	-12.02	2.01	Femur		
Add. brev. (dist.)	5	3.86	-2.57	-8.34	Pelvis	0.06	-0.39	-13.28	1.97	Femur	0.08	
	6	4.09	-2.58	-8.45	Pelvis		0.02	-14.52	1.87	Femur		
Add. long.	1	5.25	-0.92	-6.64	Pelvis	0.03	1.54	-17.44	1.68	Femur	0.07	
	2	5.44	-1.16	-6.89	Pelvis		1.84	-18.64	1.52	Femur		
	3	5.57	-1.37	-7.19	Pelvis		2.16	-19.86	1.44	Femur		
	4	5.63	-1.56	-7.51	Pelvis		2.49	-21.09	1.39	Femur		
	5	5.61	-1.73	-7.85	Pelvis		2.80	-22.31	1.29	Femur		
	6	5.50	-1.88	-8.20	Pelvis		3.07	-23.52	1.10	Femur		
Add. magn. (dist.)	1	-2.10	-7.10	-4.85	Pelvis	0.35	5.66	-36.31	-2.54	Tibia	0.38	
	2	-1.51	-6.71	-5.57	Pelvis		5.66	-36.31	-2.54	Tibia		
	3	0.21	-5.78	-7.03	Pelvis		5.66	-36.31	-2.54	Tibia		
Add. magn. (mid.)	1	-2.79	-6.90	-4.94	Pelvis	0.10	1.82	-19.92	1.43	Femur	0.11	
	2	-2.50	-6.68	-4.53	Pelvis		1.82	-19.92	1.43	Femur		
	3	-2.12	-6.60	-5.53	Pelvis		2.65	-23.01	0.99	Femur		
	4	-1.87	-6.42	-5.18	Pelvis		2.65	-23.01	0.99	Femur		
	5	-1.25	-6.21	-6.24	Pelvis		3.41	-26.12	0.90	Femur		
	6	-1.06	-6.07	-5.98	Pelvis		3.41	-26.12	0.90	Femur		
Add. magn.(prox.)	1	1.86	-4.50	-7.74	Pelvis	0.12	0.03	-10.75	1.54	Femur	0.19	
	2	0.39	-5.33	-6.76	Pelvis		0.55	-12.77	1.52	Femur		
	3	1.13	-4.92	-7.25	Pelvis		1.07	-14.80	1.50	Femur		
	4	1.86	-4.50	-7.74	Pelvis		1.58	-16.82	1.48	Femur		
Bic. fem. CL	1	-3.78	-6.09	-1.71	Pelvis	0.50	1.63	-45.15	4.62	Tibia	0.72	
Bic. fem. CB	1	0.58	-19.35	1.77	Femur	0.17	1.63	-45.15	4.62	Tibia	0.72	
	2	1.81	-23.83	1.34	Femur		1.63	-45.15	4.62	Tibia		
	3	2.68	-28.65	1.60	Femur		1.63	-45.15	4.62	Tibia		
Ext. dig. long.	1	2.49	-51.38	3.75	Tibia	0.23	17.36	-96.59	6.79	Phal.	1.90	
	2	2.90	-47.38	4.50	Tibia		17.36	-96.59	6.79	Phal.		
	3	3.39	-44.82	5.18	Tibia		17.36	-96.59	6.79	Phal.		
Ext. hal. long.	1	4.12	-66.43	3.48	Tibia	0.13	21.52	-93.48	4.97	Phal.	0.33	
	2	3.45	-61.01	3.27	Tibia		21.52	-93.48	4.97	Phal.		
	3	2.89	-55.52	3.48	Tibia		21.52	-93.48	4.97	Phal.		
Flex. dig. long.	1	6.40	-54.90	0.81	Tibia	0.12	17.58	-96.88	5.87	Phal.	2.14	
	2	7.16	-60.18	0.93	Tibia		17.58	-96.88	5.87	Phal.		
	3	7.24	-64.27	1.11	Tibia		17.58	-96.88	5.87	Phal.		
Flex. hal. long.	1	2.22	-58.59	2.83	Tibia	0.13	22.00	-94.84	4.55	Phal.	0.32	
	2	3.01	-63.93	2.81	Tibia		22.00	-94.84	4.55	Phal.		
	3	3.80	-69.41	2.81	Tibia		22.00	-94.84	4.55	Phal.		
Gastrocn. (lat.)	1	3.43	-37.75	2.21	Femur	0.58	2.90	-81.98	-1.89	Hindf.	0.47	
Gastrocn. (med.)	1	5.04	-36.71	-1.48	Femur	0.73	3.01	-82.21	-2.74	Hindf.	0.65	
Gemellus (inf.)	1	-6.50	-4.05	-2.86	Pelvis	0.39	-3.24	0.64	4.28	Femur	0.41	
Gemellus (sup.)	1	-5.56	0.86	-5.02	Pelvis	0.39	-2.11	-0.12	3.72	Femur	0.41	
Glut. max. (sup.)	1	-7.91	7.77	-1.57	Pelvis	0.32	-4.04	5.70	7.47	Femur	0.28	
	2	-8.98	5.51	-3.46	Pelvis		-4.31	2.63	7.74	Femur		
	3	-9.64	2.73	-5.01	Pelvis		-4.73	-0.44	7.99	Femur		
	4	-9.13	8.91	-2.68	Pelvis		-2.40	5.45	7.74	Femur		
	5	-10.33	6.77	-4.69	Pelvis		-2.60	2.37	8.02	Femur		

Glut. max. (inf.)	6	-10.94	3.94	-6.19	Pelvis		-3.09	-0.69	8.26	Femur	
	1	-10.74	-0.83	-7.52	Pelvis	0.25	-5.61	-7.16	4.07	Femur	0.37
	2	-9.87	-1.49	-7.31	Pelvis		-5.07	-8.47	3.75	Femur	
	3	-9.05	-2.56	-7.35	Pelvis		-3.66	-10.78	3.38	Femur	
	4	-10.25	-0.16	-6.86	Pelvis		-5.61	-7.16	4.07	Femur	
	5	-9.38	-0.82	-6.65	Pelvis		-5.07	-8.47	3.75	Femur	
Glut. med. (ant.)	6	-8.65	-2.00	-6.80	Pelvis		-3.66	-10.78	3.38	Femur	
	1	0.40	9.48	4.46	Pelvis	0.19	-3.03	-0.25	5.90	Femur	0.19
	2	1.43	9.03	4.56	Pelvis		-2.25	-0.44	6.19	Femur	
	3	2.49	8.19	4.26	Pelvis		-1.53	-0.54	6.42	Femur	
	4	0.93	9.95	5.22	Pelvis		-3.36	-1.09	6.20	Femur	
	5	1.80	9.36	5.09	Pelvis		-2.68	-1.50	6.56	Femur	
Glut. med. (post.)	6	2.81	8.47	4.72	Pelvis		-1.96	-1.60	6.79	Femur	
	1	-3.88	11.87	2.51	Pelvis	0.39	-3.85	0.88	4.50	Femur	0.04
	2	-6.02	10.15	-0.41	Pelvis		-4.01	0.86	3.97	Femur	
	3	-6.82	7.21	-2.31	Pelvis		-4.24	0.76	3.62	Femur	
	4	-4.81	13.46	2.07	Pelvis		-3.85	0.88	4.50	Femur	
	5	-7.34	12.41	-1.03	Pelvis		-4.51	0.39	4.66	Femur	
Glut. min. (ant.)	6	-8.41	9.93	-3.06	Pelvis		-4.76	0.26	4.34	Femur	
	1	-0.08	7.89	3.31	Pelvis	0.42	-1.50	-2.27	6.16	Femur	0.65
Glut. min. (mid.)	1	-2.26	7.55	1.73	Pelvis		-1.50	-2.27	6.16	Femur	
Glut. min. (post.)	1	-4.03	6.51	0.07	Pelvis		-1.50	-2.27	6.16	Femur	
Gracilis	1	1.65	-4.88	-7.39	Pelvis	0.18	7.70	-48.16	0.27	Tibia	0.96
	2	3.67	-3.46	-7.98	Pelvis		7.70	-48.16	0.27	Tibia	
Iliacus (lat.)	1	-2.95	13.23	2.75	Pelvis	0.34	-2.34	-5.12	0.37	Femur	0.82
	2	-1.13	11.48	2.92	Pelvis		-2.34	-5.12	0.37	Femur	
	3	-0.34	10.01	2.78	Pelvis		-2.34	-5.12	0.37	Femur	
Iliacus (mid.)	1	-5.58	13.54	0.03	Pelvis	0.27	-2.34	-5.12	0.37	Femur	0.82
	2	-4.32	11.03	-0.21	Pelvis		-2.34	-5.12	0.37	Femur	
	3	-3.08	8.61	-0.38	Pelvis		-2.34	-5.12	0.37	Femur	
Iliacus (med.)	1	-5.27	12.75	-3.90	Pelvis	0.33	-2.34	-5.12	0.37	Femur	0.82
	2	-4.67	10.77	-3.51	Pelvis		-2.34	-5.12	0.37	Femur	
	3	-3.68	8.13	-3.61	Pelvis		-2.34	-5.12	0.37	Femur	
Obt. ext. (inf.)	1	-0.04	-4.83	-6.75	Pelvis	0.14	-4.50	-5.54	2.77	Femur	0.59
	2	1.89	-3.95	-7.98	Pelvis		-4.50	-5.54	2.77	Femur	
Obt. ext. (sup.)	1	3.88	-1.77	-8.02	Pelvis	0.29	-3.09	-1.18	2.56	Femur	0.21
	2	2.11	-3.26	-7.72	Pelvis		-3.09	-1.18	2.56	Femur	
	3	-0.04	-4.33	-6.87	Pelvis		-3.09	-1.18	2.56	Femur	
Obturator int.	1	-2.22	2.19	-4.19	Pelvis	0.39	-2.68	0.26	4.00	Femur	0.82
	2	-1.98	0.35	-4.92	Pelvis		-2.68	0.26	4.00	Femur	
	3	-0.93	-1.28	-5.90	Pelvis		-2.68	0.26	4.00	Femur	
Pectineus	1	3.47	1.38	-5.13	Pelvis	0.27	-1.82	-7.67	1.58	Femur	0.12
	2	3.97	1.03	-5.48	Pelvis		-1.66	-8.54	1.59	Femur	
	3	4.47	0.67	-5.83	Pelvis		-1.50	-9.41	1.60	Femur	
	4	4.97	0.32	-6.18	Pelvis		-1.82	-7.67	1.58	Femur	
Peroneus brev.	1	2.59	-60.53	3.39	Tibia	0.08	7.57	-89.43	3.62	Midf.	0.34
	2	3.16	-65.19	3.29	Tibia		7.57	-89.43	3.62	Midf.	
	3	3.78	-69.69	3.23	Tibia		7.57	-89.43	3.62	Midf.	
Peroneus long.	1	1.67	-48.99	4.08	Tibia	0.20	7.18	-87.15	3.54	Midf.	0.18
	2	1.90	-52.73	3.73	Tibia		7.18	-87.15	3.54	Midf.	
	3	2.16	-56.43	3.40	Tibia		7.18	-87.15	3.54	Midf.	
Peroneus tert.	1	4.33	-68.61	3.55	Tibia	0.10	11.08	-92.42	4.51	Midf.	0.41
	2	3.64	-63.48	3.51	Tibia		11.08	-92.42	4.51	Midf.	
	3	3.08	-58.34	3.49	Tibia		11.08	-92.42	4.51	Midf.	
Piriformis	1	-10.07	2.31	-7.42	Pelvis	0.91	-3.48	0.88	2.74	Femur	0.43
Plantaris	1	2.83	-38.59	3.73	Femur	1.01	4.51	-81.41	-2.33	Hindf.	--
Popliteus	1	2.74	-41.05	4.49	Femur	0.35	6.21	-51.18	0.37	Tibia	0.70
	2	2.74	-41.05	4.49	Femur		4.91	-47.08	-0.08	Tibia	
Psoas minor	1	-5.06	25.28	-5.61	Pelvis	0.78	1.59	-1.79	-0.80	Femur	0.20
Psoas major	1	-5.74	22.64	-5.56	Pelvis	0.26	-2.34	-5.12	0.37	Femur	0.82
	2	-2.91	18.44	-5.96	Pelvis		-2.34	-5.12	0.37	Femur	
	3	-2.81	14.20	-5.88	Pelvis		-2.34	-5.12	0.37	Femur	

Quadratis fem.	1	-0.90	-4.98	-6.30	Pelvis	0.43	-4.65	-2.43	2.81	Femur	0.42
	2	-1.54	-5.24	-5.50	Pelvis		-4.60	-3.22	2.87	Femur	
	3	-2.17	-5.50	-4.69	Pelvis		-4.54	-4.01	2.93	Femur	
	4	-2.80	-5.76	-3.89	Pelvis		-4.48	-4.80	2.99	Femur	
Rectus fem.	1	3.02	4.27	2.03	Pelvis	0.45	9.46	-35.06	3.48	Patella	0.06
	2	3.02	4.27	2.03	Pelvis		8.86	-35.03	4.48	Patella	
Sartorius (prox.)	1	3.20	7.49	3.50	Pelvis	0.50	7.94	-47.72	0.38	Tibia	1.06
Sartorius (dist.)	1	3.20	7.49	3.50	Pelvis	0.50	7.94	-47.72	0.38	Tibia	1.06
Semimembr.	1	-2.80	-6.61	-2.03	Pelvis	0.71	4.12	-43.84	-2.97	Tibia	0.81
Semitend.	1	-4.03	-6.07	-2.78	Pelvis	0.49	7.22	-49.29	-0.24	Tibia	0.60
Soleus (med.)	1	1.85	-54.40	2.79	Tibia	0.45	2.90	-81.98	-1.89	Hindf.	0.35
	2	1.57	-51.72	2.92	Tibia		2.90	-81.98	-1.89	Hindf.	
	3	0.97	-47.81	3.08	Tibia		2.90	-81.98	-1.89	Hindf.	
Soleus (lat.)	4	7.63	-58.10	0.81	Tibia	0.46	4.18	-81.71	-2.71	Hindf.	0.33
	5	7.21	-54.96	0.57	Tibia		4.18	-81.71	-2.71	Hindf.	
	6	6.50	-52.52	0.27	Tibia		4.18	-81.71	-2.71	Hindf.	
Tensor fasc. l.	1	2.83	7.99	4.76	Pelvis	0.32	4.68	-38.51	5.40	Tibia	0.40
	2	2.37	9.01	5.13	Pelvis		4.68	-38.51	5.40	Tibia	
Tibialis ant.	1	5.78	-46.65	4.26	Tibia	0.23	14.55	-87.06	1.79	Midf.	0.38
	2	6.36	-49.36	3.89	Tibia		14.55	-87.06	1.79	Midf.	
	3	6.38	-54.64	2.94	Tibia		14.55	-87.06	1.79	Midf.	
Tibial post. (med.)	1	5.04	-50.06	2.22	Tibia	0.18	11.30	-83.54	1.54	Midf.	0.55
	2	5.51	-54.88	2.03	Tibia		11.30	-83.54	1.54	Midf.	
	3	6.12	-61.14	2.09	Tibia		11.30	-83.54	1.54	Midf.	
Tibial post. (lat.)	1	2.91	-54.31	3.38	Tibia	0.13	11.30	-83.54	1.54	Midf.	0.55
	2	3.74	-61.64	3.13	Tibia		11.30	-83.54	1.54	Midf.	
	3	4.64	-68.75	3.29	Tibia		11.30	-83.54	1.54	Midf.	
Vastus interm.	1	5.41	-22.86	2.55	Femur	0.32	9.46	-35.06	3.48	Patella	0.06
	2	3.71	-17.44	2.95	Femur		9.46	-35.06	3.48	Patella	
	3	1.62	-11.67	3.74	Femur		9.46	-35.06	3.48	Patella	
	4	4.74	-23.17	3.53	Femur		8.86	-35.03	4.48	Patella	
	5	2.92	-17.81	4.11	Femur		8.86	-35.03	4.48	Patella	
	6	1.01	-11.97	4.64	Femur		8.86	-35.03	4.48	Patella	
Vastus lat. (inf.)	1	2.69	-29.27	2.17	Femur	0.27	8.86	-35.03	4.48	Patella	--
	2	2.09	-24.72	2.18	Femur		8.86	-35.03	4.48	Patella	
	3	1.19	-20.26	2.39	Femur		8.86	-35.03	4.48	Patella	
	4	-0.01	-15.88	2.81	Femur		8.86	-35.03	4.48	Patella	
	5	-1.51	-11.59	3.44	Femur		8.86	-35.03	4.48	Patella	
	6	-3.30	-7.38	4.28	Femur		8.86	-35.03	4.48	Patella	
Vastus lat. (sup.)	7	-2.66	-3.32	6.10	Femur	0.27	8.86	-35.03	4.48	Patella	--
	8	-0.90	-1.61	5.16	Femur		8.86	-35.03	4.48	Patella	
Vastus med. (inf.)	1	4.17	-29.43	0.75	Femur	0.40	9.46	-35.06	3.48	Patella	--
	2	5.25	-29.22	0.78	Femur		9.46	-35.06	3.48	Patella	
Vastus med.(mid.)	3	3.68	-24.91	1.22	Femur	0.40	9.46	-35.06	3.48	Patella	--
	4	4.73	-24.71	1.26	Femur		9.46	-35.06	3.48	Patella	
Vastus med. (sup.)	5	2.59	-19.76	1.76	Femur	0.40	9.46	-35.06	3.48	Patella	--
	6	3.55	-19.58	1.79	Femur		9.46	-35.06	3.48	Patella	
	7	1.21	-14.60	2.29	Femur		9.46	-35.06	3.48	Patella	
	8	2.17	-14.42	2.32	Femur		9.46	-35.06	3.48	Patella	
	9	-0.08	-8.01	2.98	Femur		9.46	-35.06	3.48	Patella	
	10	0.42	-7.92	2.99	Femur		9.46	-35.06	3.48	Patella	

Appendix B: Joint Coordinate Systems

Table B: Comparing the model outputs and biomechanical definitions for the three modelling approaches.

Model	Spine Model (Superior)	Hip-Spine Model (Superior)	Visual 3D (Superior)
Coordinate system	 (Rt.)	 (Rt.)	 (Rt.)
	(Anterior)	(Anterior)	(Anterior)
Spine Flexion/Extension	-z/+z	-z/+z	-x/x
Spine Lateral Bend Rt. / Lt.	x/-x	x/-x	y/-y
Spine Axial Twist Rt./Lt.	-y/y	-y/y	-z/z
Hip Flexion/Extension		-z/+z	-x/x
Right Hip Adduction/Abduction		x/-x	y/-y
Left Hip Adduction/Abduction		-x/x	-y/y
Rt. Hip Axial Rotation Medial/Lateral		y/-y	-z/z
Lt. Hip Axial Rotation Medial/Lateral		-y/y	z/-z
Compression	-y	-y	-z
A-P Shear	-x	-x	-y
Spine M-L Shear (Rt)	z	z	x
Right Hip M-L Shear		z	x
Left Hip M-L Shear		-z	-x

*Where possible to avoid confusion data will be presented using naming conventions (i.e. compression rather than symbols (-y)).

**TLEM data is congruent to the SM and HSM coordinate systems, which follows Wu (2002).

***These conventions are true for angles, but since internal moments are calculated in V3D the polarity is reversed.

Appendix C: Passive Tissue Torque-Angle Curves – Tuning the model

This was an initial attempt to evaluate passive torque-angle curves with the HSM prior to the enhancements and changes made in this thesis. Notice the behaviour of the model poorly represents the biological data and therefore an explanation of this poor fit was examined. Below are the breakdowns of passive force by muscle during the virtual motion of the hip and the subsequent forces produced. There was a clear issue with the moment arms since the muscle produced smaller and smaller moments while at the same time producing more force with more stretch. The geodesics and wrapping techniques used here improved the biofidelity of the model estimates.

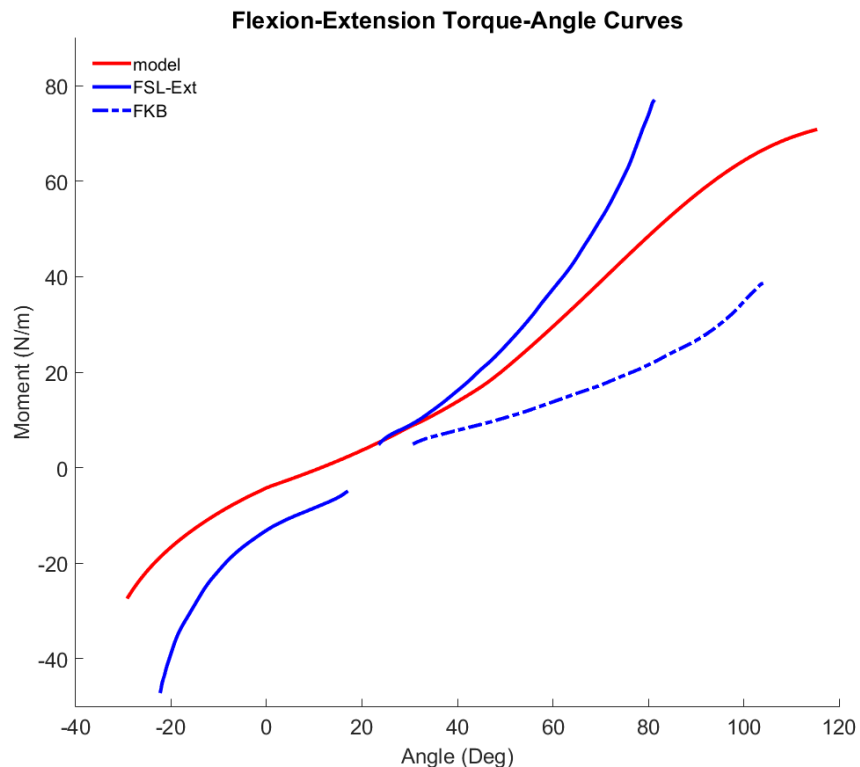
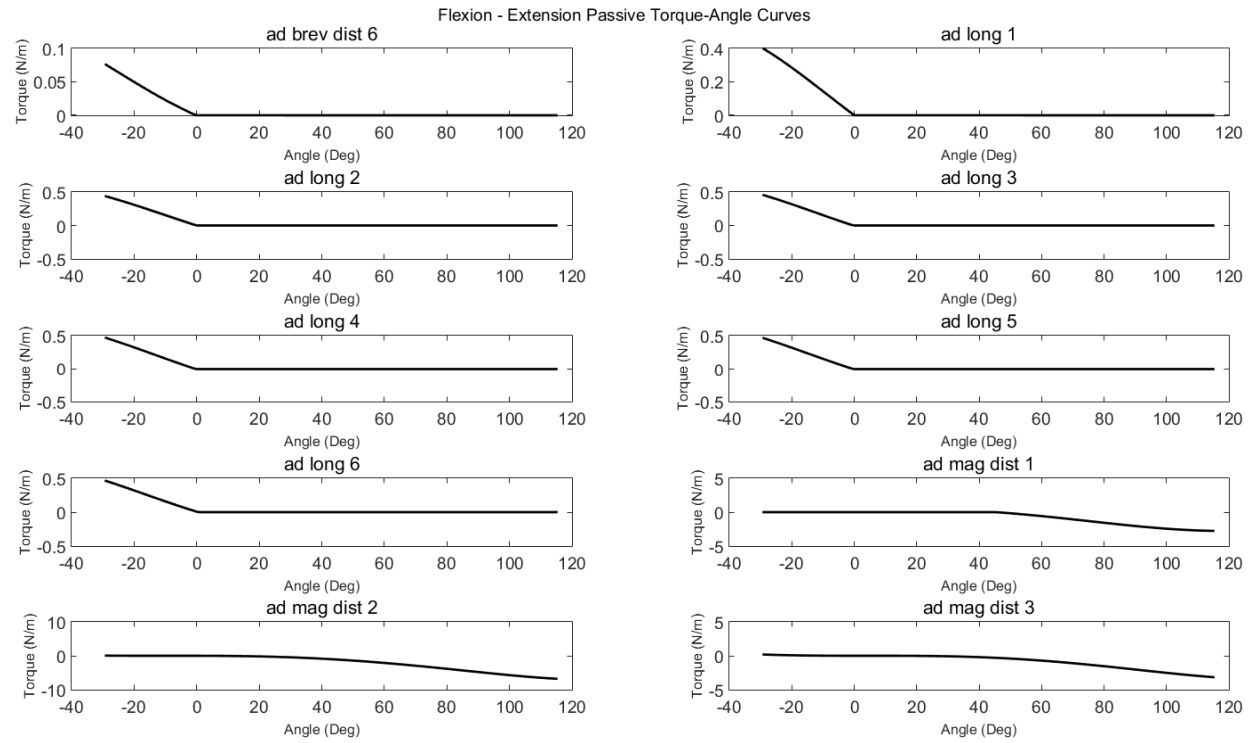
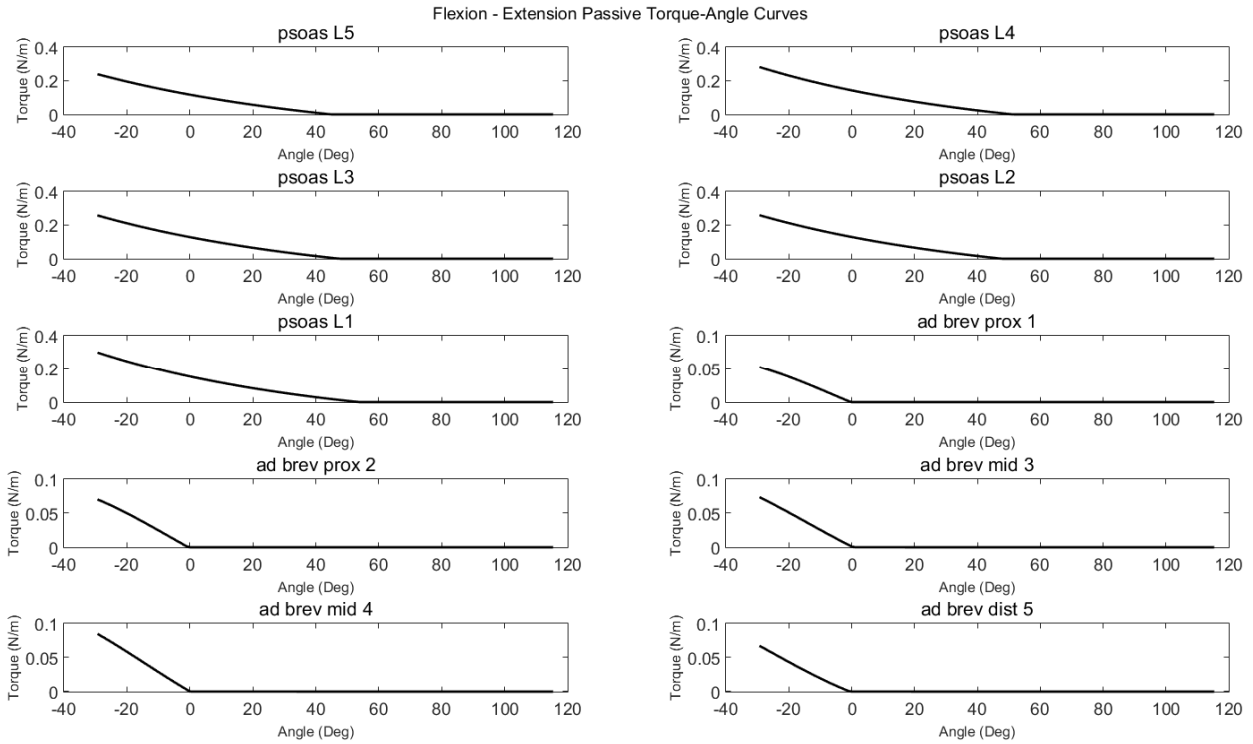
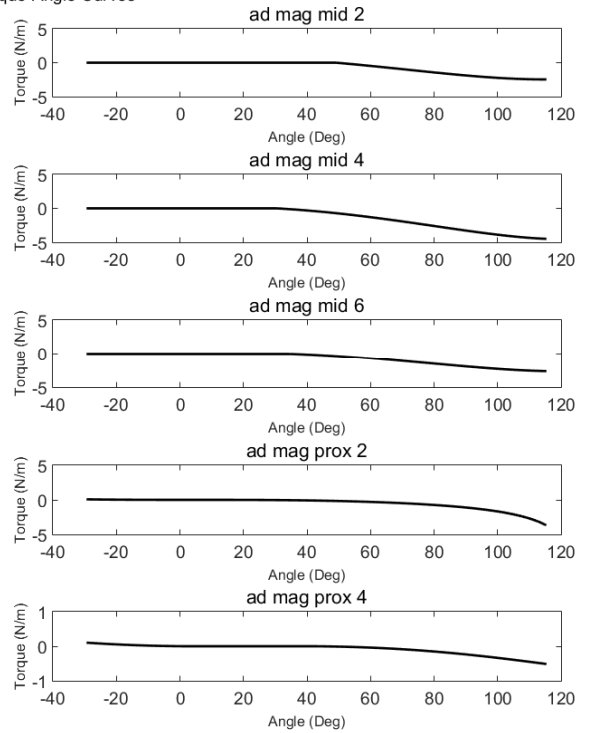
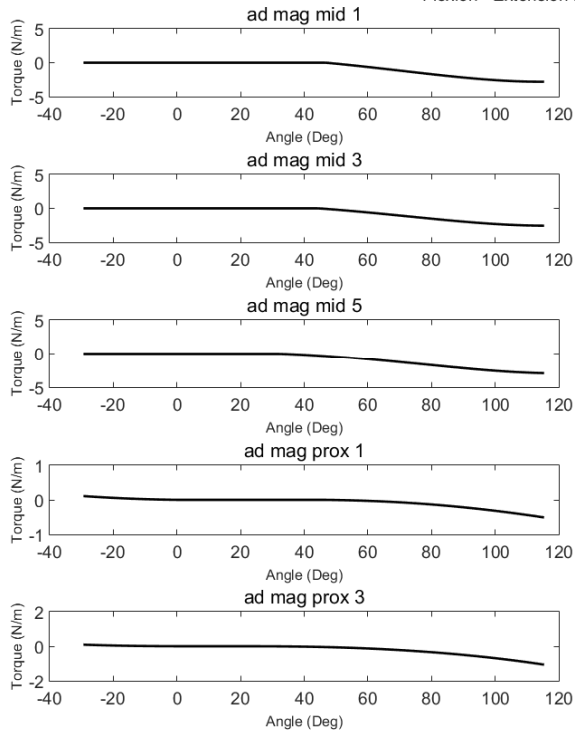


Figure C1: Mean male passive torque-angle curves and model predictions from 30 degrees of extension to 115 degrees of flexion. Currently the model under estimates both flexion and extension moments at the hip. There is also an inaccurate trend above ~70 degrees of hip flexion. This can be explained by the individual muscle moment arms and errors in moment arm estimations.

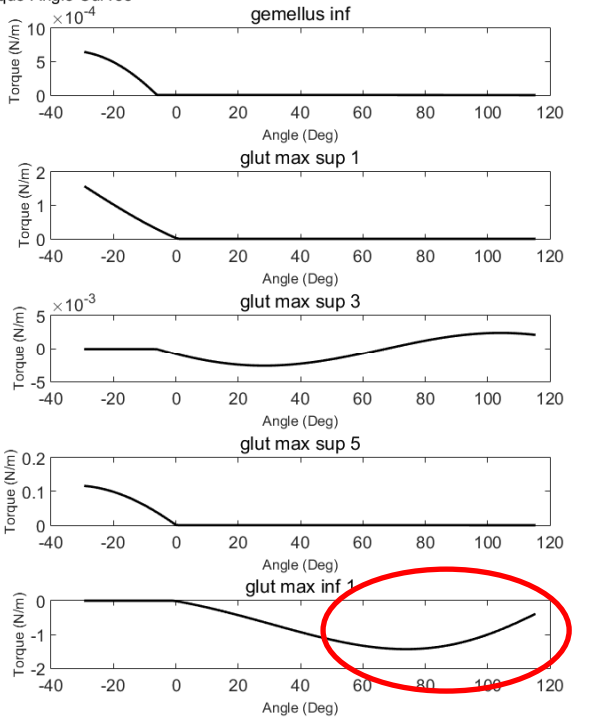
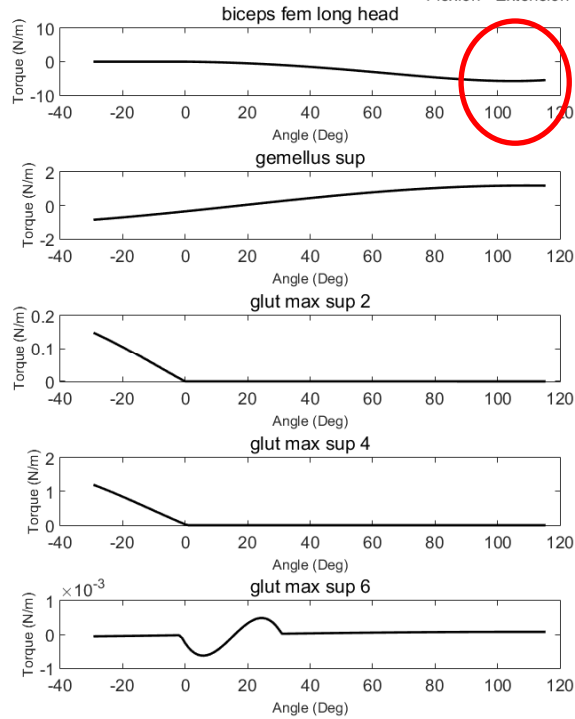
Here are the following muscle contributions which sum to the joint moment.



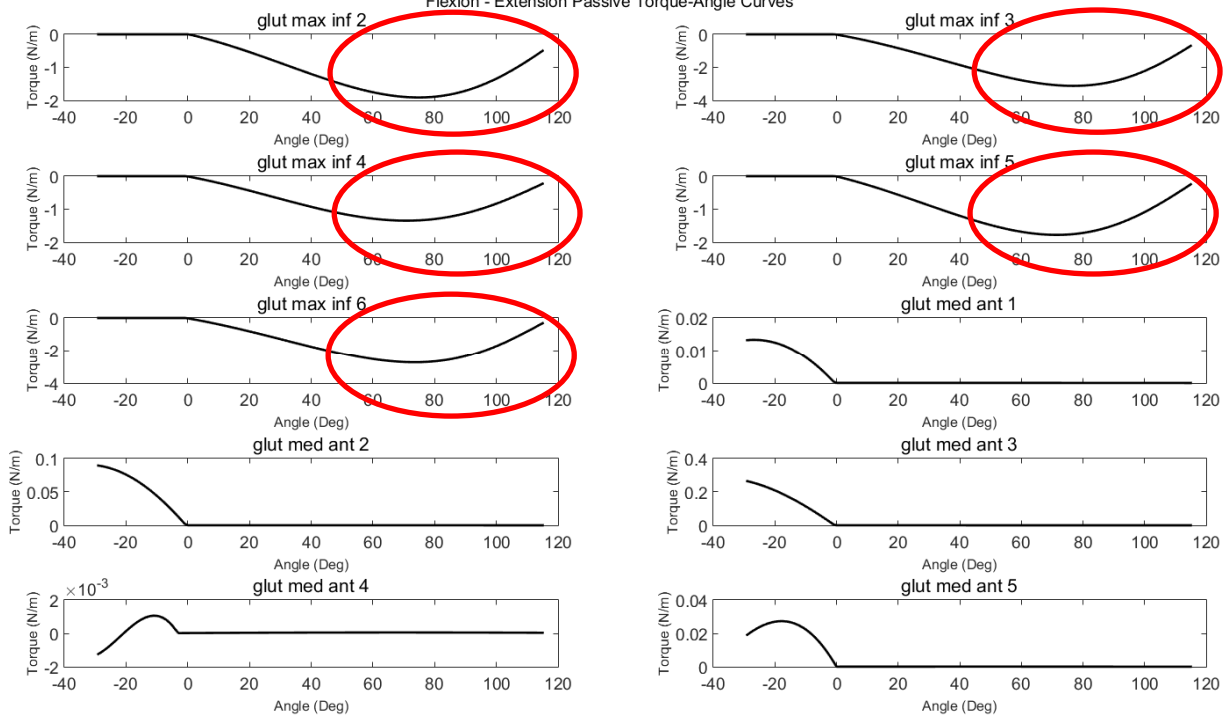
Flexion - Extension Passive Torque-Angle Curves



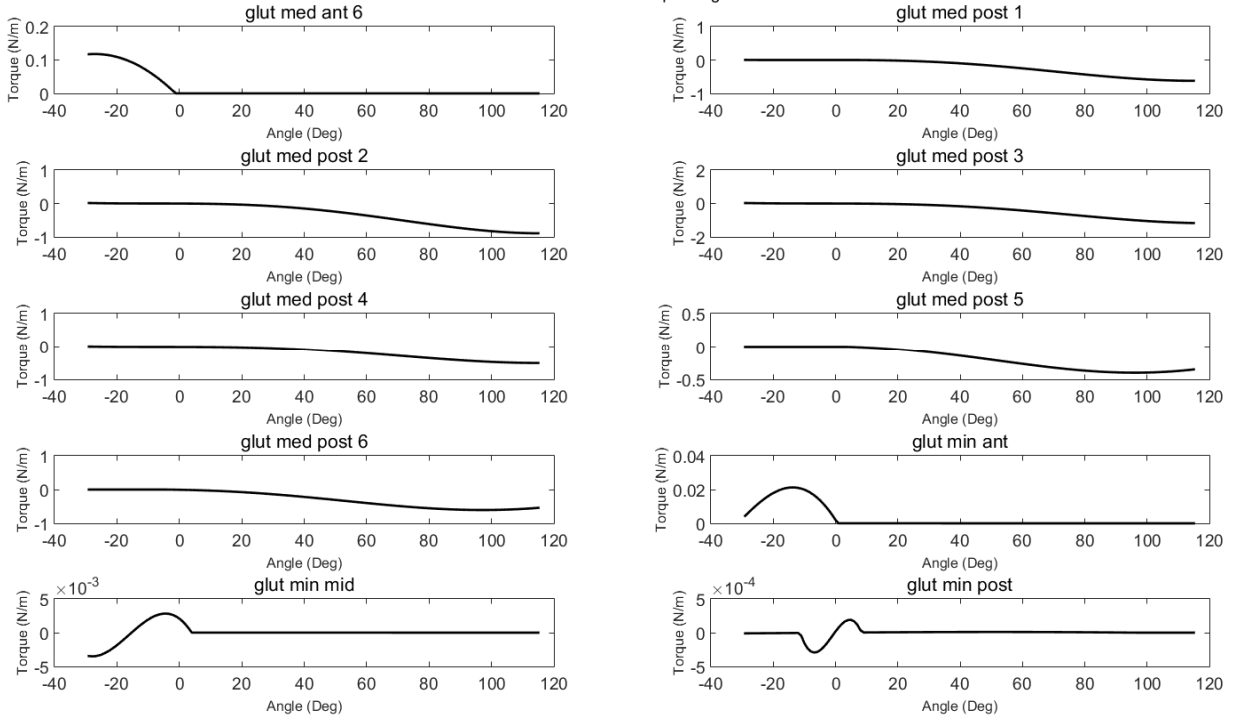
Flexion - Extension Passive Torque-Angle Curves



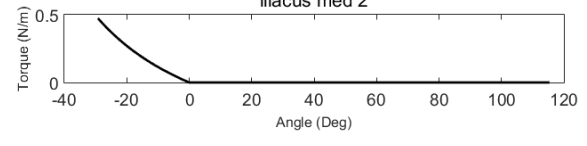
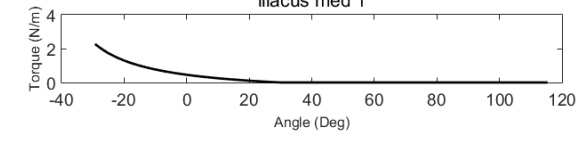
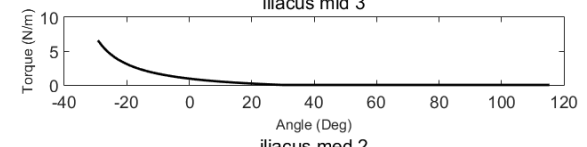
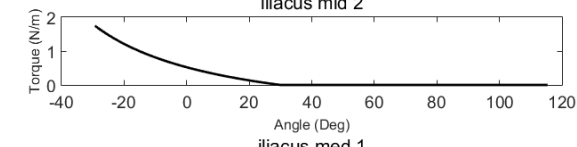
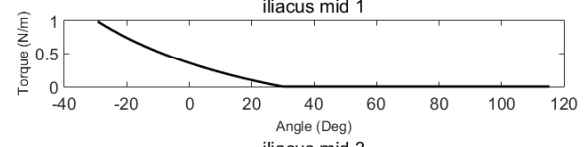
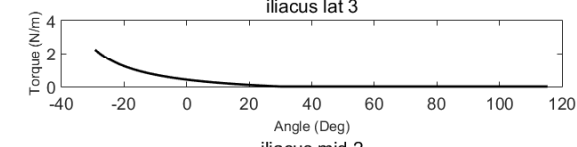
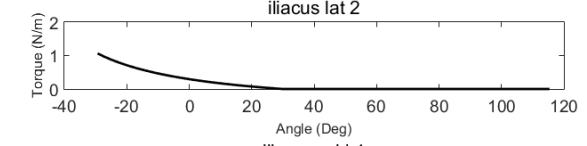
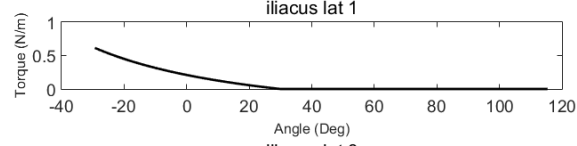
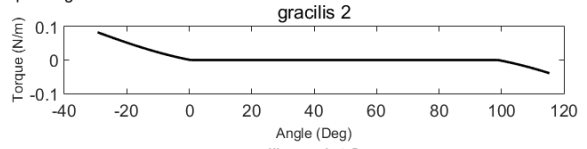
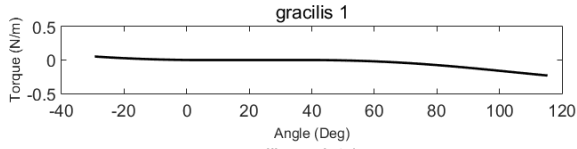
Flexion - Extension Passive Torque-Angle Curves



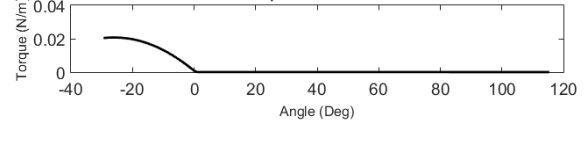
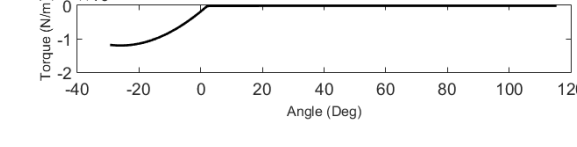
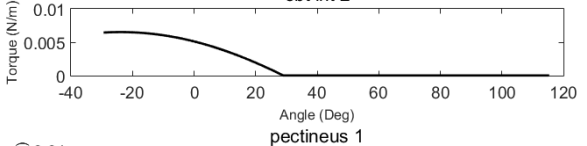
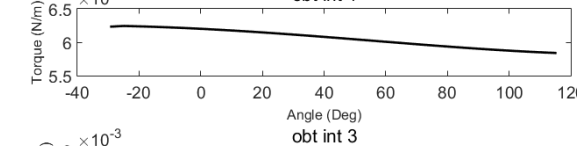
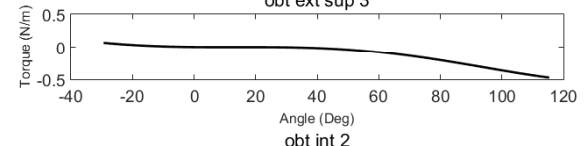
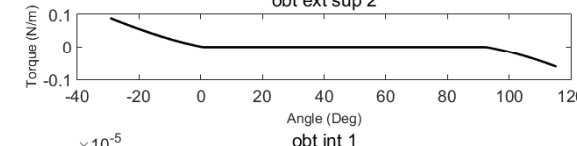
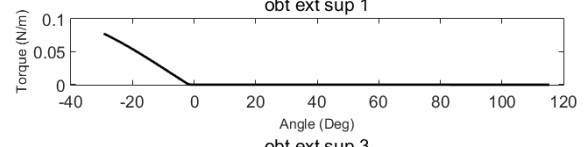
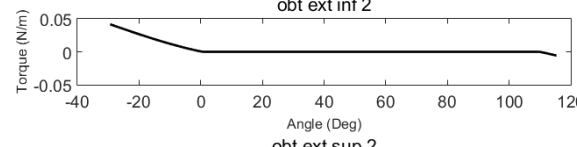
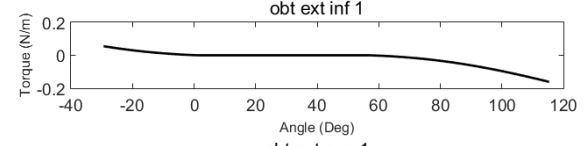
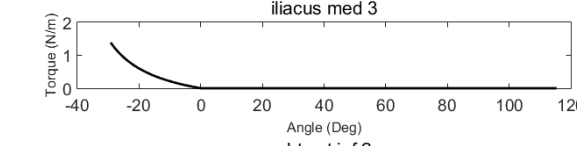
Flexion - Extension Passive Torque-Angle Curves



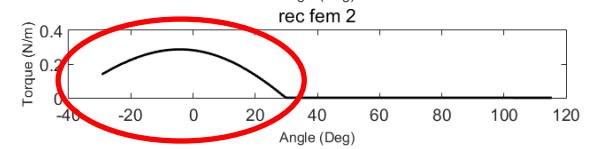
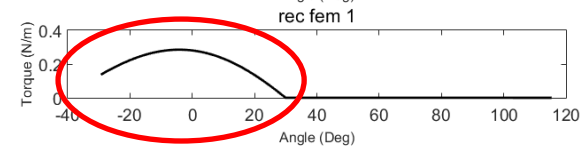
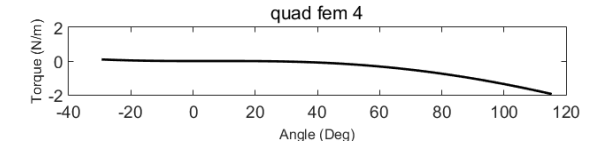
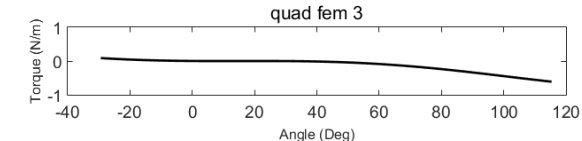
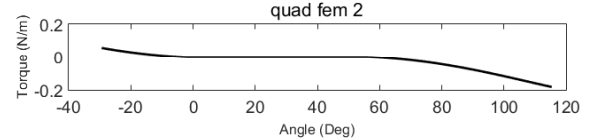
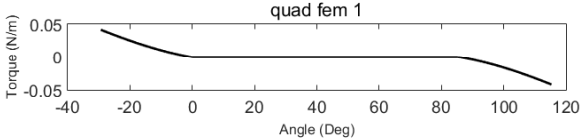
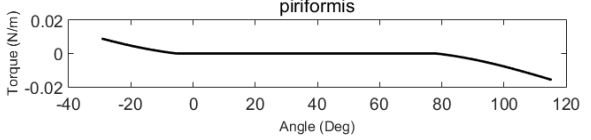
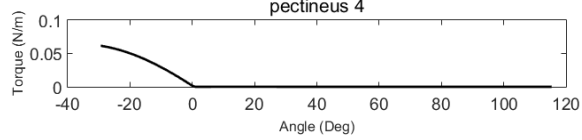
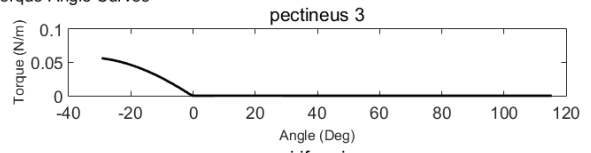
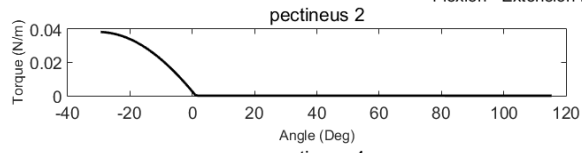
Flexion - Extension Passive Torque-Angle Curves



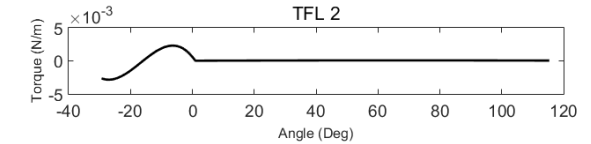
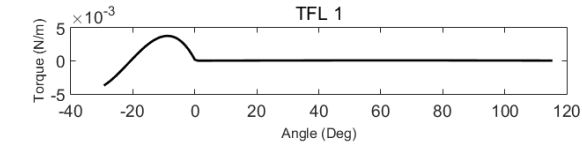
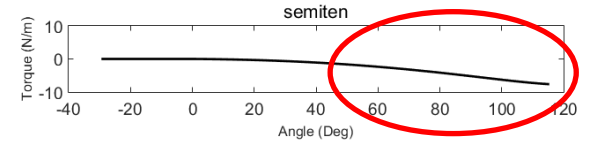
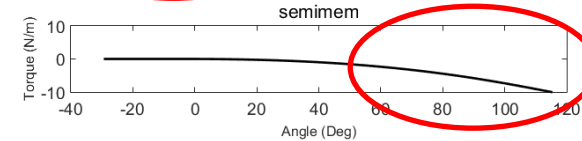
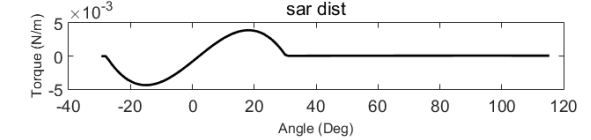
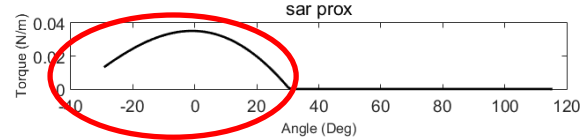
Flexion - Extension Passive Torque-Angle Curves



Flexion - Extension Passive Torque-Angle Curves



Flexion - Extension Passive Torque-Angle Curves



Appendix D: Data Collection, Processing and Analysis

Data Collection

Three-dimensional kinematic data was captured using eight optoelectronic motion capture cameras (Vicon MX20+, Vicon Motion Systems, Oxford, UK). These cameras monitored the position of reflective markers (Vicon, MX, 12.5mm diameter, Vicon Motion Systems, Oxford, UK) in a free marker (adhered individually to the skin) and marker-clusters (fixed to a rigid plate and adhered to the subject). Free markers defined segment geometry parameters for V3D each segment is described in Table D1. EMG data was collected using 3-8 channel differential amplifiers (AMT-8: Bortec Biomedical Ltd., Calgary, AB, Canada) . The AMT-8 amplifiers have an input impedance of 10M Ω , a built-in bandpass analog filter from 10 to 1000Hz, a CMR of 115dB at 60Hz. EMG signals were analog-to-digital converted (Vicon MX 64-channel analog-to-digital interface unit, Vicon Motion Systems, Oxford, UK) using a 16-bit converter (Vicon MX 20 MX control box, Vicon Motion Systems, Oxford, UK) with a ± 2.5 V range. Finally, two force plates, mounted in the floor, were used to capture kinetic data (OR6/7 AMTI Force and Motion, Advanced Mechanical Technology, Inc. Waterdown, MA, USA). Force plate calibration matrices and the physical location in the global space (laboratory) were pre-assigned to the Vicon Nexus software (Vicon Motion Systems, Oxford, UK) for real-time calibrated 3D space during data collection. These data were captured using Vicon Nexus 1.8.5 software (Vicon Motion Systems, Oxford, UK) and stored for post-collection processing.

Table D1: Visual 3D Segments

	Land Marks		Rigid Body Cluster Position
Segment	Proximal End	Distal End	
Torso	Lateral most aspect of Iliac crests	Acromioclavicular Joint	Over the T12-L1 (4 markers)
Pelvis	Lateral most aspect of Iliac crests	Greater Trochanters	Over the sacrum (5 markers)
Thigh	Greater Trochanter	Femoral epicondyles	Laterally over the mid thigh (5 markers)
Shank	Femoral epicondyles	Malleoli	Laterally over the mid-calf (4 markers)
Foot	Malleoli	Head of the 1 st and 5 th Metatarsal	Superiorly over the dorsum of the foot.

Data Processing

Data processing began in the Nexus software with model templates which labelled the reflective markers. Gaps in the kinematic data were filled using the "pattern fill" function (an algorithm which generates a trajectory based on a second marker - "parent marker"). When gaps appeared in the data less than ten frames (0.166 seconds) they were carefully analysed for an appropriate "parent marker" on the same rigid cluster, filled and then carefully examined for consistency in trajectory pattern. Gaps greater than ten frames rarely occurred, however when gaps exceeded ten frames, they were either filled or left unlabeled based on the ability of the "pattern fill" function to accurately project the trajectory. No gap larger than thirty frames was ever filled and it is also important to note that these gaps were rarely, if ever, seen in segments of critical importance (i.e. most gaps were seen in the quadruped position on the foot clusters - ankle joint angles were not required for analysis in these positions). Redundancy in the rigid marker clusters (four or five markers per cluster) allowed for gaps in single marker tracking and un-

labelling of poorly tracked markers, which typically occurred when only two adjacent cameras were able to detect a marker. However, gaps were filled since additional tracking markers will reduce error in kinematic processing described below when a least squares function is used to calculate local coordinate systems.

Data was then batch processed from Nexus software and exported for further analysis. Visual3D software (Version 4.96.11; C-Motion Inc., Rockville, MD) was used to calculate kinematic and inverse dynamics measures. Visual 3D models were built from anatomical markers and clusters were used to track segment position and orientation of each segment during the motion trials. Functional joint centers (FJC) and functional joint axes (FJA) were computed from "Functional Joint Center" motion trials during the calibration process for the hip and knee, respectively. For the hip FJC, these trials consisted of a circumduction motion, five clockwise and five counter clockwise rotations, with a radius of approximately 20 cm, bilaterally. For the knee FJA, five continuous cycles of flexion and extension were performed, typically from zero to 90 degrees of knee flexion, bilaterally.

Next, segments were defined as listed in Table D1. Additional anthropometric data (including chest depth, pelvis depth and trochanteric width) were collected and used as scaling measures in V3D software. Each segment was created from the anatomical markers and tracked in the motion trials with the segments' marker cluster. Joints were then created between adjacent segments automatically and could be modified with desired parameters. The spine was kinematically restricted to 3 degrees of freedom (3 rotations) as was the hip. The knee was unstrained as was the angle.

Lastly, processing pipelines were created to filter, process and export the desired output variables. The kinematic data were low pass filtered at 6 Hz and the kinetic data were low pass filtered at 15 Hz. The Visual 3D pipelines were then used to calculate joint angles, forces and moments at the spine, hips and knees, which were exported and used for analysis or input variables into the HSM.

Appendix E: Model Congruency

Below are representative Figures of the MATLAB program which was constructed to evaluate moment outputs from the HSM and inverse dynamics estimations and select the regions of the moments used to calculate the gain factor. As you can see the HSM, driven by EMG, response is less stable than the inverse dynamics estimates. Nonetheless the magnitude and congruence are subjectively excellent. Below – Subject 6 ACL setting the “gain” values for RHip, LHip, and Spine.

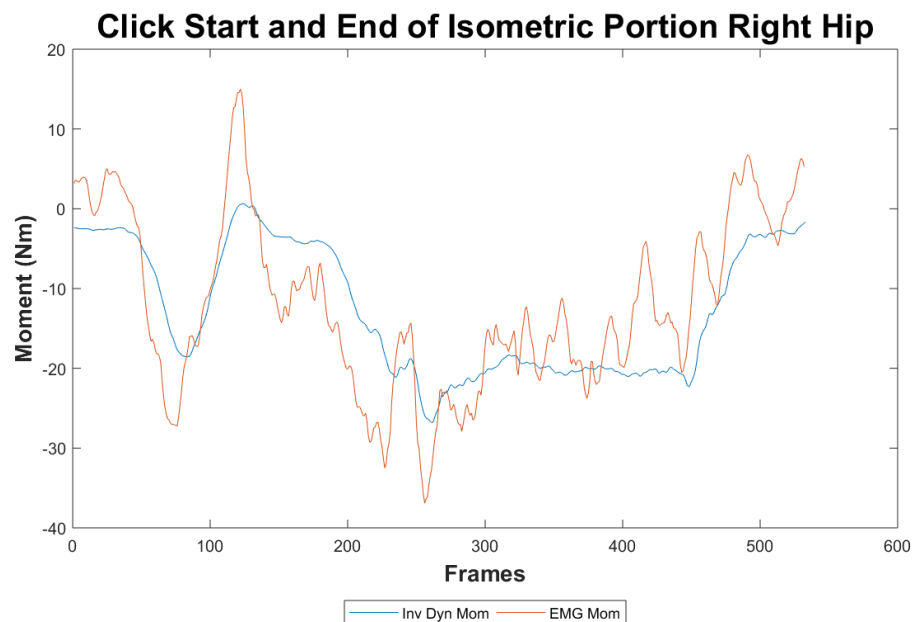


Figure E.1: Screen shot of HSM running a MATLAB script to identify section of the trail used to calculate gain between the HSM and ID estimates (right hip).

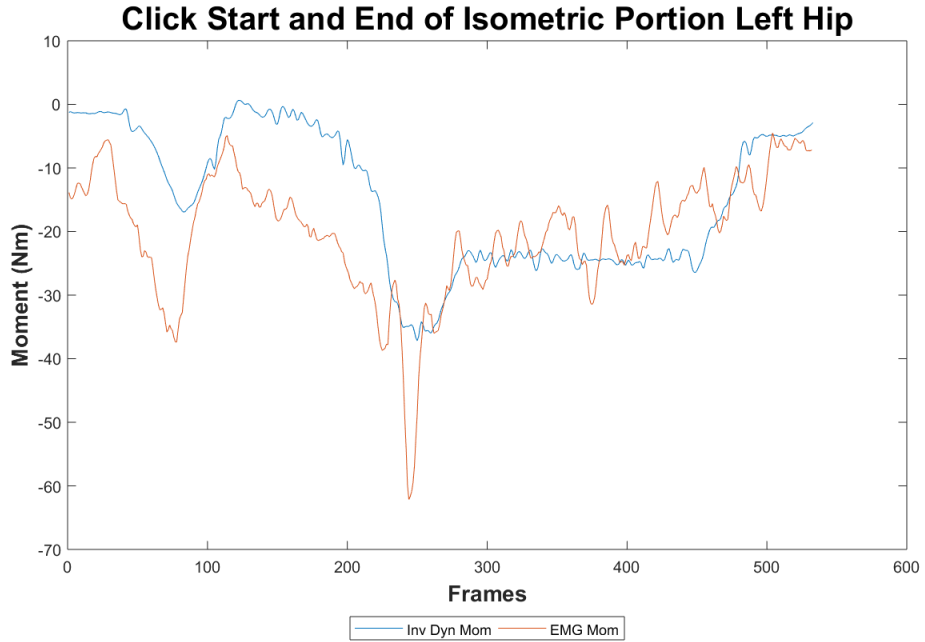


Figure E.2: Screen shot of HSM running a MATLAB script to identify section of the trail used to calculate gain between the HSM and ID estimates (left hip).

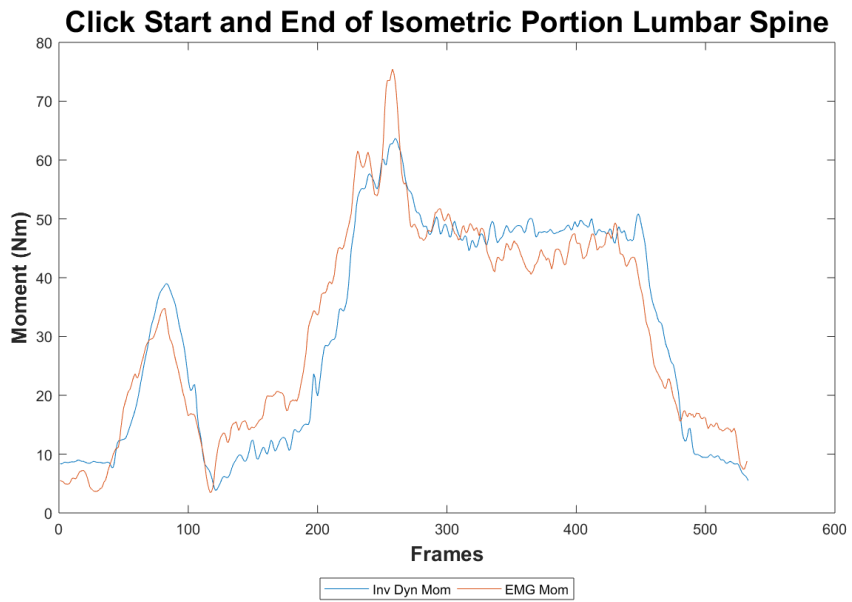


Figure E.3: Screen shot of HSM running a MATLAB script to identify section of the trail used to calculate gain between the HSM and ID estimates (spine).

Intermediate steps comparing the newly coded MATLAB – HSM with the original Visual basic code from the McGill Model. Figure E.4 demonstrates to calculate muscle length from kinematic data the two models are an exact match. This confirms the rotations and anatomical details between the original model and the current model are perfect.

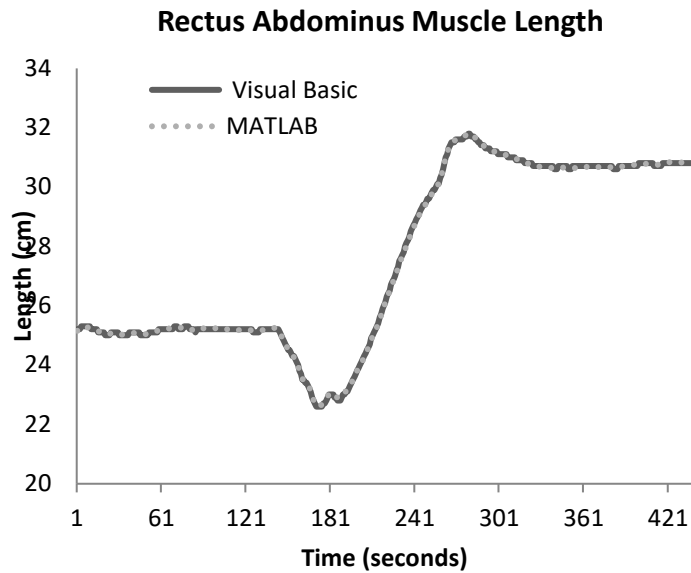


Figure E.4: A trail of sit-to-stand kinematics used to evaluate the model during a simple range of motion task. There models are a perfect match for rectus abdominis.

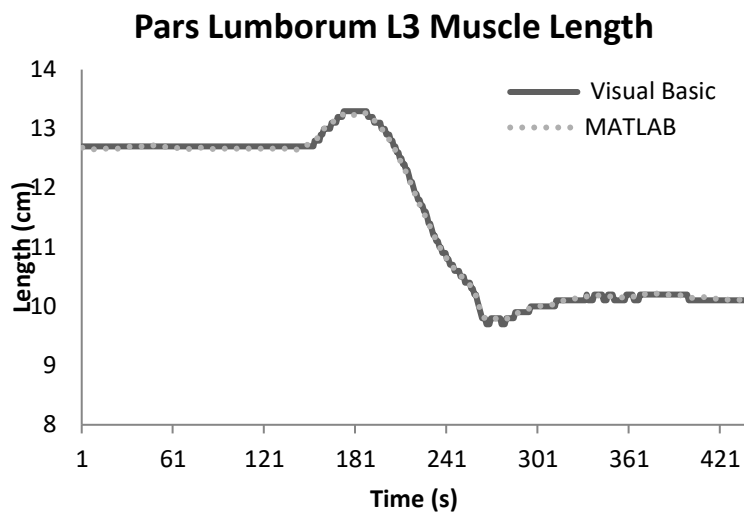


Figure E.5: A trail of sit-to-stand kinematics used to evaluate the model during a simple range of motion task. There models are a perfect match for pars lumborum L3 segment.

Appendix F: Data from Hip Passive Resistance & Stiffness

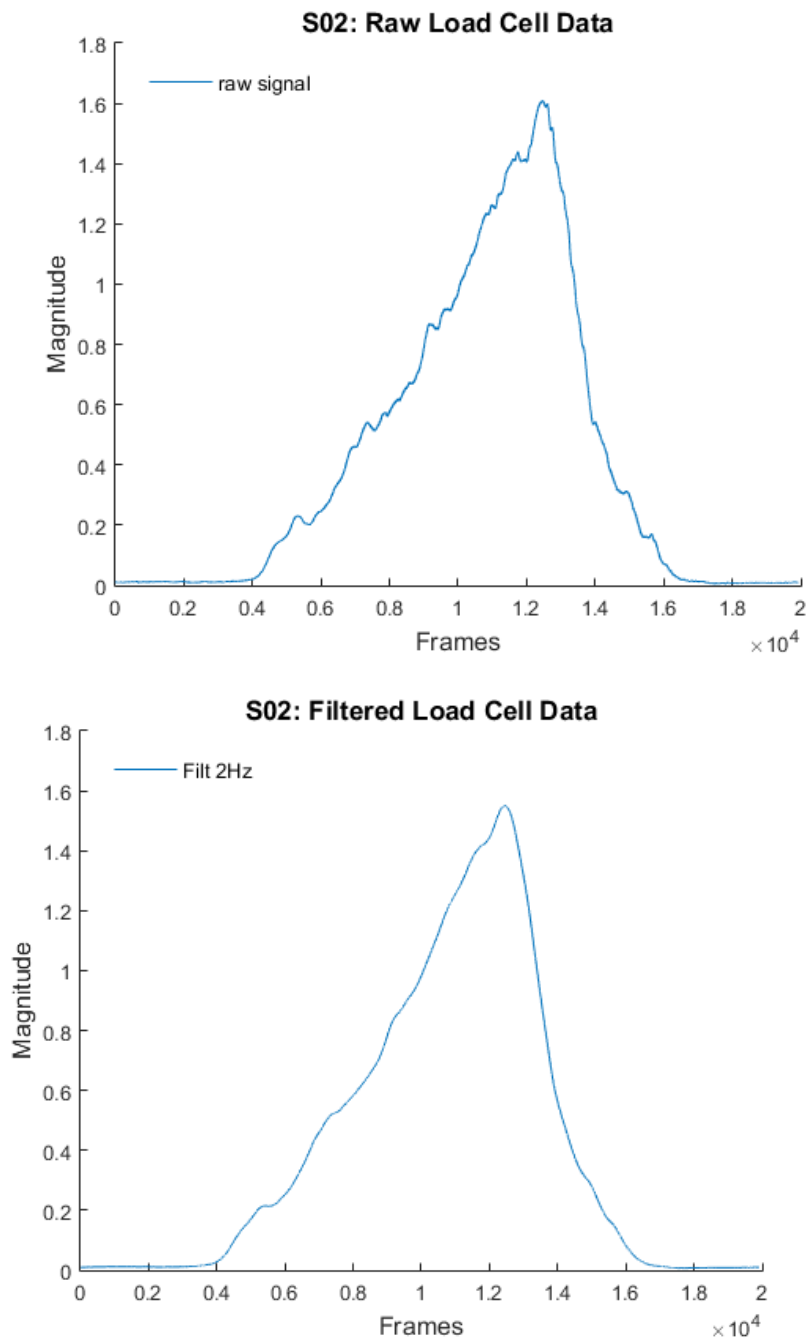


Figure F1: Sample of filter effects on load cell data filtered with low pass Butterworth filter at 2Hz raw signal (top) and filtered (bottom) (S02 from male data set).

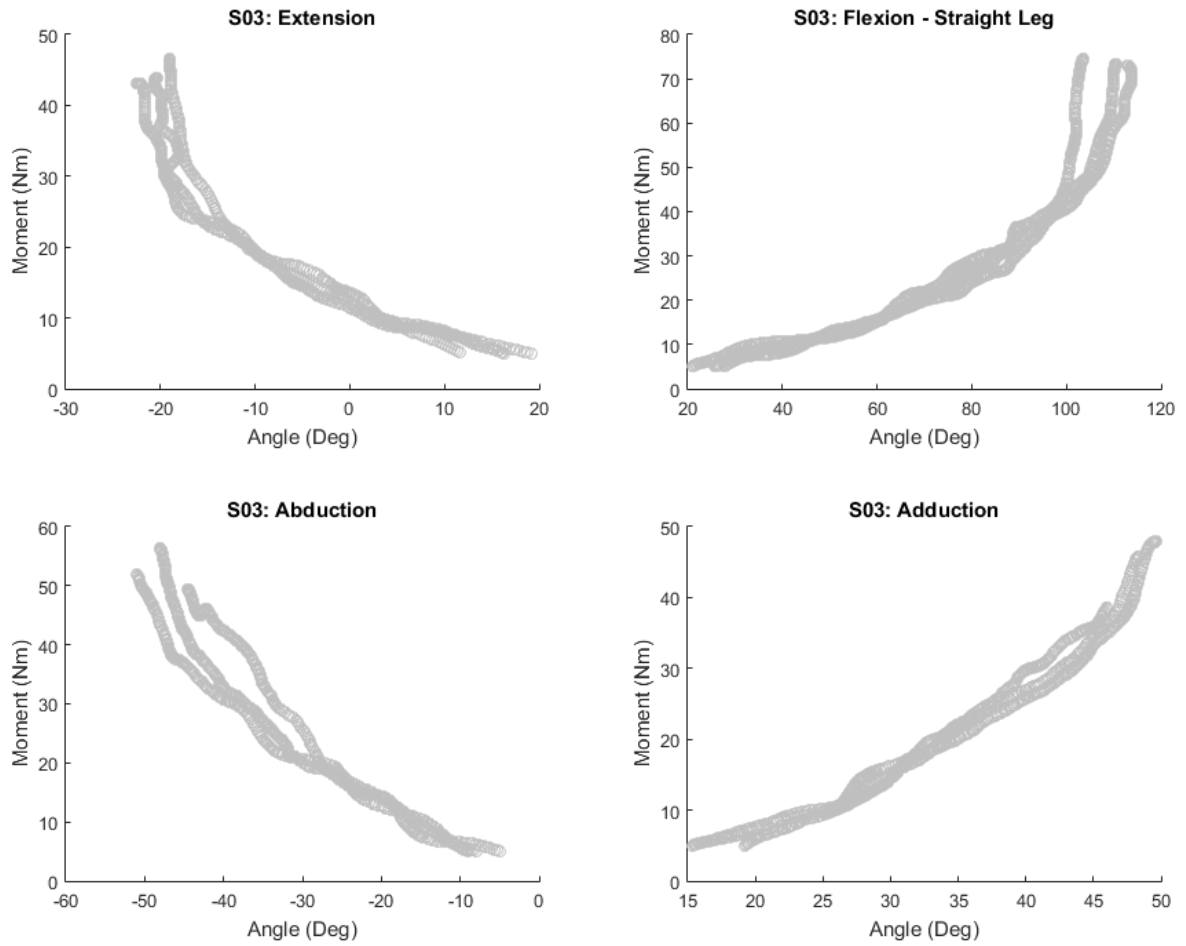


Figure F2: Angle-moment curves of one representative subject (female) for FSL, Ext, Abd, and Add. Note: Moments have not be adjusted for joint coordinate system (raw moment = force x distance).

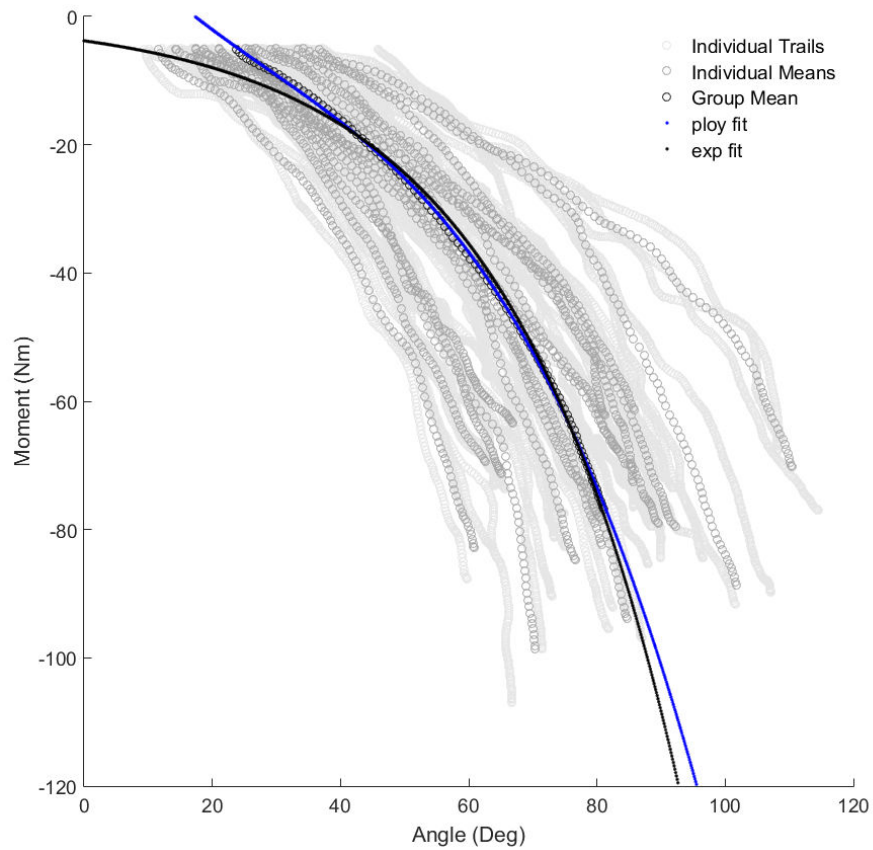


Figure F3: Passive hip resistance male flexion straight leg trials, individual means, and group means with a fitted polynomial and exponential curve to the group mean.

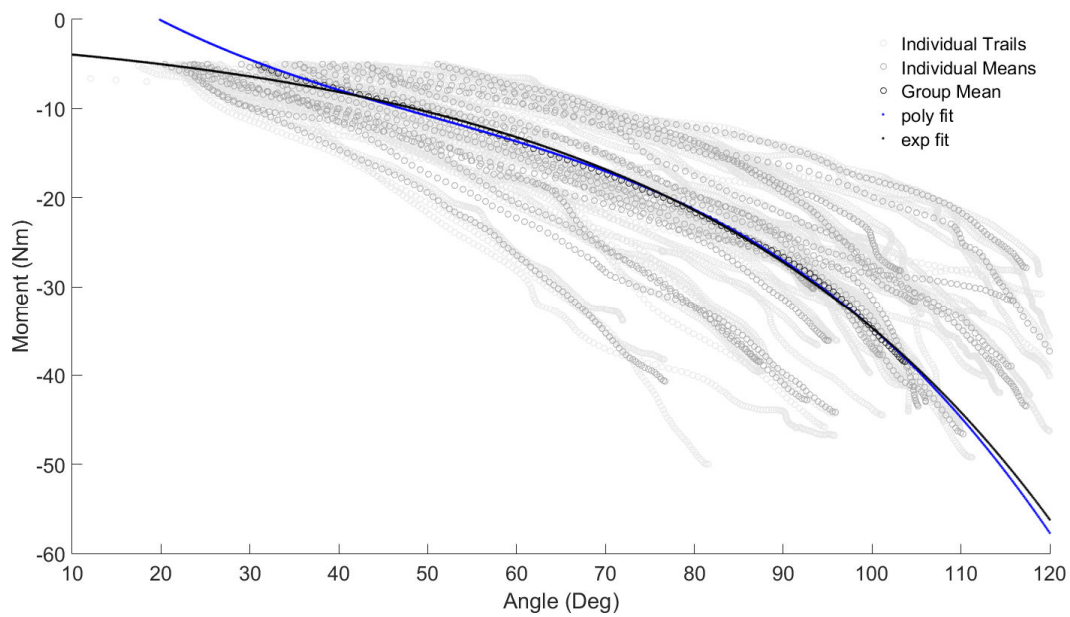


Figure F4: Passive hip resistance male flexion knee bent trials, individual means, and group means with a fitted polynomial and exponential curve to the group mean.

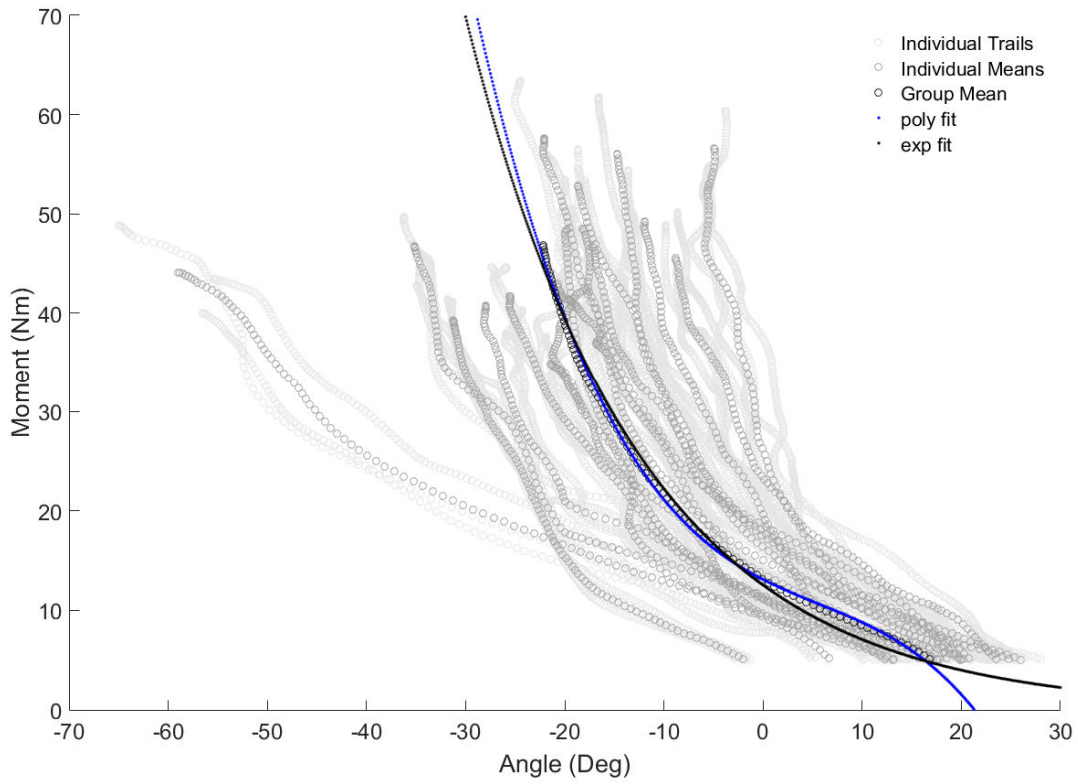


Figure F5: Passive hip resistance male extension trials, individual means, and group means with a fitted polynomial and exponential curve to the group mean.

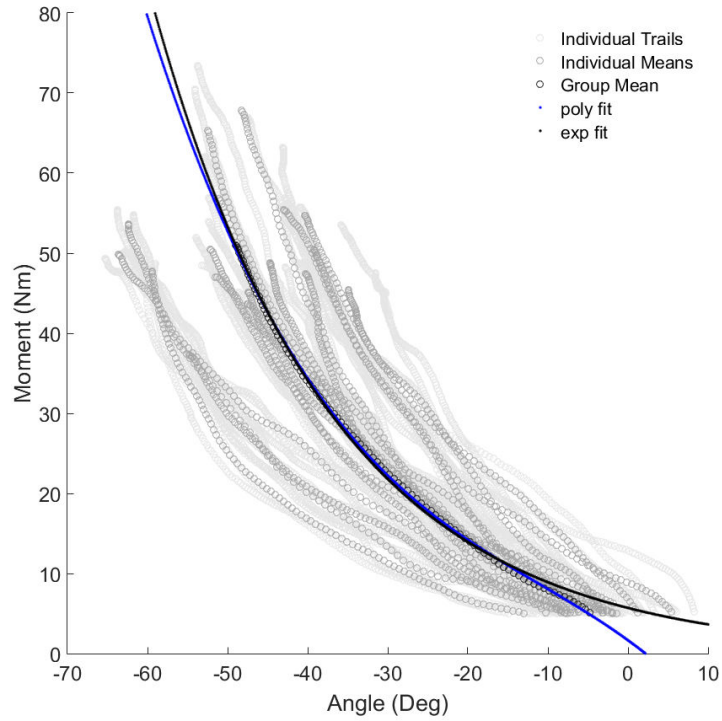


Figure F6: Passive hip resistance male abduction trials, individual means, and group means with a fitted polynomial and exponential curve to the group mean.

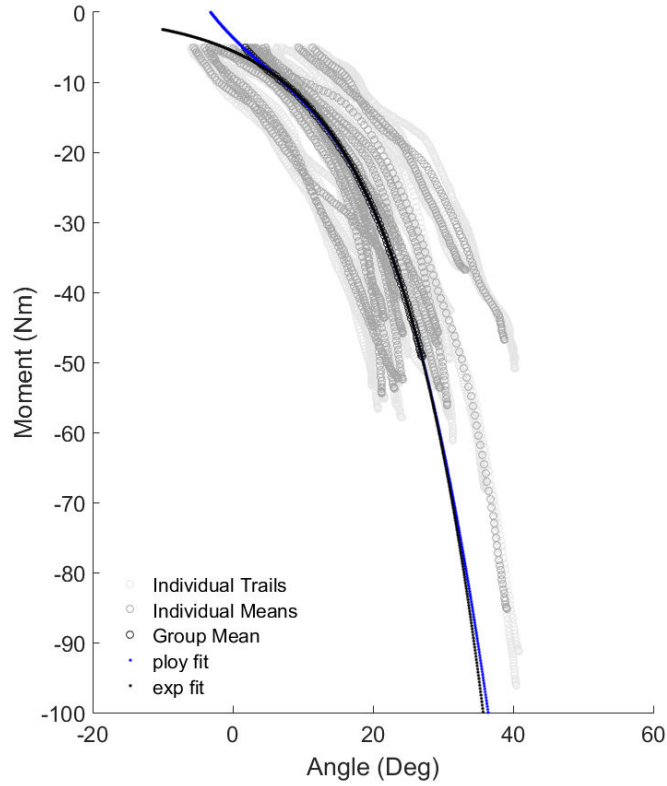


Figure F7: Passive hip resistance male adduction trials, individual means, and group means with a fitted polynomial and exponential curve to the group mean.

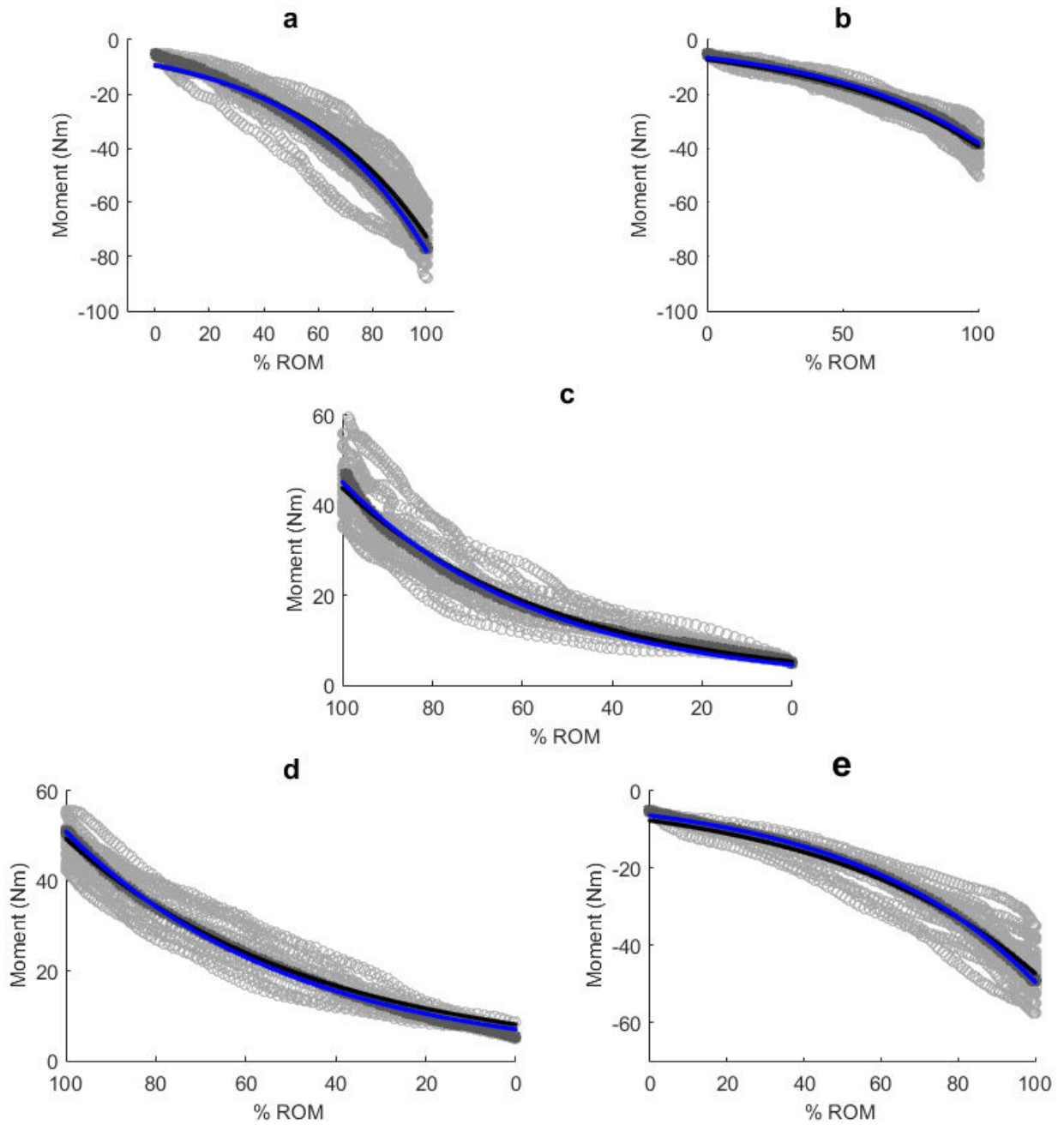


Figure F8: Torque-ROM curves with exponential curves fitted (blue) to the group mean (dark grey) versus the fitted curve (black) to the individual trials (light grey) for (a) FSL, (b) FKB, (c) Ext, (d) Abd, (e) Add.

Table D.1a: Equations of curve fit and goodness of fit measures for mean angle-moment data (males).

	3rd Order Polynomial Equation	sse	R²	rmse
Flexion – Straight Leg	$y = -0.00021647x^3 + 0.018558x^2 - 1.227x + 16.7949$	22.9222	0.9996	0.4861
Flexion – Knee Bent	$y = -8.1018e-05x^3 + 0.012265x^2 - 0.89945x + 13.6145$	9.7673	0.9990	0.3173
Extension	$y = -0.0011079x^3 + 0.018582x^2 - 0.50637x + 13.1141$	26.5175	0.9985	0.5229
Abduction	$y = -0.00036213x^3 - 0.012188x^2 - 0.72577x + 1.6558$	12.5848	0.9994	0.3602
Adduction	$y = -0.0020913x^3 + 0.031476x^2 - 1.0146x - 3.6025$	0.3879	1.0000	0.063
Abduction-Adduction	$y = -0.00041469x^3 - 0.01788x^2 - 0.92876x - 0.72244$	276.2389	0.9985	1.1812

Table D.2: Equations of curve fit and goodness of fit measures for mean moment-ROM data (females).

	3rd Order Polynomial Equation	sse	R²	rmse
Flexion – Straight Leg	$y = -0.00021647x^3 + 0.018558x^2 - 1.227x + 16.7949$	22.9222	0.9996	0.4861
Flexion – Knee Bent	$y = -8.1018e-05x^3 + 0.012265x^2 - 0.89945x + 13.6145$	9.7673	0.9990	0.3173
Extension	$y = -0.0011079x^3 + 0.018582x^2 - 0.50637x + 13.1141$	26.5175	0.9985	0.5229
Abduction	$y = -0.00036213x^3 - 0.012188x^2 - 0.72577x + 1.6558$	12.5848	0.9994	0.3602
Adduction	$y = -0.0020913x^3 + 0.031476x^2 - 1.0146x - 3.6025$	0.3879	1.0000	0.063
Abduction-Adduction	$y = -0.00041469x^3 - 0.01788x^2 - 0.92876x - 0.72244$	276.2389	0.9985	1.1812

Male Passive Hip Resistance Boundaries (N=17)

Sub	Averaged Peak Hip Joint Angle					Averaged NZ Boundary for the Hip				
	FSL_M	FKB_M	EXT_M	ABD_M	ADD_M	FSL_M	FKB_M	EXT_M	ABD_M	ADD_M
S1	89.66	117.36	-19.46	-62.41	23.68	29.85	29.06	17.61	-10.26	-4.03
S2	60.90	92.70	-58.99	-44.66	29.61	11.66	23.72	6.69	-1.84	4.32
S3	62.59	76.70	-22.35	-39.25	20.20	26.14	22.67	18.56	-6.11	-5.53
S4	85.86	115.90	-25.58	-63.67	22.92	14.38	24.15	15.70	-8.39	-3.32
S5	65.06	87.40	-20.99	-35.02	22.27	17.43	23.30	17.81	-3.19	2.66
S6	83.08	95.10	-35.19	-47.58	24.33	18.68	25.22	13.25	-6.66	2.33
S7	66.82	93.43	-31.24	-52.14	23.39	17.50	23.75	-1.96	-7.93	0.12
S8	81.28	103.19	-21.51	-40.25	33.16	26.70	33.94	13.09	-1.44	9.44
S9	76.73	100.85	-19.84	-51.55	29.34	14.23	20.45	12.30	-1.99	1.80
S10	80.74	115.66	-17.31	-43.04	38.79	29.12	30.66	24.82	5.45	11.41
S11	92.24	105.27	-14.67	-52.45	39.11	21.16	30.64	20.78	-3.08	3.28
S12	101.76	125.22	-11.97	-48.32	23.03	34.24	39.38	20.32	-7.82	-1.99
S13	70.37	95.87	-6.04	-40.34	24.24	25.71	31.77	19.89	1.20	2.87
S14	110.51	117.31	-28.45	-54.76	23.60	33.39	38.14	17.52	-7.68	2.36
S15	84.74	110.24	-18.65	-47.43	29.12	21.11	43.27	20.19	-7.23	2.39
S16	85.67	104.83	-18.20	-59.47	21.32	36.75	51.08	26.04	-12.97	-2.85
S17	80.38	106.07	-8.86	-51.06	30.62	25.26	35.65	23.50	-1.99	3.31

Female Passive Hip Resistance Boundaries (N=15)

Sub	Averaged Peak Hip Joint Angle					Averaged NZ Boundary for the Hip				
	FSL_F	FKB_F	EXT_F	ABD_F	ADD_F	FSL_F	FKB_F	EXT_F	ABD_F	ADD_F
S1	73.43	92.88	-24.02	-59.78	54.46	7.02	10.65	4.68	1.90	14.24
S2	94.79	115.74	-16.99	-39.58	33.28	8.67	29.73	9.09	3.28	13.08
S3	109.30	120.31	-20.72	-47.90	48.05	24.73	34.47	15.71	-7.34	16.67
S4	109.26	109.58	-33.58	-82.27	32.76	4.26	16.02	-5.57	-20.52	-5.41
S5	110.80	119.07	-26.41	-45.35	38.59	27.27	44.96	4.18	-3.33	13.29
S6	121.61	115.86	-19.38	-65.81	38.77	7.81	23.38	9.21	1.16	10.96
S7	106.76	103.55	-27.42	-42.77	45.02	24.87	24.15	-0.10	-4.45	11.23
S8	104.73	103.05	-23.58	-36.09	42.65	17.23	16.90	6.94	4.57	10.63
S9	94.11	104.54	-37.54	-54.98	43.14	5.37	21.79	0.45	-6.28	6.34
S10	107.82	104.70	-26.90	-61.64	25.24	25.43	34.62	-0.37	-13.05	10.66
S11	115.94	121.86	-23.58	-56.68	28.48	31.63	48.86	6.93	-14.29	6.92
S12	95.65	117.65	-18.72	-53.84	42.72	24.84	37.19	10.30	0.23	15.62
S13	112.91	117.26	-9.64	-52.91	31.85	30.74	40.87	5.42	-8.02	8.28
S14	103.93	112.38	-20.90	-47.49	38.88	20.60	31.17	17.50	1.35	13.31
S15	89.25	125.51	-18.14	-45.47	34.57	19.32	28.48	8.45	-4.32	5.96

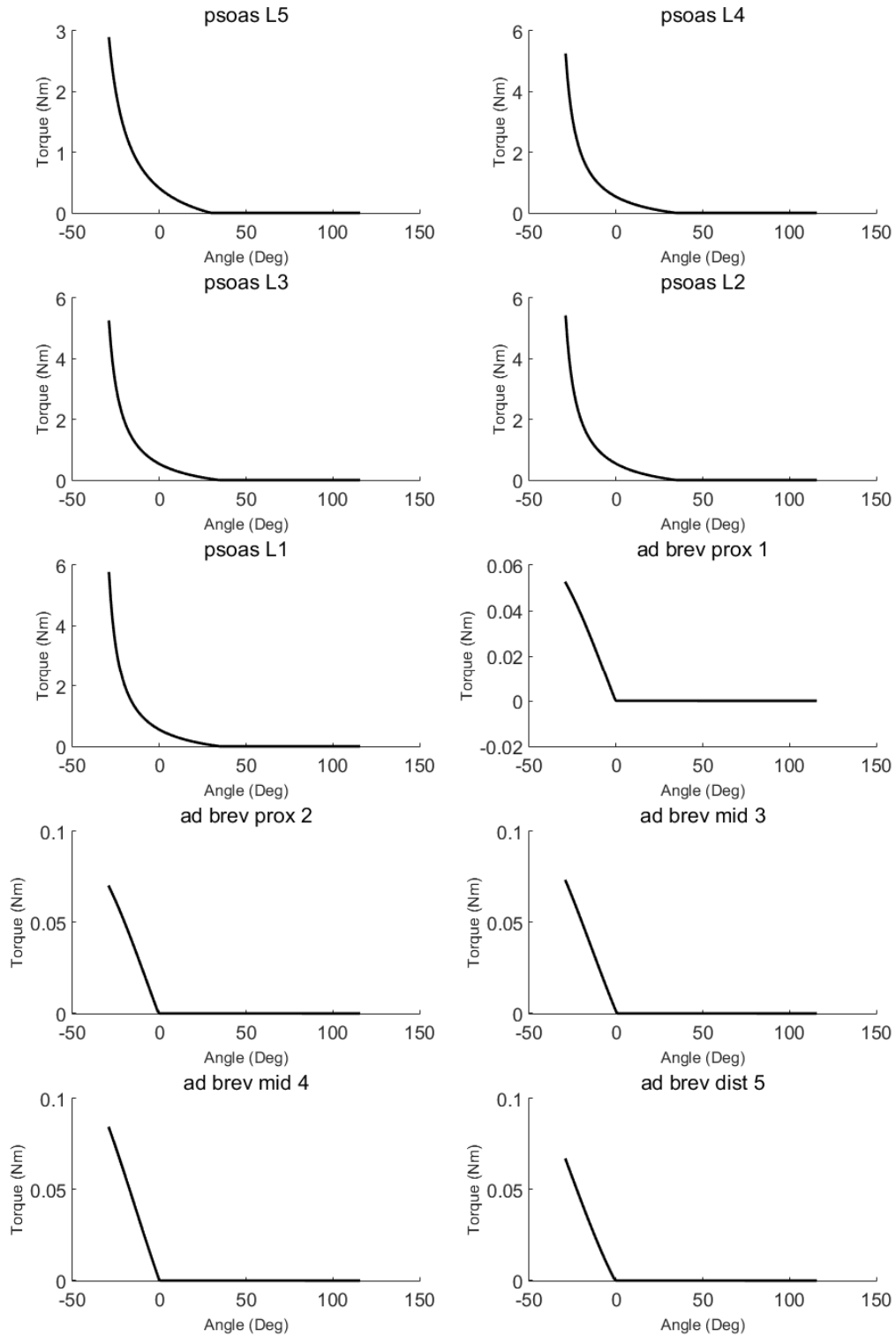


Figure F9: Flexion (straight leg) - extension passive torque-angle curves with respective contribution from Psoas (5) and Adductor Brevis (5).

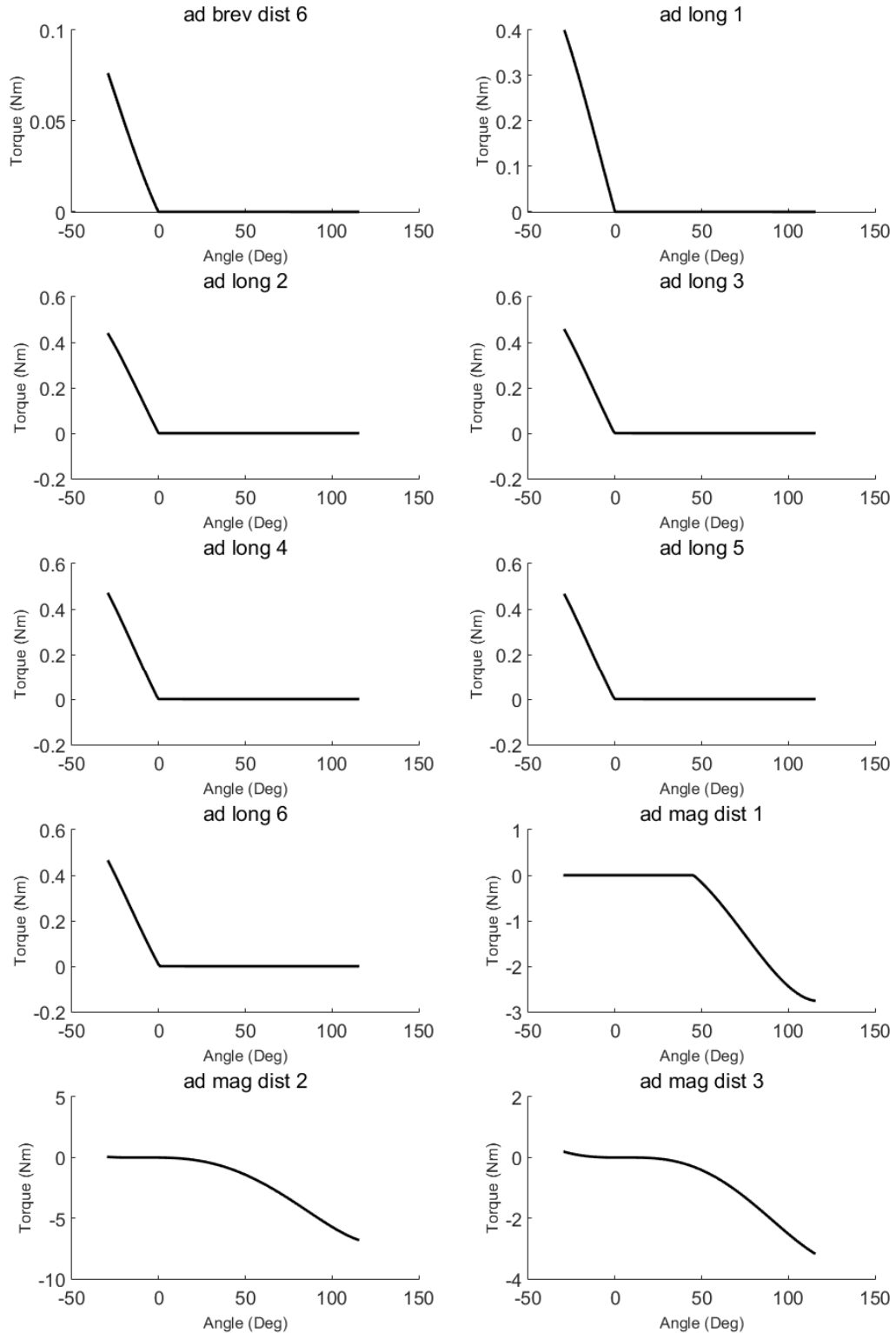


Figure F10: Flexion (straight leg) - extension passive torque-angle curves with respective contribution from Adductor Brevis (1), Adductor Longus (6), and Adductor Magnus (3).

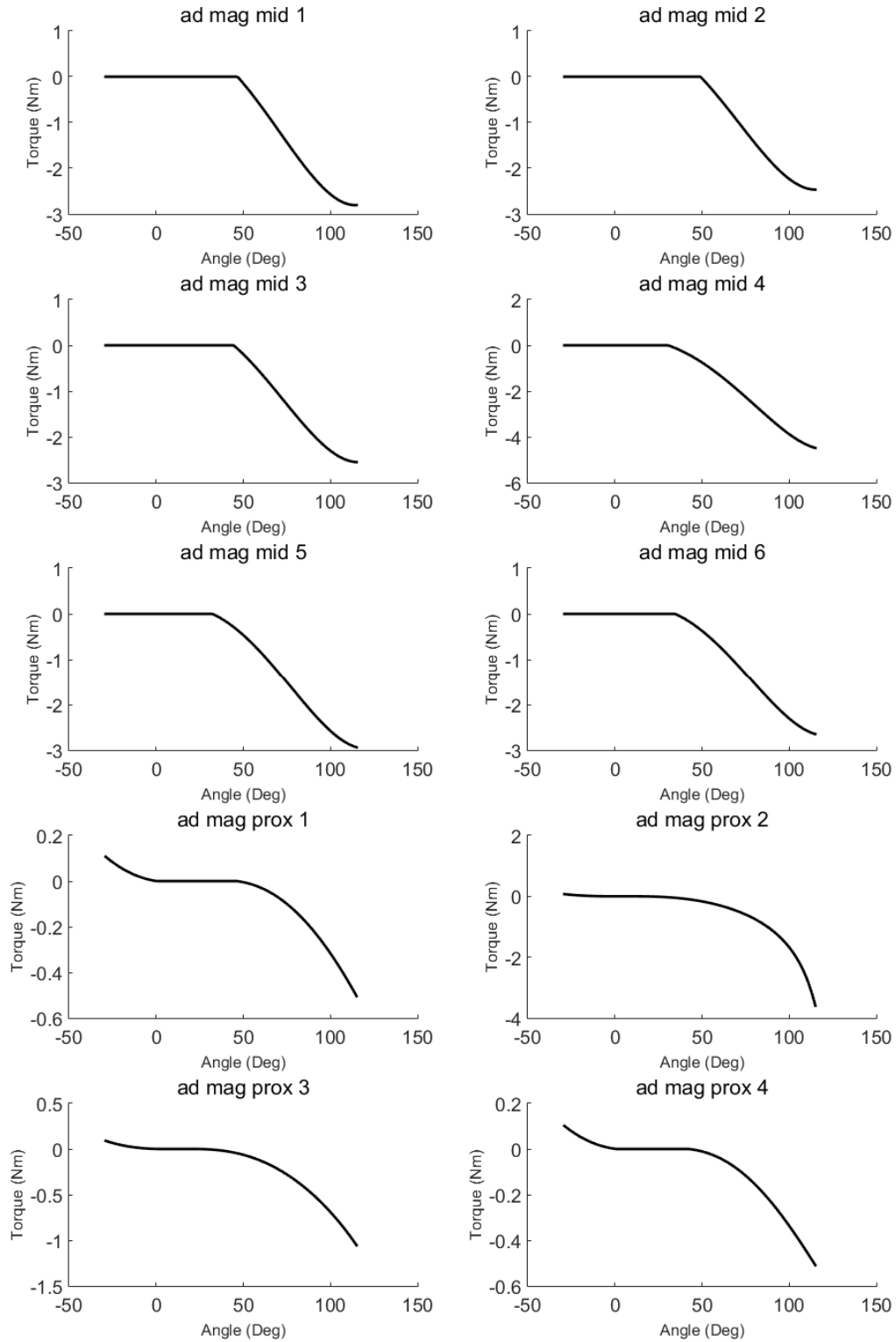


Figure F11: Flexion (straight leg) - extension passive torque-angle curves with respective contribution from Adductor Magnus (10).

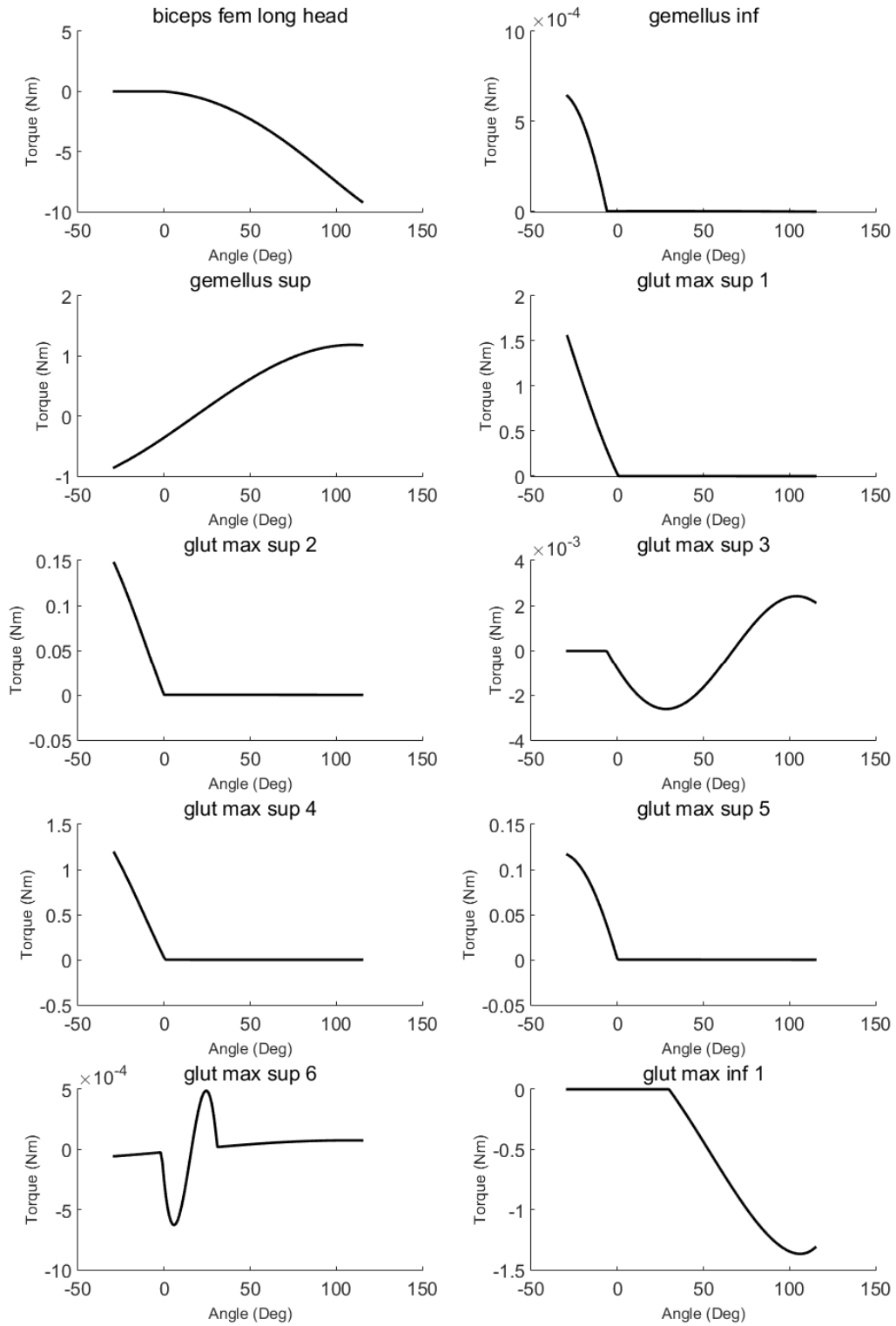


Figure F12: Flexion (straight leg) - extension passive torque-angle curves with respective contribution from Biceps Femoris, Gemellus (2), and Gluteus Maximus (7).

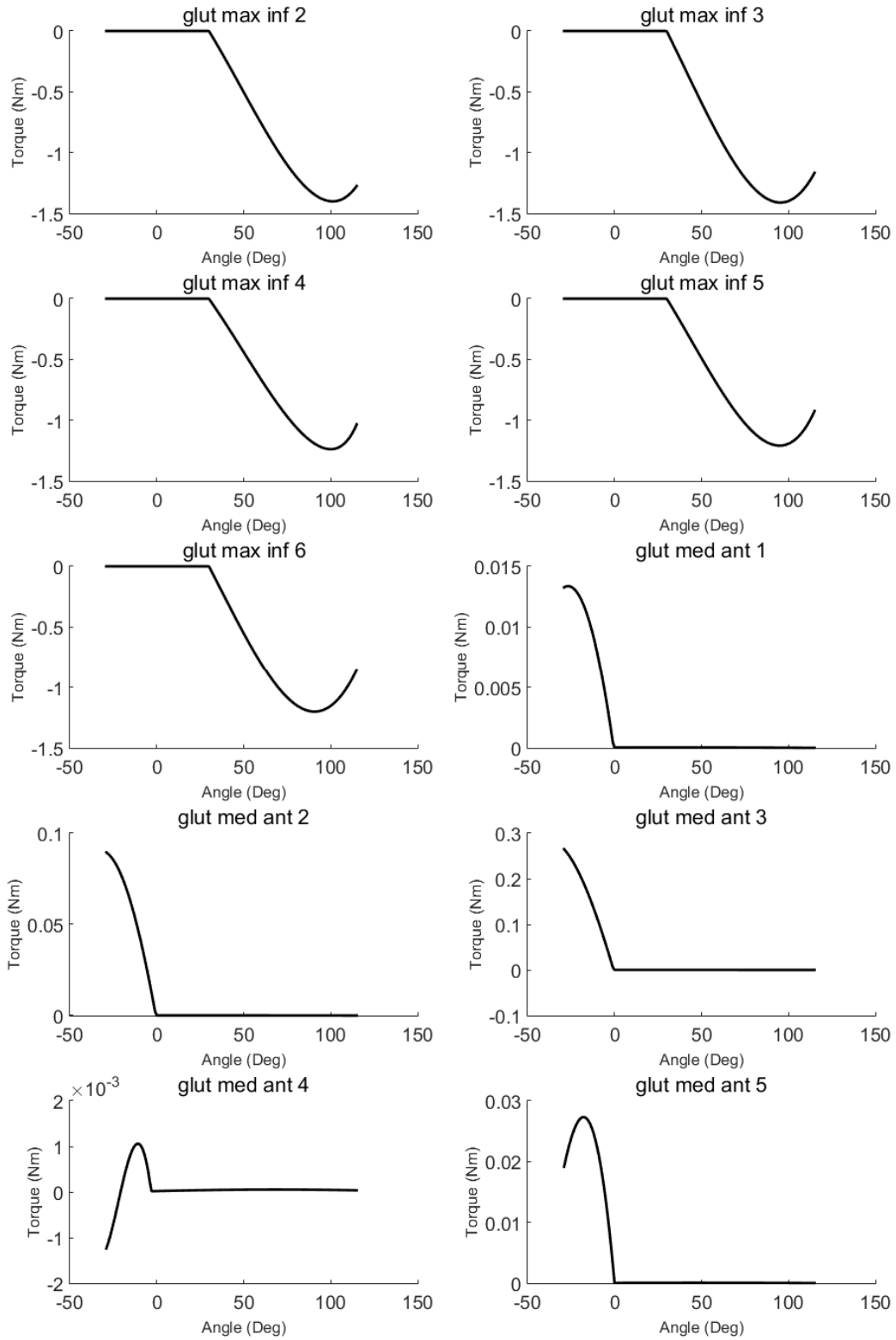


Figure F13: Flexion (straight leg) - extension passive torque-angle curves with respective contribution from Gluteus Maximus (5) and Gluteus Medius (5).

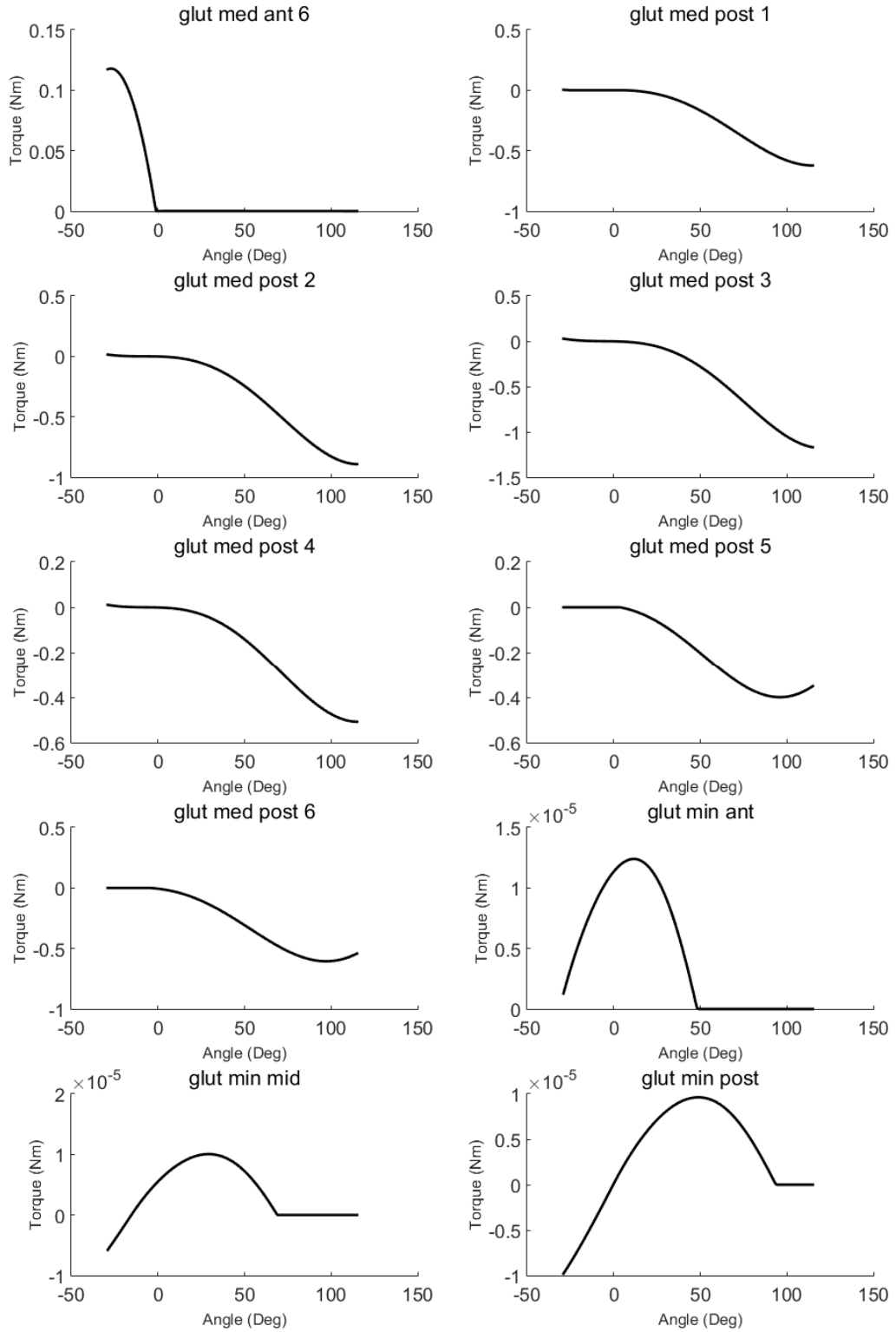


Figure F14: Flexion (straight leg) - extension passive torque-angle curves with respective contribution from Gluteus Medius (7), and Gluteus Minimus (3).

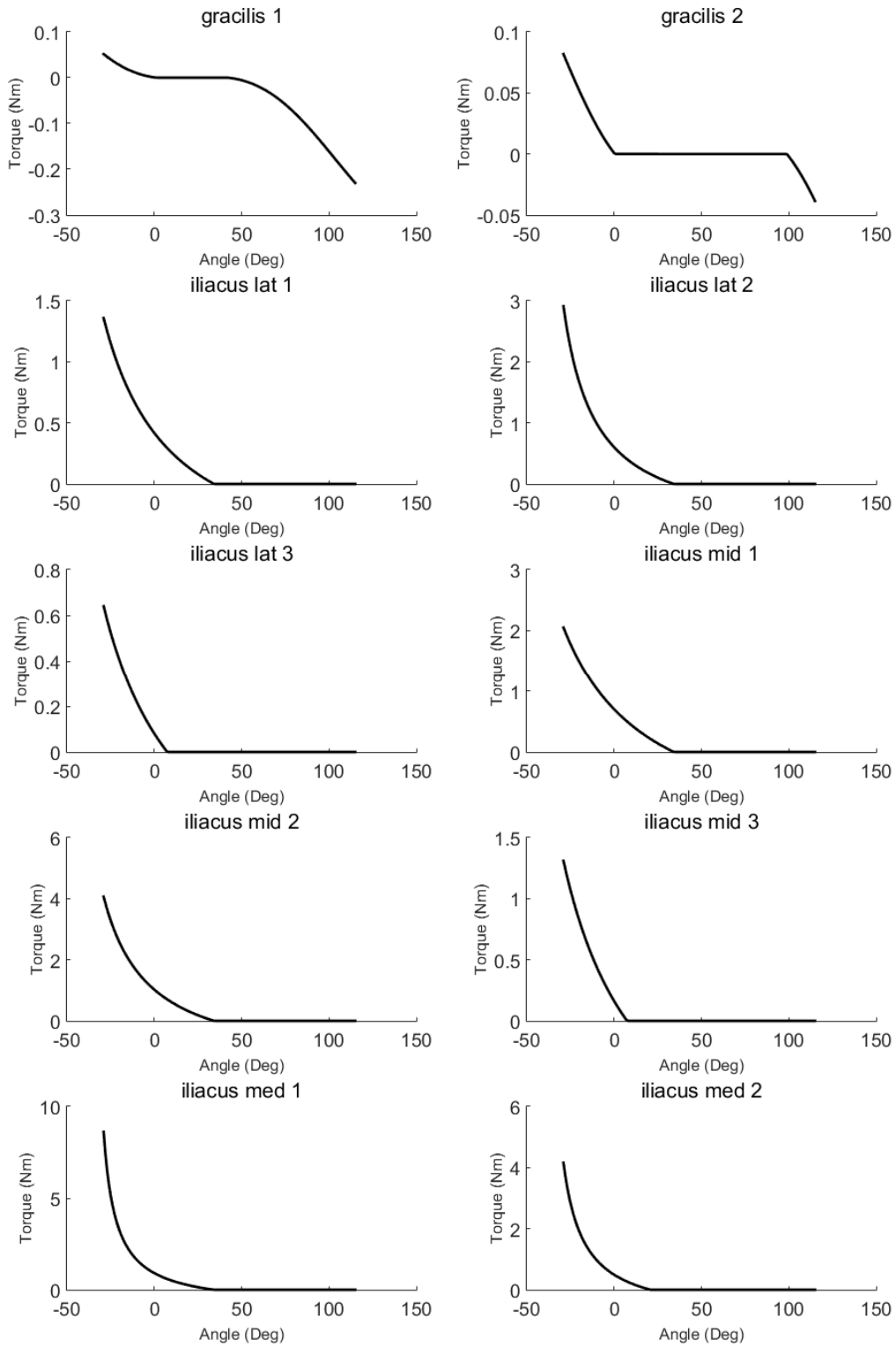


Figure F15: Flexion (straight leg) - extension passive torque-angle curves with respective contribution from Gracilis (2) and Iliacus (8).

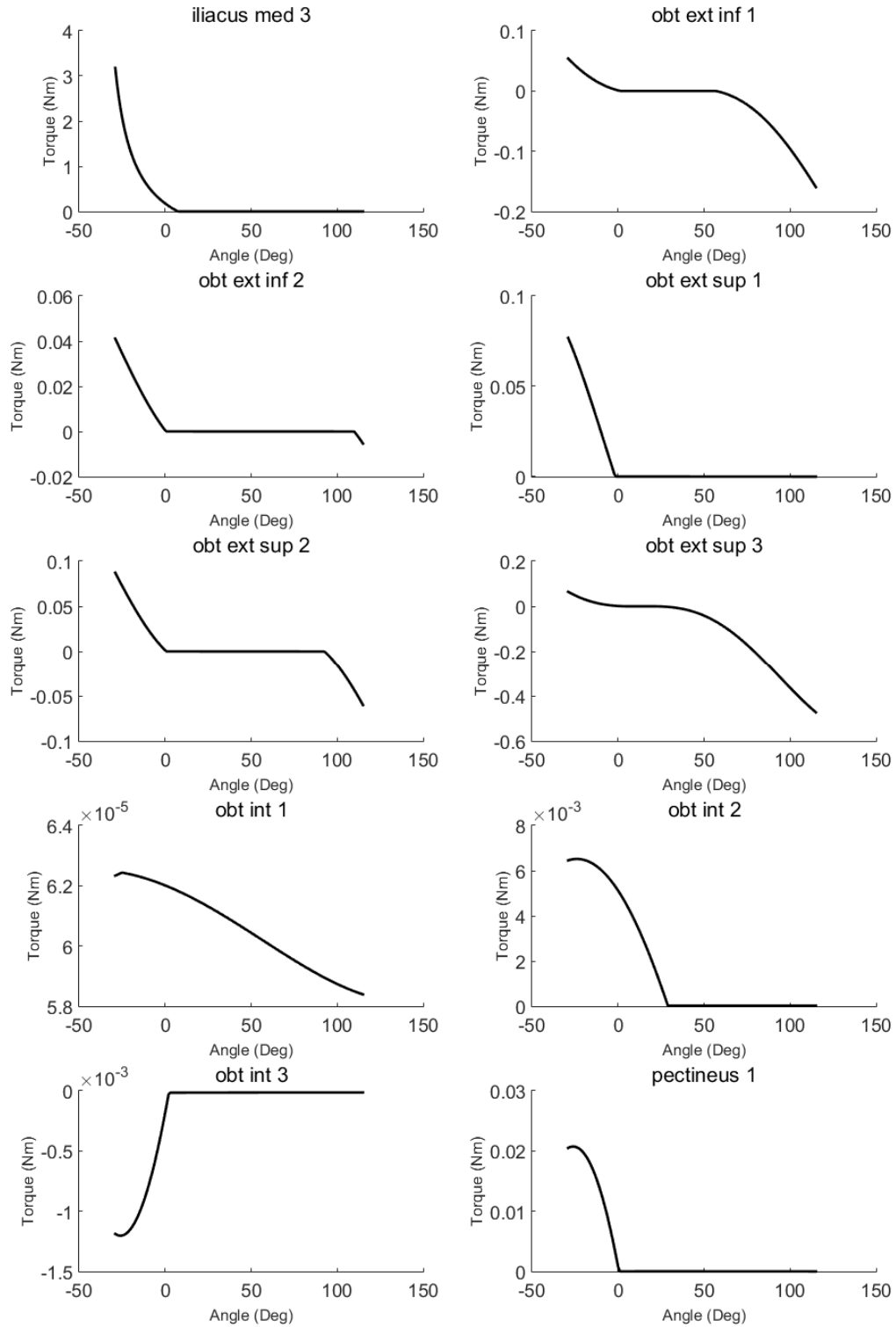


Figure F16: Flexion (straight leg) - extension passive torque-angle curves with respective contribution from Iliacus (1), Obturator Externus (5), Obturator Internus (3), and Pectineus (1).

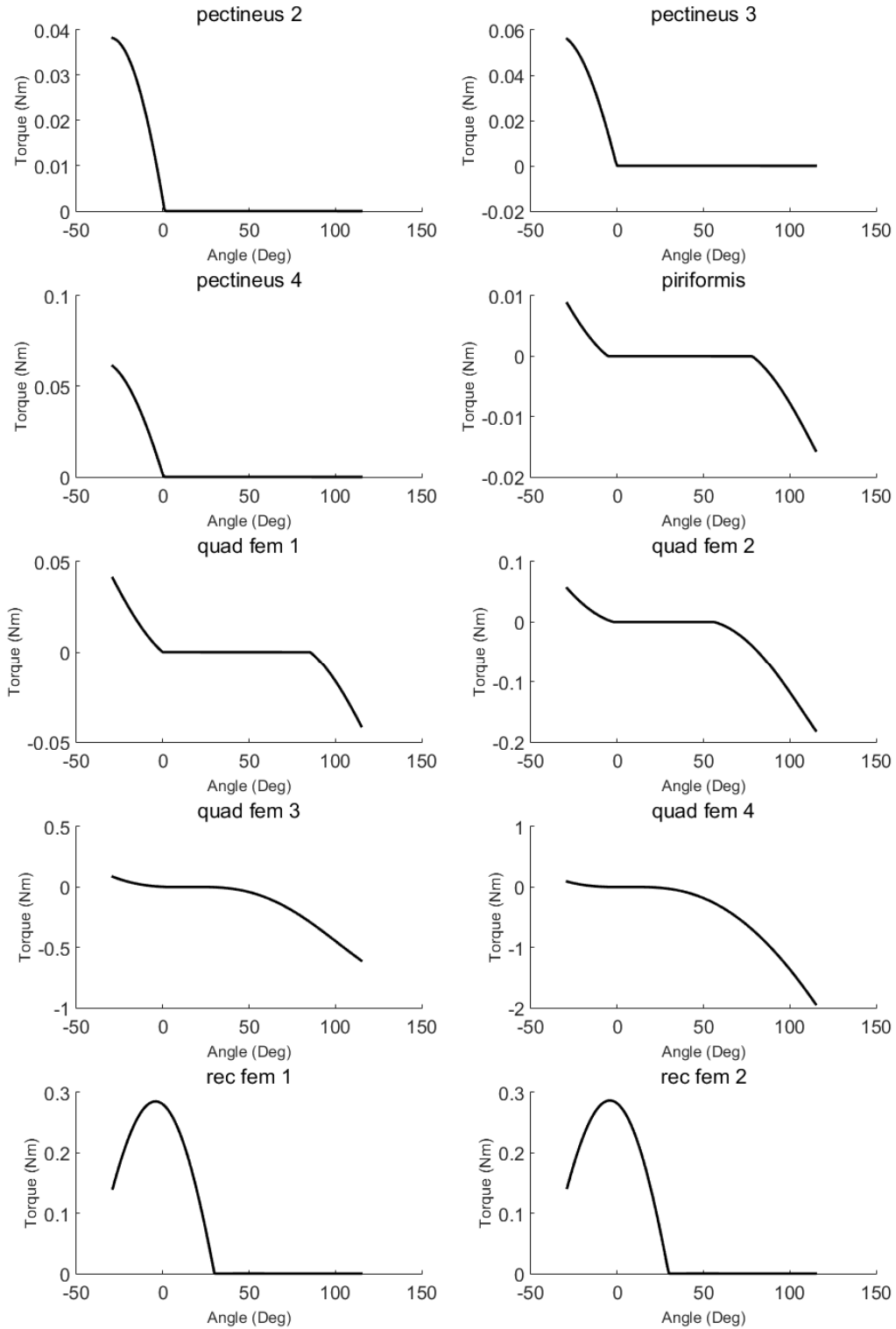


Figure F17: Flexion (straight leg) - extension passive torque-angle curves with respective contribution from Pectineus (3), Piriformis (1), Quadratus Femoris (4), and Recuts Femoris (2).

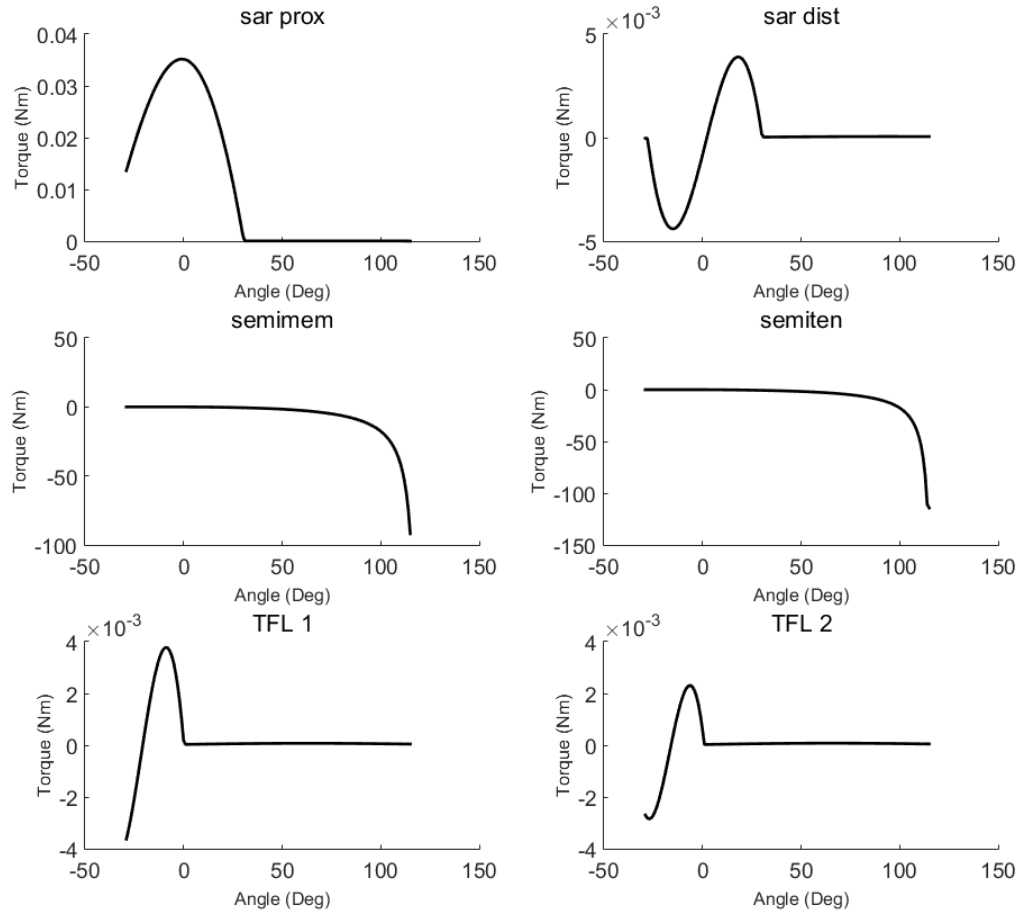


Figure F18: Flexion (straight leg) - extension passive torque-angle curves with respective contribution from Sartorius (2), Semimembranosus, Semitendinosus, and Tensor Fasciae Latae (2).

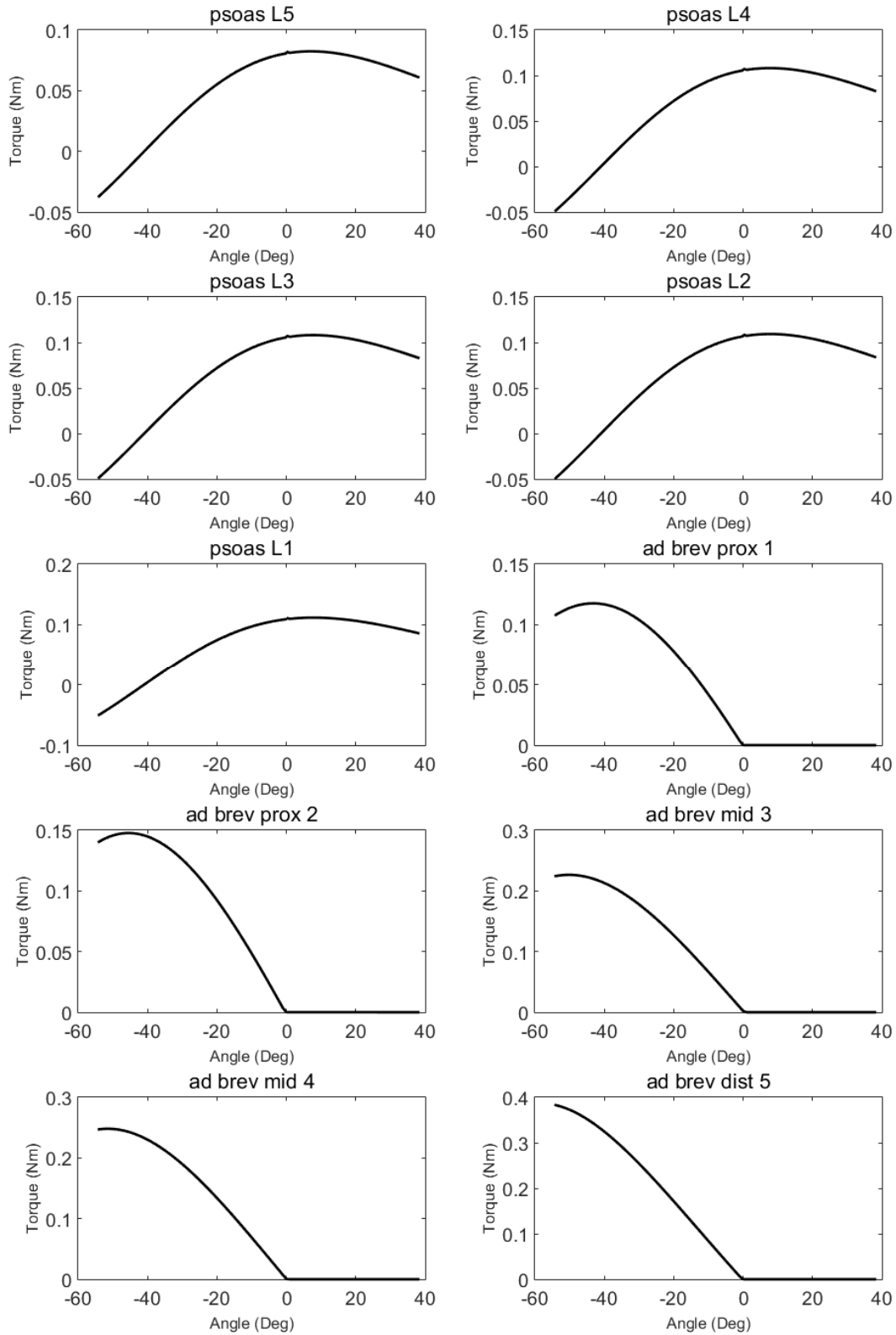


Figure F19: Abduction – Adduction passive torque-angle curves with respective contribution from Psoas (5) and Adductor Brevis (5).

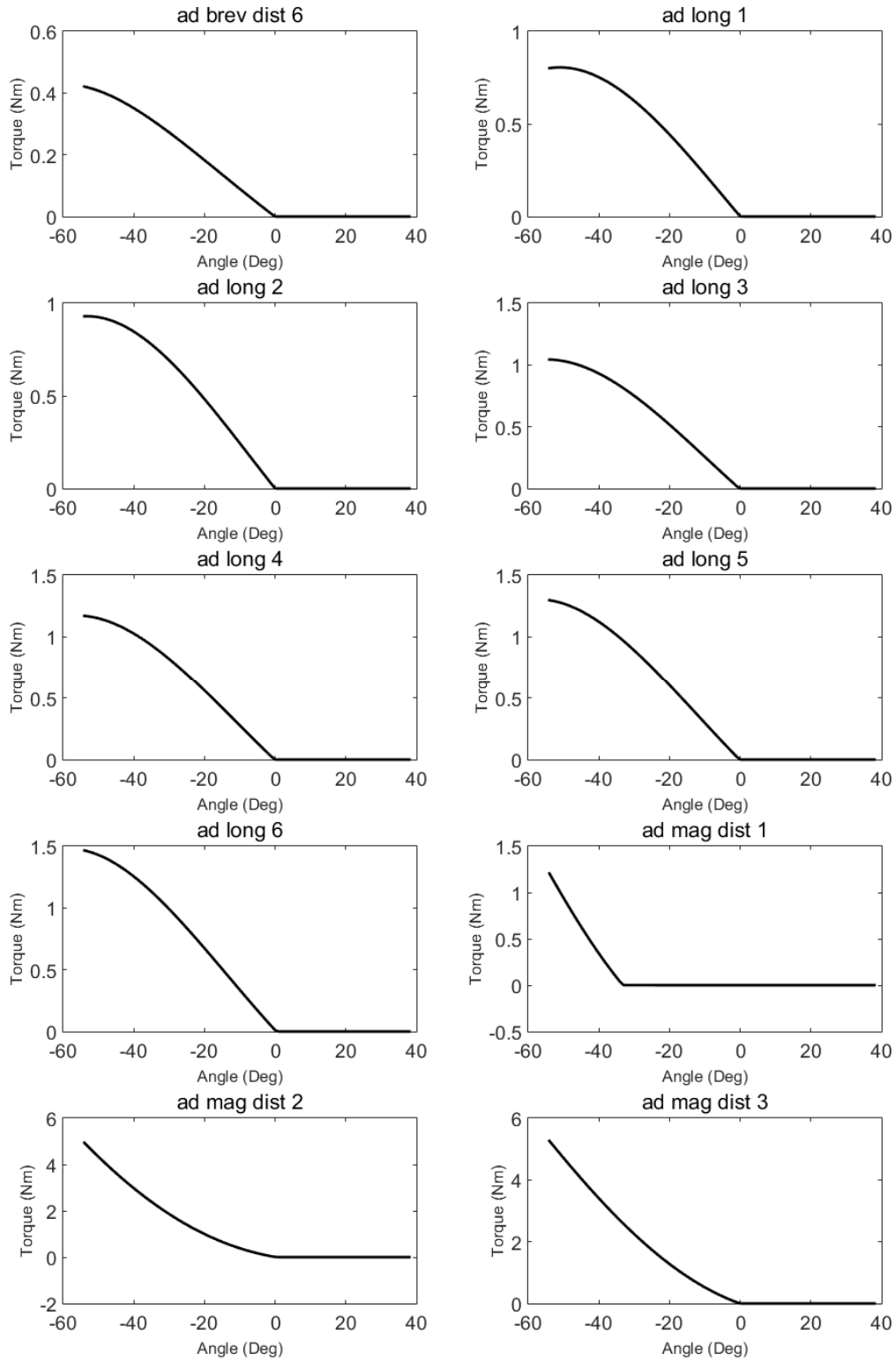


Figure F20: Abduction – Adduction passive torque-angle curves with respective contribution from Adductor Brevis (1), Adductor Longus (6), and Adductor Magnus (3).

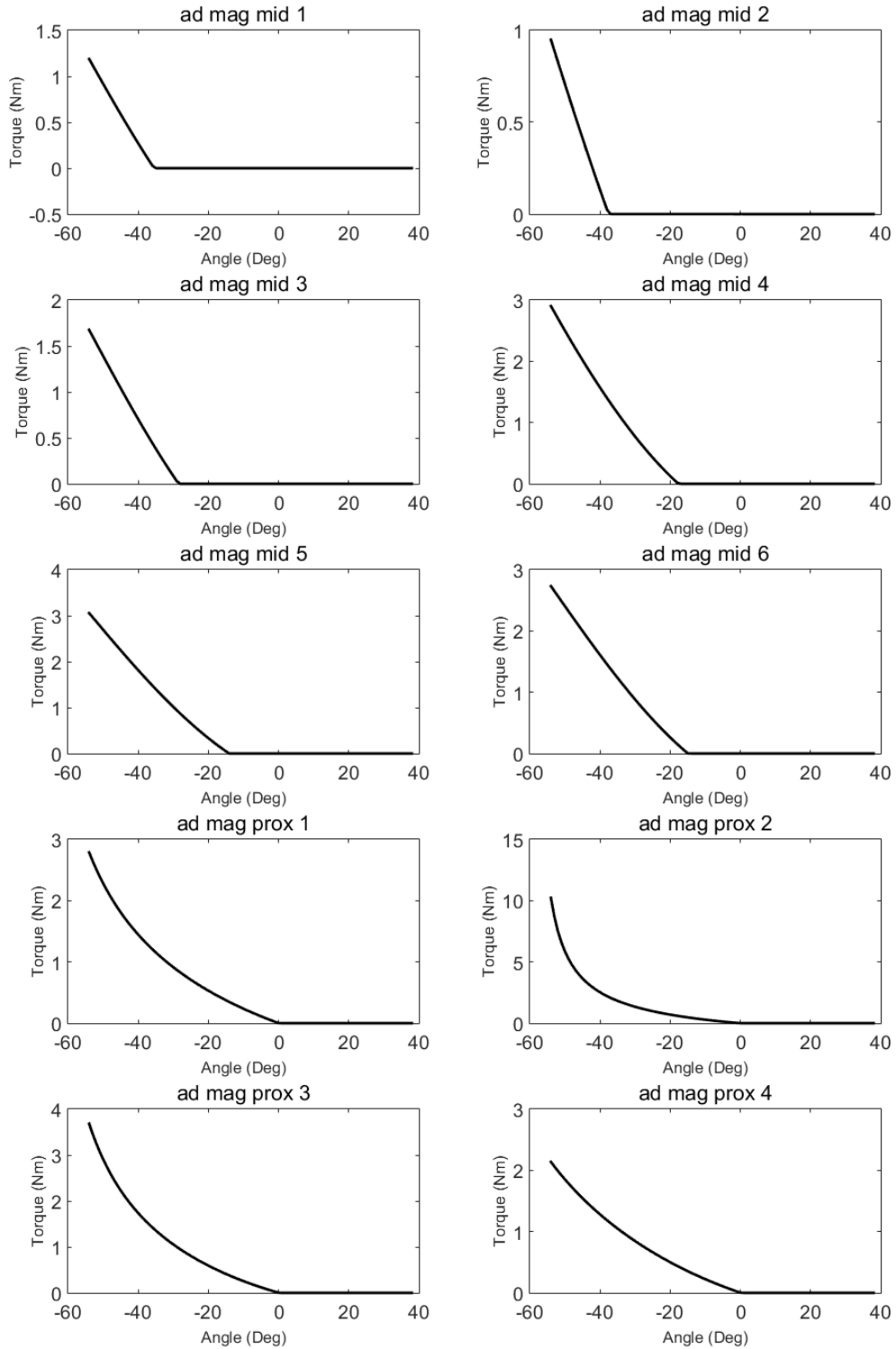


Figure F21: Abduction – Adduction passive torque-angle curves with respective contribution from Adductor Magnus (10).

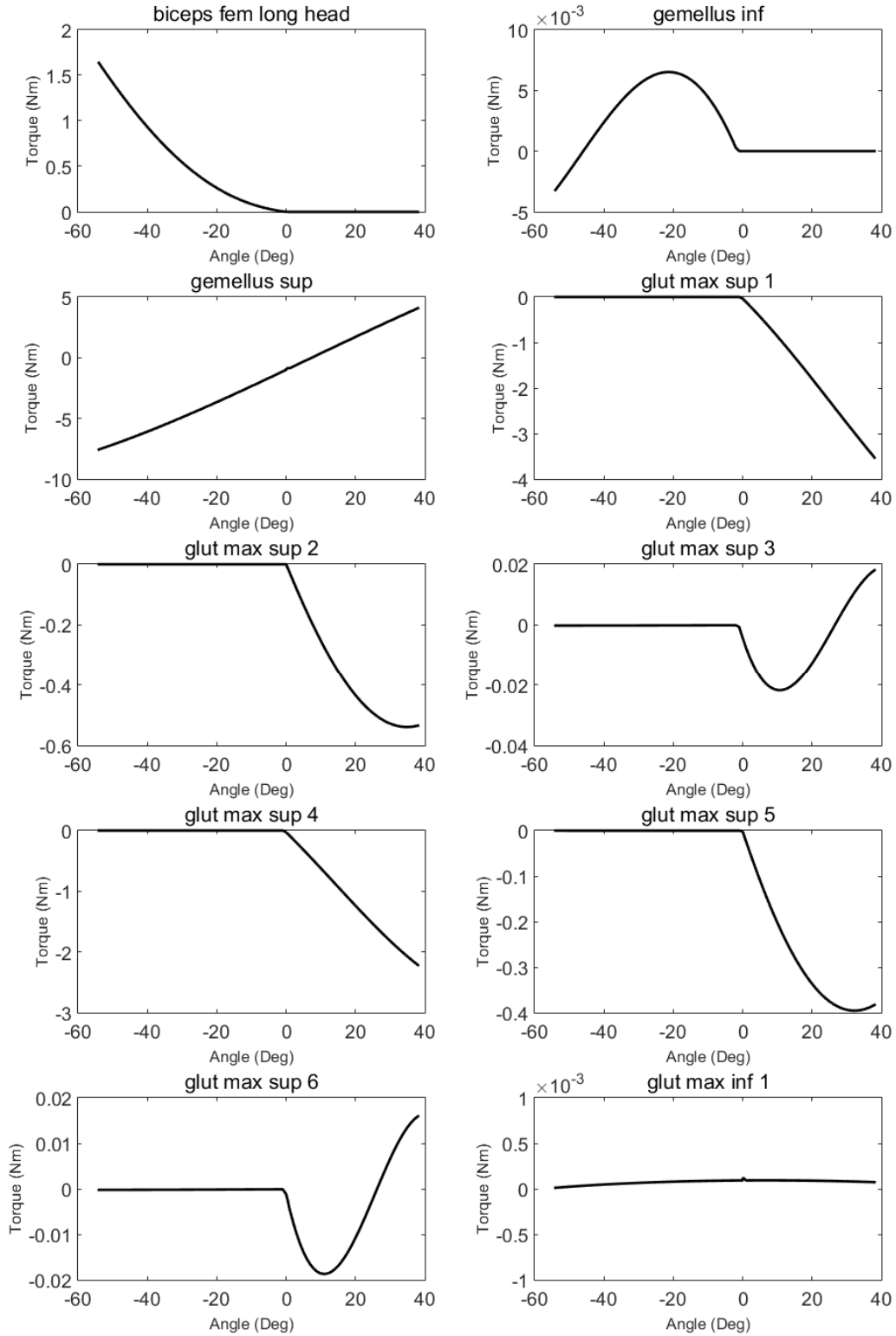


Figure F22: Abduction – Adduction passive torque-angle curves with respective contribution from Biceps Femoris, Gemellus (2), Gluteus Maximums (7).

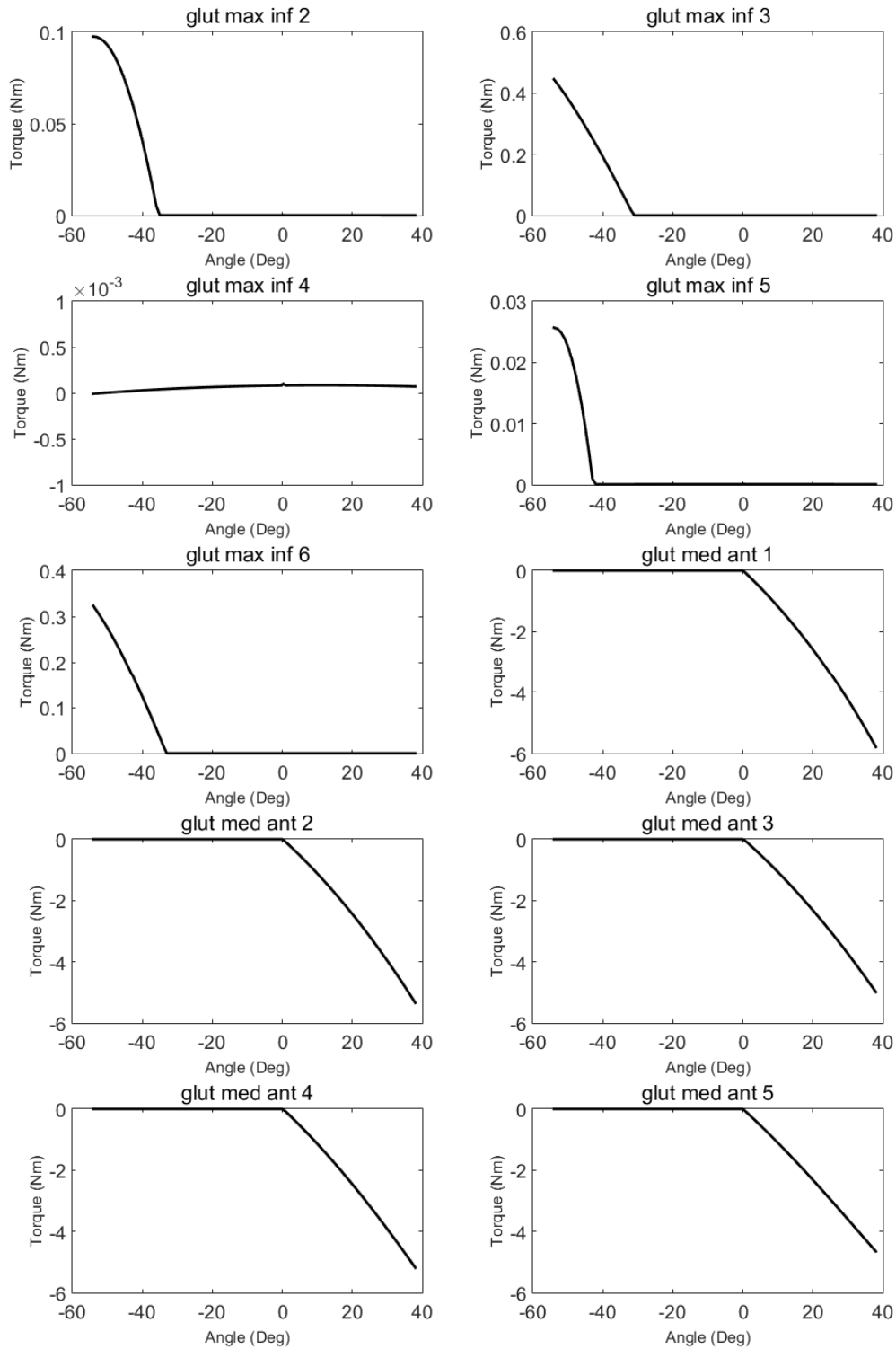


Figure F23: Abduction – Adduction passive torque-angle curves with respective contribution from Gluteus Maximus (5), and Gluteus Medius (5).

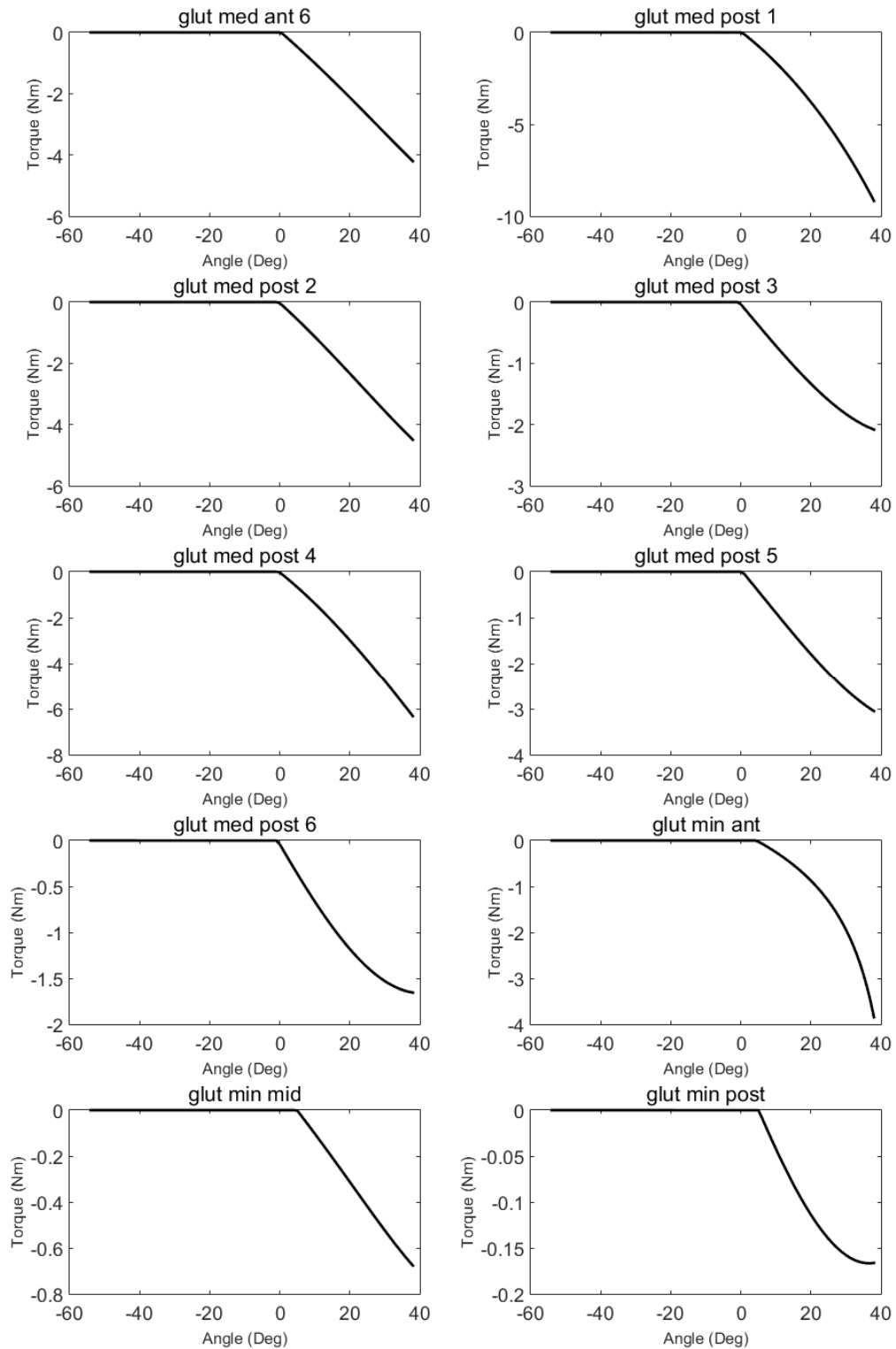


Figure F24: Abduction – Adduction passive torque-angle curves with respective contribution from Gluteus Medius (7), and Gluteus Minimus (3).

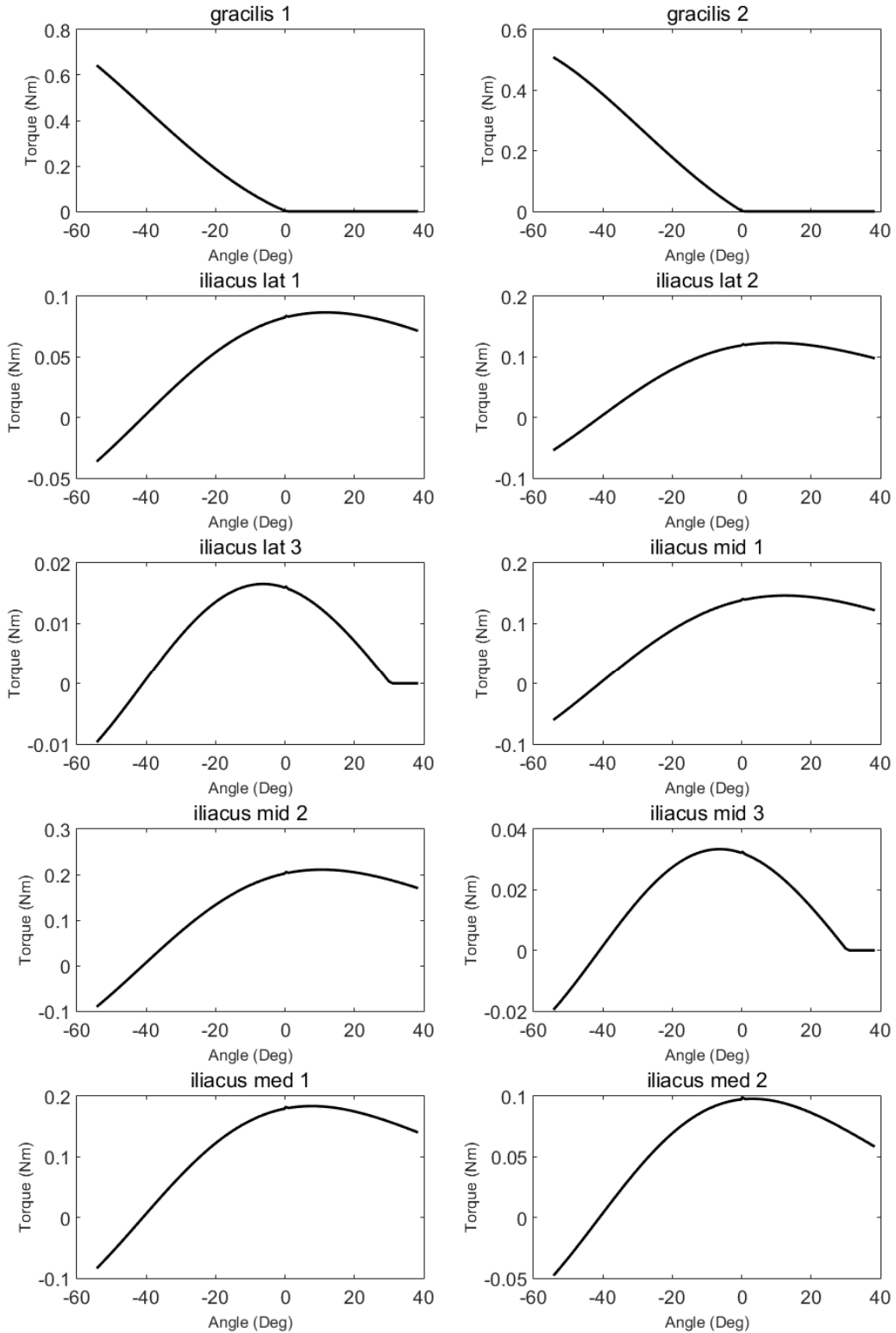


Figure F25: Abduction – Adduction passive torque-angle curves with respective contribution from Gracilis (2) and Iliacus (8).

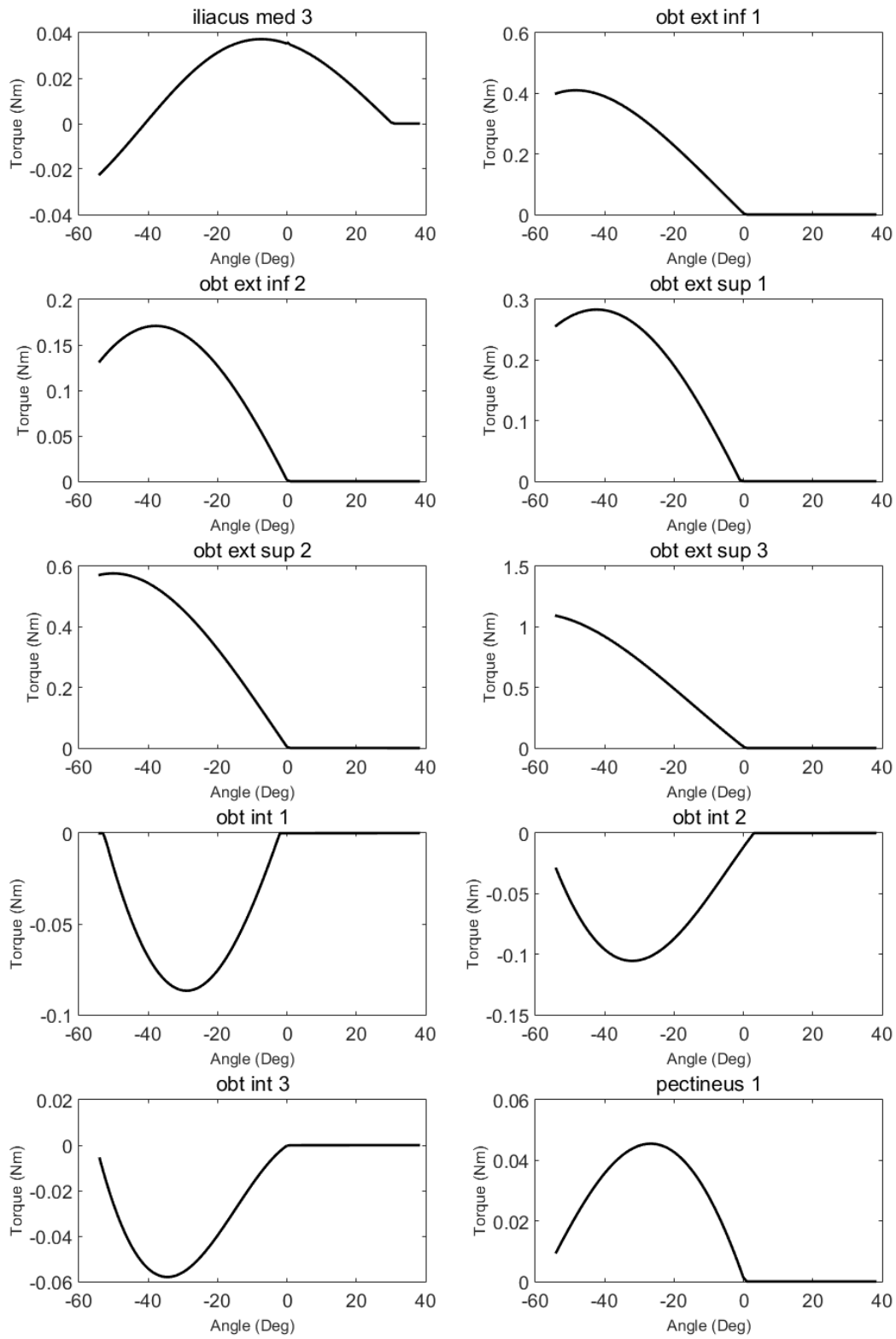


Figure F26: Abduction – Adduction passive torque-angle curves with respective contribution from Iliacus (1), Obturator Externus (4) and Pectineus (1).

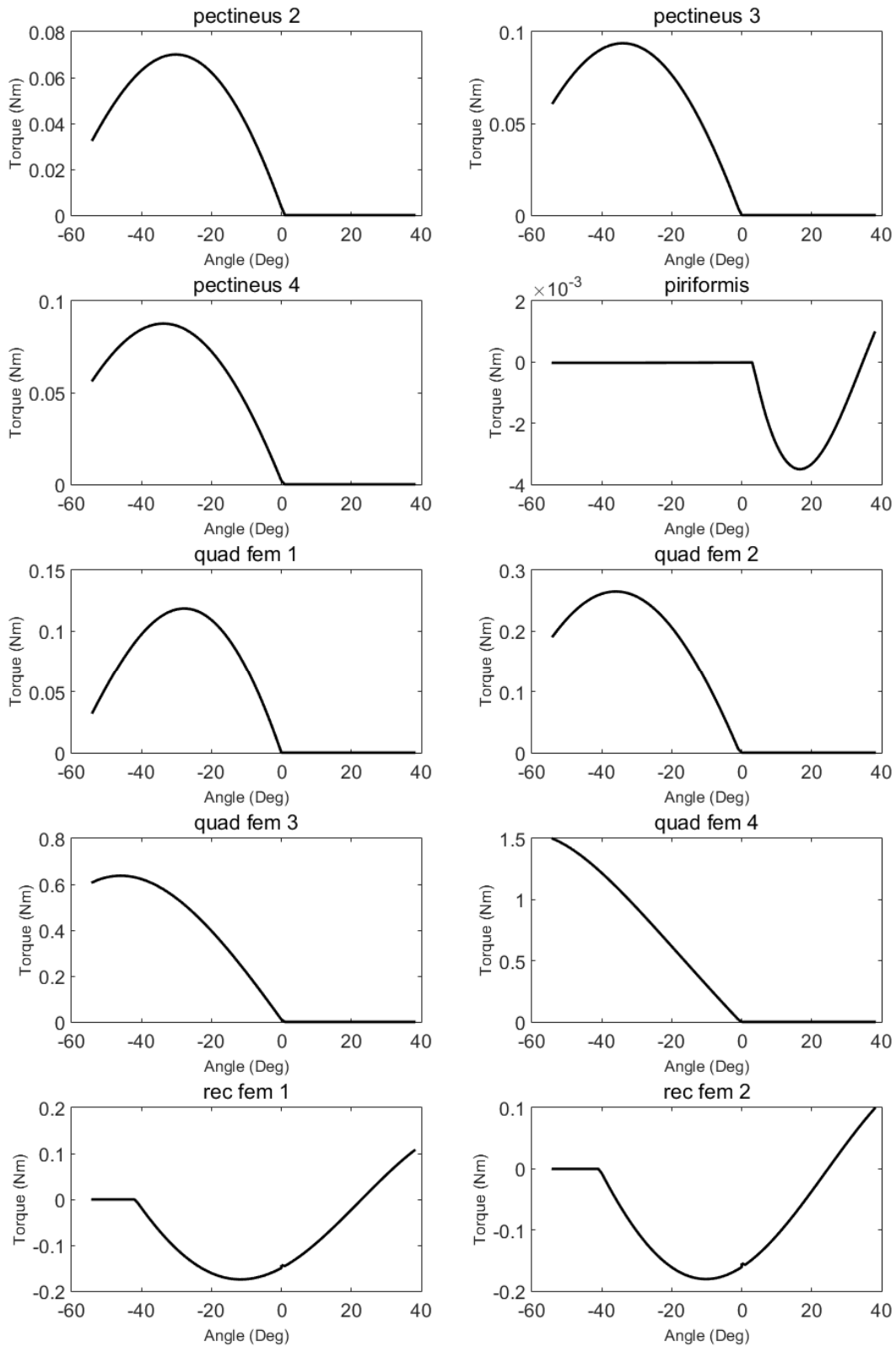


Figure F27: Abduction – Adduction passive torque-angle curves with respective contribution from Pectineus (2), Piriformis, Quadratus Femoris (4), and Rectus Femoris (2).

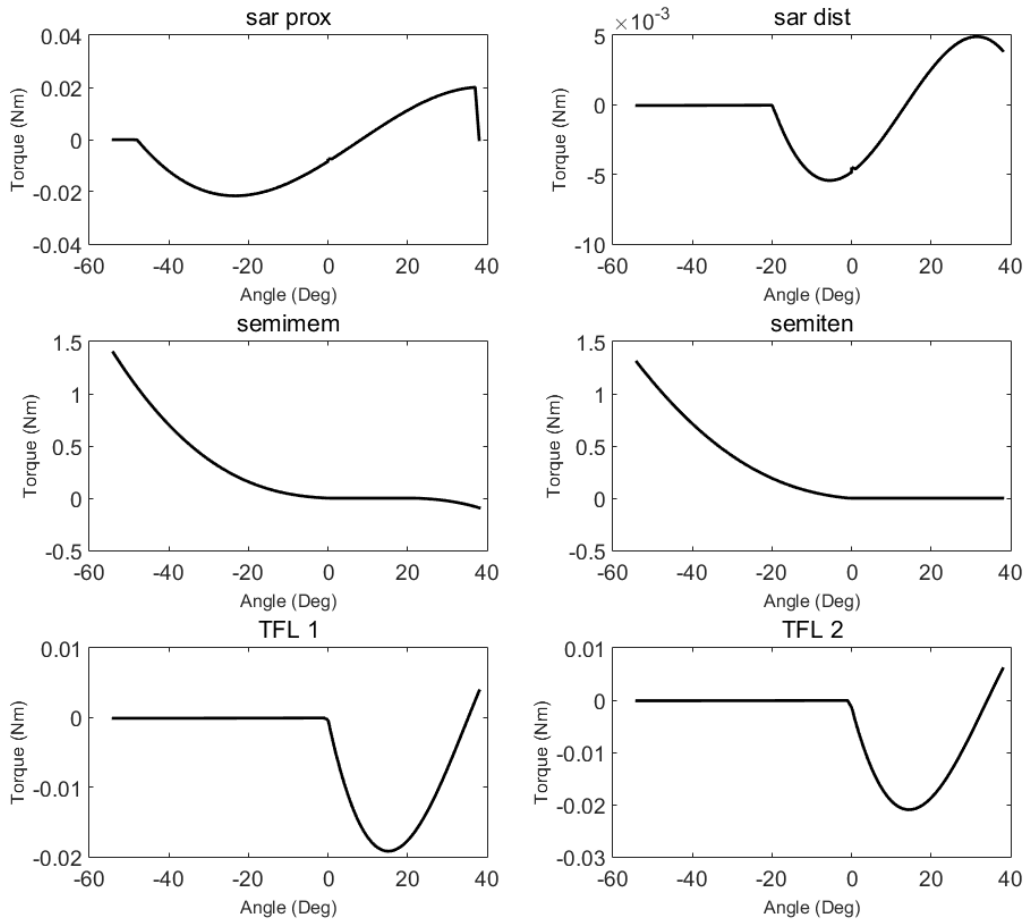


Figure F28: Abduction – Adduction passive torque-angle curves with respective contribution from Sartorius (2), Semimembranosus, Semitendinosus, and Tensor Fasciae Latae.

Appendix G: Data from ACL study – Tuning the Model

Example of ACL-S01 Right Hip Moment predictions based on Inverse dynamics (blue) and HSM (red). Muscle gain for this subject was set to 1.23, 1.18 and 0.81 for this subject's right hip, left hip and lumbar spine, respectively.

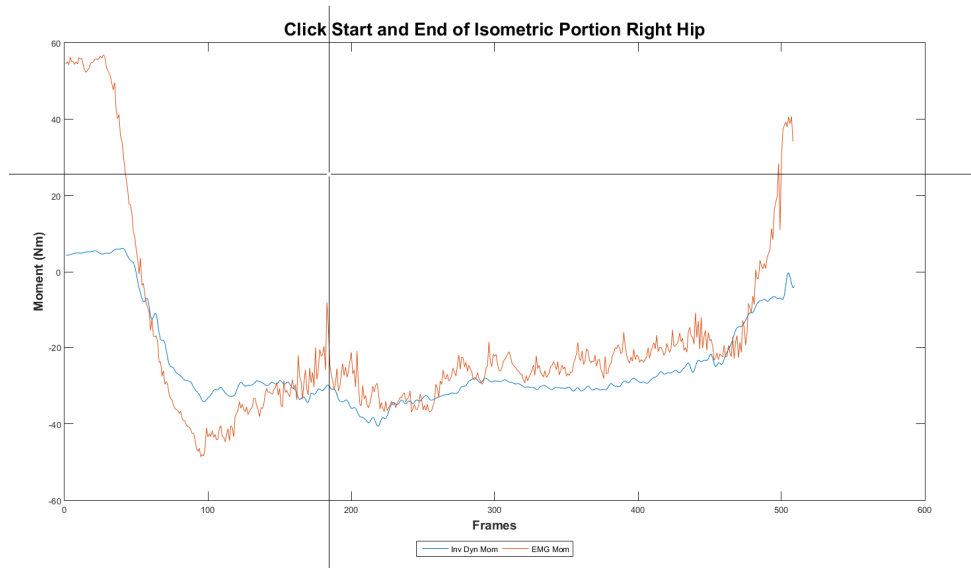


Figure G.1: Screen capture of RVC 2 trial MATLAB program allows user selected points to isolate stabilized section of RVC to calculate gain factor based on inverse dynamics and HSM predictions of right hip extension moment.

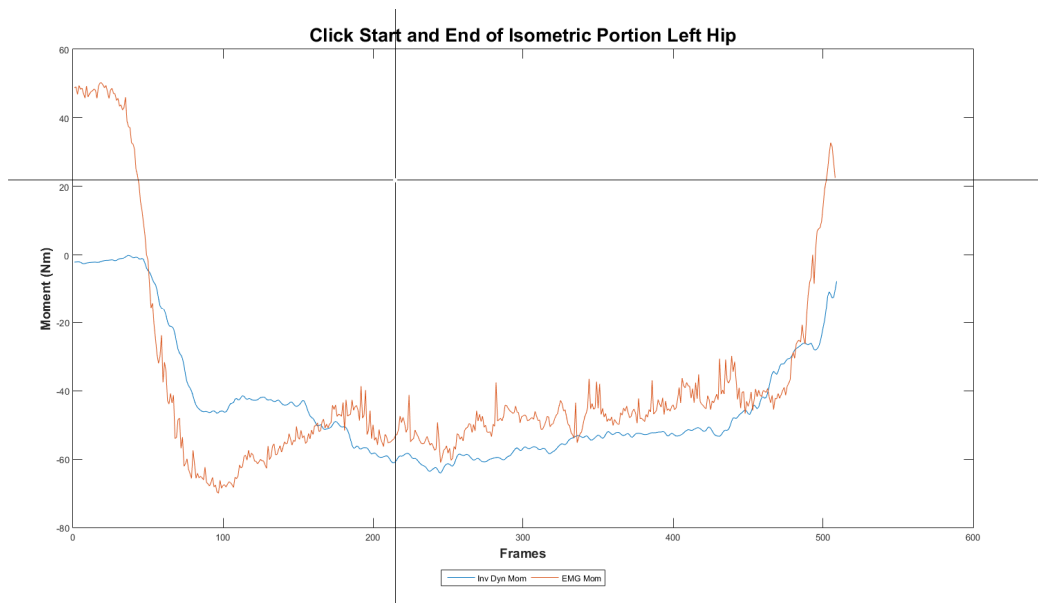


Figure G.2: Screen capture of RVC 2 trial MATLAB program allows user selected points to isolate stabilized section of RVC to calculate gain factor based on inverse dynamics and HSM predictions of left hip extension moment.

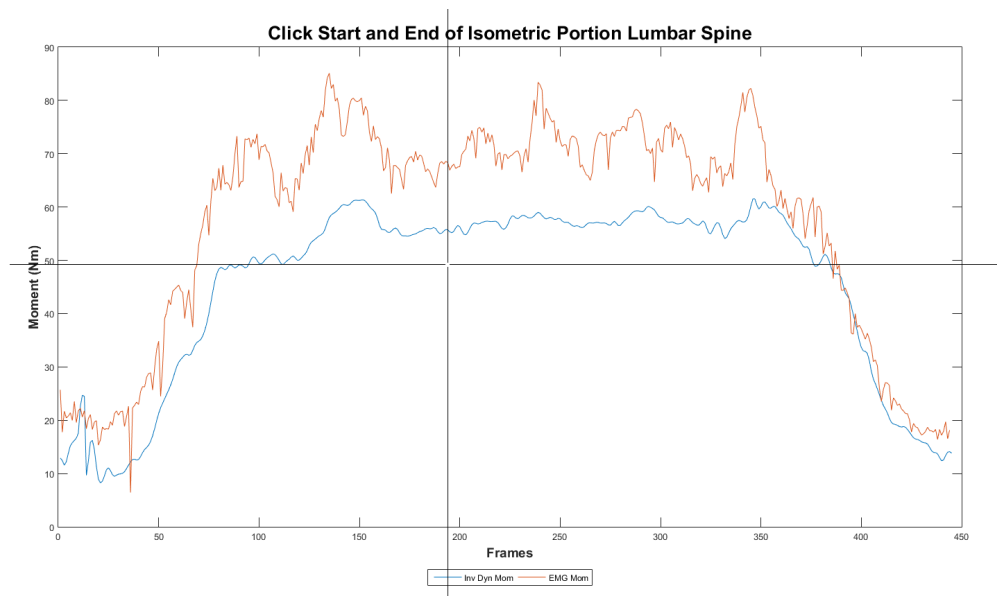


Figure G.3: Screen capture of RVC 2 trial MATLAB program allows user selected points to isolate stabilized section of RVC to calculate gain factor based on inverse dynamics and HSM predictions of spine extension moment.

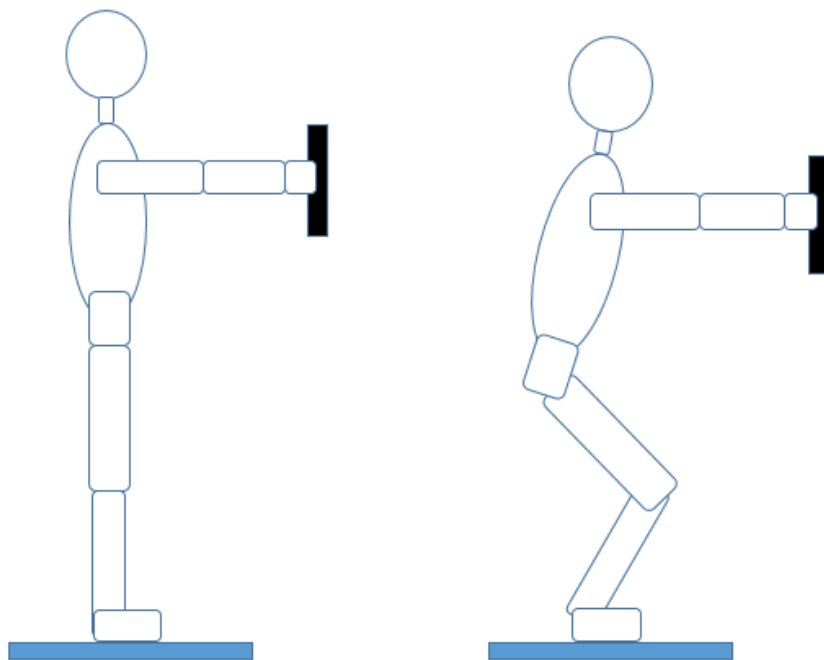


Figure G.4: Reference voluntary contraction (RVC) positions for evaluating and tuning the model, RVC 1 (left) and RVC 2 (Right).

Appendix H: Data from ACL study – Statistical Analysis

Question 1: Does one knee valgus relate and predict the other side? To address these questions a Pearson Correlation and a simple regression analysis were used. These procedures generally require large sample sizes which were simply not possible for this type of detailed biomechanical investigation. One way to artificially enlarge the sample size is to use each trial from the 18 subjects ($18 \times 3 = 54$) to get 54 data points with the intent of avoiding type II errors (not rejecting the null hypothesis). Considering this option, I examined the descriptive data and model data for both groups ($n = 18$ and $n=54$). The group data in both circumstances was very similar the difference being the regression model did not reach statistical significance (~ 0.08). Given the similarity between groups the $N = 54$ group data was used in the analysis, however both sets of data are reported here in the appendix for inspection

Regression – SPSS output Tables and graphs with interpretation. (n=54)

Table H.1: Descriptive Statistics of the Knee Valgus Peak Scores for the right and left knee on first landing.

Descriptive Statistics			
	Mean	Std. Deviation	N
Peak_MKD_R	.061529	.0378945	54
Peak_MKD_L	.057744	.0436444	54

Table H.2: Pearson Correlation of the right and left peak valgus score on first landing.

Correlations			
		Peak MKD R	Peak MKD L
Pearson Correlation	Peak_MKD_R	1.000	.420
	Peak_MKD_L	.420	1.000
Sig. (1-tailed)	Peak_MKD_R	.	.001
	Peak_MKD_L	.001	.
N	Peak_MKD_R	54	54
	Peak_MKD_L	54	54

Table H.3: Regression Model Summary

Model Summary^b

Model	R	R Square	Adjusted R Square	Std. Error of the Estimate
1	.420 ^a	.176	.160	.0347236

a. Predictors: (Constant), Peak_MKD_L

b. Dependent Variable: Peak_MKD_R

Here we see the correlation is 0.420. The $R^2=0.176$ meaning that only ~17% of the variability is account for in the independent variable. The adj. R^2 is lower in this case since even at 54 cases this is a small sample size for regression analysis.

Table H.4: The ANOVA of the regression model

ANOVA^a

Model	Sum of Squares	df	Mean Square	F	Sig.
1 Regression	.013	1	.013	11.122	.002 ^b
1 Residual	.063	52	.001		
Total	.076	53			

a. Dependent Variable: Peak_MKD_R

b. Predictors: (Constant), Peak_MKD_L

Although the correlation is moderate the about of explained variability is small the model is statistically significant $p=0.002$.

Table H.5: Regression Coefficients

Coefficients^a

Model	Unstandardized Coefficients		Standardized Coefficients	t	Sig.	95.0% Confidence Interval for B	
	B	Std. Error	Beta			Lower Bound	Upper Bound
1 (Constant)	.040	.008		5.135	.000	.025	.056
1 Peak_MKD_L	.364	.109	.420	3.335	.002	.145	.584

a. Dependent Variable: Peak_MKD_R

This is perhaps the most telling output from SPSS. Here we see a rather large 95% confidence interval which does not provide much confidence in the ability to predict knee valgus in one knee based on the score from the other.

Table H.6: Residual Statistics

Residuals Statistics ^a					
	Minimum	Maximum	Mean	Std. Deviation	N
Predicted Value	.041481	.108932	.061529	.0159065	54
Residual	-.0580789	.1000593	0E-7	.0343944	54
Std. Predicted Value	-1.260	2.980	.000	1.000	54
Std. Residual	-1.673	2.882	.000	.991	54

a. Dependent Variable: Peak_MKD_R

The mean residual score is ~0.000 meaning that the model although it does not predict the data well it represents the data well. (This is also shown below in graphical form.)

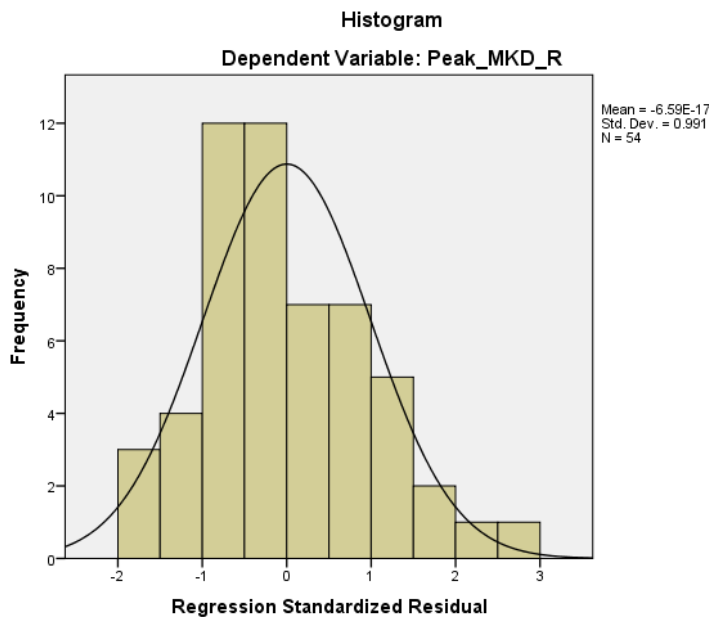


Figure H.1: Histogram of the Residual Scores

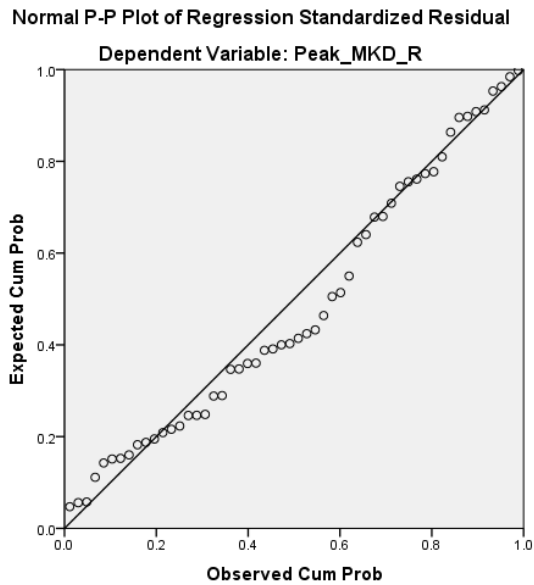


Figure H.2: A plot of the predicted and observed scores standardised. The model does a reasonably good job of fitting the data.

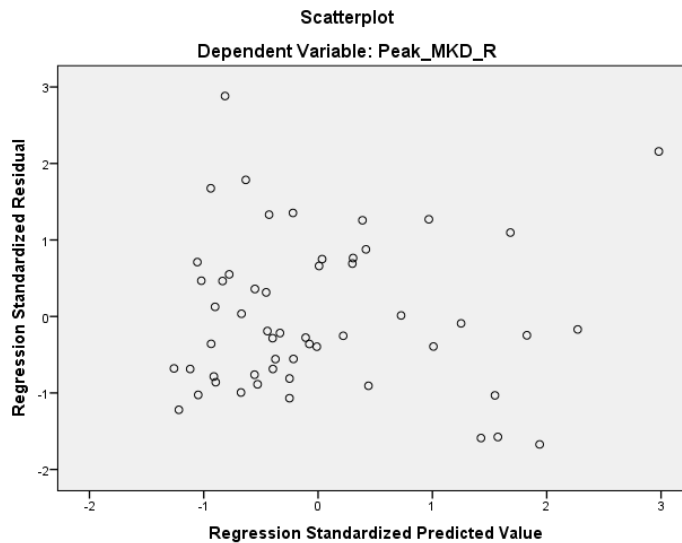


Figure H.3: The Regression Residual and Predicted Values scatter plot.

In Figure 3 there is a reasonably good spread of the data given the sample size. No further analysis of homoscedasticity was performed.

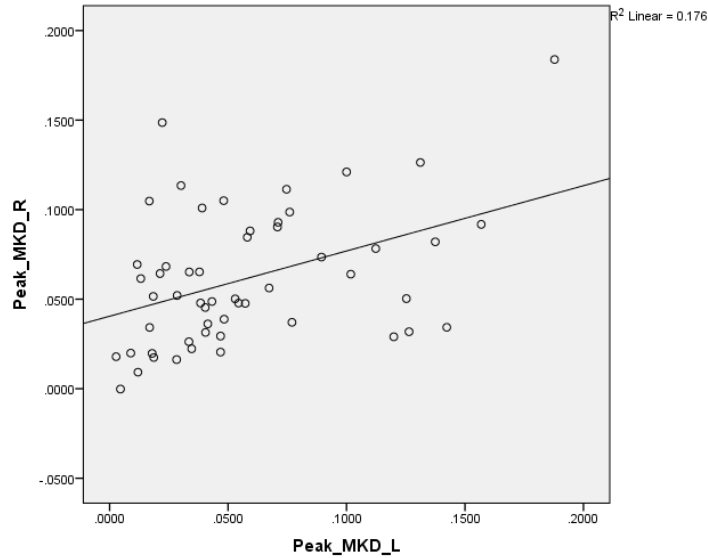


Figure H.4: A scatter plot of the peak valgus data for the right and left knee with the regression line ($R^2=0.176$).

Regression – SPSS output Tables and graphs with interpretation. (n=18)

Table H.7: Descriptive Statistics of the Knee Valgus Peak Scores for the right and left knee on first landing.

Descriptive Statistics			
	Mean	Std. Deviation	N
Peak_MKD_L	.057744	.0427296	18
Peak_MKD_R	.061529	.0356297	18

Table H.8: Pearson Correlation of the right and left peak valgus score on first landing.

Correlations			
		Peak_MKD_L	Peak_MKD_R
Pearson Correlation	Peak_MKD_L	1.000	.421
	Peak_MKD_R	.421	1.000
Sig. (1-tailed)	Peak_MKD_L	.	.041
	Peak_MKD_R	.041	.
N	Peak_MKD_L	18	18
	Peak_MKD_R	18	18

Table H.9: Regression Model Summary

Model	R	R Square	Adjusted R Square	Std. Error of the Estimate
1	.421 ^a	.177	.126	.0399560

a. Predictors: (Constant), Peak_MKD_R

b. Dependent Variable: Peak_MKD_L

Here we see the correlation is 0.421. The $R^2=0.177$ meaning that only ~17% of the variability is account for in the independent variable. The adj. R^2 is much lower in this case since 18 cases is an extremely small sample size for regression analysis.

Table H.10: The ANOVA of the regression model

Model	Sum of Squares	df	Mean Square	F	Sig.
1 Regression	.005	1	.005	3.442	.082 ^b
1 Residual	.026	16	.002		
Total	.031	17			

a. Dependent Variable: Peak_MKD_L

b. Predictors: (Constant), Peak_MKD_R

Not only is the correlation moderate the about of explained variability is small and the model is not statistically significant $p=0.082$. However, given a sample size of $n = 18$, consideration of type II error is appropriate.

Table H.11: Regression Coefficients

Model		Coefficients ^a						
		Unstandardized Coefficients		Standardized Coefficients	t	Sig.	95.0% Confidence Interval for B	
		B	Std. Error	Beta			Lower Bound	Upper Bound
1	(Constant)	.027	.019		1.390	.184	-.014	.067
	Peak MKD R	.505	.272	.421	1.855	.082	-.072	1.081

a. Dependent Variable: Peak_MKD_L

This is perhaps the most telling output from SPSS. Here we see a rather large 95% confidence interval which does not provide much confidence in the ability to predict knee valgus in one knee based on the score from the other.

Table H.12: Residual Statistics

Residuals Statistics ^a					
	Minimum	Maximum	Mean	Std. Deviation	N
Predicted Value	.032719	.094306	.057744	.0179791	18
Residual	-.0653742	.0868473	0E-7	.0387630	18
Std. Predicted Value	-1.392	2.034	.000	1.000	18
Std. Residual	-1.636	2.174	.000	.970	18

a. Dependent Variable: Peak_MKD_L

The mean residual score is ~0.000 meaning that the model although it does not predict the data well it represents the data well. (This is also shown below in graphical form.)

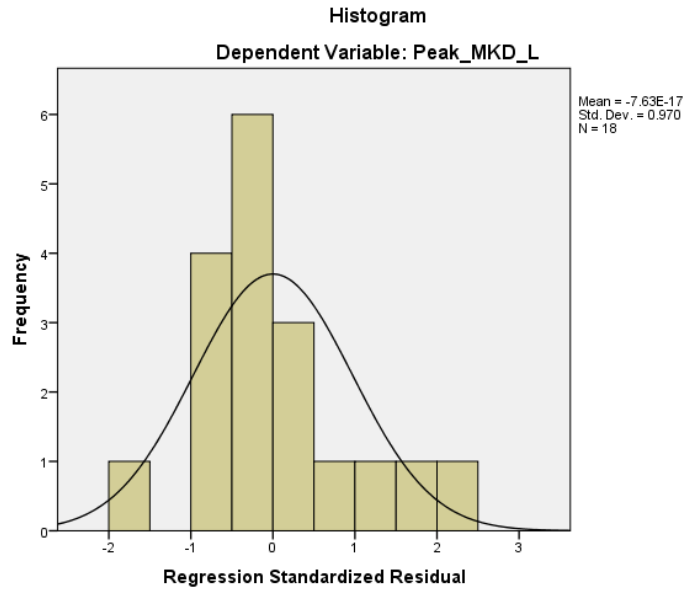


Figure H.5: Histogram of the Residual Scores

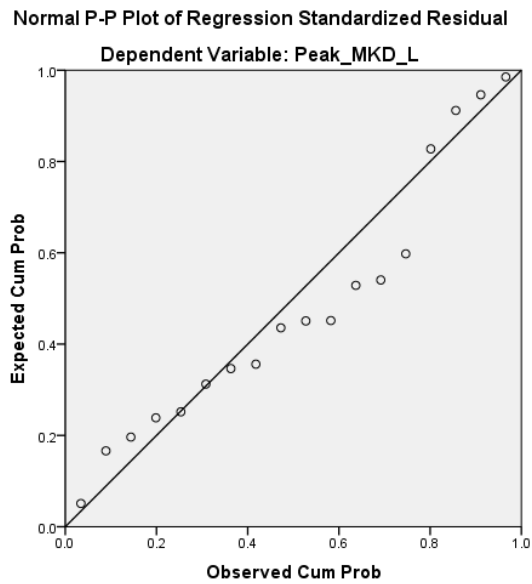


Figure H.6: A plot of the predicted and observed scores standardised. The model does a reasonably good job of fitting the data.

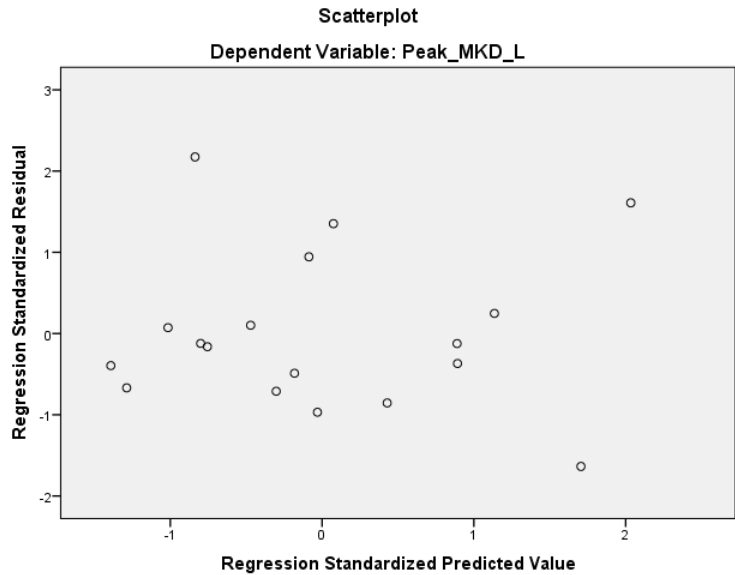


Figure H.7: The Regression Residual and Predicted Values scatter plot.

In Figure 3 there is a reasonably good spread of the data given the sample size. No further analysis of homoscedasticity was performed.

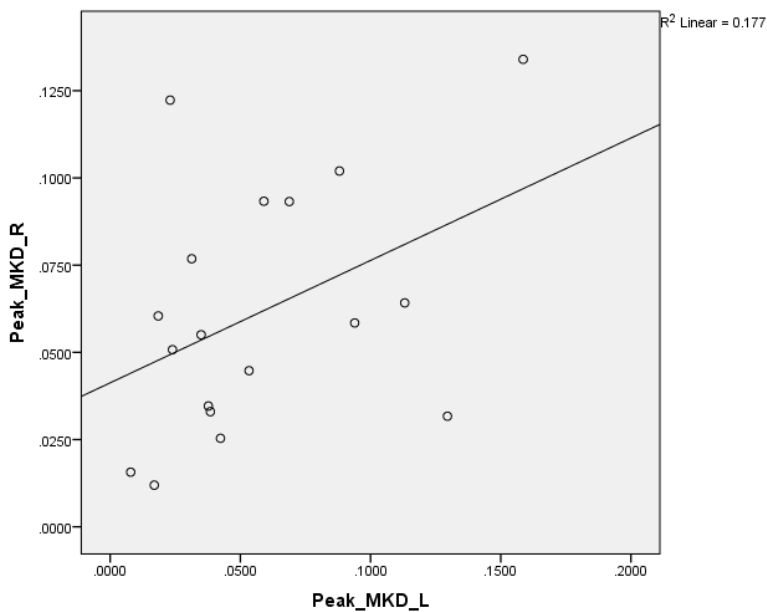


Figure H.8: A scatter plot of the peak valgus data for the right and left knee with the regression line ($R^2=0.177$).